Technische Universität München

TUM School of Medicine and Health

Development of RNAi-based antiviral therapeutic strategies

Shubhankar Sunil Ambike

Vollständiger Abdruck der von der TUM School of Medicine Health der Technischen Universität München zur Erlangung eines

Doktors der Naturwissenschaften (Dr. rer. nat.)

genehmigten Dissertation.

Vorsitz: Prof. Dr. Carsten Schmidt-Weber

Prüfende der Dissertation:

1. Prof. Dr. Ulrike Protzer
2. Prof. Dr. Matthias Feige
3. Prof. Dr. Wolfgang Wurst

Die Dissertation wurde am 18.09.2023 bei der Technischen Universität München eingereicht und durch die TUM School of Medicine and Health am 13.03.2024 angenommen.

Printed and/or published with the support of the German Academic Exchange Service

Table of Contents

Summary

Chronic hepatitis B (CHB) is a significant public health issue worldwide. Despite an effective prophylactic vaccine, approximately 296 million individuals are suffering from CHB worldwide, resulting in over 800,000 deaths yearly. Current treatment strategies can restrict hepatitis B Virus (HBV) replication efficiently but rarely eradicate it due to the persistence of the so called covalently closed circular DNA (cccDNA) in the nucleus of infected hepatocytes. Stimulation of an HBV-specific adaptive immune response against all circulating genotypes via therapeutic vaccination is a potential strategy to cure chronic hepatitis B.

HBV has been proven to take advantage of the liver's immunosuppressive environment, and its persistence has been linked to a limited virus-specific T-cell immune response mediated by an exhausted T-cell population. Therefore, more favorable outcome is attainable via novel combinatorial approaches that additionally help to sustain functional virus-specific T-cell response once activated by therapeutic vaccination. One way to achieve this could be a local suppression of immunomodulatory proteins through highly active small interfering RNAs (siRNAs).

The first part of this thesis therefore focuses on the development of highly active siRNAs against three such immunomodulatory targets, namely PD-L1, Gal-9, and TGF-ß1, with TGF-ß1 remaining the primary focus in later stages. Initially, an *in vitro* screening system based on dual-luciferase reporters was optimized for rapid and reliable siRNA screening. Furthermore, for enhancing the stability of siRNAs in serum, the candidate siRNAs were chemically modified, demonstrating a prolonged target gene knockdown. Among the different cell types found in the liver, hepatic stellate cells (HSCs) are associated with increased TGF-ß1 synthesis, contributing to the immunosuppressive environment of the liver. In the subsequent steps, the ability of HSCs to generate TGF-ß1 during HBV infection was investigated using co-culture assays. Finally, the role of TGF-ß1 in HSC activation was investigated to get insights into the effect of TGF-ß1 cell-specific knockdown in the liver.

During the second part of this thesis, novel HBV mosaic capsid particles were generated, purified, and characterized for a global application of therapeutic vaccination. These capsid particles are composed of HBcAg of genotype C and D, which are also the most abundant HBV genotypes worldwide. These capsid particles can provide a comprehensive HBcAg derived T-cell epitope repertoire against the main circulating HBV genotypes A-E. In this study, a single expression vector containing HBcAg from genotypes C and D under separate promoters enabled construction of self-assembling,

functional HBV mosaic capsid particles in a competent bacterial system. The purification procedure based on sucrose-gradient ultracentrifugation and anion-exchange chromatography was optimized to obtain pure HBV mosaic capsid particles after expression. Further structural characterization revealed that mosaic capsid particles indeed consisted of HBcAg from both genotypes.

Furthermore, the obtained know-how on optimizing siRNAs was exploited to fight the newly emerging severe acute respiratory syndrome coronavirus 2 (SARS-CoV-2). Here, a systematic analysis of RNAi-accessible replication stages of SARS-CoV-2 was conducted. It was initially demonstrated that siRNAs can target the incoming viral genome successfully, terminating the viral transcription and preventing virus-induced cell death. Surprisingly, the siRNAs were ineffective against the low-abundant negative-sense viral RNA transcripts. However, a single siRNA targeting common regions in all viral RNA transcripts (L, N, and 3' UTR) could simultaneously suppress the genomic and sub-genomic viral RNA levels. Nevertheless, efficacious targeting of SARS-CoV-2 genomic RNA with ORF1-specifc siRNAs was identified as the most promising strategy. Lastly, chemically modified siRNAs provided a proof-of-concept in a highly relevant model of human lung explants, achieving a significant reduction of SARS-CoV-2 replication.

Overall, this thesis highlights the versatility of RNAi-based strategies in devising antiviral therapeutic approaches. RNAi, as a supplementary immunotherapeutic in combination with a therapeutic vaccination, might be a promising approach for treating chronic hepatitis B. Furthermore, the efficacious knockdown of the viral genome by siRNAs offers a novel antiviral strategy against emerging viruses such as SARS-CoV-2.

Zusammenfassung

Obwohl eine wirksame Prophylaxe existiert, sind weltweit ungefähr 296 Millionen Menschen chronisch mit dem Hepatitis B Virus (HBV) infiziert, was die chronische Hepatitis B (CHB) zu einem weltweiten Gesundheitsproblem macht, welches zu etwa 800,000 Todesfällen jährlich führt. Derzeitige Therapien können die Virusreplikation beschränken, führen aber nur selten zur vollständigen Beseitigung des Virus. Grund dafür ist die sogenannte kovalent geschlossene zirkuläre DNA (cccDNA), welche in den Zellkernen von infizierten Hepatozyten persistiert. Die Stimulation einer HBV-spezifischen adaptiven Immunantwort gegen alle zirkulierenden Genotypen durch ein therapeutisches Vakzin ist eine potentielle Strategie, um chronische Hepatitis B zu heilen. Es ist erwiesen, dass HBV die immunsuppressive Umgebung der Leber ausnutzt und die virale Persistenz wurde mit einer begrenzten virusspezifischen T-Zell-Immunantwort, welche durch eine erschöpfte T-Zell Population ausgelöst wird, in Verbindung gebracht.

Daher lassen sich bessere Ergebnisse durch neuartige kombinatorische Ansätze erzielen, die zusätzlich dazu beitragen, eine funktionelle virusspezifische T-Zell-Antwort aufrechtzuerhalten, sobald sie durch ein therapeutisches Vakzin aktiviert wurde. Eine Möglichkeit dies zu erreichen, ist eine lokale Suppression immunmodulatorischer Proteine durch hoch aktive kleine interferierende RNAs (siRNAs). Daher fokussiert sich der erste Teil dieser Thesis auf die Entwicklung von hoch aktiven siRNAs gegen drei solche immunmodulatorische Ziele, PD-L1, Gal-9 und TGF-ß1, wobei auf TGF-ß1 der primäre Fokus in späteren Untersuchungen liegt. Zunächst wurde ein *in vitro* Screening System optimiert, welches auf Dual-Luciferase Reportern basiert, um ein schnelles und zuverlässiges siRNA Screening zu ermöglichen. Außerdem wurden die vielversprechenden siRNA Kandidaten chemisch modifiziert, um deren Stabilität in Serum zu verbessern und dadurch ein längeres Knockdown der Zielgene zu ermöglichen.

Unter den verschiedenen Zelltypen in der Leber sind die hepatischen Stellatzellen (HSCs) mit erhöhter TGF-ß1 Synthese assoziiert, wodurch sie zu der immunsuppressiven Umgebung in der Leber beitragen. In den folgenden Schritten wurde die Fähigkeit der HSCs TGF-ß1 während einer HBV-Infektion zu produzieren in Co-Kultur Assays untersucht. Abschließend wurde die Rolle von TGF-ß1 in der HSC Aktivierung untersucht, um Einblicke in den Effekt eines TGF-ß1 zellspezifischen Knockdown in der Leber zu erlangen.

Im zweiten Teil dieser Thesis wurden neuartige Mosaik-Kapsid Partikel generiert, gereinigt und mit Hinblick auf eine globale Anwendung als therapeutische Vakzine charakterisiert. Diese Kapside bestehen aus HBcAg der Genotypen C und D, welche die am meisten verbreiteten Genotypen weltweit sind. Die Kapside bieten damit ein übergreifendes HBcAg abgeleitetes T-Zell Epitop Repertoire gegen die häufigsten zirkulierenden HBV Genotypen A-E.In dieser Studie wurde ein Expressionsvektor, welcher für die HBcAg Genotypen C und D mit seperaten Promotoren kodiert, verwendet. Dieser ermöglichte die Konstruktion von sich selbst formenden, functional HBV Mosaik-Kapsiden im kompetenen Bakterien System. Die Reinigung der Kapside basiert auf einer Ultrazentrifugation eines Suchrose-Gradienten und anschließender Anionenaustausch Chromatography. Dieses Reinigungsprotokoll wurde so optimiert, dass reine HBV Mosaik-Kapside gewonnen werden konnten. Weitere strukturelle Charakterisierung zeigte, dass die Mosaik Kapside wie erwartet aus HBcAg beider Genotypen bestehen.

Weiterhin wurde das erlangte Know-how der siRNA Optimierung ausgenutzt, um das neu aufgekommene severe acute respiratory syndrome coronavirus 2 (SARS-CoV-2) zu bekämpfen. Hierfür wurde eine systematische Analyse von RNAi-erreichbaren Replikationsstadien des SARS-CoV-2 durchgeführt. Anfangs wurde gezeigt, dass siRNAs das eintretende Virusgenom zielgerichtet erkennen und damit die virale Transkription terminieren und den Virus-induzierten Zelltod verhindern können. Überraschenderweise waren die siRNAs gegen die geringen negative-sense viralen RNA-Transkripte nicht effektiv. Allerdings konnte eine siRNA, welche verbreitete Regionen in allen viralen RNA-Transkripten (L, N, and 3’ UTR) erkennt, sowohl die genomischen, als auch sub-genomischen viralen RNA Level unterdrücken. Dennoch wurde die gezielte Erkennung von SARS-CoV-2 genomischer RNA mit ORF-1-spezifischen siRNAs als meist versprechende Strategie identifiziert. Zuletzt konnten chemisch modifizierte siRNAs als Proof-of-concept in einem hoch relevanten Modell von humanen Lungen-Explantaten genutzt werden, wo sie eine signifikante Reduzierung der SARS-CoV-2 Replikation erzielten.

Zusammenfassend hebt diese Thesis die vielseitigen Anwendungen von RNAi-basierten Strategien im Hinblick auf antivirale therapeutische Ansätze hervor. RNAi ist, in Kombination mit einem therapeutischen Vakzin, ein vielversprechender Ansatz für die Behandlung von chronischer Hepatitis B. Außerdem stellt das gezielte Knockdown viraler Genome durch siRNA eine neuartige Strategie gegen neu aufkommende Viren wie SARS-CoV-2 dar.

List of Abbreviations

2’-F	2' Fluoro
2’-MOE	2'-O-Methoxyethyl
2’-OMe	2'-O-Methyl
3’UTR	3' Untranslated region
AAV	Adeno associated virus
ACE2	Angiotensin converting enzyme 2
ACTA2	Actin alpha 2
Ago2	Argonaute 2
AHT	Anhydrotetracycline
ALT	Alanine transaminase
WHO	World health organization
ARDS	Acute resipratory distress syndrome
ASGPR	Asialoglycoprotein receptor
aSMA	Alpha smooth muscle actin
ASO	Antisense oligonucleotides
Bim	Bcl-2 interacting mediator of cell death
BirA	*E. coli* biotin ligase
C_{Δ}	C-terminally truncated genotype C HBcAg
$C_{\Delta}D$	HBV mosaic capsid particles containing C-terminally truncated genotype C HBcAg and full-length genotype D HBcAg
$C_{\Delta}D_{bt}$	HBV mosaic capsid particles containing C-terminally truncated genotype C HBcAg and full-length, N-terminally biotinylated genotype D HBcAg
cccDNA	covalently closed circular DANN
CDC	Centers for disease control and prevention
CDS	Coding sequence
CM	Convulated membrane
CMV	Cytomegalovirus
CTL	Cytotoxic T-lymphocyte
CTLA4	Cytotoxic T-lymphocyte-associated antigen 4
D	HBV capsid particles containing full-length genotype D HBcAg
DCs	Dendritic cells

DMVs	Double-membraned vesicles
ds	double stranded
E	SARS-CoV-2 Envelope protein
ER	Endoplasmic reticulum
ERGIC	ER-Golgi mediated compartment
ETV	Entecavir
FBS	Fetal bovine serum
Gal-9	Galectin-9
GalNAc	N-acetylgalactosamine
GFP	Green fluorescent protein
gRNA	Genomic RNA
hATTR	Hereditary transthyretin amyloidosis
HBcAg	HBV core antigen
HBcrAg	HBV core related antigen
HBeAg	HBV e antigen
HBsAg	HBV surface antigen
HBV	Hepatitis B Virus
HBVenv	HBV envelope protein
HBx	HBV x protein
HCC	Hepatocellular carcinoma
HCV	Hepatitis C Virus
HDV	Hepatitis D Virus
HIV-1	Human Immunodeficiency Virus-1
hPCLS	Human precision cut lung slices
HSC	Hepatic stellate cells
HSPG	Heparan sulfate proteoglycans
IC50	Half-maximal inhibitory concentration
IDO	Indoleamine 2,3-dioxgenase
IEX	Ion-exchange chromatography
IFN	Inteferon
IL-10	Interleukin 10
IPTG	Isopropyl-ß-D-thiogalactopyranoside
ISG	Inteferon stimulated gene
Kb	Kilobases
kD	Kilo dalton

L	SARS-CoV-2 Leader sequence
LB_{Kan}	Luria broth containing kanamycin
LNA	Locked nucleic acid
LNP	Lipid nanoparticles
LSEC	Liver sinusoidal endothelial cells
Luc	Firefly luciferase
M	SARS-CoV-2 membrane protein
MDSCs	Myloid-derived suppressor cells
miRNAs	MicroRNAs
MOI	Multiplicity of infection
mRNA	Messenger RNA
MVA	Modified Vaccinia Ankara Virus
N	SARS-CoV-2 nucleocapsid protein
NAG-MLP	GalNac conjugated melittin like peptide
NAGE	Native agarose gel electrophoresis
NAs	Nucleic acid analogues
NK Cells	Natural killer cells
NMR	Nuclear magnetic resonance
NTCP	Na+-taurocholate cotransporting polypeptide
ORF	Open reading frame
ORF1	SARS-CoV-2 open reading fram 1 a/b
P	HBV polymerase protein
PBS	Phosphate buffer saline
PCR	Polymerase chain reactions
PD-1	Programed-cell death protein 1
PD-L1	PD-1 ligand
PEG	Polyethylene glycol
PEG-IFNα	Pegylated interferon alpha
PEI	Polyethylenimine
pgRNA	Pre-genomic RNA
pHSCs	Primary hepatic stellate cells
PIV	Human Parainfluenza Virus
POTS	Potential offt-targeting score
preC-C	HBV precore and core region
preS-S	HBV presurface and surface region

PS	Phosphorothioate linkage
qPCR	Quantitative polymerase chain reaction
RBD	Receptor binding domain
rcDNA	Relaxed circular DANN
RDRP	RNA dependent RNA polymerase
RISC	RNA induced silencing complex
RNAi	RNA interference
RNP	Ribonucleoprotein
RSV	Respiratory Syncytial Virus
S	SARS-CoV-2 spike protein
SARS-CoV-2	Severe acute respiratory syndrome coronavirus 2
sgRNA	Subgenomic RNA
shRNA	Small-hairpin RNA
siNC	Negative control siRNA
siRNA	Small interferring RNA
SVP	Sub-viral particles
TAF	Tenofovir-Alafenamid
TDF	Tenofovir-Disoproxil
Tet	Tetracycline
TGF-ß1	Transforming growth factor beta 1
TH cells	Helper T cells
TIM-3	T cell immunoglobulin and mucin domain-containing protein 3
TMPRSS2	Transmembrane protease, serine 2
Tregs	Regulatory t cells
TRS	Transcription regulatory sequence
TRS-L	Leader transcription regulatory sequence
TSP	Total soluble proteins
TTR	Transthyretin
UNA	Unlocked nucleic acid
UTR	Untranslated region
VLP	Virus-like particles
VOCs	Variants of concern
WHV	Woodchuck Hepatitis Virus

1 Introduction

The pandemics of Hepatitis B Virus (HBV) and Severe Acute Respiratory Syndrome Coronavirus 2 (SARS-CoV-2) reached unprecedented proportions, infecting millions of people across continents and posing a significant challenge to global public health systems. There is a constant demand for novel antiviral therapies due to persistent challenges posed by these infectious diseases, their global impact, and the limitations of existing treatment options. A post-transcriptional gene-silencing phenomenon known as RNA interference (RNAi) involving the use of complementary small interfering RNA (siRNA) molecules to facilitate the sequence-specific destruction of target mRNA with the help of Argonaute family proteins (M. Muller, Fazi, & Ciaudo, 2019), could be a viable strategy. RNAi enables a precise targeting of a host gene to modulate immune response (Won et al., 2022) as well as the viral nucleic acids (A. Levanova & Poranen, 2018) by delivering exogenous siRNAs to the infected organ or cell. This thesis, therefore, deals with the application of RNAi in developing alternate treatment strategies with HBV and SARS-CoV-2 in focus.

1.1 Hepatitis B Virus (HBV)

The first part of this thesis is focused on optimizing a combinatorial therapeutic strategy utilizing RNAi and therapeutic vaccination against chronic hepatitis B. The subsequent chapters thus cover the structural components of the HBV virion, the molecular biology of the virus, viral pathogenesis, immune response against HBV, and current therapeutic options. Additionally, the necessary background information required to address the topic of this thesis is presented.

1.1.1 Structure and genome organization of HBV

HBV is a small, enveloped DNA virus, belonging to the *Hepadnaviridae* family. It has a 3.2 kilo bases (kb) partial double-stranded (ds) genome, and the virion is about 42 nm in diameter (Figure 1, A). It was first described in 1970 by Dane et *al*. and therefore, the complete virion is also referred to as the ‘Dane particle’ (Dane, Cameron, & Briggs, 1970). The partial dsDNA genome, also known as the relaxed circular DNA (rcDNA), is coupled with the viral polymerase, a reverse transcriptase, and is engulfed/encapsulated in an icosahedral capsid, that is assembled by the hepatitis B core protein (HBcAg). The viral capsid is composed of 180-240 HBcAg monomers (Datta, Chatterjee, Veer, &

Chakravarty, 2012). The capsid is enveloped by a lipid layer derived from the host cell, consisting of three variants of hepatitis B envelope proteins (HBVenv): S, M and L (Nassal, 2015; Ning et al., 2018).

In addition to the infectious virus particles, infected cells also give rise to spherical and filamentous subviral particles of about 22 nm, which lack the viral DNA and thus, are non-infectious (Tsukuda & Watashi, 2020). These subviral particles are more abundant in the serum of infected individuals and are up to 100,000-fold more prevalent than the complete virions (J. Hu & Liu, 2017).

Most of the HBV capsids have T=4 icosahedral symmetry and are made of 240 copies of HBcAg monomers while, a relatively small fraction (approximately 5% of total) of capsids are made of 180 monomers of HBcAg (Niklasch, Zimmermann, & Nassal, 2021). Both particles are about 35 and 30 nm in diameter, respectively (Chen, Wang, & Zlotnick, 2011). The viral capsid shields the viral genome from damage and transports it to the host cell during infection (H. Kim, Ko, Lee, & Kim, 2021)The unique ability of the capsids to undergo reversible disassembly and re-assembly for the uptake and release of the viral nucleic acids is essential for the viral replication. The N-terminal of HBcAg is capable of self-assembly and is responsible for capsid formation, whereas the C-terminal domain is more responsible for binding to the pre-genomic RNA (pgRNA) (Chen et al., 2011; Z. Tan et al., 2015). Given the significance of the capsid in the viral replication cycle, it is an attractive target for new antiviral therapies (Taverniti et al., 2022).

Based on the varying serological reactivity, HBV can be further divided into four serotypes - *adw*, *adr*, *ayw*, and *ayr* (Le Bouvier et al., 1972). Whereas, based on the genetic variance, at least 10 genotypes of HBV, namely A-J, have been identified with distinct regional distribution (Velkov, Ott, Protzer, & Michler, 2018). Distinct genotypes have been reported to have significant impact on the clinical outcome of HBV infection including the risk of developing a chronic infection, progression to hepatocellular carcinoma (HCC), host immune response as well as responsiveness to antiviral therapy (Lin & Kao, 2011; Yuen et al., 2003). Therefore, in line with the focus of this thesis, contemplating the HBV genotypes is essential to formulate prophylactic as well as novel therapeutic strategies.

The HBV genome is highly organized due to its finite coding capacity of only 3.2 kb (Figure 1, B). It consists of four partially overlapping open reading frames (ORF), namely precore-core (preC-C), presurface-surface (preS-S), Polymerase (P) and X (Nassal, 2015). The three viral surface proteins S, M and L are encoded by the preS-S region of the genome by differential translation initiation. The S-protein is expressed by translation of the S region alone. The M-protein is formed by the addition of the preS2 region.

Whereas a further extension with the preS1 region leads to formation of the L-protein. (Ganem & Prince, 2004). HBcAg and HBeAg are both encoded in the preC-C region.

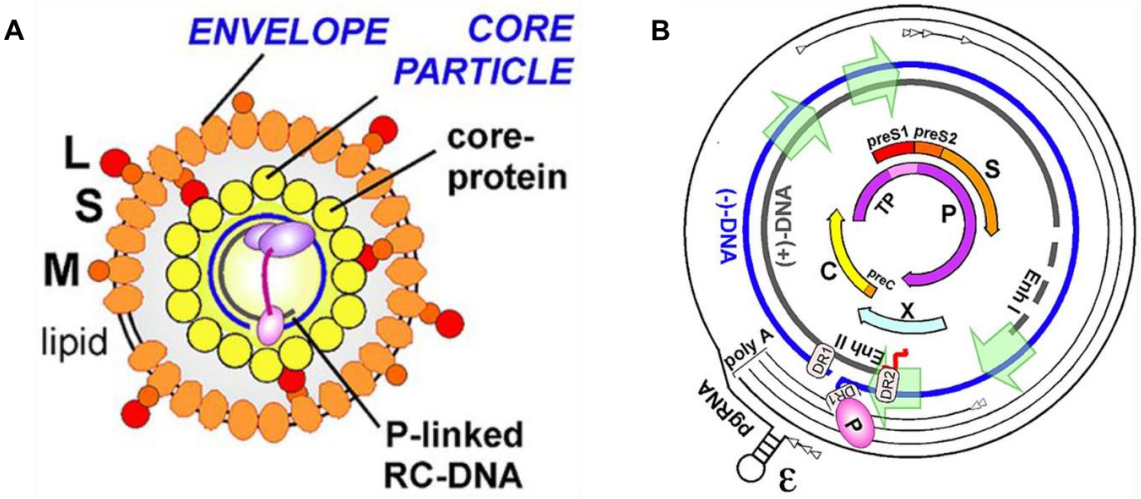

Figure 1: Structure of HBV virion and HBV genome organization. (A) Morphology of HBV virion. The partial double-stranded viral DNA is associated with the viral polymerase, enclosed in the icosahedral viral capsid, formed by the HBcAg. Host-derived lipids and hepatitis B envelope proteins S, M and L form a lipoprotein membrane covering the capsid. **(B)** Genomic organization of HBV. The HBV genome consists of four ORFs – preC-C, preS-S, P and X. Outer lines indicate viral transcripts with start of transcription at the small white arrowheads. ε signifies the encapsidation signal for the pgRNA. Green arrows indicate promotors, transcriptional enhancers, DR1/DR2 direct repeats and terminal protein domain of polymerase protein (Nassal, 2015).

The internal start codon in the C region results in a 21 kD HBc, whereas translation of a complete ORF forms a pre-Core protein carrying a signal sequence leading to its translocation into the endoplasmic reticulum. Subsequent cleavage by cellular proteases, a 16 kD peptide, the HBeAg, is generated and thereafter secreted (Takahashi et al., 1983). A 90 kD multifunctional enzyme, the viral polymerase is encoded by the P region. It performs a variety of functions such as reverse transcription of pgRNA, DNA synthesis and RNA encapsidation (Seeger & Mason, 2015). Lastly, the X ORF encodes the viral X protein (HBx), which controls host-cell signal transduction and can alter host and viral gene expression both, directly and indirectly. While the complete function of the X-protein remains unclear, its activity has been shown to be necessary for initiation and maintenance of viral replication post infection (Ganem & Prince, 2004; Lucifora et al., 2011).

1.1.2 HBV replication cycle

Replication of HBV begins with attachment to the host cell, accomplished by an unspecific, reversible interaction between the myristoylated preS1 domain and heparan sulfate proteoglycans (HSPG). Subsequently, the virions specifically bind to the sodium taurocholate cotransporting polypeptide (NTCP) receptor, the functional receptor of HBV on the cell surface (Herrscher, Roingeard, & Blanchard, 2020). In the subsequent steps, the virus is endocytosed by the fusion with endosomal membrane followed by the release of the viral nucleocapsid into the cytosol. The capsid is afterwards transported to the nucleus, where the HBV rcDNA is released. In the nucleus, the rcDNA is repaired with the help of the host cell repair machinery to generate the episomal HBV covalently closed circular DNA (cccDNA) (Ji & Hu, 2017). cccDNA serves as the replication template pool, from which viral mRNAs are constantly transcribed, followed by translation of viral proteins (Figure 2). Aside from the structural viral proteins, HBx and HBeAg are also translated in the host cell. While HBeAg has been reported to have an immunoregulatory function (Milich & Liang, 2003), the HBx protein acts as an enhancer for viral transcription and is thought to have a role in the progression to HBV-associated HCC (Levrero & Zucman-Rossi, 2016; Y. Li et al., 2019). cccDNA also generates the pre-genomic RNA (pgRNA) and is packed into viral capsids after binding to the HBV polymerase (Figure 2). Inside of the capsids, the viral polymerase reverse transcribes the pgRNA into rcDNA (Seeger & Mason, 2015). Following on, the viral nucleocapsid can be shuttled back to the nucleus to replenish or enlarge the pool of cccDNA or can be released from the host cell (Niklasch et al., 2021). For the release of the progeny virus, the nucleocapsids are enveloped at the endoplasmic reticulum (ER) and the virions are released via multivesicular bodies (Bruss & Ganem, 1991; Watanabe et al., 2007). In addition to the infectious virions, HBV releases vast volumes of empty virus particles and subviral particles (SVPs), assembled in pre-Golgi compartment of the infected cell (Huovila, Eder, & Fuller, 1992) (Figure 2). The SVPs are non-infectious, rcDNA-free and are spherical or filamentous particles. These are mainly seen in the serum of infected individuals as soluble HBsAg. Spherical SVPs appear to be produced via the ER secretory pathway, whereas filaments appear to be released via the multivesicular bodies (Niklasch et al., 2021).

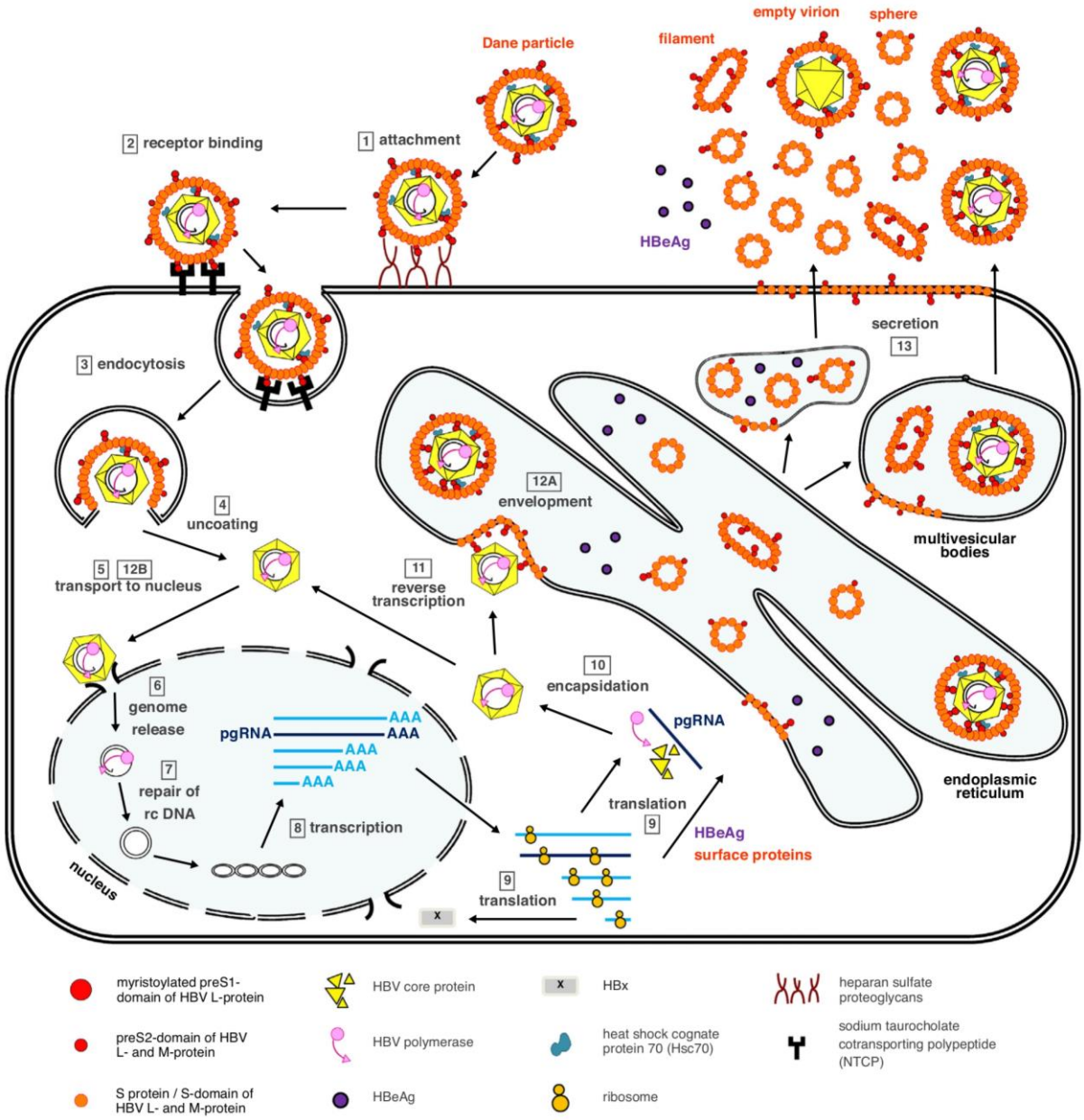

Figure 2: HBV replication cycle. (1) Upon non-specific and irreversible binding to heparin sulfate proteoglycans, **(2)** the virion binds specifically to NTCP. **(3)** The virus is then endocytosed and **(4)** the nucleocapsid is released into the cytoplasm by fusion of the viral envelope with the endosomal membrane. **(5)** The nucleocapsid is transported to the nucleus, where **(6)** the rcDNA is released and **(7)** repaired to form cccDNA. **(8)** The cccDNA serves as a template for the synthesis of mRNAs, which are transported back to the cytoplasm for **(9)** translation using the host machinery. Additionally, pgRNAs are transcribed from cccDNA which associate with the viral polymerase and **(10)** are encapsidated, followed by **(11)** reverse transcription in the capsids. The viral nucleocapsid then can be **(12A)** enveloped in the ER or **(12B)** transported back to the nucleus. **(13)** The formation of multivesicular bodies facilitates the secretion of infectious virions. In addition to the virions, HBeAg, empty virus particles and spherical and filamentous subviral particles are

also released from the cells. Besides the secreted particles, HBVenv proteins S, M and L can additionally reside on the surface of the infected cell (Ko, Michler, & Protzer, 2017).

1.1.3 Course of HBV infection

Hepatitis B virus infection can be an acute self-limiting or a persistent chronic infection, posing a high risk of developing liver cirrhosis and hepatocellular carcinoma to chronically infected individuals (Hadziyannis, Vassilopoulos, & Hadziyannis, 2013). HBV can be transmitted via perinatal route (vertical transmission) or via exposure to infected body fluids (horizontal transmission) (Umar, Hamama Tul, Umar, & Khan, 2013). In general, HBV infection in adults mostly results in self-limited diseases where no treatment is required. Contrastingly, in perinatal infections as well as in young children, the infected individuals often fail to control the virus. As a result, these individuals are at increased risk of a chronic infection (Noordeen, 2015). Certain factors such as age at the time of infection, route of infection, antiviral immune response, status of vaccination and the size of the inoculum contribute to the prevalence of chronic HBV infection (Asabe et al., 2009; Zhao, Shi, Lv, Yuan, & Wu, 2021).

1.1.3.1 Acute HBV infection

Most of the individuals with acute HBV infection experience symptoms such as icteric skin and sclera, gastrointestinal signs such as poor appetite, nausea and vomiting, liver pain and fatigue (Du et al., 2017). Typically, the diagnosed individuals are provided with supportive symptomatic treatment (Du et al., 2017). Majority of the infected individuals with a competent immune system are able to rapidly eliminate the infection, without any therapeutic requirements(Tripathi & Mousa, 2023). As fulminant hepatitis, characterized by rapid liver failure, is rarely seen, the mortality rate associated with acute HBV infection is between 0.5-1% (Peeridogaheh et al., 2018). Acute infections are usually resolved within 6 months (Noordeen, 2015). In relevant *in vivo* study models of HBV and a closely related Woodchuck hepatitis virus (WHV), it was reported that the initial weeks post infection are characterized by nominal innate and adaptive immune activation, where the virus spreads throughout the hepatocytes in the liver. Within the following weeks, the onset of an efficient, virus-specific adaptive immune response mediated by the cytotoxic T lymphocytes (CTLs, CD8+ T cells) leads to killing of majority of HBV-infected hepatocytes (Thimme et al., 2003; S. Wieland, Thimme, Purcell, & Chisari, 2004; S. F. Wieland, Spangenberg, Thimme, Purcell, & Chisari, 2004). On the similar lines, a strong,

multispecific T-cell response is observed with the viral clearance after acute hepatitis along with undetectable serum HBV-DNA levels andnormal alanine amino transferase (ALT) levels with seroconversion to HBsAg-specific antibodies (Chisari, Isogawa, & Wieland, 2010; Rehermann, Ferrari, Pasquinelli, & Chisari, 1996).

1.1.3.2 Chronic HBV infection

According to the World Health Organization's (WHO), about 296 million individuals are living with chronic hepatitis B, resulting in more than 820,000 deaths due to related liver diseases in 2019 (WHO, 2022). Therefore, HBV infection is a major global health problem. The children under the age of five are at increased risk, where 30-90% infected children fail to eliminate the infection during their lifetime (Peeridogaheh et al., 2018). The presence of HbsAg in blood or serum for more than six months is the major serological indicator of chronic hepatitis B. In patients with chronic infection, the illness spectrum may vary. In the majority of the cases, the infection remains asymptomatic and may not cause a significant liver damage. In other cases, however, it could lead to further disorders such as fibrosis, cirrhosis, and an elevated risk of HCC (Peeridogaheh et al., 2018). In addition to the factors such as age, sex and viral genotype, a co-infection with HIV, Hepatitis D or C virus (HDV or HCV) as well as over-consumption of alcohol could accelerate the progression of liver diseases (Alberti et al., 2005; Honer Zu Siederdissen & Cornberg, 2016; Peeridogaheh et al., 2018; Weldemhret, 2021). As opposed to the individuals with acute infection, a weak, narrowly focused adaptive immune response mediated by an exhausted T-cell population is associated with chronic hepatitis B and fails to achieve viral clearance (Chisari et al., 2010; B. Ye et al., 2015). Therefore, restoring the virus-specific adaptive immune response through therapeutic vaccination or further combinatorial therapies to be promising approaches for the treatment of chronic HBV infection (Bunse, Kosinska, Michler, & Protzer, 2022; Kosinska, Zhang, Lu, & Roggendorf, 2010).

1.1.4 Adaptive response during HBV infection

The course of HBV infection majorly relies on the virus-specific T-cell response. During an acute resolving infection, the host immune system fights HBV effectively and quickly. The robust and multi-specific CD8+ T cells play an important role in HBV clearance (Maini et al., 1999; Thimme et al., 2003). In particular, HBV core specific CD8+ T cells have been associated with viral clearance (Webster et al., 2004). Additionally,

neutralizing antibodies produced by B cells against HBsAg can be protective and inhibit the virus from spreading to non-infected hepatocytes (Bertoletti & Ferrari, 2016).
The liver has been described to possess a unique immune-regulatory environment to prevent needless induction of immune responses against harmless antigens (Thomson & Knolle, 2010). As a result, it could raise an opportunity for persistent viral infections. Although the mechanisms of viral persistence in the liver are only partially understood, there is evidence that it can be related to a high antigenic load as well as to the contribution of immunomodulatory proteins by parenchymal as well as non-parenchymal liver cells (Protzer, Maini, & Knolle, 2012).

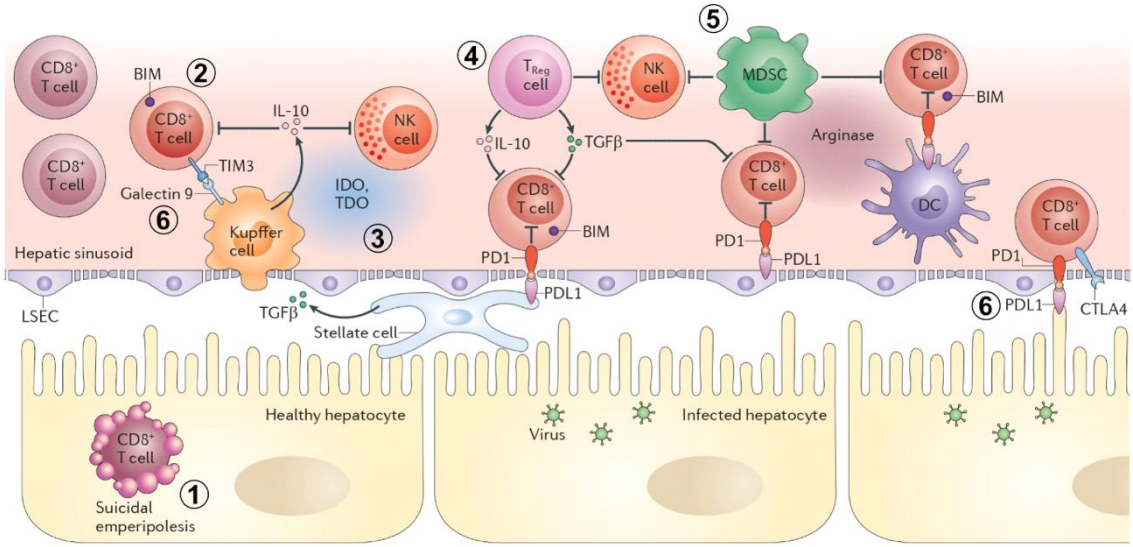

Figure 3: Mechanisms promoting persistence of liver infection. (1) Suicidal emperipolesis in hepatocytes eliminating T cells. **(2)** T cells expressing BIM undergo apoptosis. **(3)** High levels of IDO and arginase in the liver inhibit Natural kill cells (NK cells) and T cells. **(4)** T_{regs} produce anti-inflammatory cytokines such as Interleuikin-10 (IL-10) and TGFß. T_{regs} and **(5)** Myeloid-derived suppressor cells (MDSCs) prevent expansion and functions of NK cells and T cells. **(6)** Co-inhibitory receptors PD1, TIM-3 and CTLA4 provide inhibitory signals through binding of their respective ligands on infected hepatocytes, Kupffer cells, liver sinusoidal endothelial cells (LSECs), hepatic stellate cells (HSCs) and dendritic cells (DCs). Modified from (Protzer et al., 2012).

In case of HBV, high HBsAg levels in serum of infected individuals have been associated with chronic infection and an exhausted CD8+ T-cell profile (Lumley, McNaughton, Klenerman, Lythgoe, & Matthews, 2018). This exhausted state is characterized by impaired effector functions such as cytotoxic activity and cytokine secretion along with expression of certain co-inhibitory receptors (or checkpoint inhibitors) such as Programmed cell death-1 (PD-1), cytotoxic and T-cell immunoglobulin domain and mucin

domain 3 (TIM-3) (Lumley et al., 2018; B. Ye et al., 2015). Interestingly, the exhausted phenotype observed during chronic hepatitis B is limited to the HBV-specific T cells, which represent only a fraction of the total population (Boni et al., 2007). Moreover, blockade of factors contributing to T-cell exhaustion such as the checkpoint inhibitors have demonstrated restoration of T-cell effector functions to some extent (Bengsch, Martin, & Thimme, 2014; W. Wu et al., 2012). Therefore, a majority of the cells could remain functional and thus available for priming via immunotherapeutic strategies such as the therapeutic vaccination.

Adding to this exhausted state, certain host factors have been proposed to assist the development of chronic liver infections such as hepatocyte-mediated degradation of CD8+ T cells (Benseler et al., 2011) (Figure 3, (1)), T-cell apoptosis mediated BCL-2 interacting mediator of cell death (Bim) (Holz et al., 2008) (Figure 3, (2)), high levels of enzymes such as Indoleamine 2,3-dioxygenase (IDO) (Figure 3, (3)), presence of immunosuppressive cytokines like Transforming growth factor beta1 (TGFß-1) (Tinoco, Alcalde, Yang, Sauer, & Zuniga, 2009), T-regulatory cell (T_{reg}) and myeloid-derived suppressor cells (MDSC) mediated control of immune cells in the liver (Figure 3, (4, 5)) (Stross et al., 2012), and inhibition by checkpoint inhibitors (Figure 3, (6)).

1.1.5 Prophylaxis and treatment for HBV infection

1.1.5.1 Prophylactic HBV vaccination

Vaccination against hepatitis B virus (HBV) infection began on a large scale in the early 1980s, with a first-generation vaccine prepared from plasma of chronic carriers containing HBsAg. Following that, it was replaced with a second-generation vaccine comprising of HBsAg produced in yeast cells (Gerlich, 2015). The prophylactic vaccination is recommended by the WHO for all infants, particularly in the endemic regions such as Africa and south-east Asia. Additionally, it is recommended for certain groups such as healthcare personnel, who could be at elevated risk of occupational exposure. Vaccination within 24 hours of birth, if followed by two further doses, is 90-95% effective in preventing HBV infection (WHO, 2015). The vaccination results in protective anti-HBs antibodies and a titre of >10 IU/L was reported as a reliable marker of protection against HBV (Jack, Hall, Maine, Mendy, & Whittle, 1999). In addition to the conventional vaccines, an alternative glycosylated vaccine produced in mammalian cells, comprising of all HBVenv proteins could be administered to non-responders (Gerlich, 2015).

When it comes to the major circulating genotypes, genotypes A and D are usually found in North Africa, Europe, and Asian countries. East Asian countries, on the other hand, have a high prevalence of genotype B and C. Genotypes A and E are common in Sub-Saharan Africa, while genotype F is found in southern America (Velkov et al., 2018). While most of the commercial prophylactic vaccines are of genotype A2, the vaccination could be less effective against non-A2 infection. During the breakthrough infections with non-A2 genotype, the infections in vaccinated individuals were subclinical and transient, and the vaccination prevented a clinical disease (Stramer et al., 2011). However, the cross-protection may vary depending on the genotype and serotype of HBV, as a gradual shift in distribution of HBV genotype has been reported in south-east Asia (Wen et al., 2011; H. Ye, Teng, Lin, Wang, & Fu, 2020). Nevertheless, the universal vaccination programs for HBV have been majorly successful due to their high effectiveness in preventing infections and onset of clinical disease caused by major circulating genotypes (Cassidy, Mossman, Olivieri, De Ridder, & Leroux-Roels, 2011). On similar lines, a therapeutic vaccination contemplating global distribution of HBV genotypes could be an effective strategy to cure chronic hepatitis B.

1.1.5.2 Current strategies to treat HBV infection

Regardless of the availability of a preventative vaccine, a significant proportion of chronic HBV carriers exists which require treatment. While the treatment for acute HBV infections is mainly supportive, chronically infected individuals are closely monitored for disease progression and are is recommended to receive appropriate antiviral treatment (WHO, 2015).

Antiviral agents capable of inhibiting HBV replication, thereby preventing progression to cirrhosis and decreasing the risk of HCC and related mortality are available. However, current treatments are unable to eradicate the virus in the majority of patients, necessitating adherence to a life-long treatment. Infected individuals with signs of liver cirrhosis or high HBV DNA levels (>2000 IU/ml) with persistently elevated ALT levels or older than 30 years with high ALT and HBV DNA levels are advised for the treatment (EASL, 2017).

Currently approved treatment options include immunomodulatory agents such as PEGylated interferon (PEG-IFNα) or nucleos(t)ide analogues (NAs). Entecavir (ETV), tenofovir disoproxil fumarate (TDF), and tenofovir alafenamide fumarate (TAF) are second-generation NAs that inhibit HBV DNA replication and are indicated as first-line, monotherapy medicines because they have a lowerrisk of drug resistance than previous

NAs (Terrault et al., 2016; WHO, 2015). PEG-IFNα can also be considered for patients with mild to moderate chronic hepatitis B, but a combination of both is not recommended. Importantly, altering the primary treatment strategy in individuals on monotherapy exhibiting low or declining HBV DNA levels is not advised (EASL, 2017). The NA therapy could be potentially discontinued upon confirmed HBsAg loss from serum, irrespective of anti-HBs seroconversion or after 12 months of therapy with undetectable HBV DNA levels and HBeAg seroconversion, but a close monitoring at regular intervals is necessary (EASL, 2017; WHO, 2015). However, HBsAg loss with undetectable levels of HBV DNA is recognized as a functional cure and not a virological cure, as the HBV cccDNA could still persist in the infected hepatocytes (Gan et al., 2023). Therefore, to completely eradicate the virus, novel therapeutic strategies are urgently needed, primarily focusing on targeting the HBV cccDNA. In such scenario, re-educating the immune system to kill the infected cells could be a viable option.

1.1.5.3 Therapeutic vaccination against chronic hepatitis B

A therapeutic vaccination is a promising technique for restoring endogenous adaptive immunity and achieving cure, by eliciting de novo or increasing existing HBV-specific T-cell and B-cell responses (Gehring & Protzer, 2019). The aims of such strategy are to prime new antiviral T-cell responses and augment existing ones, so that the balance of HBV-specific T cells switches from an exhausted to a functional state (Maini & Pallett, 2018). Currently, multiple therapeutic vaccines against chronic hepatitis B are in clinical trials (Lobaina & Michel, 2017).

While the HBsAg is sufficient to confer long term protection via prophylactic vaccination, importance of immune response against HBcAg has also been highlighted during acute hepatitis B (Ferrari et al., 1991). On these lines, a novel mucosal therapeutic vaccine, Nasvac (HeberNasvac®), was developed for the treatment of chronic hepatitis B in Cuba. It is composed of 100 µg of recombinant HBsAg and HBcAg each in 1 ml of phosphate-buffered saline (PBS), administered nasally (Aguilar, Aguiar, & Akbar, 2022). In a recently conducted phase III clinical trial in Bangladesh, Nasvac reported superior results to PEG-IFNα, where a more sustained control of HBV DNA along with clearance of HBeAg and comparatively lower progression to cirrhosis was reported (Al Mahtab et al., 2018). Another therapeutic vaccine, DV-601, consisting of HBsAg and HBcAg with a saponin-based ISCOMATRIX adjuvant was developed by Dynavax Co., Ltd. The initial dose-escalation study demonstrated a significant reduction in HBV DNA levels irrespective of the dosage in chronically infected individuals. Additionally, the vaccine

was reported to be safe and well-tolerated at all dose levels (Dynavax, 2011; Spellman M, 2011).

In addition to protein-based vaccines, several DNA-based vaccines are also under investigation. They are particularly of advantage due to induction of both, a humoral and a cellular immunity including helper T cell (T_H cells, CD4+ T cells) as well as CD8+ T cell responses (Donnelly, Wahren, & Liu, 2005). In a phase I clinical trial, immunization with 1 mg of Cytomegalovirus-based vector encoding S and M HBVenv proteins (pCMV-S2.S) resulted in decreased serum HBV DNA levels in half of the participants. While complete clearance was observed in a single case, the effects were reported to be transitory and weak (Mancini-Bourgine et al., 2004). In another multicenter phase I/II clinical trial for the pCMV-S2-S, the vaccination was unable to prevent the recurrence of infection despite an effective viral suppression by NAs in infected individuals (Fontaine et al., 2015). A combination of recombinant DNA vaccines INO-1800 and INO-9112, including plasmids coding for HBsAg and HBcAg as well as a plasmid encoding human interleukin 12, has recently been developed (Liang et al., 2015). Here, the preclinical data showed that the immune responses induced by therapeutic vaccination eliminated the adoptively transferred HBV-coated target cells (Obeng-Adjei et al., 2012). The phase I clinical trial has been conducted and further studies are ongoing (NCT02431312).

In contrast to plasmid-based vaccines, another strategy for a therapeutic vaccination is viral-vector based vaccine. TG1050 is a second-generation adenoviral-based therapeutic vaccine encoding a fused protein consisting of core, polymerase and envelope protein domains. Preclinical evaluation of TG1050 demonstrated robust and long-lasting HBV-specific T-cell response in murine models (P. Martin et al., 2015). Recently, the phase Ib trail of TG1050 reported a minor decrease of HBsAg with unquantifiable levels of HBV core-related antigen (HBcrAg) in individuals under NA therapy (Zoulim et al., 2020).

Uniting the two strategies, a heterologous protein prime/modified Vaccinia virus Ankara (MVA) vector-boost therapeutic vaccine (TherVacB) was designed (Backes et al., 2016). The protein prime phase consists of intramuscular administration of recombinant HBsAg and HBcAg followed by a boost with recombinant MVA expressing S and core proteins. Priming with particulate HBsAg and HBcAg allows induction of neutralizing antibodies, preventing further HBV spread. It could also reduce circulating HBsAg and HBeAg along with priming of CD4+ and CD8+ T cells with an appropriate adjuvant. The T-cell responses then are expanded further by the MVA boost (Dembek, Protzer, & Roggendorf, 2018). Preclinical studies have demonstrated that the TherVacB regimen

indeed induces strong anti-HBV immunity comprising of humoral and HBV-specific CD4+ and CD8+ T cell responses (Kosinska et al., 2019; Su et al., 2023).

As stated earlier, a high antigen load observed in chronic HBV infection exhibits direct immune-inhibitory effects (Lumley et al., 2018). This could obstruct achieving cure despite the administration of an effective therapeutic vaccination. Following on these lines, functional cure was achieved in murine models by therapeutic vaccination coupled with RNAi-mediated knockdown of HBV antigens (Michler et al., 2020). However, it was not clear whether a suppression of immunomodulatory components instead of HBV antigens could further enhance the efficacy of therapeutic vaccination. Moreover, the initial therapeutic vaccination strategy utilized a single HBV genotype HBcAg, abstaining the priming of adaptive immune responses against other circulating HBV genotypes. In contrast, remodelling the HBcAg to present a wider T-cell epitope repertoire, effective against major circulating HBV genotypes could be beneficial. This thesis therefore, focuses on developing a combinatorial therapeutic strategy against chronic hepatitis B, combining RNAi against immunomodulatory proteins in the liver and simultaneously improving therapeutic vaccination component.

1.2 Severe acute respiratory syndrome coronavirus 2 (SARS-CoV-2)

Severe acute respiratory syndrome coronavirus 2 (SARS-CoV-2), formerly known as 2019 novel coronavirus (2019-nCoV) is the causative agent of the coronavirus disease 19 (COVID-19) (Coronaviridae Study Group of the International Committee on Taxonomy of, 2020). It was first identified in December 2019 and caused a worldwide pandemic (Cucinotta & Vanelli, 2020). The pandemic has caused an overwhelming global economic burden and appears to be far from over after three years (Lancet, 2023; Richards et al., 2022). The following chapters introduce the molecular biology of SARS-CoV-2, characteristics of COVID-19 as well as prophylactic and therapeutic strategies against SARS-CoV-2 infection.

1.2.1 Structure of SARS-CoV-2 virion and genome organization

SARS-CoV-2 is an enveloped, single-stranded positive-sense RNA virus with a 30 kb long genome (Khailany, Safdar, & Ozaslan, 2020). The infectious virions are spherical or ellipsoidal and range in size from 60 to 140 nm in diameter and have a crown-like surface (Zhu et al., 2020). The structural components of the virions include viral spike

glycoprotein (S) embedded in the host membrane-derived lipid bilayer, together with membrane glycoprotein (M) and envelope protein (E), which composes the viral envelope. The viral RNA genome is inside the viral envelope, surrounded by a helical nucleocapsid made up of the nucleocapsid protein (N) (Figure 4 A) (Cubuk et al., 2021; Hardenbrook & Zhang, 2022).

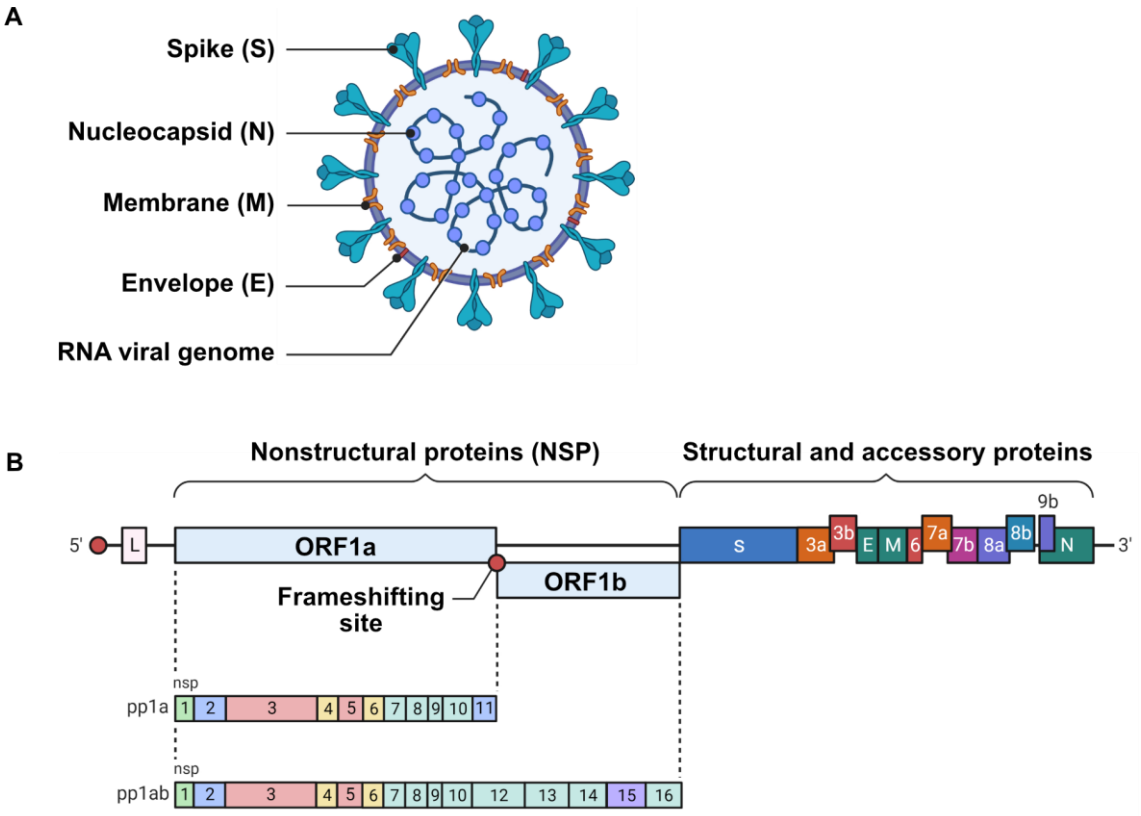

Figure 4: Morphology of SARS-CoV-2 virion and genome organization. (A) Morphology of SARS-CoV-2 virion. Structural proteins S, M, and E are embedded in a host-derived lipid bilayer, enclosing N-bound genomic RNA. (B) Genome organization of SARS-CoV-2. ORF1 spans approximately two thirds of the genome and is translationally divided into ORF1 and ORF1b. The polyproteins generated from ORF1 region are further cleaved to form 16 NSPs. The remaining third of the genome comprises structural and accessory proteins. Modified from template 'Genome organization of SARS-CoV' from BioRender.com (2023). Obtained from https://app.biorender.com/biorender-templates.

The viral genome is divided into multiple distinct sections, including the 5' untranslated region (UTR), the ORF1 region coding mainly for replication proteins, structural and accessory proteins, and the 3' UTR (Figure 4 B). The ORF1 region is translationally viewed as ORF1a and ORF1. It makes up nearly two-thirds of the genome, generating two large polyproteins, namely polyprotein 1a (pp1a) and polyprotein 1ab (pp1ab). Post

synthesis, these polyproteins are further processed by viral and cellular proteases into 16 non-structural proteins (NSPs). NSPs are primarily involved in formation of extra-nuclear double-membraned replication organelles (ROs) to initiate and carry out the viral replication (Hardenbrook & Zhang, 2022; Yan, Zheng, Zeng, He, & Cheng, 2022). In addition to virus replication, the NSPs are also involved in viral protein processing as well as in modulating host immune response (Yoshimoto, 2020).

The remaining third of the viral genome encodes several structural proteins and accessory viral proteins (Figure 4 B). Structural proteins consist of S, E, M, and N, which are essential for the assembly and release of infectious virus particles. The S protein forms a homo-trimer on the surface of the virion. The S monomer is made of two subunits, S1 and S2. The S1 domain is a receptor-binding domain (RBD) which directly binds to the entry receptor human angiotensin-converting enzyme 2 (ACE2) on the host cells. Subsequently, the S2 domain aids in the membrane fusion during the viral entry (Huang, Yang, Xu, Xu, & Liu, 2020). Whereas, E and M proteins are mainly involved in the assembly and the release of the progeny virus, altering the host signalling pathways as well as induction of host cell apoptosis (Yang et al., 2022; Zhang et al., 2022). The N protein possesses an RNA-binding function to form the ribonucleoprotein complex (RNP). Interestingly, the N protein counters the host RNAi-mediated antiviral response owing to its RNA-binding activity. The N protein is also involved in RNA transcription and immune regulation (W. Wu, Cheng, Zhou, Sun, & Zhang, 2023). The remaining accessory proteins of SARS-CoV-2 have been reported to play several important roles in viral pathogenesis. In particular, ORF3a is involved in apoptosis, ORF3b, 6, 7a and 8 are potent interferon antagonists, while other proteins impair the host immune responses through various mechanisms (Redondo, Zaldivar-Lopez, Garrido, & Montoya, 2021). However, further in-detail studies are necessary to elucidate exact functions of accessory proteins.

1.2.2 SARS-CoV-2 replication

SARS-CoV-2 replication cycle starts with attachment of the S protein to the entry receptor ACE2 on host cells (Figure 5). The S protein is cleaved at two locations namely, S1/S2 and S2, for a successful infection. Cleavage at S1/S2 by the furin protease results in a conformational alteration favoring S protein recognition by ACE2. After binding to ACE2, cleavage at the S2′ site by transmembrane serine protease 2 (TMPRSS2) facilitates viral entrance into host cells via membrane fusion (Essalmani et al., 2022; Peacock et al., 2021). The genomic RNA (gRNA) is eventually released into the host

cytoplasm by uncoating the nucleocapsid after internalization (V'Kovski, Kratzel, Steiner, Stalder, & Thiel, 2021).

Upon release, the positive sense gRNA is immediately available for translation to generate pp1a and pp1ab, and subsequently the NSPs essential for the replication of SARS-CoV-2. The genomic replication begins by assembly of double-membraned ROs by the NSPs. The ROs serve as a secure site for the synthesis of genomic and sub-genomic RNAs (sgRNA), via generation of negative-sense RNA transcripts (Roingeard et al., 2022; V'Kovski et al., 2021). The SARS-CoV-2 replication follows a discontinuous transcription and replicates via negative sense RNA transcripts which is commonly seen in Coronaviruses (Sawicki & Sawicki, 1995). The synthesis of the negative strand begins from the 3' end of the viral gRNA, it is interrupted at a transcription regulatory sequence (TRS) present upstream of most of the ORFs and is re-initiated at the TRS downstream of the leader sequence (TRS-L), continuing till the end (Y. Zhao et al., 2021). Moreover, a full-length negative-sense gRNA is also generated from the incoming genome of the virus. These negative sense intermediate RNAs are then utilized as template for the generation of monocistronic sub-genomic mRNAs as well as full-length positive-sense gRNA. Interestingly, the mRNA of an upstream ORF such as S also comprises of the complete downstream genomic sequence due to the discontinuous transcription. This unique replication process therefore results in formation of nested sgRNAs consisting of identical 5' leader (L) and 3' UTR sequences (V'Kovski et al., 2021). This is of relevance especially for the development of novel therapeutic strategies employing RNAi. Owing to the fact that each viral RNA transcript contains three common regions, namely L, N ORF and 3' UTR, a single siRNA targeting either of these regions could simultaneously suppress genomic and sgRNAs.

Viral mRNAs leave the ROs post transcription and are translated into structural and accessory proteins in the cytoplasm using the host cell machinery. The nascent positive-sense gRNA is selectively packaged with N proteins and further buds into the cisternae of the Endoplasmic reticulum-Golgi intermediate compartment (ERGIC), where the structural proteins assemble to form the complete virion. Lastly, the newly formed virions are exocytosed from the infected cells (Figure 5) (V'Kovski et al., 2021).

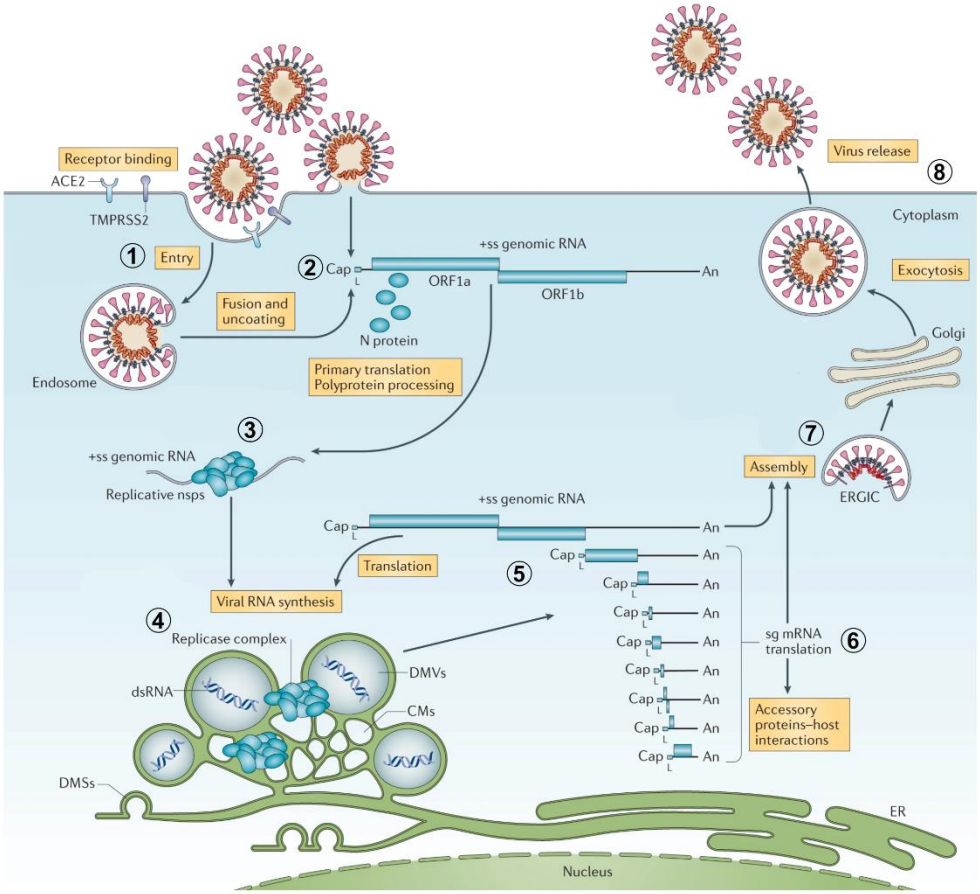

Figure 5: SARS-CoV-2 life cycle. (1) The virus enters the host cell via binding of the S protein to the ACE2 receptor, which, in conjunction with the serine protease TMPRSS2, causes viral uptake by membrane fusion. Inside the host cell, the **(2)** incoming viral gRNA is released and **(3)** immediately translated into polyproteins pp1a and pp1b, which are further processed into several non-structural proteins essential **(4)** to form ROs consisting of double-membraned vesicles (DMVs), convoluted membranes (CMs) and small open double-membraned spherules (DMSs). ROs offer a protective microenvironment for **(5)** viral genome replication and transcription of sub-genomic mRNAs. The discontinuous transcription results in nested viral mRNAs, which are **(6)** translated into corresponding structural and accessory proteins after exiting the ROs. The viral proteins then **(7)** translocate into the ER membranes and pass through the ERGIC, interacting with the N-encapsulated nascent gRNA which results in mature virions that are budding into the lumen of secretory vesicular compartments. The viral progeny is then **(8)** secreted by exocytosis. Modified from (V'Kovski et al., 2021).

1.2.3 Transmission and clinical manifestation of SARS-CoV-2 infection

The course of SARS-CoV-2 infection is variable, ranging from an asymptomatic to a severe, life-threatening illness. (Kronbichler et al., 2020). Despite the broad distribution of ACE2 receptor expression on a variety of cell and tissue types, SARS-CoV-2 primarily infects and replicates in the respiratory system (M. Y. Li, Li, Zhang, & Wang, 2020). SARS-CoV-2 spreads by having close contact with infected individuals. Here, three different viral submission routes can be described. The principal route of infection is through inhalation of small droplets and aerosol particles released by infected individuals, which can stay suspended for a long time in enclosed environments with poor ventilation and can travel up to 2 meters (Stadnytskyi, Bax, Bax, & Anfinrud, 2020). The second method requires closer contact of bigger droplets (> 5 μm) that can accumulate on exposed mucous membranes in the mouth, nose, and eye (Baselga, Guemes, Alba, & Schuhmacher, 2022). Lastly, touching mucous membranes with fluid-covered palms is the third and most ignored route (CDC, 2021). It has been reported that SARS-CoV-2 can survive on many surfaces such as plastic, metal and surgical masks for days or even weeks (Chin & Poon, 2020).

In general, the incubation period lasts between 2 to 14 days following exposure, with clinical symptoms varying widely in severity and appearance (Linton et al., 2020). The majority of infected individuals remain asymptomatic or experience mild symptoms. Individuals suffering from COVID-19 often develop flu-like symptoms such as coughing, fever, tiredness, headache and sore throat (Pascarella et al., 2020). New symptoms of infection, such as loss of taste or smell were also observed as the pandemic progressed (Samaranayake, Fakhruddin, & Panduwawala, 2020). Whereas severe COVID-19 symptoms are likely to be seen in older individuals or individuals with underlying health conditions and comorbidities (Gao et al., 2021). These severe and critical parameters associated with COVID-19 have been attributed to the complex interplay between SARS-CoV-2 and the host immune system leading to activation of numerous inflammatory pathways causing aggressive inflammation and cytokine storm. This may lead to pneumonia, hypoxia, thrombosis, multi-organ dysfunction, acute respiratory distress syndrome (ARDS) and sepsis, ultimately causing the death of the individuals (Alimohamadi, Sepandi, Taghdir, & Hosamirudsari, 2020; Colantuoni et al., 2020; Mullol et al., 2020; L. Y. Tan, Komarasamy, & Rmt Balasubramaniam, 2021). Recovery from the mild infection usually takes 7-10 days after the onset of symptoms, while it could take between 3-6 weeks to recover from a critical illness (Raveendran, Jayadevan, & Sashidharan, 2021).

In some cases, many symptoms may persist for weeks or months following SARS-CoV-2 infection, regardless of viral state. This condition is widely known as ‘Long COVID’ or post-acute sequelae of SARS-CoV-2 (Proal & VanElzakker, 2021). Long-term COVID can result in a variety of symptoms affecting organs beyond the respiratory system such as the cardiovascular system or even the nervous system. The symptoms mainly include fatigue, shortness of breath, chest pain, joint pain, myalgia, mental fog, difficulty concentrating, depression, anxiety, and sleeplessness. Other less common symptoms include loss of taste or odour, headaches, vertigo, and skin rashes (Raveendran et al., 2021). The precise cause or conditions that facilitate long COVID are only partially understood. However, the chance of getting long COVID is higher in people who are older, have pre-existing medical issues, or have had a severe initial infection (Proal & VanElzakker, 2021).

1.2.4 Prophylaxis and therapeutic strategies against SARS-CoV-2 infection

The recent development of highly effective vaccines against SARS-CoV-2 could be the key to end the pandemic. Novel therapies and modern medicines are certainly another life-saving element for breakthrough infections. Researchers all around the world have prioritized the further development of vaccines and therapeutics that provide broader protection against other variants (Le Page, 2022).

1.2.4.1 Non-pharmaceutical preventive strategies and vaccination

Apart from maintaining personal hygiene, the elemental strategy to combat SARS-CoV-2 is to limit the viral spread (Hang, Sun, & Li, 2020). Shortly after beginning of the pandemic, several countries instituted numerous measures to limit the spread of COVID-19, principally focusing on limiting human-to-human transmission. These included a strict lockdown as one of the most severe restrictions, entailed severe travel restrictions, social distancing, and closing of the majority of commercial and educational activities all over the world (Khanna, Cicinelli, Gilbert, Honavar, & Murthy, 2020). While the effectiveness of lockdowns is controversial among specialists, numerous studies have reported lower infection and mortality rates in countries with more stringent lockdown measures (Lai et al., 2020). Use of facial masks at indoor public venues, public transportation, and outdoor areas, where social distancing was difficult to achieve was another effective, globally implemented preventive strategy. Studies have demonstrated that facial masks

effectively prevent the spread of SARS-CoV-2. While surgical masks were commonly worn during regular daily activities, health-care workers who were particularly vulnerable for occupational exposure were supplemented with N95 respirators for a superior protection (Chu et al., 2020; M. S. Kim et al., 2022).

Vaccines have been used as effective preventative interventions against infectious diseases since their development. The immune system can be trained to offer protection against a natural infection by exposure to attenuated or inactivated pathogens or a structural component from pathogen. Due to the memory functions of cell-mediated immunity, the protection against a pathogen can last for years or even for a lifetime (Osiowy, 2018). Therefore, vaccines can be considered as one of the most significant medical achievements to date, having saved countless lives and prevented the spread of dangerous diseases.

Various vaccine models, such as subunit vaccines, viral vector vaccines, DNA and mRNA vaccines have been created and implemented until now (Melo et al., 2022; Rezaei & Nazari, 2022). Recently, mRNA vaccines have gained the greatest attention during the pandemic due to their speedy development as well as their high efficacy and proposed safety. These antiviral vaccines typically contain an mRNA fragment translating into a non-infectious virus antigen, which is recognized by the immune system, eliciting an effective immune response (J. Kim, Eygeris, Gupta, & Sahay, 2021). SARS-CoV-2 vaccines from Pfizer-BioNTech (BNT162b2) and Moderna (mRNA502 1273), both with a similar design of lipid nanoparticles encasing an mRNA-encoding SARS-CoV-2 S, are well-known examples of recently developed mRNA vaccinations (Bettini & Locci, 2021). In clinical trials, the Pfizer-BioNTech and Moderna vaccines showed 95% and 94.1% efficacy in preventing COVID-19 after two doses given 21 and 28 days apart, respectively (Kronbichler et al., 2021; Polack et al., 2020). Many countries including the United States, the United Kingdom, and the European Union, allowed their emergency use in December 2020, rendering them the first commercially available vaccines during the pandemic. Furthermore, vaccinations have been demonstrated to be effective in reducing severe disease, hospitalization, as well as COVID-19 related mortality (Rahmani et al., 2022). Recently, the pharmaceutical companies are focusing on revising the vaccination strategies considering the emerging variants of concerns (VOCs) to decrease the mutation-induced immune escape.

The Oxford-AstraZeneca (ChAdOx1 nCoV-19), a viral vector vaccine, is another type of COVID-19 vaccine that has been widely utilized. Vaccines employing an innocuous viral vector such as an adenovirus transport the genetic material into target cells, where the immunogenic viral protein is synthesized. This vaccine employed a chimpanzee

adenovirus carrying a gene encoding the SARS-CoV-2 S protein (Joe et al., 2022). However, this vaccine reported a lower efficiency of 70% after two doses provided 4-12 weeks apart, compared to the mRNA vaccines (Voysey et al., 2021).

It should be noted that, the development of a vaccine is a very stringent process and can take many years. The general stages in vaccine development include discovery, preclinical testing, optimizing manufacturing process, clinical trials and vaccine approval (CDC, 2023b). However, in response to the imperative need and to halt the spread of the pandemic, the development and distribution of COVID-19 vaccines were surprisingly accelerated to less than one year. This unprecedented milestone could have been reached with the prioritization and streamlining of the review and approval processes for COVID-19 vaccines by regulatory agencies, as well as the advanced vaccine technology platform and global collaboration (Barbier, Jiang, Zhang, Wooster, & Anderson, 2022).

1.2.4.2 Therapeutic strategies to treat COVID-19

The hyperactive inflammatory response or the cytokine storm in response to SARS-CoV-2 infection plays a crucial role in development of COVID-19 (Ragab, Salah Eldin, Taeimah, Khattab, & Salem, 2020). Therefore, several immune-modulators such as Interleukin-6 antagonists, Corticosteroids such as dexamethasone and Janus kinase inhibitors are used for reducing inflammation and severity of COVID-19 (NIH, 2023; van de Veerdonk et al., 2022)

The number of treatments designed to treat SARS-CoV-2 infection has significantly expanded since the start of the COVID-19 epidemic (CDC, 2023a). A quicker method to treat newly emerging novel pathogens could be to reposition already-approved broad-spectrum antiviral drugs. The nucleoside analogues such as Remdesivir, Molnupiravir, and Favipiravir, have been shown to inhibit the replication of various viruses mainly by interfering with a key viral protein, RNA-dependent RNA polymerase (RdRp) (Kabinger et al., 2021; Kaptein et al., 2020; Kokic et al., 2021). On these lines, double-blind, randomized, placebo-controlled trial of intravenously applied Remdesivir reported a reduction of recovery time (Beigel et al., 2020) while molnupiravir demonstrated reduced risk of hospitalization or mortality in high-risk unvaccinated adults with COVID-19 (Jayk Bernal et al., 2022). Favipiravir, mainly distributed in Japan, Russia and China also showed therapeutic potential against COVID-19 in terms of disease progression and viral clearance (Cai et al., 2020; Ivashchenko et al., 2021). While these drugs have demonstrated antiviral activities against SARS-CoV-2 to various extents, none of these

are specific to the SARS-CoV-2. Therefore, a highly specific siRNA-based antiviral therapy, directly suppressing the SARS-CoV-2 RNA, could be more beneficial.

Considering the specificity towards SARS-CoV-2, monoclonal antibody-based therapies could be another viable option. Monoclonal antibodies created by combining classic antibody identification and isolation procedures with novel synthetic antibody library methodologies and high-throughput screening might thus be employed to develop an efficient strategy to combat COVID-19 (Hwang et al., 2022). On these lines, Casirivimab and Imdevimab, a combination medicine and a cocktail of monoclonal antibodies, was devised as a potential therapy against SARS-CoV-2, which was later approved for emergency use in few countries (Copin et al., 2021; Deeks, 2021). Moreover, another monoclonal antibody, namely Sotrovimab, was approved for emergency use in many countries, which has been shown to have a high affinity towards the conserved receptor binding domain (RBD) of SARS-CoV-2 S protein, displaying the same mode of action as Casirivimab and Imdevimab (Heo, 2022). These monoclonal antibodies have been proven to lower the incidence of hospitalization and mortality in high-risk patients with mild to moderate COVID-19 (Miguez-Rey, Choi, Kim, Yoon, & Sandulescu, 2022). In addition to monoclonal antibodies, several patients with severe COVID-19 have been treated with convalescent plasma from individuals recovered from COVID-19. From the therapeutic point of view, the convalescent plasma primarily includes antibodies that can help to fight the virus, and it has been found to minimize the risk of death in individuals suffering from COVID-19 (Senefeld et al., 2023).

Several studies have recently highlighted RNAi as a potential therapeutic strategy against SARS-CoV-2 (Fopase, Panda, Rajendran, Uludag, & Pandey, 2023; Kokic et al., 2021; Raghav et al., 2020). An early report with the closely related SARS-CoV-1 have demonstrated the potential of RNAi-based therapy to efficiently suppress infection in non-human primates (B. J. Li et al., 2005). As the siRNAs are highly sequence specific and given the recent technological advances in the field of chemical modifications, RNAi could be a viable alternative for SARS-CoV-2 specific antiviral treatment.

1.3 RNA interference (RNAi)

This thesis primarily focuses on development of therapeutic siRNAs to target immunomodulatory genes and viral nucleic acids. The following chapters introduce the history, applications of RNAi and the advancements in the field of siRNA-based antiviral therapeutic strategies.

1.3.1 Discovery and mechanism of RNAi

RNAi is a vital mechanism of post-transcriptional gene regulation that has been reported in a wide variety of eukaryotic organisms (He & Hannon, 2004). This phenomenon of gene regulation was first discovered in 1998 by Fire et al., where introduction of exogenous dsRNA could suppress the expression of an endogenous gene in *C. elegans* (Fire et al., 1998). This ground-breaking discovery further led to a Nobel Prize in Physiology or Medicine in 2006 ("The Nobel Prize in Physiology or Medicine 2006," 2006). The main hallmark of RNAi is its specificity towards the target gene. Therefore, RNAi quickly rose as a powerful tool for studying gene functions and developing novel therapeutic strategies (Dorsett & Tuschl, 2004).

The pilot studies reporting the application of dsRNA as gene regulators in *C. elegans*, proposed that the injection of longer dsRNA in a cell subsequently triggers an internal mechanism, ultimately leading to the degradation of mRNA (Fire, Albertson, Harrison, & Moerman, 1991; Fire et al., 1998). Upon successful introduction of dsRNAs, they are first cleaved into smaller RNA duplexes of approximately 21-23 nucleotides, by an RNase III family endonuclease Dicer (Bernstein, Caudy, Hammond, & Hannon, 2001) (Figure 6, (1, 2)). These small duplexes or the siRNAs then join as a guide to the effector complex, forming the (RISC), which is the key mediator of the mRNA cleavage (Paroo, Liu, & Wang, 2007) (Figure 6, (3)). The siRNAs can alternatively be introduced in the cytoplasm directly. The RISC comprises of two key components – the antisense guide strand of the siRNA and the Argonaute family proteins. It has been identified that, Argonaute 2 (Ago2) is responsible for the cleavage of the mRNA in mammals, hence known as the catalytic driver of RNAi (J. Liu et al., 2004). Prior to binding RNA-induced silencing complex to the mRNA, the RISC complex is pre-organized for an increased efficiency of binding to the target mRNA complementary to the guide strand (Salomon, Jolly, Moore, Zamore, & Serebrov, 2015) (Figure 6 (4)). The cleavage of mRNA upon RISC binding begins in the middle section of the siRNA binding site (Iwakawa & Tomari, 2022) (Figure 6 (5)). Upon successful cleavage, the cleaved mRNA is handed over to the RNA decay machinery in

the cell lead by the exonucleases (Orban & Izaurralde, 2005) (Figure 6 (6)). An alternative pathway of RNAi mediated by microRNAs (miRNAs) processed by another RNase III nuclease, Drosha has also been described (Carthew & Sontheimer, 2009), however, is not the focus of this thesis.

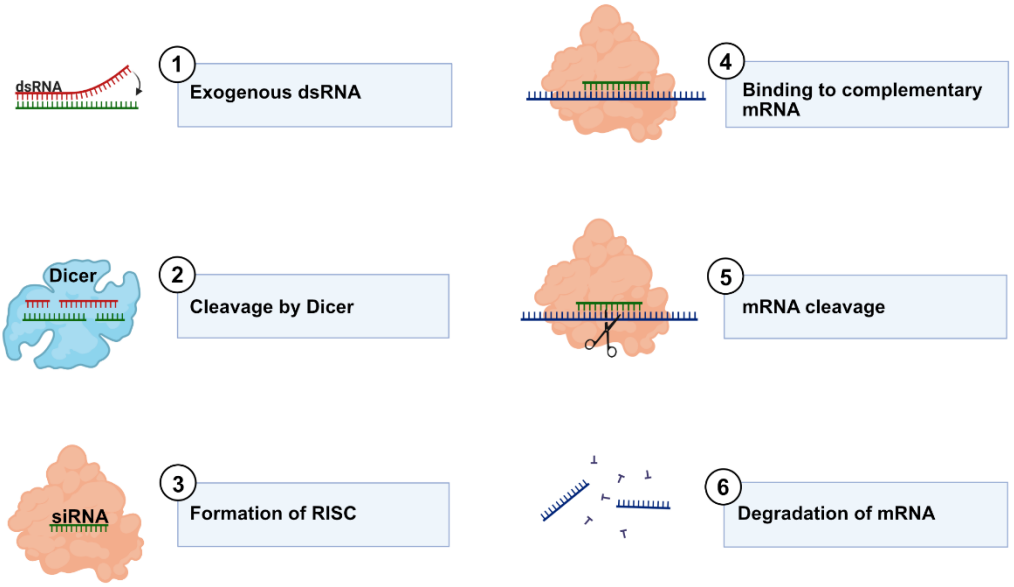

Figure 6: Post-transcriptional gene silencing by RNAi. (A) Exogenous dsRNA is processed by **(B)** Dicer into shorter siRNA fragments of about 21-23 nucleotides long. **(C)** The antisense strand of the siRNA is recruited by the Ago2 proteins to form the RISC. **(D)** Subsequently, the antisense RNA guides the RISC to the target mRNA, which is then **(E)** cleaved and **(F)** degraded, suppressing the gene expression. Modified from template 'RNAi Mechanism' from BioRender.com (2023). Obtained from https://app.biorender.com/biorender-templates.

1.3.2 Designing of siRNAs

siRNAs are the mediators of RNAi in the cell. Functional siRNAs can be of varying length, with 18-25 nucleotides being the average (Tokatlian & Segura, 2010). The design of siRNAs is the first and most critical stage in the development of siRNA-based therapeutic strategies. A successful siRNA designing results in a unique RNA duplex of a sense and an antisense strand, capable of effectively targeting a complementary mRNA target sequence. While the siRNAs largely rely on sequence complementarity for their activity, any complimentary short stretch of RNA may not always be a functional siRNA. The efficiency of siRNAs depend on a variety of aspects such as target availability, position of nucleotides, secondary structures of target mRNA and relative stability (Safari, Rahmani Barouji, & Tamaddon, 2017). Addressing these factors, several guidelines

have been previously published, to allow an efficient designing of siRNAs (Naito, Yamada, Ui-Tei, Morishita, & Saigo, 2004; Ui-Tei et al., 2004).

Considering potential off-target effects is of utmost importance when it comes to siRNA design (Jackson et al., 2003). Off-targeting primarily occurs when the seed region (nucleotides 2–8 of the anti-sense RNA) binds to sequences within the 30-nucleotide UTR of unintended mRNAs, thereby inducing a translational repression and transcript destabilization, similar to micro-RNA-based silencing (Jackson et al., 2006). This off-target effect could render the siRNAs toxic, even at lower concentrations. Among multiple siRNA designing algorithms available online (Gong et al., 2008; Naito et al., 2004), siSPOTR additionally offers a deeper insight into possible off-target effects of potential siRNA sequences (Boudreau et al., 2013). While following the usual guidelines for siRNA designing, siSPOTR additionally calculates a potential off-targeting score (POTS) for each siRNA sequence designed. Given this advantage, siSPOTR was utilized to design siRNAs in this thesis. In general, designing multiple siRNAs against a single target gene is advised and a rigorous experimental screening is recommended to define a candidate siRNA against a target (Boudreau et al., 2013).

1.3.3 History and applications of RNAi

RNAi has been extensively used in various branches of biology since more than two decades. Within the first few years of its discovery, numerous researchers primarily aimed at defining the underlying mechanisms and biochemical processes concerning the phenomenon RNAi. At the beginning of the 21st century, RNAi was successful implemented in human cells (Elbashir et al., 2001). Subsequently, RNAi become an influential tool in molecular biology enabling highly specific and potent silencing of any known RNA sequence (Pereira & Lopes-Cendes, 2013). RNAi has been successfully employed in several fields of biology including but not limited to developmental biology, cancer therapy, antiviral therapeutics, agriculture, genomic screens and epigenetics (Dai, Yusuf, Farjah, & Brand-Saberi, 2005; Das & Sherif, 2020; Kara, Calin, & Ozpolat, 2022; Muthusamy, Bosenberg, & Wajapeyee, 2010; Pereira & Lopes-Cendes, 2013; van den Berg et al., 2020).

Furthermore, RNAi contributed significantly to the understanding of gene regulation and function in diverse organisms (Novina & Sharp, 2004) and has widely been used to understand and modulate the role of particular genes involved in development, behavior or diseases. One early study reported up to 70% increase in lifespan of *C. elegans* using RNAi-based inactivation of genes (Hamilton et al., 2005). Additionally, RNAi-based

approaches also play an important role in regulating stem-cell towards fully differentiated cells for tissue repair, underlining its applications in regenerative medicine (Q. Wu, Wang, Wang, Liang, & Li, 2020). In line with the focus of this thesis, RNA-based therapeutics employing RNAi-technology are gaining attention as upcoming treatment options for infectious and non-infectious diseases (Brown et al., 2022). In a widely-known example, potential of RNAi-based approaches in developing therapies against one of the most lethal cancers such as pancreatic cancer have also been reported, where efficient delivery of siRNAs against certain genes to cancer cells, inhibited the invasiveness of pancreatic tumors in mice (Taniuchi, Yawata, Tsuboi, Ueba, & Saibara, 2019). Moreover, siRNA-based targeting of certain transcription factors, promoting invasion and proliferation of cancerous cells, has exhibited potential applications against HCC (Khan, Alanazi, Jabeen, Chauhan, & Ansari, 2019; J. Xu et al., 2021). Irrespective of such wide applications, stability and delivery of the siRNAs to a relevant cell or organ still remain as the major hurdles (Truong, Medina-Cruz, & Mostafavi, 2023).

1.3.4 Chemical modifications of siRNAs and targeted delivery to the liver

Numerous obstacles such as poor pharmacokinetics, off-target effects, activation of immune system and precise delivery to the relevant cell or organ hinder the clinical translation of RNAi-based therapeutic strategies (Alshaer et al., 2021). These challenges can be overcome by sequence-specific chemical modifications of the siRNAs. This strategy has also been employed in this thesis to improve the activity of siRNAs.

The significance of ribose modifications in siRNA-based therapeutic approaches is widely known (Kurreck, 2009). Especially, alteration of 2-O' of the sugar moiety has been of central interest and are employed most frequently (Braasch et al., 2003; Kraynack & Baker, 2006). The reported modifications mainly include 2'-*O*-Methyl (2'-OMe), 2'-Fluorine (2'-F) and 2'-*O*-Methoxyethyl (2'-MOE). (Kraynack & Baker, 2006; Song et al., 2017; J. K. Watts et al., 2007). In addition to these modifications, inclusion of phosphorothioate (PS) linkage at the terminal positions, replacing the phosphodiester linkages, is another widely employed strategy (Jahns et al., 2015). These are the most frequent chemical modifications used in therapeutic siRNAs, however, several alternative strategies are constantly in development. These mainly include modifications such as locked nucleic acids (LNA), unlocked nucleic acids (UNA), 5'-*O*-methyl, 2'-*O*-2-Thio, 4-Thio, N6-methyl and others (Chiu & Rana, 2003; Dande et al., 2006; Elmen et al., 2005; Imaeda et al., 2019; Laursen et al., 2010; Prakash, Naik, Sioufi, Bhat, &

Swayze, 2009; Terrazas & Kool, 2009). While these modifications are beneficial in overcoming the hurdles mentioned earlier, incorporation of these modifications ameliorates the RNAi activity (Friedrich & Aigner, 2022).

Apart from the intra-strand modified nucleotides, conjugation of biomolecules at the terminal positions is a pivotal strategy for therapeutic siRNA development. These mainly include N-acetylgalactosamine (GalNAc), cholesterol, folic acid, polyethylene glycol (PEG) and peptide conjugation to either 5' or 3' end of the sense or 5' end of antisense strand of the siRNA (Balkhair et al., 2020; Gaziova, Baumann, Winkler, & Winkler, 2014; Haraszti et al., 2018; Sajid et al., 2022; Springer & Dowdy, 2018). Such bioconjugation of the siRNAs primarily assist in targeted delivery of the siRNAs but may enhance their efficiency as well (Chernikov, Vlassov, & Chernolovskaya, 2019).

Traditionally, the siRNA delivery to the liver is achieved by lipid nanoparticles (LNP) and synthetic nanoparticles (Kulkarni, Witzigmann, Chen, Cullis, & van der Meel, 2019). Due to their positive charge at low pH, LNPs mask the negatively charged siRNAs to protect them from chemical degradation by intra- and inter-cellular nucleases and mainly aid a rapid endosomal escape into the cytoplasm (Yonezawa, Koide, & Asai, 2020). LNP delivery vehicles are typically about 50 nm in diameter. They are usually composed of ionisable cationic lipids and co-lipids such as cholesterol, phospholipids and PEG-lipids. The formation of LNP-siRNA and release of siRNAs is majorly driven by the change of pH (Kulkarni et al., 2019) (Figure 7). At a lower pH, initial mixing of an organic-lipid phase with the nucleic acids aqueous buffer causes the trapping and particle formation. However, stable LNP-siRNA complexes are formed at a neutral pH. These complexes consist of a hydrophobic oil-core, majorly comprised of ionisable lipid encircled by siRNA complexed to the lipids in a bilayer configuration (Kulkarni et al., 2018). The ionisable cationic lipids facilitate the interaction with the cell membrane inducing the internalization of complexes. Once internalized, the ionisable lipids are protonated at acidic pH of the endosome, interacting, and thereby destabilizing the endosomal membrane for endosomal escape of the encapsulated siRNA to cytoplasm (B. Martin et al., 2005; Sun & Lu, 2023). Early studies on identifying ideal formulations enabling liver directed siRNA delivery (Adami et al., 2011; Love et al., 2010) have highlighted the efficacy of LNP-mediated siRNA delivery in preclinical models of liver diseases upon intravenous administration (Akinc et al., 2008; Morrissey et al., 2005). Subsequent advancements in development and optimization of various formulations ultimately resulted in Patisiran, the first approved siRNA drug (Adams et al., 2018; Coelho et al., 2013). The siRNA of Patisiran targets the Transthyretin (TTR) gene and is delivered specifically to hepatocytes with LNPs. It is used for treatment of hereditary transthyretin amyloidosis

(hATTR) with polyneuropathy, caused by deposition of hepatocyte-derived transthyretin amyloid in peripheral nerves (Kristen et al., 2019). In addition to siRNAs, several LNP formulations are under current investigation as vehicles for a targeted delivery of mRNA, DNA and various drugs (Hou, Zaks, Langer, & Dong, 2021; Luo & Lu, 2023; Mashima & Takada, 2022; Schnichels et al., 2023).

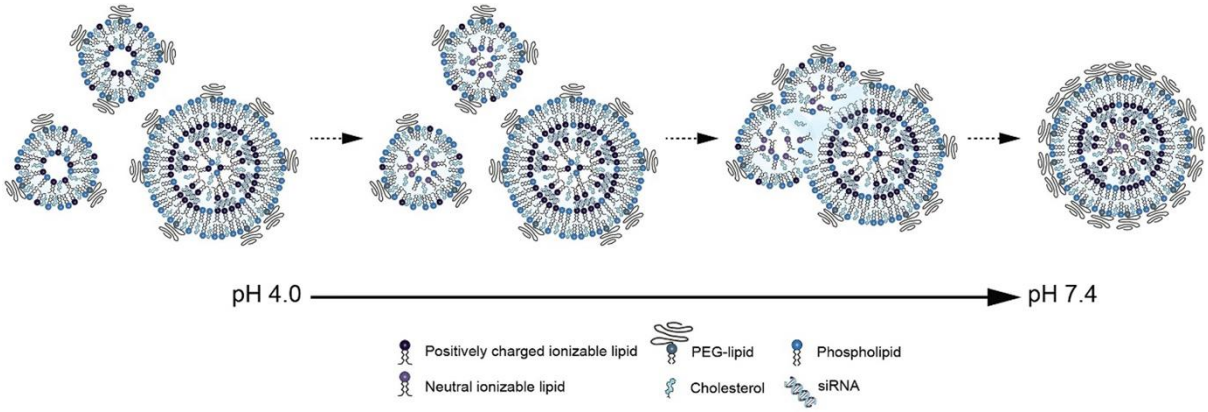

Figure 7: Formation and structure of LNP vehicles. Small particles are generated during rapid mixing at acidic pH (4.0; left). Final LNP-siRNA complexes are generated through fusion of metastable particles as the pH is neutralized (center). The final structures consist of siRNAs sandwiched between layers of lipid and the lipid core (right) (Kulkarni et al., 2019).

Apart from delivery vehicles, conjugate-mediated siRNA distribution is a growing area of study. Particularly, identification of GalNAc as a compound that can deliver siRNAs specifically to hepatocytes has provided a new opportunity for the advancement of RNA-based treatments for liver diseases (S. Matsuda et al., 2015; Springer & Dowdy, 2018). Asialoglycoprotein receptor (ASGPR) is abundantly expressed on the hepatocytes while minimal expression was reported on extra-hepatic cells (D'Souza & Devarajan, 2015) and has a high affinity towards GalNAc. Specifically promoting the endocytosis of glycoconjugates fused with GalNAc units, ASGPR enables siRNA targeting in the hepatocytes, with minimal concerns of toxicity (Janas et al., 2018). Given the advantages, four of the current approved siRNA drugs – Givosiran, Lumasiran, Inclisiran and Vutrisiran are based on the GalNAc-conjugation chemistry (Mullard, 2022; Padda, Mahtani, & Parmar, 2023). GalNAc conjugated siRNAs usually consist of three GalNAc molecules clustered and conjugated to a single siRNA molecule. Binding of GalNAc to the ASPGR promotes a rapid clathrin- mediated endocytosis of the conjugated siRNAs. During maturation of the endosome, GalNAc dissociates from the ASPGR and is degraded in the lysosome. The siRNAs are released slowly over an extended period while ASGPR is recycled back to the cell surface (Figure 8) (Springer & Dowdy, 2018).

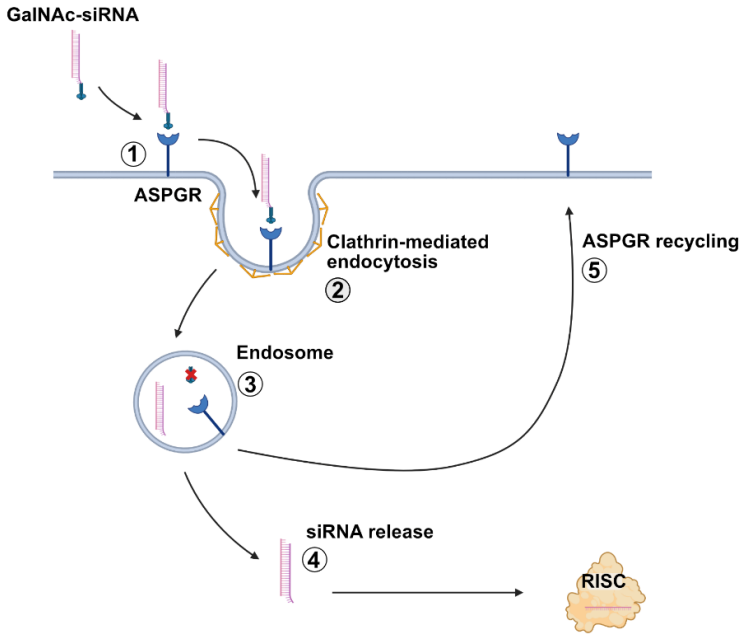

Figure 8: GalNAc-mediated delivery of siRNAs in hepatocytes. (1) ASPGR expressed on surface of hepatocytes promotes **(2)** rapid endocytosis of GalNAc-siRNA conjugates, mediated by Clathrin. **(3)** Acidification of endosomes causes dissociation of siRNA and GalNAc from ASGPR and **(4)** siRNAs are further released slowly to cytoplasm for their activity **(5)** while, the ASPGR receptors are recycled to the cell surface. Modified from template 'Mechanism of Action – Diptheria Toxin' from BioRender.com (2023). Obtained from https://app.biorender.com/biorender-templates.

In addition to synthetic siRNAs, short hairpin RNAs (shRNAs) are other mediators of therapeutic RNAi. Delivered by a viral vector, shRNAs are intracellularly expressed from a strong polymerase III promotor (such as U6) and are processed by Dicer to yield functional siRNAs (Siolas et al., 2005) (Figure 9). Even with the current advancements of chemical modifications and versatile carriers, repeated dosage of siRNAs is essential to achieve a prolonged knockdown of the target gene. On the other hand, shRNAs delivered by recombinant lentiviral vectors or Adeno-associated virus (AAV) could yield a long-term expression of siRNAs and thus a comparatively prolonged knockdown in a single dose (Koornneef et al., 2011; Manjunath, Wu, Subramanya, & Shankar, 2009). Several studies have previously demonstrated the application of AAVs to reprogram the liver cells, primarily mediated by the capsid serotype (Adrian, Zeman, Erdley, Lisa, & Sim, 2011; Baatartsogt et al., 2023; Grimm, Pandey, Nakai, Storm, & Kay, 2006; Rezvani et al., 2016). Various serotypes of AAVs exhibit variable cell tropism among different liver

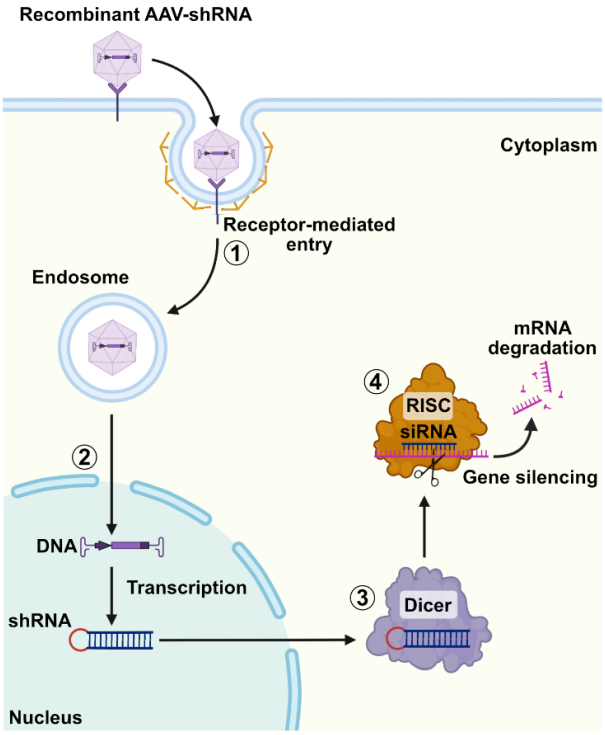

Figure 9: shRNA-mediated gene silencing. A recombinant viral vector harboring shRNA sequence **(1)** enters the cell via receptor-mediated endocytosis. Post unpacking, shRNAs are **(2)** constantly transcribed from the DNA in the nucleus of the target cell. After exported to the cytoplasm, shRNAs are **(3)** processed by the Dicer enzyme to form functional siRNAs, **(4)** which carry out the gene silencing via RISC. Modified from template 'Viral vs Non-viral Gene therapy' from BioRender.com (2023). Obtained from https://app.biorender.com/biorender-templates.

cells (Ho et al., 2008; Rezvani et al., 2016; Tomczyk et al., 2020). This characteristic could be beneficial as a majority of factors contributing to the immune tolerance in the liver and thereby persistence of liver diseases are produced by non-parenchymal cells such as Kupffer cells, Liver sinusoidal endothelial cells (LSECs), hepatic stellate cells (HSCs) and more (Protzer et al., 2012).

1.3.5 Current state of siRNA-based antiviral therapeutic strategies

The use of RNAi to suppress viral pathogens has been under development since more than a decade. Early works in the 2000s demonstrated the application of chemically synthesized siRNAs to inhibit replication several viruses such as Human immunodeficiency virus 1 (HIV-1), HBV, Respiratory syncytial virus (RSV) and parainfluenza virus (PIV) (Bitko, Musiyenko, Shulyayeva, & Barik, 2005; Klein et al., 2003; Novina et al., 2002). However, due to the challenges faced in targeted delivery as described earlier, the clinical applications of siRNAs remain limited.

siRNAs exhibit a major therapeutic potential as any gene of interest can be targeted by siRNAs. Since siRNAs act by complementarity to the target mRNA, they could be advantageous over other small molecule inhibitors and monoclonal antibody drugs which function via recognition of specific conformation of certain proteins. Therefore, in comparison to the small molecule inhibitors or antibodies, screening and development of a therapeutic siRNA could be much shorter. In general, siRNAs offer a viable alternative for several viral diseases which are not treatable using current therapeutic strategies (B. Hu et al., 2020).

Many of the siRNA-based antivirals are being considered for clinical purpose in coming years and a few have already been in clinical trials (Burnett, Rossi, & Tiemann, 2011). In order to combat RSV, a common cause of respiratory illness in new-born and young children, ALN-RSV01 was developed as a siRNA-based antiviral treatment. Alnylam Pharmaceuticals and Cubist Pharmaceuticals collaborated to start the development of ALN-RSV01 (Gottlieb et al., 2016). A lipid nanoparticle formulation was used for a targeted delivery of the siRNA, which specifically targeted the Nucleocapsid (N) gene of the RSV genome. In animal models, preclinical research showed that ALN-RSV01 decreased viral replication and enhanced lung function (Crehuet Gramatyka et al., 2022). In phase I and II clinical trials, ALN-RSV01 was reported to be safe and well tolerated in healthy adults (Gottlieb et al., 2016). Subsequently, in a randomized, double-blind, placebo-controlled phase IIb trial, ALN-RSV01 showed about 38% reduction in the incidence of RSV infection in high-risk adult populations (DeVincenzo et al., 2010). Despite the phase III trial's failure in achieving its primary endpoint, the earlier success opened the door for the creation of additional siRNA-based antiviral therapeutics.

Another promising siRNA-based antiviral therapeutic strategy by Alnylam Pharmaceuticals was the ALN-HBV, for the treatment of chronic HBV infection. This strategy was composed of a chemically modified, metabolically stable siRNA characterized in pre-clinical models for a potent and durable activity, delivered by GalNAc conjugation (Sepp-Lorenzino, 2016). ALN-HBV was designed to effectively target all viral transcripts of HBV and was pan-genotypic to target all major circulating HBV genotypes. During the pre-clinical development, ALN-HBV showed approximately 2 log reduction of Hepatitis B surface antigen (HBsAg) *in vivo*, where a single dose could silence the HBV transcripts for over 70 days (Stuart Milstein, 2017). In contrast to the preclinical studies, a transient, asymptomatic, and dose-dependent elevation in blood ALT levels ≥3 times the upper limit of normal levels was reported in 5 out of 18 healthy subjects treated with ALN-HBV (ClinicalTrials.gov Identifier: NCT02826018). Such an effect was not observed with other candidates in development with similar chemistry,

suggesting a sequence-dependent effect (Schlegel et al., 2022). In addition to ALN-HBV, another RNAi drug ARC-520 (Arrowhead Pharmaceuticals) was designed to combat chronic hepatitis B (ClinicalTrials.gov Identifier: NCT02452528). ARC-520 contained two equimolar siRNAs conjugated with cholesterol (siHBV-74 and suHBV-77), delivered specifically to hepatocytes using novel vehicle ARC-EX1, containing GalNAc conjugated melittin-like peptide (NAG-MLP) (Wooddell et al., 2013). In the randomized, double-blind, placebo-controlled phase I clinical trial, a single, intravenous does of ARC-520 was well-tolerated in 54 healthy volunteers (Schluep et al., 2017). Interestingly, in phase II trials in chronically infected individuals, strong reduction of HBsAg was noted in individuals positive as well as negative for Hepatitis B envelope antigen (HBeAg) (Yuen et al., 2020). This variance in response was further investigated in non-human primates, where the integration of HBV DNA in host genome was reported as the dominant source of HBsAg. These transcripts however, lacked the sites for siRNAs in ARC-520 (Wooddell et al., 2017). Later, in other two similar and randomized, multicenter, multi-dosed phase II studies, both, HBeAg negative and HBeAg positive groups significantly reduced HBsAg levels compared to placebo treatment. Along with these results, participants of the HBeAg positive group also showed a dose-dependent reduction in HBeAg levels. Unfortunately, the further development of ARC-520 and a subsequent drug ARC-521, which has also been developed against chronic HBV infection was discontinued, possibly due to the toxicity associated with the ARC-EX1 (Pharmaceuticals, 2016).

Despite their failure, these pioneering clinical studies have promoted the development of siRNA-based therapeutic strategies for other as well as emerging viral diseases (Kraft et al., 2015; Scott et al., 2020). The progressions made in the area of chemistry and formulation, aimed at achieving targeted delivery of siRNAs and other challenges mentioned previously, hold the potential for a more promising future for RNAi-based antiviral therapeutic strategies.

1.4 Aims of the work

The current treatment options for chronic hepatitis B are very limited. A cure is rarely achieved, and infected individuals remain at risk of recurrence with subsequent development of hepatocellular carcinoma (HCC) if the therapy is discontinued. A therapeutic vaccination could be a way to cure chronic hepatitis B, primarily through activation of antiviral adaptive immunity for the clearance of HBV infected hepatocytes (Buchmann et al., 2013). Recently it was shown that additional suppression of HBV antigens by RNAi could achieve functional cure in murine models (Michler et al., 2020).

However, it was unclear whether a further suppression of certain immunomodulatory components contributing to the immunosuppressive environment of the liver could also enhance the efficacy of therapeutic vaccination.

Building upon this, this thesis mainly focuses on transforming both, RNAi and therapeutic vaccination components of this combinatorial approach. The leading hypothesis was that a local suppression of immunomodulatory components such as PD-L1, Gal-9 and TGF-ß1 in the liver can further enhance the therapeutic vaccination by promoting T-cell effector functions. The first part of this thesis was mainly aimed at designing highly active siRNAs against three genes of interest and defining candidate siRNAs through rigorous screening for therapeutic use in a combinatorial approach with the therapeutic vaccine. It was investigated if development of therapeutic siRNAs is feasible and moreover if incorporation of position-specific chemical modifications are further beneficial for their silencing activities. In the later parts, TGF-ß1 remined as the target of interest with a question whether strong suppression of TGF-ß1 in the liver could in turn suppress the regulatory T cells to enhance the T-cell effector function post vaccination.

Furthermore, the second part of this thesis was aimed at generating novel HBV mosaic capsid particles to further optimize the current therapeutic vaccination strategy. Development of such novel capsid particles has not been described before and this is the first-of-its kind study. The main question addressed in this section was whether the mosaic capsid particles are indeed composed of HBcAg of both the genotypes and whether they can be purified in an intact form. Successful generation of the mosaic capsid particles is beneficial for a global application of the therapeutic vaccination, contemplating the global HBV genotype distribution.

Lastly, the focus of work was extended towards SARS-CoV-2 soon after its emergence. Previous research from numerous groups have demonstrated the potential of siRNAs to suppress other related coronaviruses, thus suggesting RNAi as a potential approach to combat COVID-19 (Medeiros et al., 2021; Shawan et al., 2021). However, it was still unclear which coronaviral replication steps are accessible for siRNA-based targeting. Extending from this, it was hypothesized that highly-active siRNAs targeting various genomic regions of the SARS-CoV-2 can efficiently suppress the viral replication and spread. This third part of the thesis is primarily aimed at analyzing siRNA-accessible SARS-CoV-2 replication steps inside the host cells. This included a series of comparative experiments between siRNAs targeting only the viral genomic RNA and siRNAs additionally targeting the sub-genomic RNAs, to determine the ideal antiviral therapeutic strategy. As a proof-of-concept, it remained essential to investigate the antiviral activity of siRNAs in a more physiological relevant model such as human lung slices.

Overall, this thesis underlines the applications of RNAi in therapeutic setting to combat a variety of viral threats and portrays a crucial step for the development of an efficient combinational therapy approach against CHB.

2 Results

In accordance with the aims of the thesis, this part reports the key findings from the two projects pursued. The first part of results is majorly focused on optimizing both components of a combinatorial immunotherapy against chronic HBV infection; while the latter is focused on developing a siRNA-based therapeutic strategy to combat the SARS-CoV-2.

2.1 Optimizing a combinatorial immunotherapy against chronic HBV infection constituting RNAi and therapeutic vaccination

As reported earlier, RNAi against HBV along with a therapeutic vaccination could achieve functional cure in murine models (Michler et al., 2020). On the same lines, this thesis focuses on developing an alternative approach by simultaneously revising the RNAi component and improving the therapeutic vaccine component for a finer combinatorial therapeutic approach.

2.1.1 *In vitro* screening of siRNAs

siRNA designing heavily relies on the prediction tools constructed as an inference from previously reported studies. Not every predicted siRNA allows in gene silencing. Therefore, in the first step, the designed siRNAs were screened for their activity to silence the target genes *in vitro*. Before proceeding for the screening of siRNAs against all 3 genes, an optimized system for the screening of multiple siRNAs was established only using a commercial Silencer Select® siRNA targeting PD-L1 in mice-derived cell lines.

2.1.1.1 Optimising an *in vitro* system for RT-qPCR based screening of siRNAs

Firstly, optimal conditions to assess the knockdown of gene of interest via quantitative Polymerase Chain reaction (qPCR) were derived. Therefore RAW 264.7 (murine macrophages) and AML-12 (murine hepatocytes) were forward transfected with 10 nM siRNA targeting PD-L1 using different transfection agents and the efficiency of the gene knockdown was determined after 48 hours. Cells treated with a negative control siRNA (siNC) served as controls.

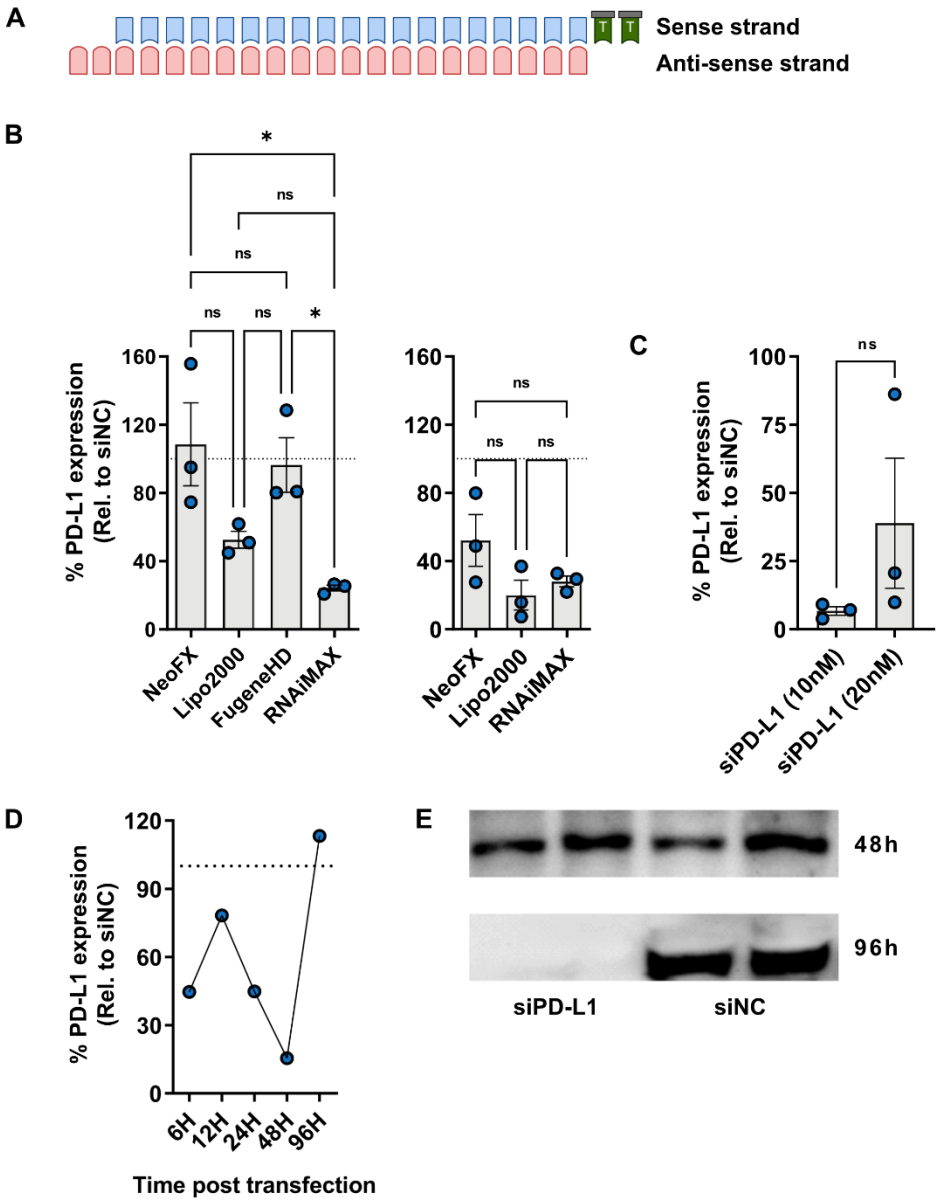

Figure 10: Lipofectamine® RNAiMAX is the suitable commercial transfection agent for in-vitro screening of siRNAs. (A) Schematic representation of siRNA design. Each siRNA is composed of a 21-nucleotide antisense RNA strand annealed with a 19-nucleotide long sense strand, harboring a dTdT overhang at 3' end of the sense strand. **(B)** Comparison of different transfection agents. 10 nM siRNA targeting PD-L1 was transfected in RAW 264.7 (left) and AML-12 cells (right) using different transfection agents. Relative PD-L1 mRNA expression was quantified 48 hours post transfection. **(C)** Comparison of two different siRNA concentrations. Similar experimental setup as (B) except, only RAW 264.7 cells were reverse transfected with two different siRNA concentrations, 10 nM and 20 nM with RNAiMAX to compare relative PD-L1 mRNA levels with qPCR 48 hours post transfection. **(D)** Kinetics of PD-L1 mRNA knockdown. Similar experimental setup as (B) except the qPCR was performed at different time points as indicated in RAW 264.7 cells. **(E)** PD-L1 knockdown at protein levels. RAW 264.7 cells were

reverse transfected with 10 nM siRNA targeting PD-L1 and total soluble proteins were extracted using RIPA buffer 48 and 96 hours post transfection. PD-L1 protein expression was determined using western blotting. Cells treated with negative control siRNA targeting GFP (siNC) served as negative control for all experiments. **(B-D)** Percent mRNA expression of PD-L1 relative to siNC transfected group. Individual values of biological triplicates for all the groups are shown and error bars indicate SEM. Statistical significance was calculated using (B) ordinary one-way Anova and (C) non-parametric unpaired T-test. ns– Non-significant; *P < 0.05; **P < 0.01.

It was observed that, Lipofectamine® RNAiMAX showed an upper hand in knockdown of PD-L1 in RAW 264.7 cells as compared to other transfection agents (Figure 10 B). However, in AML-12 cells, RNAiMAX did not show a significant improvement over other transfection agents, still achieving a similar level of knockdown as observed in RAW.264.7 cells. When transfected with Fugene® HD, AML-12 showed a great extent of cell toxicity, therefore was excluded from the qPCR analysis.

The total amount of RNA content from RAW 264.7 cells was consistently higher than the AML-12. Moreover, RAW 264.7 cells expressed relatively higher levels of PD-L1 as compared to AML-12. Therefore, further experiments were continued with RAW 264.7. In the next step, the resulting knockdown effect of two different siRNA concentrations, 10 nM and 20 nM was assessed and surprisingly, a lower concentration of siRNA with commercially recommended amount of transfection reagent (1.5 ml) was found to be more effective and thus selected for further experiments (Figure 10 C). The siRNA mediated knockdown was assessed further at various time points in the RAW 264.7 cells to define an optimal time frame for the siRNA screening (Figure 10 D). As expected, the siRNA showed more than 50 % knockdown at the earliest time point of 6 hours post transfection. Surprisingly, the siRNA activity was reduced at 12 hours however, it further improved till 48 hours post transfection, where it achieved the maximum. After 96 hours, the siRNA exhibited a complete loss of its activity when screened at the mRNA levels. These observations thus indicated use of RNAiMAX and screening at 48 hours post transfection as optimal conditions for further siRNA screening.

To further validate the siRNA activity, the knockdown at protein level was determined by western blotting (Figure 10 E). Interestingly, a complete knockdown was observed only at 96 hours post transfection. While the siRNA targeted against PD-L1 had shown near to 80 % knockdown at mRNA levels after 48 hours of transfection, required 48 hours more to translate at protein levels. Even though PD-L1 is a labile protein with a half-life of about 4 hours (Cha, Chan, Li, Hsu, & Hung, 2019), murine macrophages have been already reported to express significant levels of PD-L1 on their surface(Cha et al., 2019;

J. F. Hu, Zhang, Zuo, Tan, & Bai, 2020; H. Y. Li et al., 2017) Therefore, it is likely to expect a reduction in protein levels only after a significant amount of time post mRNA knockdown. Therefore, these findings defined the time interval of 96 hours for analyzing a decrease in protein expression post siRNA transfection.

2.1.1.2 siRNA screening by conventional methods suggests potential candidates, however, lacks reliability

In the subsequent steps, all the 28 chemically unmodified siRNAs targeted against three genes – PD-L1, Gal-9 and TGF-ß1 were screened for their activities at mRNA and protein levels. For a successful RNAi strategy, it is rather more crucial to assess how mRNA knockdown is translated to the protein expression, as a single mRNA transcript can be translated into multiple copies of protein (C. Wang, Han, Zhou, & Zhuang, 2016). Therefore, based on the mRNA knockdown, top 5 active siRNAs were selected for a screening at protein level for each gene.

It was quite evident that out of 28, 26 siRNAs showed mRNA knockdown to some extent for each gene (Figure 11 A, C and E). In case of siRNAs targeting PD-L1, all the siRNAs except siPD-L1#1 showed silencing of mRNA (Figure 11 A). None of the siRNAs however, showed comparable knockdown of PD-L1 mRNA levels to that of the commercial siRNA. Such a result was expected due to the lack of chemical modifications in the self-designed siRNAs. On the other hand, all the siRNAs designed against Gal-9 showed suppression of mRNA, with two of the siRNAs siGAL-9#5 and siGal-9#8 showing around 90 % knockdown (Figure 11 C). Similarly, all but siTGF-ß1#10 showed substantial mRNA knockdown (Figure 11 E).

To define the candidate siRNAs for further development, 5 of the best performing siRNAs at this stage were chosen for screening at protein level. As expected, the commercial siPD-L1 showed a visible knockdown of PD-L1 protein in comparison to the negative control siRNA. However, from the self-designed siRNAs only siPD-L1#4 showed a visible reduction in protein levels (Figure 11 B). All the other siRNAs which showed a clear knockdown of PD-L1 mRNA, failed to demonstrate expected reduction of PD-L1 protein levels. Moreover, the cells treated with siPD-L1#3 even showed a strong upregulation of PD-L1 levels unexpectedly while, a discrepancy was observed within the duplicates of siPD-L1#7 and siPD-L1#10 treated cells. Similar results were observed upon repeating the whole series of experiments. Following on these lines, similar inconclusive results were obtained with the screening of siRNAs targeting Gal-9 (Figure 11 D). Poorly visible

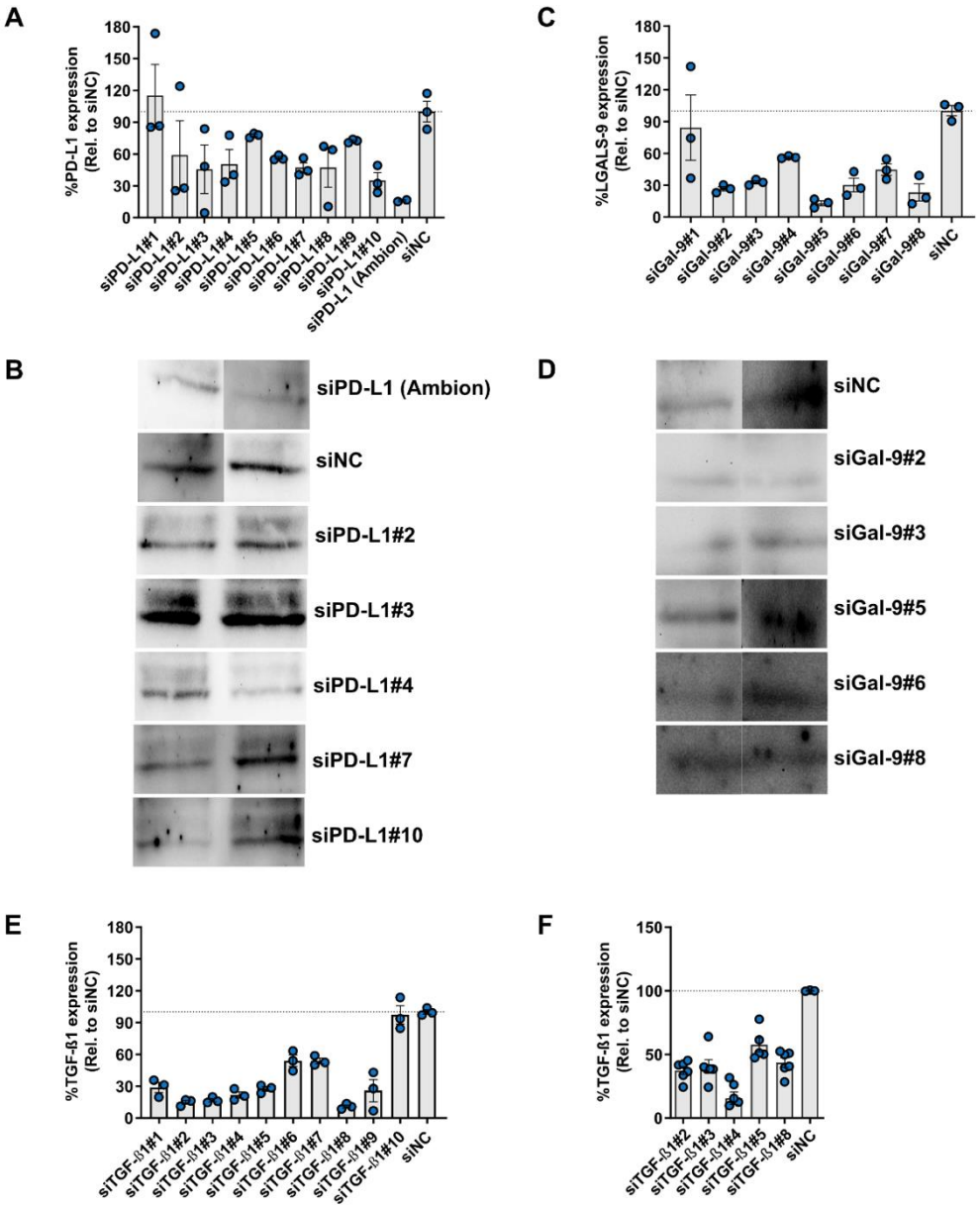

Figure 11: Screening of siRNAs in RAW 264.7 cells suggest potential candidates for further development. (A-F) Screening of siRNAs targeting genes of interest. RAW 264.7 cells were reverse transfected with 10 nM siRNAs against genes of interest individually. RNA and total soluble proteins or supernatants were isolated 48 and 96 hours post transfection respectively to assess knockdown by qPCR and western blot or ELISA as indicated. **(A, B)** Screening of siRNAs targeting PD-L1. Relative PD-L1 mRNA levels (A) were determined by qPCR and PD-L1 protein (B) was detected by western blotting. **(C, D)** Screening of siRNAs targeting Gal-9. Relative Gal-9 mRNA levels (C) were determined by qPCR and Gal-9 protein (D) was detected by western blotting. **(E, F)** Screening of siRNAs targeting TGF-ß1. Relative TGF-ß1 mRNA levels (E) were determined by qPCR and secreted TGF-ß1 protein (F) was detected by sandwich ELISA from supernatants of treated cells. Cells treated with negative control siRNA targeting GFP served as negative control for all experiments. (A, C, E, F) Individual values of at least biological triplicates for all the groups are shown and error bars indicate SEM. siNC – negative control siRNA; siPD-

L1#1-10 – PD-L1-specific siRNAs; siGal-9#1-8 – Galectin-9-specific siRNAs; siTGF-ß1#1-10 – TGF-ß1-specific siRNAs.

blots were obtained multiple times while detecting Gal-9 levels upon siRNA treatment. Very weak bands obtained with negative control siRNA treatment suggest a low basal Gal-9 expression in RAW 264.7 cells. Nevertheless, two of the siRNAs, siGal-9#2 and #3 showed a reduction of Gal-9 levels. On the other hand, TGF-ß1 being a secretory cytokine, supernatant from siRNA transfected cells was analyzed for secretory TGF-ß1 levels 96 hours post transfection by sandwich ELISA instead of western blotting. Here, the readouts were more reliable and all 5 chosen siRNAs showed at least 50 % inhibition of TGF-ß1 secretion (Figure 11 F). Since the conventional approach was inconclusive for screening of siRNAs against two out of three genes, a more reliable and rapid alternative approach for siRNA screening was employed in further steps.

2.1.1.3 psiCHECK2.0™, a dual luciferase-based reporter system constitutes a rapid and reliable *in vitro* siRNA screening method

In the subsequent steps, a more reliable screening system based on psiCHECK2.0™ reporter vector was established to screen all the siRNAs used above against three genes indicated earlier.

The psiCHECK2.0™ based screening was successful in indicating the candidate siRNAs for further development. Out of 8 siRNAs designed against Gal-9, three siRNAs siGal-9#2, #5 and #8 showed around 90 % reduction in the *Rluc* activity (Figure 12 A). On the other hand, only 2 out of 10 siRNAs targeting TGF-ß1, siTGF-ß1#2 and #8 showed a major reduction of *Rluc* activity (Figure 12 B). Presence of the complete CDS of the target gene in the reporter construct render this screening approach as an alternative for the screening at both mRNA and protein levels. The results clearly indicated the potential siRNA candidates for further chemical modifications. At this point, the siRNAs targeting PD-L1 were handed over to Dr. Till Bunse (Institute of Virology, TU Munich) and the screening was continued for siRNAs targeting Gal-9 and TGF-ß1.

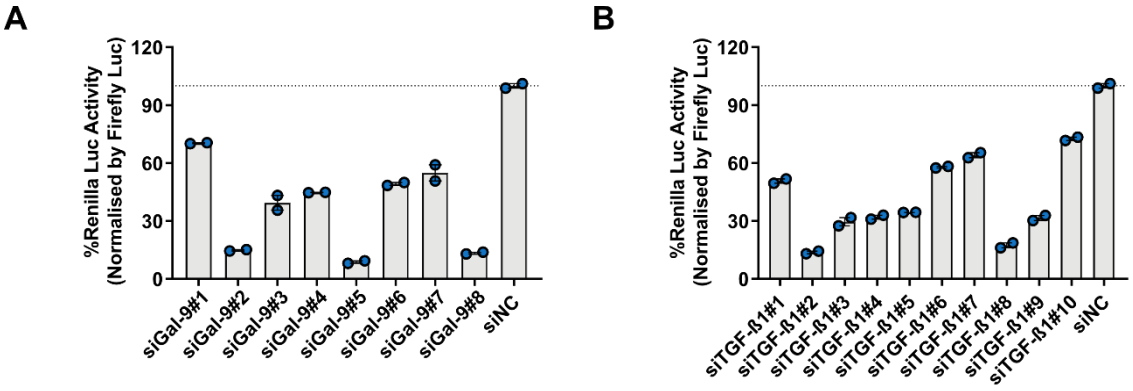

Figure 12: siRNA screening with psiCHECK2.0^{TM} based dual-luciferase reporter assay precisely identifies potential siRNA candidates. (A, B) Dual luciferase reporter-based screening of siRNAs targeting genes of interest. HEK293T cells were co-transfected with reporter plasmid harbouring target gene and respective siRNAs or the negative control siRNA. Dual luciferase assay was performed after 48 hours of co-transfection from cell lysates. **(A)** Screening of siRNAs targeting Gal-9. **(B)** Screening of siRNAs targeting TGF-ß1. Cells co-transfected siRNA targeting GFP (siNC) along with reporter vector containing gene of interest served as the negative control. Both graphs indicate normalised Renilla luciferase activity corresponding to siRNA silencing activity. Firefly luciferase activity was used for normalization for each readout and percent Renilla luciferase activity was calculated with respect to that of the negative control. Individual values of biological duplicates for all the groups are shown and error bars indicate SEM. siGal-9#1-8 – Gal-9-specific siRNAs; siTGF-ß1#1-8 – TGF-ß1-specific siRNAs; siNC – negative control siRNA.

2.1.2 Chemical modifications of siRNAs

The chemical modifications were employed in a position specific manner and mainly included 2'OMe, 2'F and PS linkages. These chemical modifications have been already characterized and were known to offer nuclease resistance, improved potency, RISC loading capacity, cellular uptake, reduced immune stimulation and cytotoxicity (Allerson et al., 2005; Ayensu & Tchounwou, 2006; Choung, Kim, Kim, Park, & Choi, 2006; Deleavey, Watts, & Damha, 2009; Kenski et al., 2012; Kraynack & Baker, 2006; A. A. Levanova et al., 2020; J. K. Watts, Deleavey, & Damha, 2008; S. Y. Wu et al., 2014)

2.1.2.1 Position specific chemical modification of siRNAs offer nuclease resistance in serum

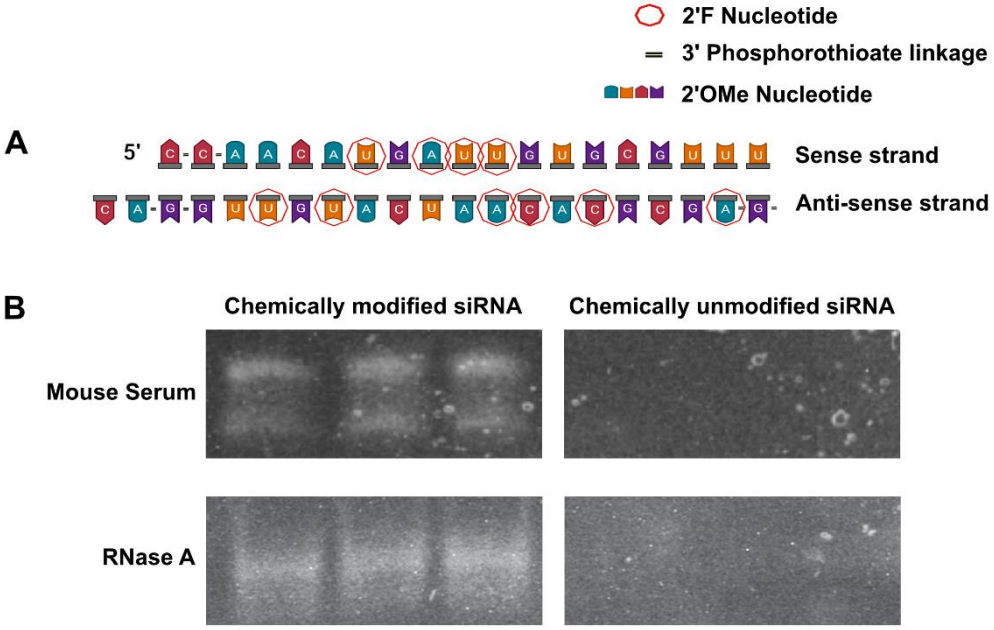

Figure 13: Chemically modified siRNAs can withstand serum as well as pure RNase A treatment. (A) Schematic representation of an asymmetrical, chemically modified siRNA with U-G mismatch wobble. Sense strand of the siRNA is 19 nt long while the antisense strand is 21 nt long. Chemical modifications incorporated in each nt are indicated in right. **(B)** Stability testing of chemically modified siRNAs as compared to unmodified siRNAs. siRNAs of either chemistry were incubated at 37 ˚C in either 90 % serum diluted in PBS or 20 μg of RNaseA for different time points. Reducing 8 M Urea PAGE of the siRNAs after serum or RNase A treatment was performed to visualize the integrity of siRNAs. White bands indicate presence of intact siRNAs. 2'F – 2'-Fluoro modification, 2'Ome – 2'-O-Methyl modification, RNase A – Ribonuclease A.

Candidate siRNAs chosen in previous experiments were further subjected to positions specific chemical modifications majorly at 2' position of sugar moiety. Chemically modified siRNAs were designed as asymmetric duplex described previously (Foster et al., 2018), following a modification pattern of an approved drug, Lumasiran (sold under the name OXLUMO®) (CRASTO, 2020). In brief, all the nucleotides on both strands were modified with 2'OMe modifications except nucleotides on positions 7, 9, 10 and 11 from 5' end of sense strand and 2, 6, 8, 9, 14 and 16 from 5' end of antisense strand. These nucleotides were rather incorporated with a 2'F modifications. Additionally, two 5' terminal nucleotides on sense strand and two nucleotides of both terminals on antisense strand were modified with phosphorthioate linkages (Figure 13 A). Subsequently,

stability of one chemically modified and an unmodified siRNA, siTGF-ß1#8, in mouse serum and in presence of RNase A was compared. Briefly, 50 pmoles of siRNA were incubated in 90 % mouse serum diluted in PBS (kindly provided by Jakob Zillinger, Institute of Virology, TU Munich) and 20 µg of pure RNaseA at 37 °C till 5 hours. Post incubation, the siRNAs were analyzed by denaturing 8 M Urea PAGE to assess their integrity (Figure 13 B). Upon visualization, it was quite evident that the chemically modified siRNAs were stable for extended time points as compared to unmodified siRNAs. These observations underlined the importance of chemical modifications of the siRNAs for *in vivo* or *ex vivo* use.

2.1.2.2 Chemical modifications yield a prolonged knockdown *in vitro*, however, may result in loss of siRNA activity

In the subsequent set of experiments, the effect of chemical modifications on the activity of siRNAs was assessed *in vitro* using dual luciferase assay. Three siRNAs targeting Gal-9 and six siRNAs targeting TGF-ß1 were subjected to chemically modifications. Firstly, to compare the effect of the chemical modifications on the activity of siRNAs, a dual luciferase reporter assay was performed for each siRNA individually. As expected, most of the siRNAs retained their activities post chemical modifications (Figure 14 A and B). While some of the siRNAs showed an improvement in the activity, a few were contrary and demonstrated a slight yet significant loss of activity. Chemically modified siGal-9#5 among the three exhibited superior activity achieving about 98 % knockdown *in vitro*. On the other hand, siTGF-ß1#4 and #8, among the six siRNAs could achieve about 90 % knockdown, with a slight improvement upon chemical modification. Interestingly, two of the chemically modified siRNAs, siTGF-ß1#2 and #5 showed a significant loss of activity than their unmodified counterparts (Figure 14 B). A possible explanation for the same could be that the chemical modification at a prime position on the antisense strand could hinder the RNAi mechanism at a specific step as reported previously (Amarzguioui, Holen, Babaie, & Prydz, 2003). Furthermore, the chemically modified siRNAs were tested for their activity at protein level in RAW 264.7 cells by ELISA. Here, siTGF-ß1#8 achieved a maximum knockdown (70 %) among all the siRNAs, indicating its suitability as the candidate siRNA for further experiments (Figure 14 C).

It must be noted that, a slight loss of siRNA activity could in theory be compensated by achieving a stable knockdown for a longer period. Thus, the ability of chemically modified siRNAs to yield a prolonged knockdown as compared to its unmodified counterpart was subsequently assessed. In brief, siTGF-ß1#8 as candidate siRNAs in modified and

unmodified chemistry were co-transfected with a dual luciferase reporter vector in HEK293T cells individually to assess their ability to reduce *Rluc* expression. It was evident that the chemically modified siTGF-ß1#8 achieved a more stable knockdown over the period of 96 hours than the unmodified siRNA. Initially, after 48 hours of transfection, both the siRNAs showed nearly identical activity. However, a constant loss of activity was observed over the span of next 48 hours only for the unmodified siRNA (Figure 14 D). Lastly, the determination of half maximal inhibitory concentration revealed the additional benefit of chemical modification in rather gain of activity for siTGF-ß1#8 (Figure 14 E and F). Therefore, these results indicate that the chemical modifications may not always be advantageous for the potency of the siRNAs but rather help improve the siRNA stability to enable a prolonged silencing. With these observations, the siRNAs – siGal-9#5 and siTGF-ß1#8 were identified as candidate siRNAs and characterized further for their *in vivo* use in future experiments. At this point, only the TGF-ß1 remained as the focus of this project while Gal-9 targeting siRNAs were handed over to Ms. Merve Gültan (Institute of Virology, TU Munich).

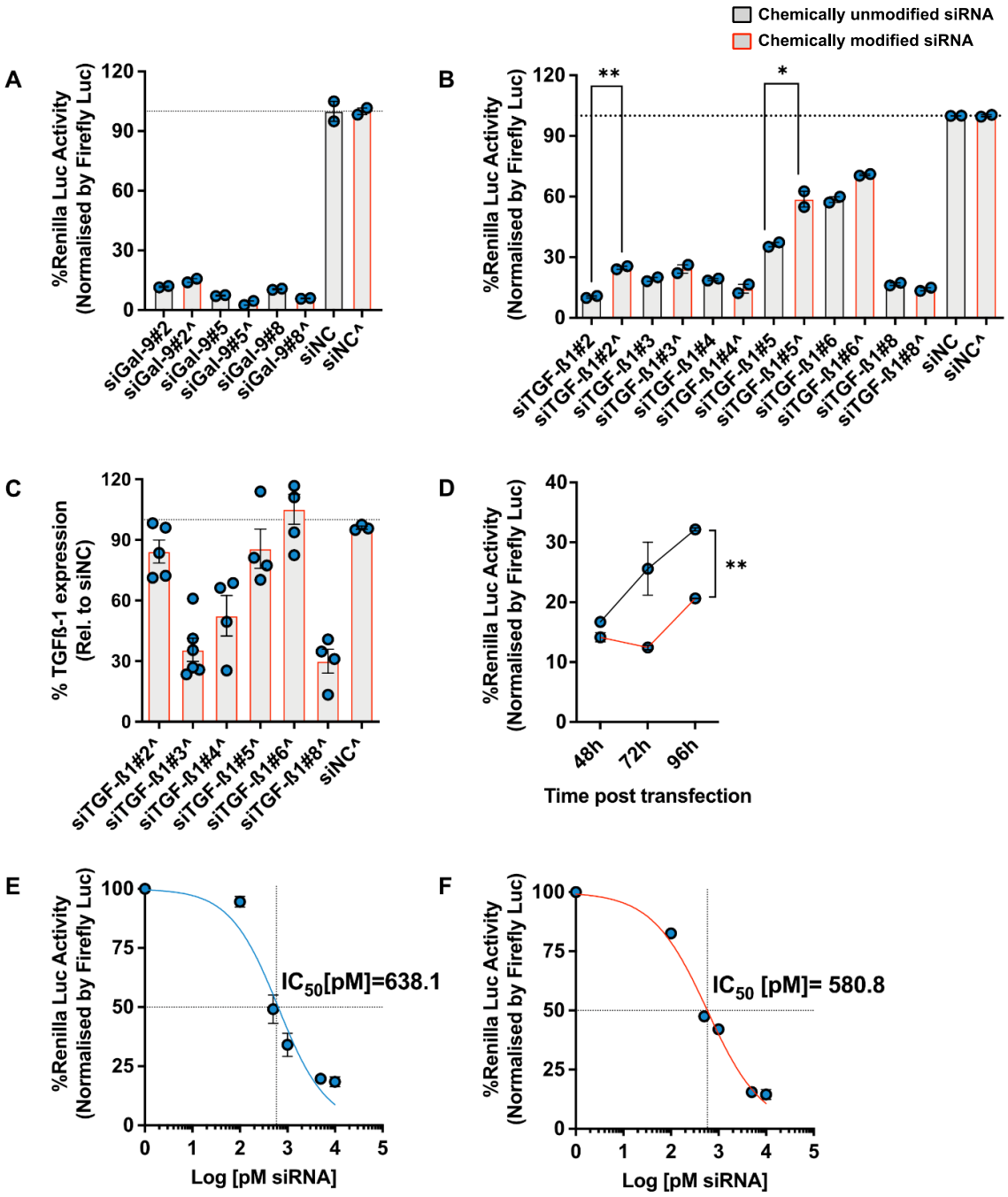

Figure 14: Position specific chemical modification of siRNAs can alter the efficacy, however, yield a longer knockdown. (A, B) Comparison of siRNA activity between chemically modified and unmodified siRNAs targeting genes of interest. HEK293T cells were co-transfected with reporter plasmid harbouring target gene and respective siRNAs. Dual luciferase assay was performed after 48 hours of co-transfection from cell lysates. **(A)** Comparison between Gal-9-specific siRNAs of either chemistry **(B)** Comparison between TGF-ß1-specific siRNAs of either chemistry. **(C)** TGF-ß1 knockdown on protein levels by chemically modified siRNAs, determined by ELISA. RAW 264.7 cells were reverse transfected with 10 nM of chemically modified TGF-ß1 siRNAs individually. Cell supernatants were harvested 96 hours post transfection and a sandwich ELISA for quantification of TGF-ß1 was performed. **(D)** Comparative kinetics of siTGF-ß1#8 in

either chemistry. Similar experimental setup as **(B)** but the dual luciferase assay was performed at various time points as indicated. **(E, F)** Half maximal inhibitory concentration determination of chemically modified (F) and unmodified (E) siTGF-ß1#8. HEK293T cells were co-transfected with a decreasing concentration of siTGF-ß1#8 in either chemistry (10, 5, 1, 0.5, 0.1, 0.05 nM) together with equal amounts of respective luciferase reporter. The dual luciferase assay was performed 48 hours post co-transfection from cell lysates. Cells co-transfected with siRNA targeting GFP (siNC) in either chemistry along with reporter vector containing target genes served as negative control as indicated. Graphs indicate normalised Renilla luciferase activity corresponding to siRNA silencing activity. Firefly luciferase activity was used for normalization of each readout and percent Renilla luciferase activity was calculated with respect to that of the negative control group. (A-C) Individual values of biological (A, B) duplicates or (C) at least triplicates for all the groups and (D-F) arithmetic mean of triplicates are shown and error bars indicate SEM. Statistical significance is calculated using standard paired T test. siNC – negative control siRNA, ^ - chemically modified siRNA, h - hours, IC_{50} – half maximal inhibitory concentration. *P < 0.05; **P < 0.01.

2.1.3 Hepatic Stellate cells (HSCs) could be the target for siTGF-ß1 therapy

Success of a siRNA-based therapeutic majorly relies on the efficiency of the delivery of siRNA to the target cell. Thus, identifying the cell type majorly secreting TGF-ß1 during the HBV infection was of focus for this project to formulate an appropriate delivery agent. Since the potential of HSC-derived TGF-ß1 in liver injury and fibrosis is already well-known (Koda et al., 1996; Tahashi et al., 2002; Yata, Gotwals, Koteliansky, & Rockey, 2002), the further experiments were directed towards revealing role of HSCs in upregulating TGF-ß1 during HBV infection.

2.1.3.1 Hepatic stellate cells may upregulate TGF-ß1 secretion during HBV infection

In the subsequent experiments, it was checked whether HBV infection has an impact on activation of HSCs, thereby increasing TGF-ß1 secretion. For these experiments, LX-2 (hereafter termed as LX-2 or HSCs), a HSC-based cell line characterized previously (L. Xu et al., 2005) was used. In brief, HBV infected HepG2-NTCP cells, maintained for 96 hours, were co-cultured with HSCs with a ratio of 1:4 (HSC:Hepatocytes), for further 96 hours. Post incubation, the cells were analyzed by flow cytometry for intracellular levels of TGF-ß1 and an activation marker of HSCs- a-Smooth muscle actin (aSMA, ACTA)

(Carpino et al., 2005). From the results, it could be clearly seen that upon co-culturing with HBV infected hepatocytes, TGF-ß1 levels were upregulated in the HSCs (Figure 15 A). It could also be correlated with increased levels of aSMA, indicating an activated state of the HSCs (Figure 15 B). It must be noted that, adherence of HSCs to polystyrene

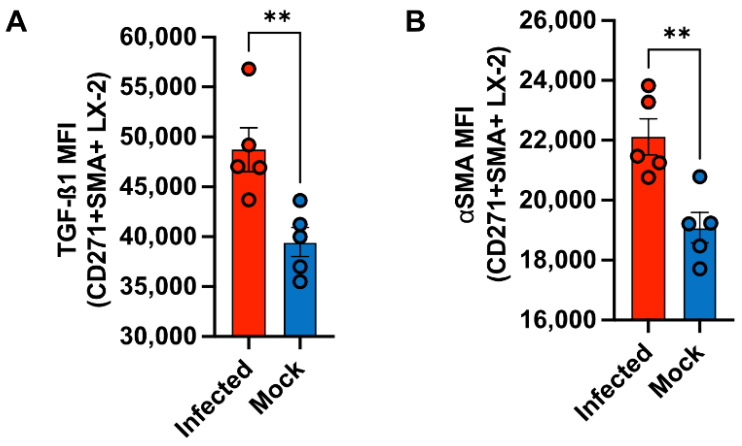

Figure 15: HBV infected hepatocytes can activate HSCs, upregulating intracellular TGF-ß1 levels. (A, B) Intracellular TGF-ß1 **(A)** and αSMA **(B)** expression in CD271+αSMA+ HSCs after co-culture with HBV infected hepatoma cells. HBV infected HepG2-NTCP cells were maintained for 96 hours and co-cultured with HSCs for further 96 hours. Post incubation, the cells were analyzed by flow cytometry for intracellular expression of TGF-ß1 and αSMA. (A, B) Graphs indicate mean fluorescence intensity of proteins of interest. Individual values of five biological replicates for all the groups are shown and error bars indicate SEM. MFI - Mean fluorescent intensity, Mock - Mock infected groups. **P < 0.01.

itself induces an activation phase in HSCs. The cells have been reported display recapitulate the features of activated HSCs around day 12 (L. Ma et al., 2018). Therefore, further experiments in a physiologically relevant setting are important before drawing significant conclusions. Nevertheless, preliminary results with the current co-culture model suggested a co-relation of HBV infection with activation of HSCs, thereby upregulating TGF-ß1 secretion.

2.1.3.2 TGF-ß1 contributes to serum induced activation of hepatic stellate cells *in vitro* and ex vivo

Ability of HSCs to undergo activation upon plating (Henderson et al., 2006) leads to higher levels of activation marker such as αSMA as well as intracellular TGF-ß1. Moreover, it has been recently reported that the bovine serum present in growth medium can also drive the activation of the HSCs (Schinagl et al., 2021). This property of HSCs could in turn render the TGF-ß1 knockdown strategies futile. Therefore, an effort was made to derive an activated and quiescent-like *in vitro* and an *ex vivo* HSC system. The

following experiments were performed at the Institute of Immunity and Transplantation at the University College London under supervision of Dr. Laura Pallett.

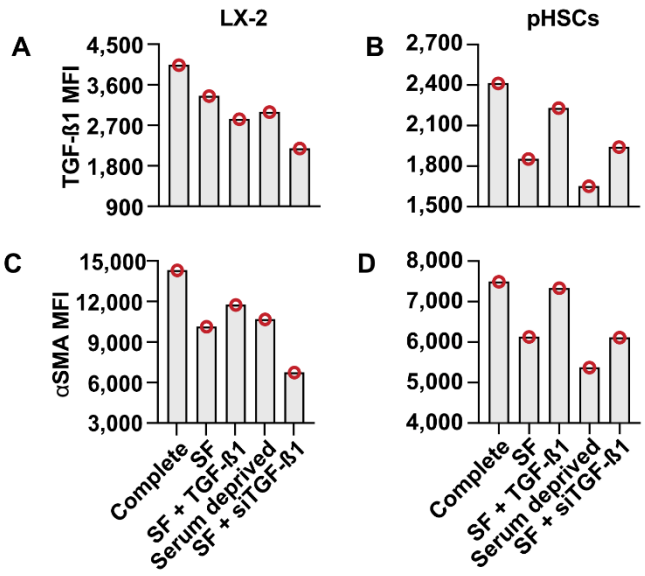

Figure 16: Absence of serum leads to a less activated state of hepatic stellate cells, which could be rescued by supplemented TGF-ß1. (A, C) LX-2 and **(B, D)** primary hepatic stellate cells (pHSCs) were maintained in various conditions as depicted and were analyzed for intracellular TGF-ß1 and αSMA levels by flow cytometry after 72 hours. **(A, B)** Mean florescence intensity of intracellular TGF-ß1 expression levels in (A) LX-2 and (B) pHSCs. **(C, D)** Mean fluorescence intensity of intracellular αSMA levels in (C) LX-2 and (D) pHSCs. Levels are indicated from a single biological replicate for each group. Complete – Growth medium containing 10 % bovine serum, SF – Growth medium without serum, SF + TGF-ß1 – SF growth medium supplemented with 20 ng/ml active TGF-ß1, Serum deprived – Cells cultivated in complete growth medium and replaced with SF media 24 hours before analysis, SF + siTGF-ß1 – Cells reverse transfected with siTGF-ß1 and cultivated in SF growth medium till analysis.

To begin with, it was checked whether a reduced serum condition or brief removal of serum, as well as silencing TGF-ß1 additionally could limit the activation of HSCs in LX-2 and primary human hepatic stellate cells (pHSCs). pHSCs were isolated from human liver explants as described before (Swadling et al., 2020). LX-2 and pHSCs were cultured in varying conditions as indicated for 72 hours and were analyzed by flow cytometry. As expected, both the cell types showed higher levels of aSMA as well as intracellular TGF-ß1 (Figure 16). In comparison, absence of serum lead to a reduced level of activation. Surprisingly, the levels of aSMA and TGF-ß1 were nearly restored completely by supplementing to TGF-ß1 externally, only in the pHSCs and not in the LX-2 (Figure 16 A and B). Moreover, a sudden serum deprivation of the cells for 24 hours before analysis exhibited lowest levels of the activation markers only in the pHSCs. In contrast, only when additionally treated with a siRNA targeting TGF-ß1 LX-2 cells showed a considerable reduction of the activation markers. However, the siRNA treatment did not result in further reducing the gene expressions in pHSCs. These findings suggest that a variety of factors present in the serum may drive the activation of cultured HSCs.

However, the pHSCs, seem more responsive to the change in serum conditions as well as TGF-ß1 treatment than LX-2 cells. Apart from being physiologically more relevant, these results also suggest pHSCs as the choice for developing a co-culture system to study the role of HSCs in inducing T_{regs}, thereby preventing T cell effector functions in chronic HBV.

With these observations, the candidate siRNA against TGF-ß1 was defined with optimal screening conditions for further use in a more sophisticated *in vivo* assessment.

2.1.4 Expression and purification of HBV mosaic capsid particles

The next results majorly focus on optimizing the therapeutic vaccination component for the combinatorial approach. The following chapters report generation, purification, and characterization of HBV mosaic capsid particles.

2.1.4.1 A single expression vector can successfully express HBcAg from two genotypes

In the first steps, the expression levels of monomeric core subunits were assessed in E. coli post induction. In brief, *T7* expressing competent E. coli BL21(DE3) were transformed with HBcAg expression construct and were differentially induced for protein expression. For a comparative assessment, the cultures were induced for either 5:15 hours or overnight (17:15 hours) and the presence of HBcAg was confirmed with SDS-PAGE and western blotting (Figure 17). HBV capsids have been previously reported to possess a tendency to form insoluble aggregates (N. R. Watts et al., 2002), which do not electrophorese completely. Therefore, as expected, the capsid aggregates were clearly visible in the SDS-PAGE analysis, which were completely absent in the non-induced group. This served as a preliminary indication for the presence of capsids in bacterial lysate. Moreover, the distinct bands of expected size for HBcAgs were clearly visualized in the SDS-PAGE (Figure 17 B). As denoted in the Figure 8, the dual-induced cultures showed presence of both the bands at 18 KD and 21 KD for C_D and D respectively, suggesting the presence of mosaic capsid particles. The cultures induced only with IPTG showed a band at 21 KD while representing D HBcAg, the cultures induced only with AHT showed a band at 18 KD representing the C_D. The non-induced cultures however, did not show distinct bands of either size as expected. To further confirm these observations, the SDS-PAGE was followed by a western blot with AD09 antibody,

capable of recognizing HBcAg of both genotypes (Figure 17, C). As shown in Figure 17 C, the dual induced cultures confirmed the presence of HBcAg from both the genotypes.

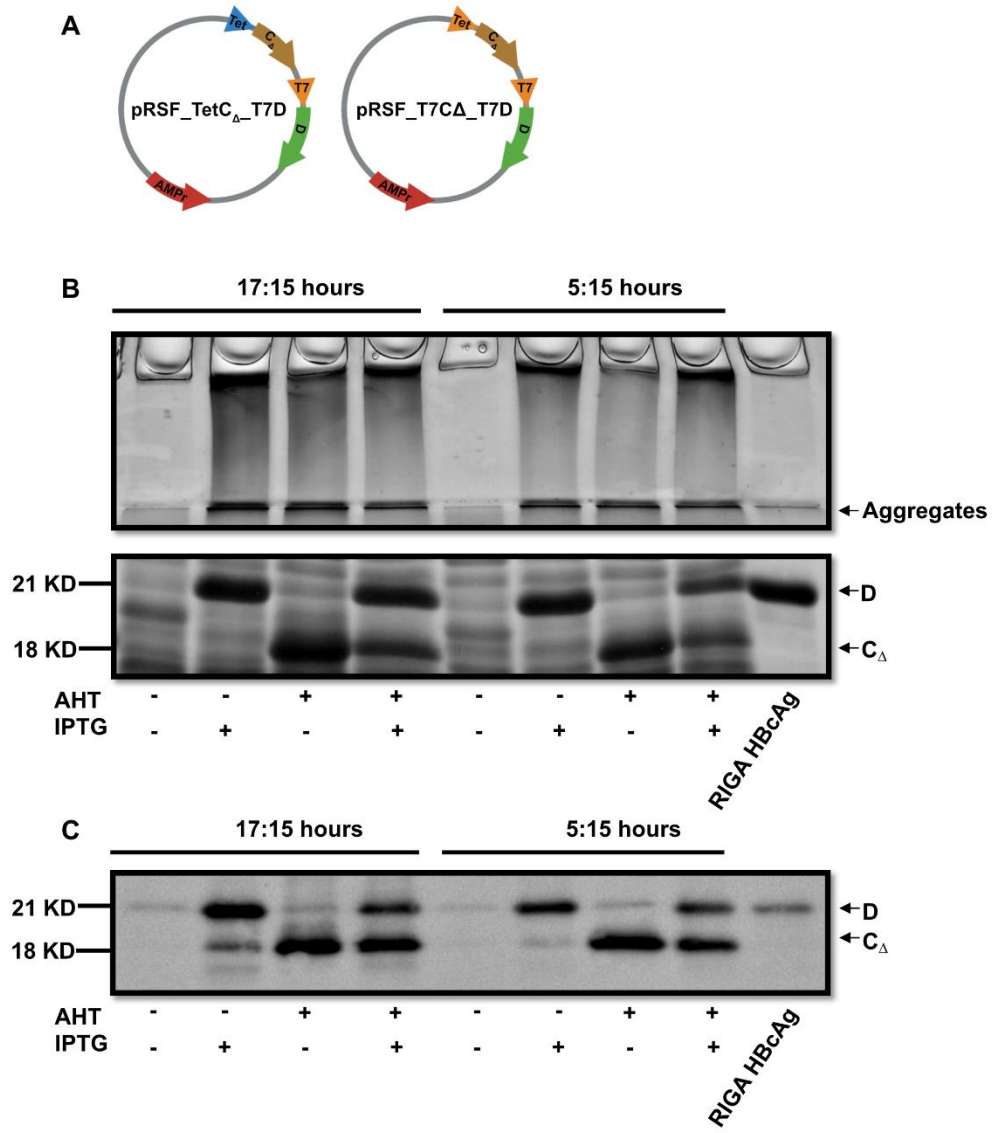

Figure 17: HBcAg from both the genotypes were successfully expressed from a single expression vector in E. coli. (A) Schematic representation of pRSF-based expression vectors used for generation of HBV mosaic capsid particles. **(B, C)** Competent E. coli harboring expression constructs were grown without induction or were induced with either Anhydrotetracycline (AHT) or Isopropyl ß-D-1-thiogalactopyranoside (IPTG) or both for either 17:15 hours or for 5:15 hours. The bacteria were harvested post induction, lysed in 1x SDS buffer and subjected to detection of HBcAg from lysate. Each well was loaded with 10 µl of sample. **(A)** SDS-PAGE from crude bacterial extract from two time points of induction. (B) Western blot of the same samples corroborating the presence of HBcAg from both the genotypes Tet – Tetracylcine promoter; T7 – T7 promoter; KD – Kilodaltons; D – genotype D HBcAg; C_{Δ} - truncated Genotype C HBcAg; AHT – Anhydrotetracycline; IPTG – Isopropyl ß-D-1-thiogalactopyranoside; HBcAg – Hepatitis B core antigen.

In line with the previous observations with SDS-PAGE, the cultures induced with either of the inducers confirmed the respective HBcAg while, the non-induced cultures showed minute amounts of D possibly due to a leaky expression. A commercially available RIGA HBcAg (Genotype D) was also used as a positive control. These results thus confirmed that a single expression vector can successfully express HBcAg from both the genotypes of interest in *E. coli*.

2.1.4.2 Density gradient-based purified HBV mosaic capsid particles show presence of HBcAg from both genotypes

In the consecutive steps, a two-step sucrose gradient ultracentrifugation method was set up for rapid purification of the mosaic capsid particles. In the past, the sucrose gradient centrifugation has proven to be a rapid, yet cost-effective method to purify HBV capsids and other virus-like particles (Rolland et al., 2001). However, owing to the novelty of the mosaic capsid, an attempt was made to set up a sucrose gradient-based centrifugation method for the purification of mosaic capsid particles. In brief, 15 mg of total soluble proteins (TSP) obtained from bacterial lysate was subjected to two consecutive runs of sucrose-gradient based ultracentrifugation (Figure 18 A and C). After each round of ultracentrifugation, the fractions were then subjected to SDS-PAGE analysis to assess the presence of HBcAg and level of purity. It was clear that the bacteria from non-induced expression cultures did not show significant presence of HBcAg of either genotype. However, a weak band at 21 KD was observed suggesting the leaky expression of D under *T7* promoter. Further as expected, the single induced cultures with either IPTG or AHT (Figure 18 B) showed strong bands of expected size. Similarly, bright bands for both C_{Δ} and D were visualized in the dual induced cultures of the mosaic capsid particles. In conclusion, all the cultures showed expected presence of the HBcAg in fractions 1-8. However, the bacterial impurities were clearly visible at this stage. To further improve the quality of purification, fractions 1-8 from each group were pooled together and a second round of sucrose gradient centrifugation was performed (Figure 18 C). The SDS-PAGE followed by the 2^{nd} centrifugation showed a remarkable improvement in the purity of the capsids (Figure 18 D). Interestingly, majority of aggregates were removed during the second round of centrifugation. Although, with improved purity, a significant loss of the proteins was also noted. Out of 15, the fractions 1-7 showed distinct bands of expected size for the HBcAg, for all the expression cultures. In the subsequent steps, the sucrose from the solution was replaced with PBS containing protease inhibitor with

Vivaspin® Turbo 15 (100,000 MWCO). Approximately 0.5 mg of pure HBV mosaic capsid particles were obtained from a 500 ml of expression culture.

Lastly, for a confirmatory analysis, the purified $C_{\Delta}D$ capsids were visualized by transmission electron microscopy. It must be noted that the Transmission electron microscopy was performed by Dr. Julia Sacherl (Institute of Virology, TU Munich). The results clearly showed the presence of fully intact icosahedral capsids from the $C_{\Delta}D$ group (Figure 18 E). These observations constituted the first indications for the formation of HBV mosaic capsid particles made of two genotypes prior to the in-depth structural analysis.

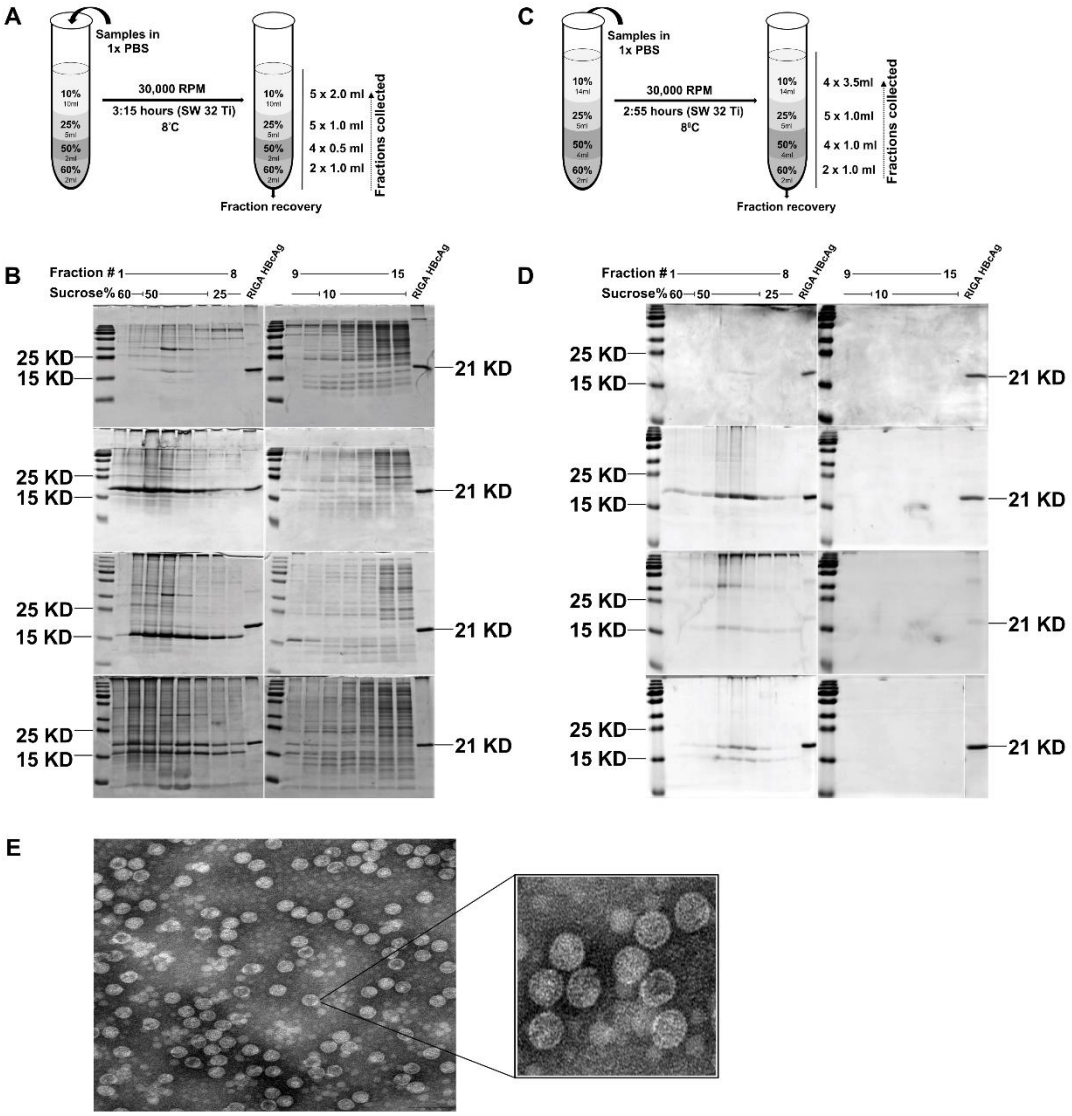

Figure 18: 2x Sucrose gradient centrifugation yields purified HBV Mosaic capsid particles. **(A-D)** 15 mg total soluble proteins were subjected to sucrose-gradient ultracentrifugation followed by SDS-PAGE. 50 µl sample from each fraction containing 1x SDS dye was heated at 95^0C for 10 minutes and 10 µl of the prepared sample was loaded in each well for the analysis. **(A, B)** First

sucrose gradient ultracentrifugation. Schematic representation of first sucrose gradient centrifugation (A), followed by SDS-PAGE analysis of each fraction (B). **(C, D)** Second round of sucrose gradient ultracentrifugation. Schematic representation of second sucrose gradient centrifugation (C), followed by SDS-PAGE analysis of each fraction (D). The gels represent four types of expression cultures non-induced, IPTG only (D), AHT only (C_{Δ}) and dual induced ($C_{\Delta}D$) from top to bottom. First lane of each gel depicts the SDS-PAGE ruler. **(E)** Negative stained transmission electron microscopy of $C_{\Delta}D$ capsids depicting completely assembled HBV capsid particles. PBS – Phosphate buffer saline, KD – Kilodaltons, HBcAg – Hepatitis B core antigen.

2.1.4.3 Anion-Exchange chromatography-based (IEX) purification yield highly pure HBV mosaic capsid particles with reduced loss of protein

In the next step, a more sophisticated capsid purification method based on IEX was established to further improve the quality and quantity of purified capsid particles. In brief, the harvested bacteria were lysed by sonication, followed by ammonium sulfate precipitation, and ultimately subjected to two successive rounds of IEX. As shown in the chromatogram (Figure 19 A and B), a real-time OD_{260} and OD_{280} measurements of elutes generated dual read-out denoting the presence of a protein component together with the nucleic acid component. Early reports on HBV capsids have revealed that, when expressed in *E. coli*, HBV capsids often encapsulate the bacterial RNA non-specifically (N. R. Watts et al., 2002). Therefore, these distinct peaks denoted the presence of nucleic-acid filled capsid particles in corresponding eluates. 10 µl samples from these

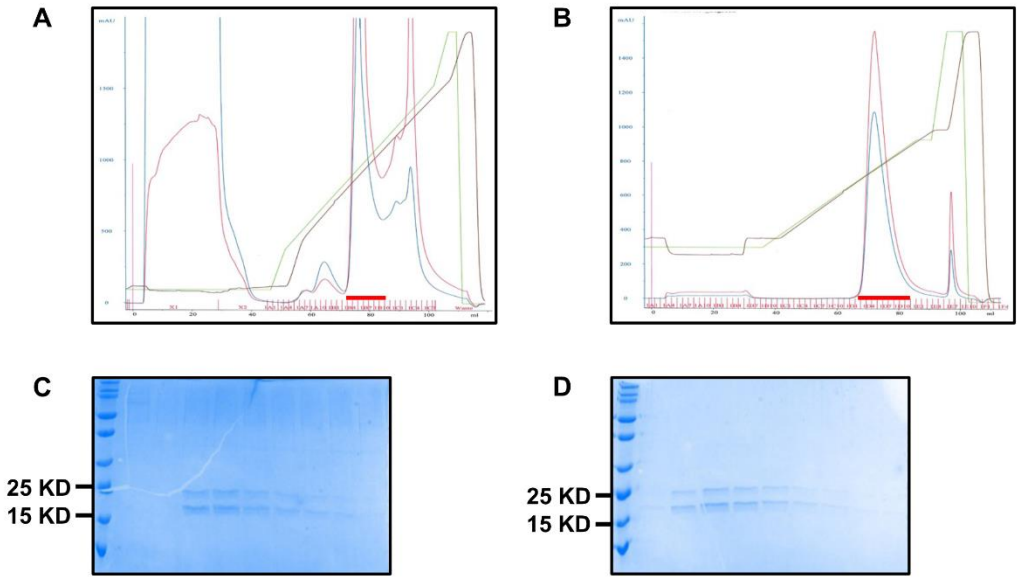

Figure 19: IEX-based purification is a more sophisticated alternative for the purification of HBV mosaic capsid particles. (A-D) Bacterial lysates were subjected to salting out and thereafter to two subsequent runs of IEX at pH 6.0 and linear gradient with varying NaCl between

the runs. **(A, B)** First IEX run. Chromatogram (A) showing the OD_{260} (blue) and OD_{280} (red) of each elute during the first IEX. Elutes constituting the distinct peak represent intact HBV capsids encapsulating bacterial RNA. SDS-PAGE (B) of elutes of interest clearly indicates presence of C_{Δ} and D HBcAg. Samples were applied at 50mM NaCl and the IEX was carried out at a linear NaCl gradient from 200-800 mM NaCl **(C, D)** Second round of IEX. Chromatogram (C) showing the OD_{260} (blue) and OD_{280} (red) of each elute during the first IEX. Elutes constituting the distinct peak represent intact HBV capsids encapsulating bacterial RNA. SDS-PAGE (D) of elutes of interest clearly indicates removal of impurities observed in the prior run with the presence of C_{Δ} and D HBcAg. Samples were applied at 150mM NaCl and the IEX was carried out at a linear gradient from 200-600 mM NaCl. KD – Kilodaltons

elutes were further subjected to SDS-PAGE to assess the presence and level of purity of HBcAg. The results revealed distinct bands of HBcAg for the both the genotypes, with minute impurities after the first round of IEX (Figure 19 C). These elutes containing HBcAg were pooled together and were subjected to a second run of IEX. Due to the presence of prior NaCl in the pooled elutes, the samples for the second IEX were applied at 150 mM NaCl concentration and were eluted again as a linear gradient ranging from 200-600 mM NaCl concentration (Figure 19 B). On the same lines as of the first IEX, distinct peaks were clearly observed in the chromatogram of the second IEX. As expected, the level of impurities was remarkably reduced post second IEX (Figure 19, C). Overall, IEX-based purification was superior to sucrose gradient-based purification in terms of level of purity and quantity. Interestingly, a total of approximately 2.36 mg of HBV capsid particles were purified with the consecutive IEXs as opposed to 0.5 mg with consecutive sucrose gradient-based purification, from equivalent volume of expression cultures.

2.1.5 Structural analysis and confirmation of the presence of HBV mosaic capsid particles

The purification steps and subsequent analysis did not rule out the possibility of the presence of C_{Δ}-only and D-only capsids as a mixture in contrast to mosaic capsid particles, in the final preparation. Therefore, to corroborate the presence of HBV mosaic capsid particles whilst ruling out the possibility of single genotype capsids, further structural analyses and confirmatory experiments were performed.

2.1.5.1 Varied mobility of $C_{\Delta}D$ capsids than single genotype capsids in Native Agarose Gel Electrophoresis (NAGE) suggest homogeneity

HBV capsids produced in *E. coli* tend to encapsulate heterologous RNA, which allows the visualization of the capsids in their native form on agarose gel (Porterfield et al., 2010). This serves as a primary indication to the occurrence of HBV capsids in the expression culture. Thus, a NAGE was performed to assess the formation of HBV mosaic capsid particles. In brief, 3 μg of total soluble proteins obtained from bacterial lysis before purification, was subjected to NAGE using 1 % agarose gel. Upon separation, the samples were first visualized for the encapsulated nucleic acid content under UV (Figure 20 A) and subsequently for the capsid particles (Figure 20 B). As marked by the black arrows, the results clearly indicate the distinct bands at identical position on the agarose gel, when visualized for the nucleic acids as well as the protein counterpart. For the different forms of capsids from left to right - C_{Δ}, D, $C_{\Delta}D$ the bands indicated a slight yet explicitly varying migration lengths. This was more clearly visualized in Figure 20 A. RIGA HBcAg particles (lane 4; also genotype D) showed a band at identical length as of D capsids. In addition to the distinct bands, one additional ill-defined band was also visualized in RIGA HBcAg particles, indicating the different lengths of encapsulated heterologous RNA.

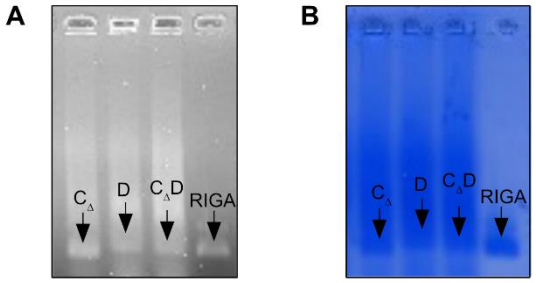

Figure 20: Mobility of $C_{\Delta}D$ capsids vary as compared to C_{Δ} and D capsids, suggesting the presence of mosaic capsid particles. (A) Roti®GelStain visualization of encapsulated RNA in HBV capsids after Native Agarose Gel Electrophoresis (NAGE). **(B)** Coomassie protein staining of the same gel depicting the presence of intact capsids at the identical location as of the encapsulated RNA. Distinct bands are marked with black arrows. The sample loading sequence for both the gels, from left to right was as follows: C_{Δ}, D, $C_{\Delta}D$ and RIGA HBcAg.

Nevertheless, a slightly varying mobility of the $C_{\Delta}D$ relative to that of C_{Δ} and D, served as a preliminary indication for the formation of single population of capsids - $C_{\Delta}D$ and not the single genotype capsids.

2.1.5.2 Pull-down of capsids consisting of biotinylated D HBcAg also shows presence of associated C_Δ HBcAg, confirming the composition and occurrence of mosaic capsid particles

To prove that the mosaic capsid particles generated in competent bacteria are indeed composed of HBcAg from both the genotypes, an alternative approach was used. For this part, a separate yet similar construct in pRSF backbone was employed (Figure 21 A; kindly provided by Prof. Dr. Michael Nassal, University of Freiburg), which made use of the AviTag™ technology (Fairhead & Howarth, 2015) to generate mosaic capsid particles with biotinylated D. Post expression of capsid particles, 1 ml of lysate was subjected to a pull-down assay (Figure 21, B) followed by detection using western blotting. In addition to biotinylated C_DD (C_DD_{bt}), non-biotinylated C_DD obtained from previous preparations were also included in the pull-down assay, to normalize the non-specific pull-down of capsids. As expected, the final eluates containing pulled-down D HBcAg also showed presence of C_D. Surprisingly, larger amounts of C_D as compared to that of biotinylated D were observed (Figure 21 C). In general, as opposed to the unbound extract, majority of protein was eluted in case of C_DD_{bt}. Looking at the C_DD, only weak bands representing non-specific pull-down were seen in the elutes, whereas rest of the protein was detected in the unbound extract. These results clearly indicated that, the mosaic capsid particles indeed occur when a single construct harboring genes coding for HBcAgs of two different genotypes is expressed in competent bacteria.

For in-depth analysis of the structure of the mosaic capsid particles, an additional Nucleic Magnetic Resonance (NMR) spectroscopy was performed in co-operation with Dr. Anne Schütz (Department of Chemistry, TU Munich). The NMR analysis clearly proved that the mosaic capsid particles are indeed composed of C_Δ-D chimeric dimers as well as homodimers of individual genotype (C_Δ-C_Δ and D-D) altogether. Additionally, an ELISA was performed to confirm the retention of antigenicity of the mosaic capsid particles. Here, an antibody recognizing only the structural epitopes of the HBV capsids showed comparable signals for recognition of mosaic as well as single genotype capsids. This experiment was performed by Dr. Julia Sacherl (Institute of Virology, TU Munich). In the next experiment, the ability of the mosaic capsid particles to induce antigen specific T-cells was confirmed in an *ex-vivo* co-culture setting. This experiment was performed by Dr. Sophia Schreiber (Institute of Virology, TU Munich). Lastly, C57BL/6 *wildtype* mice immunized with mosaic capsid particles as the part of the therapeutic vaccination showed expected induction of HBV-specific T-cell response. This experiment was

performed by Dr. Anna Kosinska (Institute of Virology, TU Munich). Since all these experiments were performed by other researchers, the data is not shown here.

Taken together, a candidate siRNA targeting the immunomodulatory TGF-ß1 was identified along with the development and characterization of novel mosaic capsid particles, for an improved combinatorial therapeutic approach to treat chronic hepatitis B.

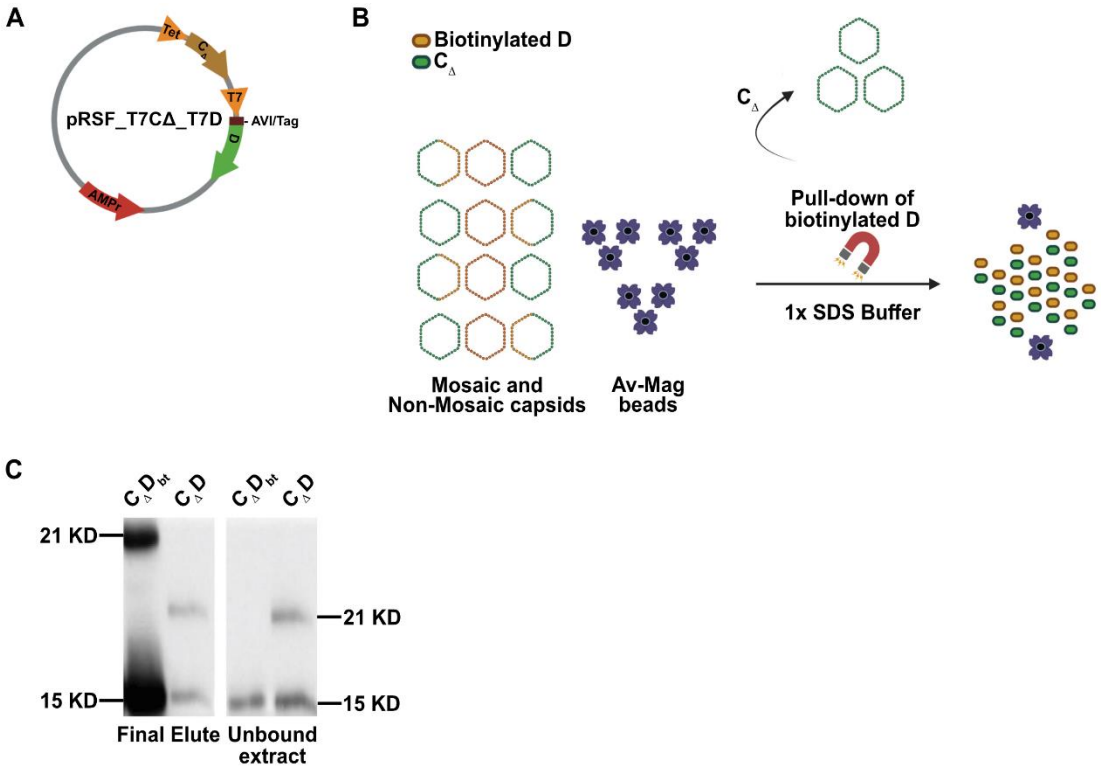

Figure 21: Pull-down of biotinylated D in mosaic capsid particles shows presence of associated C_{Δ}, confirming the composition of mosaic capsid particles. (A) A construct used for synthesizing mosaic capsid particles containing biotinylated D and C_{Δ}, under T7 promoter in pRSF backbone. **(B)** Schematic representation of the synthesis of mosaic capsid particles followed by a pull-down of biotinylated D containing capsid particles with Avidin-coated magnetic beads. **(C)** Western blotting with AD09 antibody with the final elute and unbound extract collected after the pull-down assay showing majority of C_{Δ} present in pulled-down biotinylated capsids. KD – Kilodaltons; bt – biotinylated; SDS – sodium dodecyl-sulfate.

2.2 Systematic Analysis of RNAi-accessible replication steps of Severe Acute Respiratory Syndrome Coronavirus 2 (SARS-CoV-2)

After the emergence of SARS-CoV-2, previously gained expertise on the devising therapeutic siRNAs was repurposed majorly to achieve following results. It must be noted that, majority of the observations made in this project have been already published (Ambike et al., 2022).

2.2.1 Preliminary screening of siRNAs targeting SARS-CoV-2 *in vitro*

Prior to testing the antiviral efficacy, the siRNAs were screened for their activity as well as their potential to target the incoming mRNA.

2.2.1.1 psiCHECK2.0^{TM} based screening of siRNAs reveal potential candidates as well as the sense-specific activity of N targeting siRNAs

To identify the best candidate siRNAs for the antiviral studies, the siRNAs were initially screened for their activity using the dual-luciferase reporter vectors. For the SARS-CoV-2 siRNAs, an individual reporter vector was harboring the 21-nucleotide long siRNA binding site downstream the Renilla luciferase was cloned in contrast to the siRNA screening against immunomodulatory genes. The results clearly indicated the best performing siRNAs targeting different SARS-CoV-2 genomic regions (Figure 22 A-D). For the L-specific as well as the positive sense N-specific siRNAs, the best candidates nearly achieved 80 % knockdown of the *Rluc*. On the other hand, surprisingly, the siRNAs targeting ORF1 as well as 3'UTR could achieve more than 90 % knockdown of the *Rluc*. Interestingly, the silencing activities of the siRNAs varied experimentally, among the different target regions, even though the siRNAs were predicted previously to achieve the similar levels of silencing. Considering the best performing candidates for each region, the siRNAs targeting 3'UTR achieved the highest knockdown followed by the ORF1 targeting siRNAs. For a fairer understanding, siRNAs targeting the common regions of viral transcripts – siL, siN and siU are depicted in Red whereas siRNAs targeting only the gRNA – siO are depicted in Blue henceforth. In the consequent set of experiments, siRNAs targeting positive and negative sense N gene were also screened. In theory, both strands of the siRNA possess the potential to guide the RISC complex (Wei et al., 2009). Meaning, the sense strand of the siRNA targeting the positive sense

viral RNA could in fact silence the negative sense viral RNA transcript as well, however, regarded as an off-target activity of the siRNA. Therefore, to avoid such effect, the sense specific activity of the N targeting siRNAs was tested with the luciferase reporters. For this part, two new luciferase reporters were cloned harboring the complete N gene in positive and negative sense. With such setup, the siRNA activity of each siRNA was evaluated against both positive and negative sense N gene, to identify the siRNAs with sense-specific activity (Figure 22 E). As it can be seen in the results, most of the siRNAs, indeed had a silencing effect on the opposite sense to some extent. However, this off-target effect was notably lesser than the siRNA silencing effect. In general, the siRNAs targeting the negative sense N gene exhibited a finer sense-specific activity than the siRNAs targeting the positive sense N gene. Nevertheless, siN(-)4-11 were selected as the candidate siRNAs to target negative sense viral transcript in further experiments.

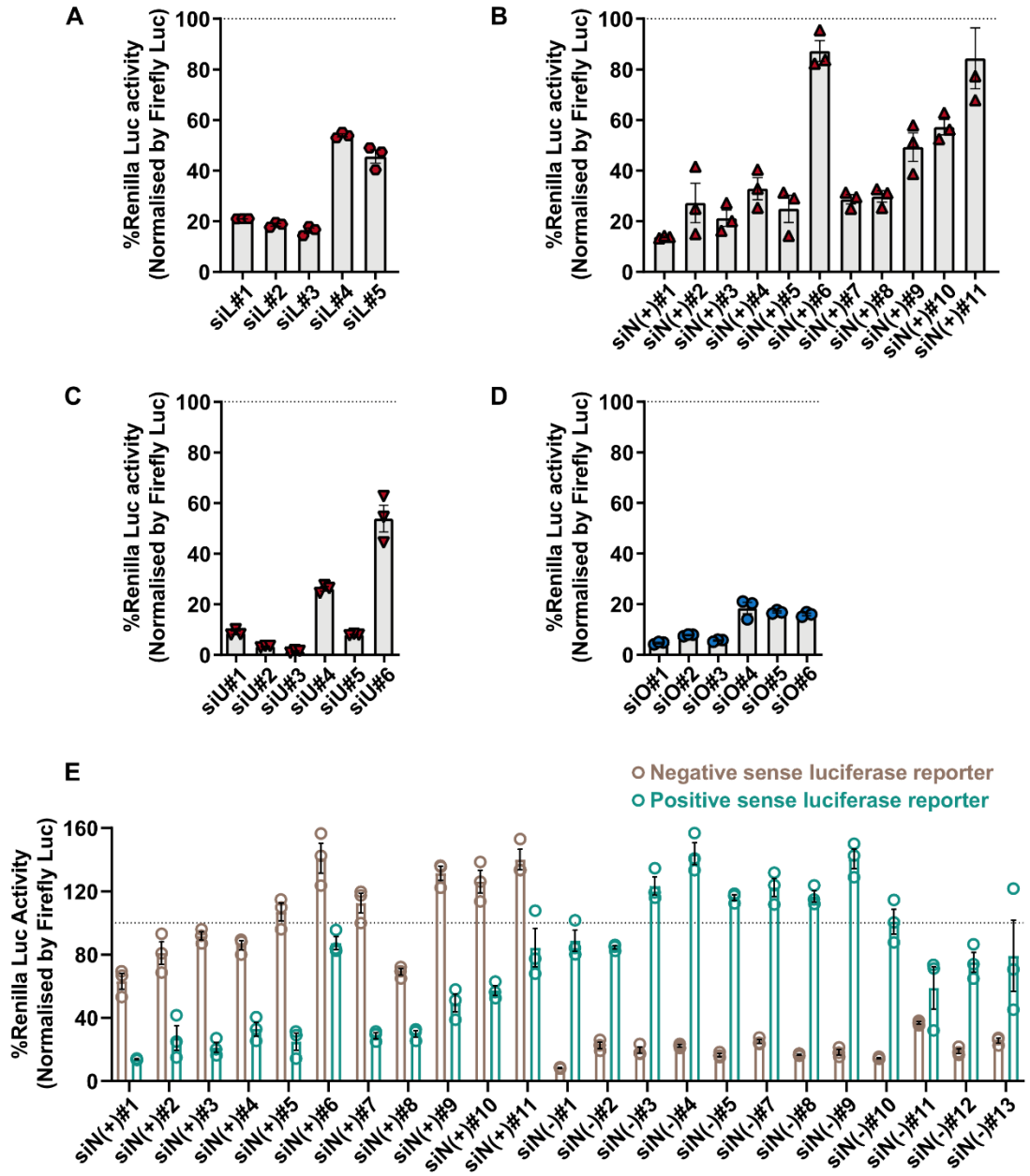

Figure 22: Screening of siRNAs exhibit reveal best performing candidates and exhibit their sense-specific activity [Adapted from: (Ambike et al., 2022)]. (A-E) HEK293T cells were co-transfected with siRNAs and respective luciferase reporters harboring siRNA binding site. Dual luciferase assay was performed 48 hours post transfection. **(A-D)** Screening of siRNAs targeting four different regions of SARS-CoV-2 genome - L (A), positive sense N (B), 3'UTR (C) and ORF1 (D). **(E)** Screening of siRNAs with sense-specific activity targeting negative sense N gene. Cells co-transfected with siRNA targeting GFP (siNC) along with reporter vector containing target sites for antiviral siRNAs served as negative control. Firefly luciferase activity was used for normalization for each readout. Percent Renilla luciferase activity was calculated with respect to that of the negative control group. Individual values of biological triplicates for all the groups are shown and error bars indicate SEM. Luc – Luciferase; siL1-5 – Leader sequence specific siRNAs;

siO1-6 – ORF1 specific siRNAs, siN(+)1-11 – positive sense Nucleocapsid gene specific siRNA; siN(-)1-13 – negative sense Nucleocapsid gene specific siRNAs; siU1-6 3'UTR specific siRNAs.

2.2.1.2 siRNAs are well tolerated by the Vero E6 cells and can target incoming mRNA

Cytopathy as an effect of some virus infections such as SARS-CoV-2, is a well-known phenomenon (Fung, Yuen, Ye, Chan, & Jin, 2020). Several mechanisms involved in virus-induced cell death have been previously explained (S. Li et al., 2020; Morais da Silva et al., 2022). Interestingly, chemically unmodified siRNAs have also been reported to be cytotoxic in target-independent manner (Fedorov et al., 2006), which can add onto the cytopathic effect in SARS-CoV-2 infected cells. Thus, an ideal RNAi-based therapy involves a well-tolerated siRNA dosage and a transfected agent that decreases toxicity while obtaining enough anti-viral efficacy. SARS-CoV-2 is a positive-sense RNA virus, and earlier siRNA screening in HEK293T cells generally involved co-transfection of a plasmid reporter with a siRNA. On these lines, the next series of experiments was performed to identify the well-tolerated concentration of the siRNAs and RNAiMAX, as well as to assess ability of siRNAs in knocking down the incoming mRNA, as a mimicking model of virus infection in Vero E6 cells.

In brief, the tolerability and activity of siGFP to silence incoming GFP mRNA was tested at various concentrations in Vero E6 cells with CellTitre-Blue® assay and fluorescent microscopy. As the results indicate, the cells could tolerate most of the siRNA-RNAiMAX combinations, except at the lowest concentrations of 10 nM siRNA with highest amount of 2.5 µl RNAiMAX. As expected, a deterioration (about 15 %) of the viability was observed with highest concentration of the siRNAs except when supplemented with increased amount of RNAiMAX. Moreover, a diminutive difference on cell viability was observed with either 1.5 or 2 µl of RNAiMAX. Considering these observations, RNAiMAX concentration of 1.5 µl was chosen along with 50 nM of siRNA concentration. This allowed a 5 times higher concentration of siRNA with a minute (about 5 %) loss of viability as compared to the lowest concentrations in future experiments. Additionally, a fluorescently labelled (AF647) siRNA (kindly provided by Prof. Dr. Olivia Merkel, Department of Pharmacy, Ludwig Maximilian University of Munich) was reverse transfected into Vero E6 cells, with chosen combination of siRNA and RNAiMAX to assess the siRNA transfection efficiency in the Vero E6 cells. The results indicated that almost all the cells contained the siRNA 24 hours post transfection, exhibiting the suitability of the chosen siRNA and RNAiMAX concentration (Figure 23 B). Henceforth,

50 nM final concentration of siRNAs was used in all the experiments, unless indicated otherwise.

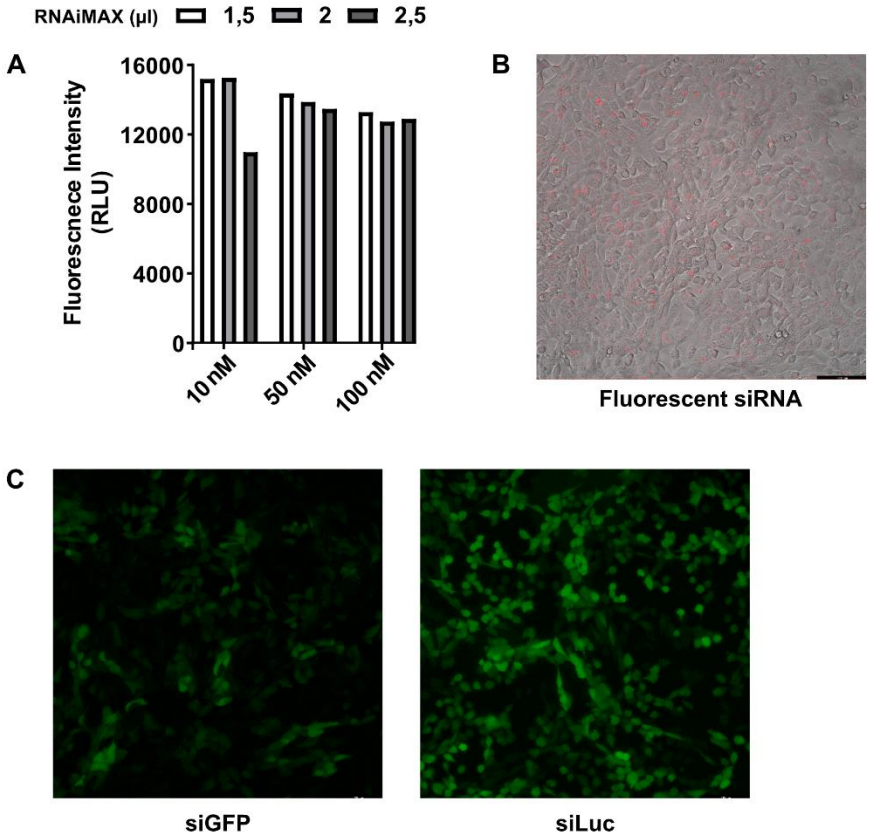

Figure 23: Chemically unmodified siRNAs are well tolerated in Vero E6 cells and can target incoming mRNA (A) Viability of cells transfected with siGFP. The cells were reverse transfected with various combinations of concentrations of siRNA and RNAiMAX. RNAiMAX values used for each group are denoted on top. CellTitre-Blue® assay was performed 48 hours post transfection. The graph represents the fluorescence intensity emitted by Resorufin reduced from Resazurin by metabolically active cells. **(B)** siRNA transfection efficiency in Vero E6 cells. VeroE6 cells were transfected with 50 nM of fluorescent siRNA using 1.5 µl RNAiMAX. Cells were visualized for the presence of intracellular siRNA molecules 24 hours post transfection. The fluorescently labelled (AF647) siRNA molecules are visualized as red dots within the cells. **(C)** siRNA-based silencing of incoming GFP mRNA. Vero E6 cells were reverse transfected with 50 nM siRNA targeting GFP. 6 hours post siRNA transfection, 250 ng of in vitro transcribed mRNA was transfected into the cells. Reduction of GFP was visualized under fluorescence microscope 48 hours post mRNA transfection. siRNA targeting Firefly luciferase was used as negative control. **(A)** Bars indicate individual values of a single replicate for each group. **(B, C)** Representative images from biological triplicates are shown here. RLU – Relative Light Units; nM – nanomolar; GFP – Green Fluorescence Protein, Luc – Firefly Luciferase.

Next, to assess the ability of siRNAs to silence the incoming RNA, in vitro transcribed mRNA coding for GFP as a mimicking model of incoming viral mRNA was used. In brief, 50 nM siRNA targeting GFP was reverse transfected into Vero E6 cells, followed by transfection of 250 ng GFP mRNA (pretested concentration, data not shown; kindly provided by Dr. Andreas Oswald, Institute of Virology, TU Munich). From the results, it was clear that the cells transfected with siGFP indeed showed a significant reduction in GFP signal as compared to siLuc (siNC) (Figure 23 C). These findings inferred that a 50 nM concentration of chemically unmodified siRNA was indeed tolerable to Vero E6 cells and that the siRNAs can target the incoming GFP mRNA.

2.2.1.3 The half maximal inhibitory concentration (IC50) of the candidate siRNA targeting various regions determined with dual luciferase reporters do not significantly differ from each other

One of the aims of this project was to compare the antiviral efficacy of the siRNAs targeting the common regions of the SARS-CoV-2 genomic and sgRNA, against the siRNAs targeting only the gRNA. For an equitable comparison of siRNAs targeting various regions, it was crucial to avoid the siRNA-designing bias as explained earlier.
Hence, IC50 values for each candidate siRNA were determined using respective luciferase vector harboring only the siRNA-binding site. IC50 values differed to some extent within a group as well as between the groups (Figure 24 A). Among all the siRNAs, siU3 was identified as the most potent siRNA against the luciferase reporters, with an IC50 value of 0.0011 nM. On the other hand, siN(+)3 exhibited the least potency among all. It was also observed that siO1-3, as a group were slightly more potent than other group of siRNAs. Therefore, another comparison of IC50 values is depicted with grouping all the siRNAs targeting common regions against the ORF1 targeting siRNAs (Figure 24 B). Here, a slight trend towards the benefit of ORF1 siRNAs was observed, but the IC50 values did not significantly differ between the groups.

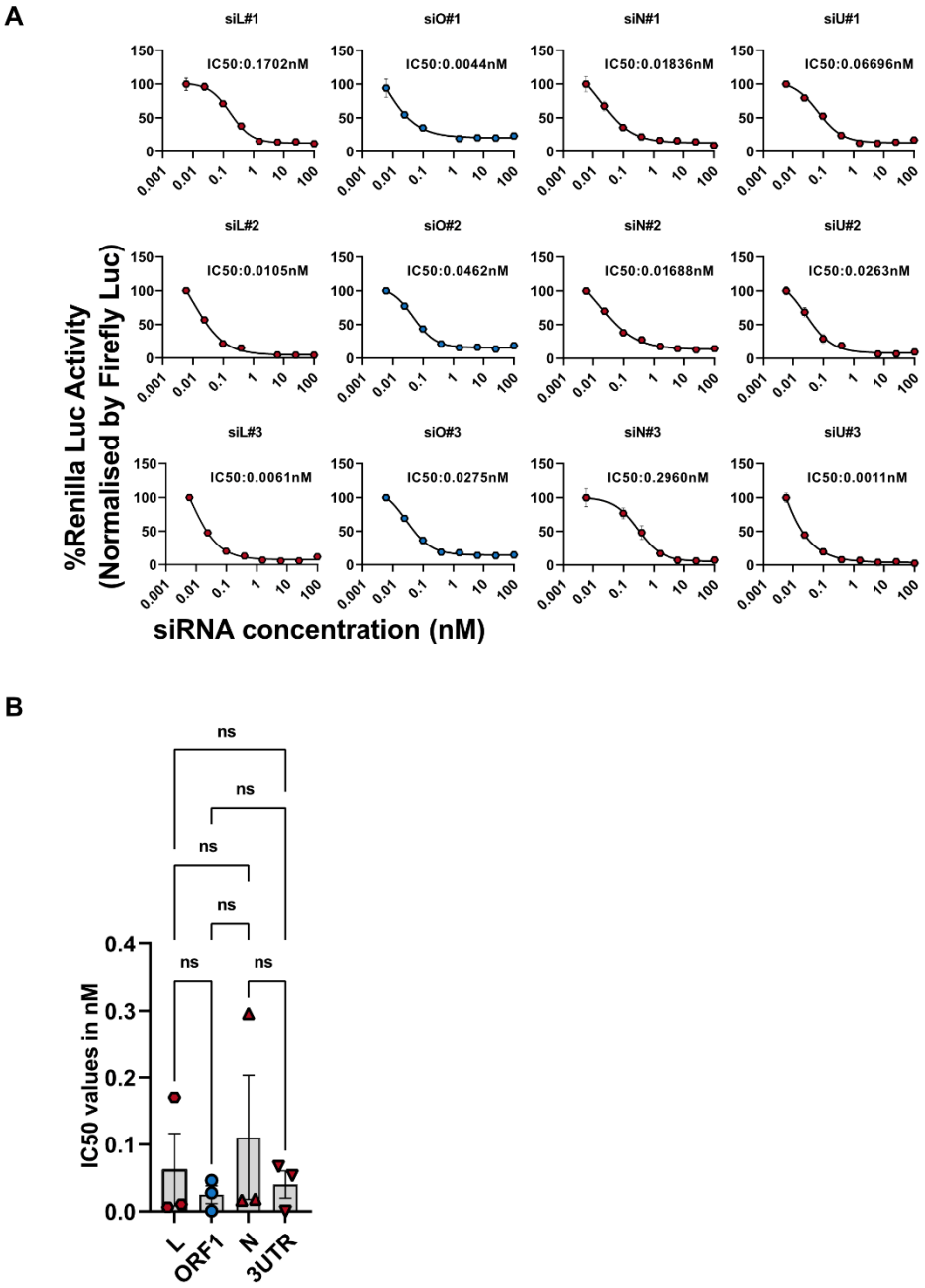

Figure 24: siRNAs targeting various regions of SARS-CoV-2 do not differ significantly in silencing activities against respective luciferase reporters [Adapted from: (Ambike et al., 2022)]. (A) Dual luciferase assay-based determination of mean inhibitory concentration (IC50) of siRNAs. HEK293T cells were co-transfected with decreasing concentrations of siRNAs (100, 25, 6.25, 1.56, 0.39, 0.098, 0.024 and 0.006 nM) and 200 ng of luciferase reporters. The dual luciferase assay was performed 48 hours post transfection. Cells co-transfected with negative control siRNA targeting GFP along with respective reporter vector served as negative control. Firefly luciferase activity was used for normalization for each readout. Percent Renilla luciferase activity was calculated with respect to that of the negative control group. IC50 values were calculated using non-linear regression using GraphPad 9.0. **(B)** Comparison of observed IC50 values between siRNAs targeting common regions of all viral transcripts (L, N and 3'UTR) and

only genomic RNA (ORF1). (A) Arithmetic mean of triplicates with error bars indicating SEM or (B) median of arithmetic mean of triplicates for all groups is shown. Statistical significance was calculated using Mann-Whitney test. siL1-3 – Leader sequence specific siRNAs; siO1-3 – ORF1 specific siRNAs, siN(+)1-3 – positive sense Nucleocapsid gene specific siRNA; siU1-6 3'UTR specific siRNAs; nM – nanomolar; ns – non-significant.

2.2.2 Antiviral activity of siRNAs

In the consequent experiments, the antiviral activity of the siRNAs to inhibit SARS-CoV-2 replication and virus-induced cell death was tested.

2.2.2.1 siRNAs terminate SARS-CoV-2 transcription and limit viral spread by targeting incoming viral genome

In the first set of experiments, the ability of the siRNAs to directly target the incoming viral genome was tested. Since ORF1 is present only in the gRNA of SARS-CoV-2, the siRNAs only targeting ORF1 were used in these experiments. Moreover, for a rapid, real-time monitoring of virus spread, a recombinant rSARS-CoV-2-GFP was employed resulting in GFP expression in infected cells (Figure 25 A). In brief, siRNA transfected Vero E6 cells were infected with rSARS-CoV-2-GFP (MOI 1.0) and were monitored for real-time virus spread for 68 hours post infection using Incucyte® Live-cell Analysis. It must be noted that, SARS-CoV-2 infection for all the experiments henceforth performed in this project were done by Dr. Cho-Chin Cheng (Institute of Virology, Technical University of Munich).

The real-time monitoring clearly showed a reduction in number of GFP^+ cells beginning in 12 hours post infection, reaching about 50 % before 24 hours post infection (Figure 25 B). A clear reduction of GFP^+ cells can also be seen from the superimposed images (Figure 25 C). These results confirmed that the siRNAs transfected before infection, can directly target the incoming genome of SARS-CoV-2 and can limit the spread. For a further, more relevant testing, the effect of same siRNAs was tested in identical setting against the *wildtype* SARS-CoV-2 (MOI 0.1), 24 hours after infection. As the results indicate, about 80 % of reduction in both gRNA and total RNA was observed as compared to the mock group (Figure 25 D and E). Therefore, it was concluded that the silencing of incoming gRNA by siRNAs in-turn lead to termination of transcription, limiting the sgRNA expression, and thereby significantly reducing the total viral RNA levels.

Since the reduction of GFP^+ cells was observed within 12 hours of infection, the next set of experiments were performed to shed a light on the effects of siRNAs on early time-

points of the virus infection. Thus, a similar experimental setup was used for this part. However, to examine a region-specific effect avoiding the differential siRNA activity within siRNAs targeting the same region, a pool of siRNAs targeting ORF1 ($siORF1_{pool}$) was transfected into Vero E6 cells before infection and the RT-qPCRs were performed 1h, 6h and 12h post infection instead of 24h post infection. Interestingly, it was noted that siORF1 can target the incoming viral genome immediately as the reduction was observed as early as 1h post infection (Figure 25 F). As expected, the effect of the siRNAs became robust as the time persisted, achieving about 85 % reduction of both gRNA and total RNA 12 hours after infection (Figure 25 F and G). At each time-point, the total RNA expression was slightly lesser than that of the gRNA. This suggested that a swift control of gRNA could be key in controlling SARS-CoV-2 infection. Collectively, these results could conclude that the siRNAs can terminate the transcription of SARS-CoV-2 within few hours of infection because of silencing the gRNA.

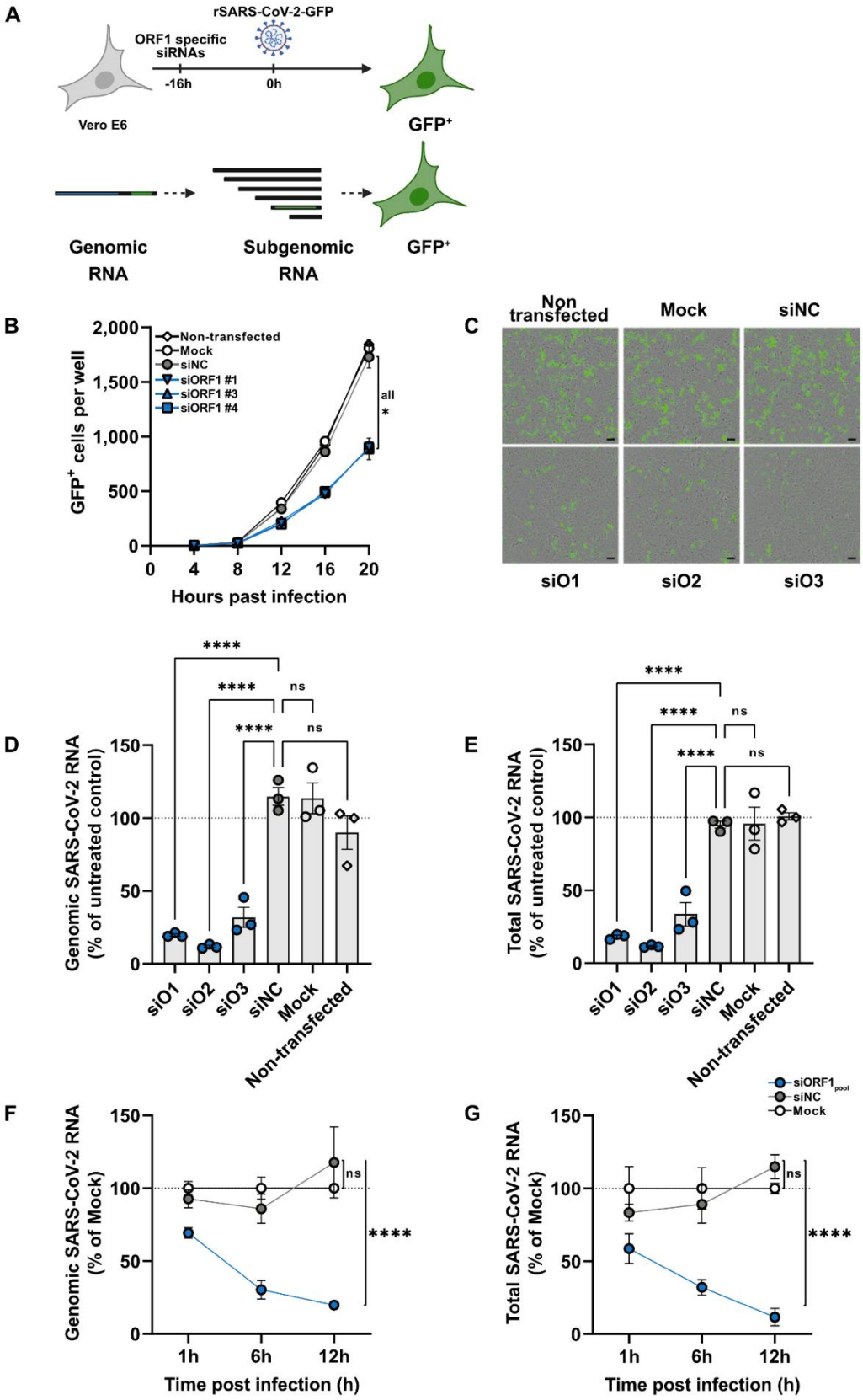

Figure 25: siRNAs target incoming genome of SARS-CoV-2 thereby terminating viral transcription and spread reporters [Adapted from: (Ambike et al., 2022)]. (A) Experimental

setup used in (B, C). Vero E6 cells were reverse-transfected with siRNAs targeting ORF1. 16 hours post transfection, the cells were infected with rSARS-CoV-2-GFP with an MOI 1.0 and the number of GFP+ cells monitored in real-time using Incucyte® Live-Cell Analysis. Cells receiving no siRNAs (Non-transfected), Mock-transfected (Mock) cells as well as siRNA targeting Firefly luciferase (siNC) served as controls. **(A, bottom)** Schematic representation of rSARS-CoV-2-GFP transcription leading to formation of virus-infected GFP^+ cells. **(B)** Real-time monitoring of viral spread showing number of GFP^+ cells determined by Incucyte S3 software post siRNA treatment. **(C)** Representative superimposed images of fluorescent channel and phase-contrast channel from Incucyte® Live-Cell Analysis indicating GFP^+ cells 24 hours post rSARS-CoV-2-GFP infection. **(D, E)** Vero E6 cells were reverse transfected with siRNAs targeting ORF1 individually. 6 hours post transfection, cells were infected with *wildtype* SARS-CoV-2 (MOI 0.1). RT-qPCR was performed to assess the knockdown of **(D)** gRNA and **(E)** total SARS-CoV-2 RNA. **(F, G**) Vero E6 cells were reverse transfected with pool of 3 siRNAs targeting ORF1. 6 hours post transfection, cells were infected with *wildtype* SARS-CoV-2 (MOI 0.1). RT-qPCR was performed at various time points to determine SARS-CoV-2 **(F)** gRNA and **(G)** total RNA knockdown. siRNA concentration of 50 nM was used in all the experiments for individual as well as the pool. Mock-transfected (Mock) cells as well as siRNA targeting Firefly luciferase (siNC) served as controls. (D, E) Individual values and (B, F and G) Arithmetic mean of biological triplicates for all groups are shown and error bars indicate SEM. Statistical significance was calculated by ordinary one-way Anova (D) or by multiple comparisons of means using 2-way Anova (B, E) in GraphPad Prism 9.0. GFP – Green Fluorescent Protein; siO1-3 – ORF1 specific siRNAs; ns – non-significant. *P < 0.05; **P < 0.01; ***P < 0.001; ****P < 0001.

2.2.2.2 Silencing of SARS-CoV-2 gRNA improves cell viability and prevents cell-death

It is well established that SARS-CoV-2 infection could result in host cell death (Fung et al., 2020; S. Li et al., 2020; Morais da Silva et al., 2022). The major pathways leading to cell death upon SARS-CoV-2 infection have been studied previously (X. Li, Zhang, Wang, Gutierrez-Castrellon, & Shi, 2022). Improving cell viability along with a potent antiviral activity thus describes an ideal therapeutic strategy against COVID-19. Hence, the following set of experiment was focused on assessing whether the antiviral activity of siORF1 is associated with improved cell viability. Briefly, the Vero E6 cells were reverse transfected with $siORF1_{pool}$ 16 hours before infection with *wildtype* SARS-CoV-2 with a higher MOI of 1.0; and the cell viability was assessed at 24 hours post infection. It could be demonstrated that, the siRNA treatment indeed improved the cell viability post virus infection (Figure 26 A). As expected, the non-infected cells showed maximum viability among the experimental groups. When treated with the siNC, the viability of the

cells decreased drastically to about 50 % as of the non-infected control. On the other hand, the siRNA treatment before infection could significantly reduce the loss of viability upon virus infection. However, the siRNA treatment could not completely retain the viability of the cells. To further elucidate this effect, the infected cells were monitored in real-time for virus-induced cell death. To increase comparability considering the potential cytotoxic effects of siRNA transfection, non-infected as well as siRNA-transfected groups were also used as controls. Undoubtedly, the siRNA treatment could exceptionally reduce the virus-induced cell death over time (Figure 26 B). The number of dead cells in general increased over time as expected, achieving the maximum at 56 hours post infection. All the non-infected controls showed nearly the identical levels of cell death. The siRNA treatment on the other hand, could alleviate the virus-induced cell death by approximately 60 %. Additionally, the visualization of cells under fluorescent channel at 56h post infection could clearly corroborate the prevention of cell death by siRNAs as compared to the Mock and siNC treatments (Figure 26 C). In continuation with the previous observations, it was concluded the siRNAs targeted against gRNA of SARS-CoV-2 can additionally dampen the virus-induced cell-death in Vero E6 cells.

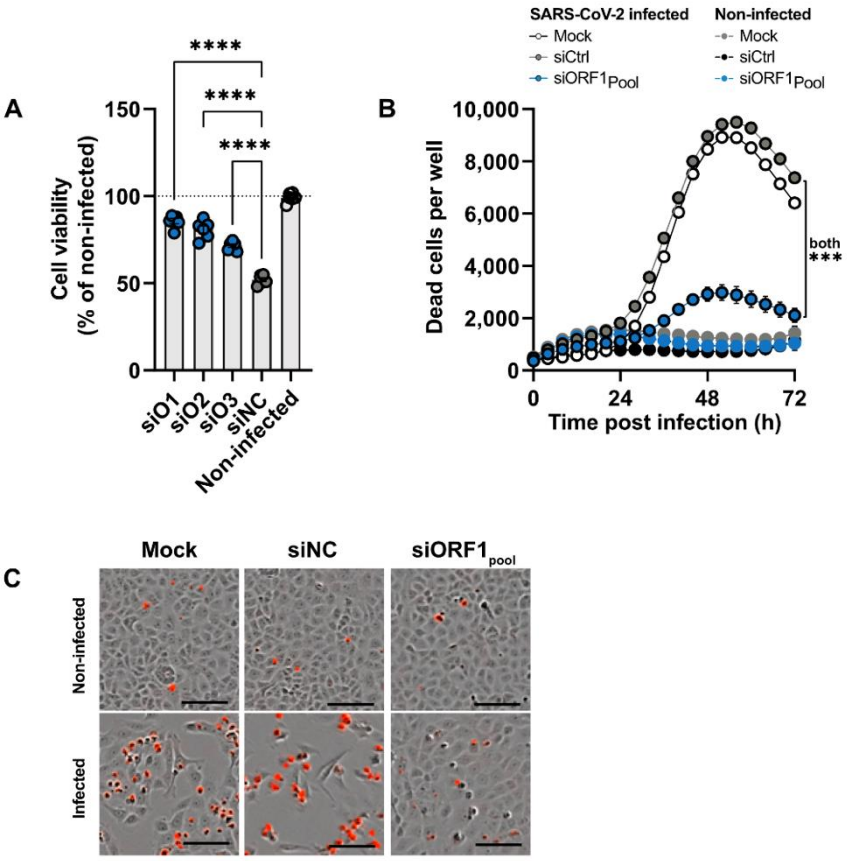

Figure 26: Knockdown of SARS-CoV-2 gRNA improves cell viability and prevents cell-death [Adapted from: (Ambike et al., 2022)]. (A) Cell viability of SARS-CoV-2 infected Vero E6

cells after siRNA treatment. Vero E6 cells were reverse-transfected with siO1-3 individually and were infected with *wildtype* SARS-CoV-2 at a high MOI of 1.0. CellTitre-Blue® Cell Viability assay was performed 24h post infection. Cell viability was measured as Resorufin fluorescence reduced from Resazurin by metabolically active cells. (B, C) Vero E6 cells were reverse transfected with a pool of siO1-3, 6 hours before SARS-CoV-2 infection. The dead cells were visualized in real-time in Incucyte® Live-Cell Analysis system using Incucyte® Cytotox Red dye and were quantified using Incucyte S3 software. **(B)** Time kinetics of dead cells quantified every 4 hours for the period of 72 hours. **(C)** Representative superimposed images of fluorescent channel and phase contrast channel from Incucyte® Live-cell Analysis system showing dead cells in red. The images were taken at 56h post infection, where maximum number of dead cells were seen. Non-infected cells, Mock-transfected (Mock) cells as well as negative control siRNA targeting Firefly luciferase (siNC) served as controls wherever indicated. (A) Individual values and (B) arithmetic mean of triplicates for each group are shown and the error bars indicate SEM. Statistical significance was calculated using (A) ordinary Anova and (B) repeated measures one-way Anova in GraphPad 9.0. Ctrl – control; Mock – Mock transfected group; siNC – negative control siRNA; siO1-3 – ORF1 specific siRNAs; $siORF1_{pool}$ – pool of siO1-3. ***P< 0.001; ****P < 0.0001.

2.2.2.3 siRNAs targeting negative sense viral RNA transcripts do not exhibit any antiviral effect

SARS-CoV-2 replicates through negative sense RNA intermediates (D. Kim et al., 2020). Previous reports suggest that the negative sense RNA intermediates generated during the transcription of SARS-CoV-2 are between 10 to 100 times lower than positive sense RNA (Alexandersen, Chamings, & Bhatta, 2020; Bartas et al., 2022). siRNA-based suppression of these low-abundant transcripts could be thus key in controlling SARS-CoV-2 replication. However, it was not yet clear if the viral RNA of certain polarity is accessible for RNAi. Prior to using the siRNAs, the kinetics of negative and positive sense viral RNA transcripts were inspected at early time points. Surprisingly, positive as well as negative sense gRNA were detected within 1h post infection. On the other hand, the sgRNAs were barely detectable (Figure 27 A). Interestingly, at 6h post infection, the levels of negative sense gRNA exceeded than the positive sense gRNA whereas, the negative sense sgRNA levels were about 25-folds lower. These results suggest the possibility that, such low-abundant negative sense sgRNAs could be sufficient as templates to generate 25-fold higher amounts of viral mRNA.

In the next set of experiments, the possibility of siRNAs targeting negative sense genomic and sgRNA to suppress viral replication was tested. Initially, the siRNAs

demonstrating the sense-specific activity against the negative sense N (see 2.2.1.1; Figure 22 E) were previously tested against the rSARS-CoV-2-GFP.

Unexpectedly, none of the siRNAs targeting the negative sense N gene could limit the viral spread even to a slight extent (Figure 27 B). To further confirm these findings, the antiviral activity of these siRNAs was tested against the *wildtype* SARS-CoV-2. As expected, only the siRNAs targeting the positive sense N coding sequence could suppress the sgRNA expression whereas the siRNAs targeting the negative sense N failed to achieve a significant knockdown (Figure 27 C). It was thus concluded that, the negative sense viral transcripts are inaccessible for siRNA treatment.

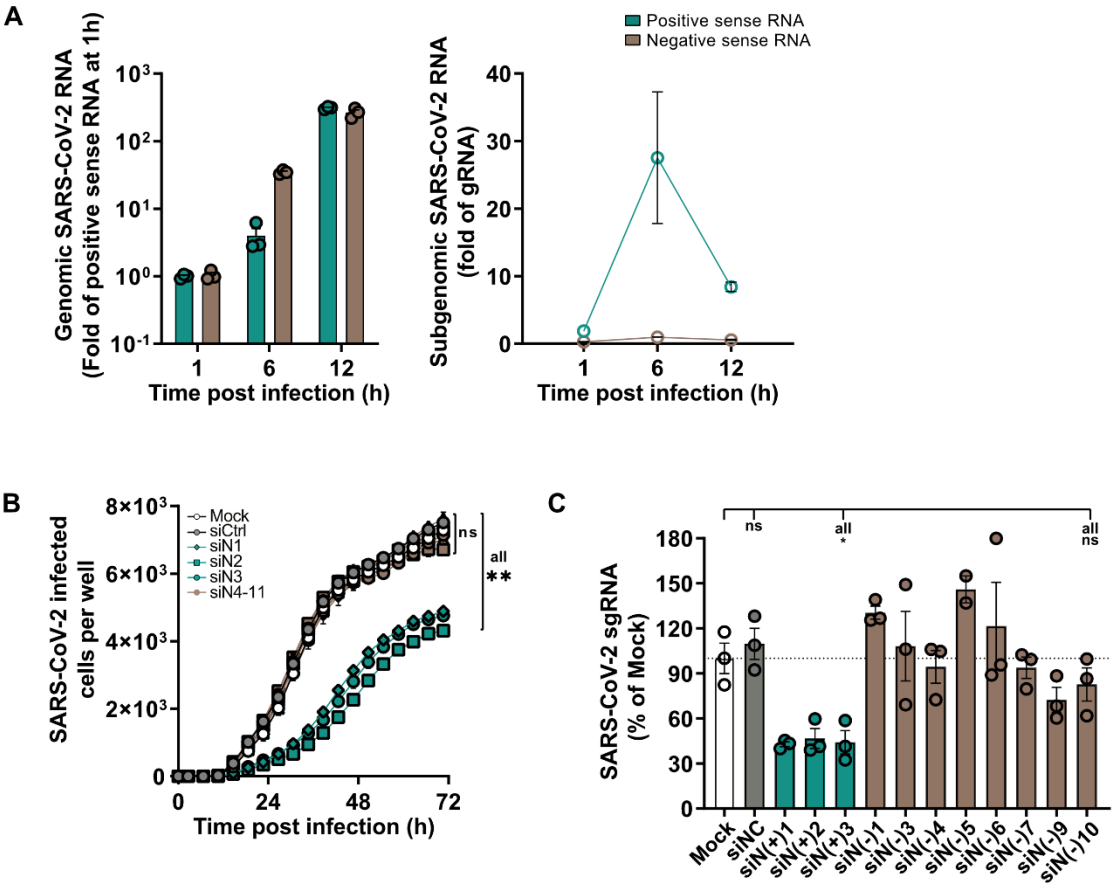

Figure 27: Negative sense RNA transcripts are inaccessible to siRNA-based suppression [Adapted from: (Ambike et al., 2022)]. (A) Kinetics of viral RNA transcripts. RT-qPCR indicating kinetics of positive and negative sense genomic RNA (left) and subgenomic RNA (right) during early time points of infection. Vero E6 cells were infected with *wildtype* SARS-CoV-2 (MOI 0.1) and the cells were lysed at 1h, 6h and 12h post infection. Negative and positive sense RNA was transcribed to cDNA using either poly-A or poly-T primers respectively and subsequently subjected to qPCR. **(B)** Real-time monitoring of GFP+ cells indicating viral spread post siRNA

treatment. Vero E6 cells were reverse transfected individually with siRNAs targeting negative or positive sense N gene, 6h before infection with rSARS-CoV-2-GFP (MOI 1.0). GFP^+ cells were monitored for 72h with images taken at the intervals of 4h in Incucyte® Live-Cell Image Analysis system. **(C)** Effect of siRNA treatment on SARS-CoV-2 subgenomic RNAs determined by RT-qPCR. Similar experimental setup as (B) however, cells were infected with *wildtype* SARS-CoV-2 (MOI 0.1) and were lysed at 24h post infection. Non-infected cells, Mock-transfected (Mock) cells as well as siRNA targeting Firefly luciferase (siNC) served as controls wherever indicated. Individual values (A left, C) or arithmetic means of triplicates (A right, B) are shown, and the error bars indicate SEM. Statistical significance was calculated using (B) two-way Anova and ordinary one-way Anova (C) in GraphPad 9.0. h – hours; ns – non-significant; siNC – negative control siRNA targeting Firefly Luciferase; Mock – Mock transfected; siN(+)1-3 – positive sense N-specific siRNAs; siN(-)1-10 – negative sense N-specific siRNAs. *P < 0.05; **P < 0.01.

2.2.2.4 siRNAs targeting common regions of SARS-CoV-2 RNA transcripts achieve simultaneous suppression of gRNA and sgRNA but are less efficient than siRNAs targeting only gRNA.

For an ideal therapeutic strategy, it is of utmost importance to identify the determinants for an efficient suppression of viral replication. Therefore, to pinpoint the best genomic region and RNA species to achieve maximum inhibition of SARS-CoV-2 by siRNAs, the following comparative experiments were performed. The candidate siRNAs against all four regions of interest – L, ORF1, N and 3' UTR, were tested for their ability to silence gRNA and sgRNA of SARS-CoV-2. In brief, the siRNA activity of individual pools of 3 siRNAs targeting each region was assessed in infected Vero E6 cells. As anticipated, all the siRNA pools showed a significant reduction of SARS-CoV-2 gRNA. Interestingly, among the four, $siORF1_{pool}$ indeed showed the most efficient knockdown of SARS-CoV-2 gRNA (Figure 28 A). This was the first indication towards concluding that siORF1 treatment before infection is a more plausible strategy to target incoming SARS-CoV-2 genome.

Besides targeting only, the incoming gRNA, it was still unclear if a simultaneous reduction of replicating gRNA and sgRNA is more efficacious to control the virus replication. As it was already observed that suppressing gRNA prior to transcription, significantly reduced the expression of both viral RNA species, an alternative experimental setup was needed to avoid the bias towards siRNAs targeting ORF1. Therefore, this time, the siRNAs were transfected into the cells 3 hours post infection, to avoid targeting the incoming gRNA and rather allow targeting of replicating gRNA and sgRNAs for a fair comparison. From the first looks, it was clear that the siRNAs targeting

the common regions indeed showed suppression of gRNA and sgRNA simultaneously. On the other hand, the siRNAs against ORF1 showed only the suppression of gRNA, as expected (Figure 28 B). The silencing of sgRNA was calculated by subtracting relative levels of gRNA from relative levels of total SARS-CoV-2 RNA. The common region targeting siRNAs also showed a significant reduction of viral gRNA as compared to the negative control siRNA treatment. However, siORF1 treatment still showed a stronger knockdown. These observations again pointed towards the practicability of siORF1 treatment in suppressing gRNA.

For a further comparison to identify the most efficient strategy, a similar experiment was performed where cells were transfected 3 hours post infection of rSARS-CoV-2-GFP (MOI 1.0) with individual siRNAs and the real-time viral spread was monitored. The results again exhibited a trend towards better control of viral spread when treated with siRNAs targeting ORF1 (Figure 28 C) as compared to other siRNAs. Notably, with common regions targeting siRNAs, an exponential increase in viral spread was observed as compared to a linear increase with ORF1-specific siRNAs at the later time points (from 56h post infection). Therefore, for an adequate comparison, the doubling times of GFP^+ cells were compared as representation of viral spread (Figure 28 D). In the siRNAs targeting ORF1 i.e. only the gRNA showed higher doubling times of viral spread as compared to the siRNAs additionally targeting the sgRNAs. Meaning, that, the efficient targeting of gRNA was consistently proved as a finer strategy to control SARS-CoV-2.

Lastly, the ability of the siRNA pools to prevent the cell-death was also compared. In brief, Vero E6 cells were transfected with different siRNA pools 6h before infection and were infected with *wildtype* SARS-CoV-2 (MOI 1.0). The number of dead cells at previously identified time point of 56h post infection was quantified with Incucyte® Live-cell imaging Analysis system using Incucyte® Cytotox red dye as described previously (Figure 28 E). In the absence of SARS-CoV-2 infection, all groups transfected with siRNA pools showed similar, yet very low levels of cytotoxicity as expected. Interestingly, in the infection settings, treatment with $siORF1_{pool}$ again proved advantageous in preventing cell-death as compared to other siRNAs. Collectively, these results repeatedly indicated the superiority of siRNAs targeting ORF1 over common region targeting siRNAs. It was thus concluded that, targeting genomic RNA of SARS-CoV-2 allows an efficient inhibition of viral replication, spread, and can prevent the virus-induced cell death.

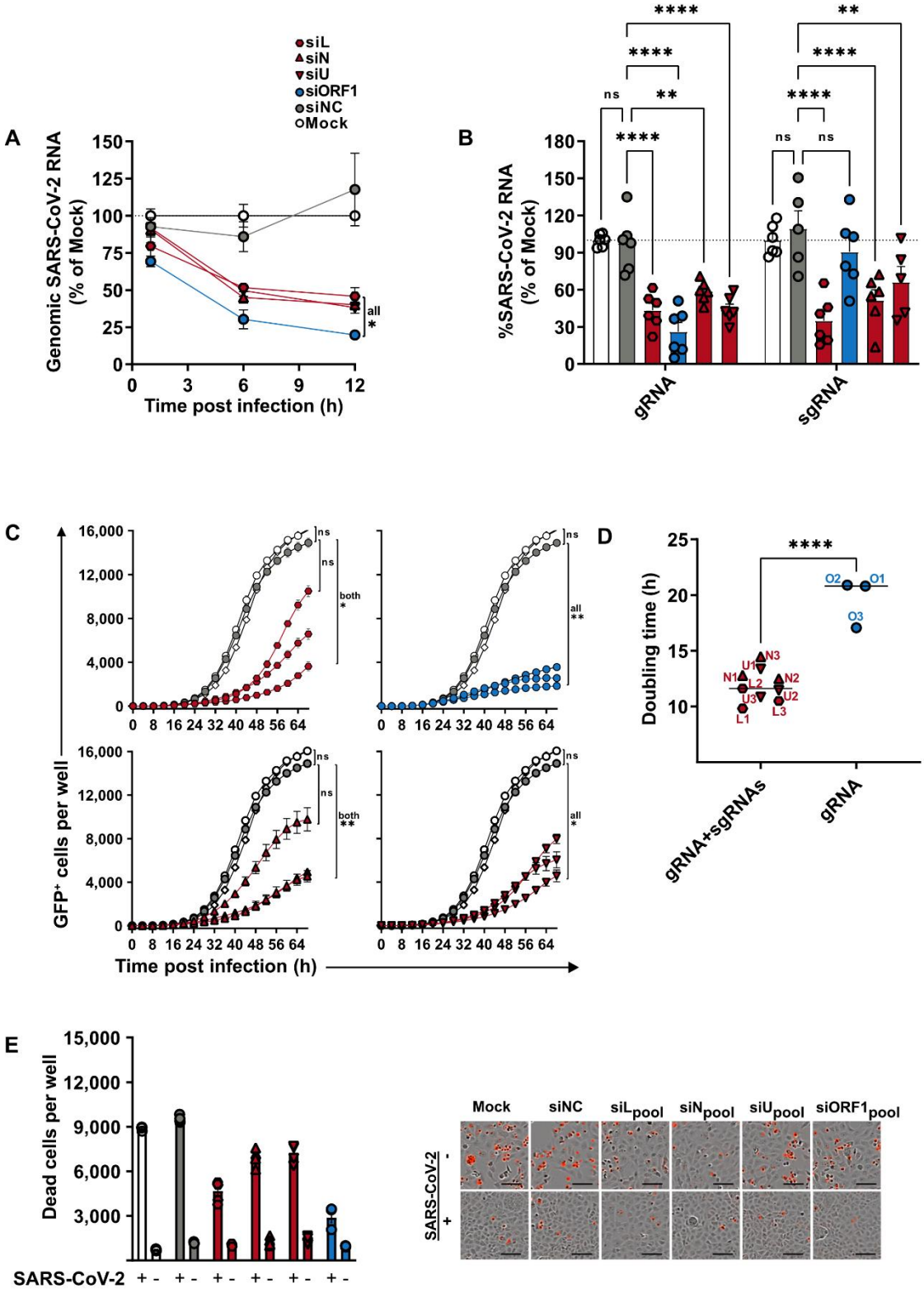

Figure 28: siRNAs targeting common regions can simultaneously suppress genomic and sub-genomic RNA but exhibit a lower efficiency than siRNAs targeting ORF1 [Adapted from: (Ambike et al., 2022)]. (A, B) Vero E6 cells were reverse transfected with pools of 3 siRNAs targeting separate regions of SARS-CoV-2 genome, either (A) 6 hours before infection or (B) 3 hours after infection with *wildtype* SARS-CoV-2 (MOI 0.1). The cells were lysed (A) at

different time points as indicated or (B) 24 hours post infection and viral RNA levels were quantified with RT-qPCR. **(A)** Effect of siRNAs targeting different SARS-CoV-2 regions on viral gRNA determined by qPCR. **(B)** Relative levels of genomic and sub-genomic SARS-CoV-2 RNAs upon siRNA treatment determined by RT-qPCR. **(C)** Real-time monitoring of GFP+ cells indicating viral spread in Vero E6 cells post siRNA treatment. Similar setup as (A) however, Vero E6 cells were infected with rSARS-CoV-2-GFP (MOI 1.0) and the viral spread was monitored for 68h with images taken at intervals of 4h. GFP+ cells with Incucyte® Live-Cell Analysis and were quantified with Incucyte® S3 software. **(D)** The doubling time in hours of GFP+ cells as an indication of viral spread in (C). **(E)** Number of dead cells per well upon siRNA treatment with and without infection in Vero E6 cells. Similar setup as (A) however, Vero E6 cells were infected with *wildtype* SARS-CoV-2 (MOI 1.0) and the number of dead cells was quantified 56 hours post infection with Incucyte® Cytotox Red dye. Images on the right depicts representative images from each group. Non-infected cells, Mock-transfected (Mock) cells as well as siRNA targeting Firefly luciferase (siNC) served as controls wherever indicated. (A, C) Arithmetic mean of triplicates or (B, E) individual values for each group is shown and the error bars indicate SEM. (D) Median of arithmetic mean for each group is indicated. Statistical significance is calculated using (A, E) ordinary one-way Anova and (B, C) two-way Anova with GraphPad 9.0. Mock – Mock transfected; h – hours; ns – non-significant; GFP – Green fluorescent protein; siNC – negative control siRNA targeting Firefly Luciferase; L1-3/siL#1-3. – L-specific siRNAs; O1-3/siORF1#1-3 – ORF1-specific siRNAs; N1-3/siN#1-3 – N-specific siRNAs; U1-3/siU#1-3 – 3'UTR-specific siRNAs; siL/siL$_{pool}$ – pool of siL1-3; siO/siORF1$_{pool}$ – pool of siO1-3; siN/siN$_{pool}$ – pool of N1-3; siU/siU$_{pool}$ – pool of siU1-3. *P < 0.05; **P < 0.01; ***P< 0.001; ****P < 0.0001.

2.2.2.5 Highly abundant sgRNAs can outcompete siRNAs targeting sgRNA additionally but not the siRNAs targeting gRNA only

In order to understand the underlying mechanisms for a finer activity of ORF1-specific siRNAs, the next set of experiments was performed. To begin with, the IC50 levels of the siRNA candidates were determined in the rSARS-CoV-2-GFP infection model (Figure 29 A). Evidently, the ORF1-specific siRNAs were more potent than the common region targeting siRNAs in the infection settings as compared to when tested with the dual-luciferase reporters (Figure 29 B). In continuation with previous results, this observation particularly strengthens the point that the siRNAs targeting only the gRNA outperforms the siRNAs targeting the common regions of SARS-CoV-2 only in the presence of replicating virus. In simpler words, it was observed that the SARS-CoV-2 replication has a significant impact on the siRNA activity.

This led to a hypothesis that highly abundant sgRNAs can outcompete the siRNAs targeting genomic and sgRNAs simultaneously, which is not the case with siRNAs

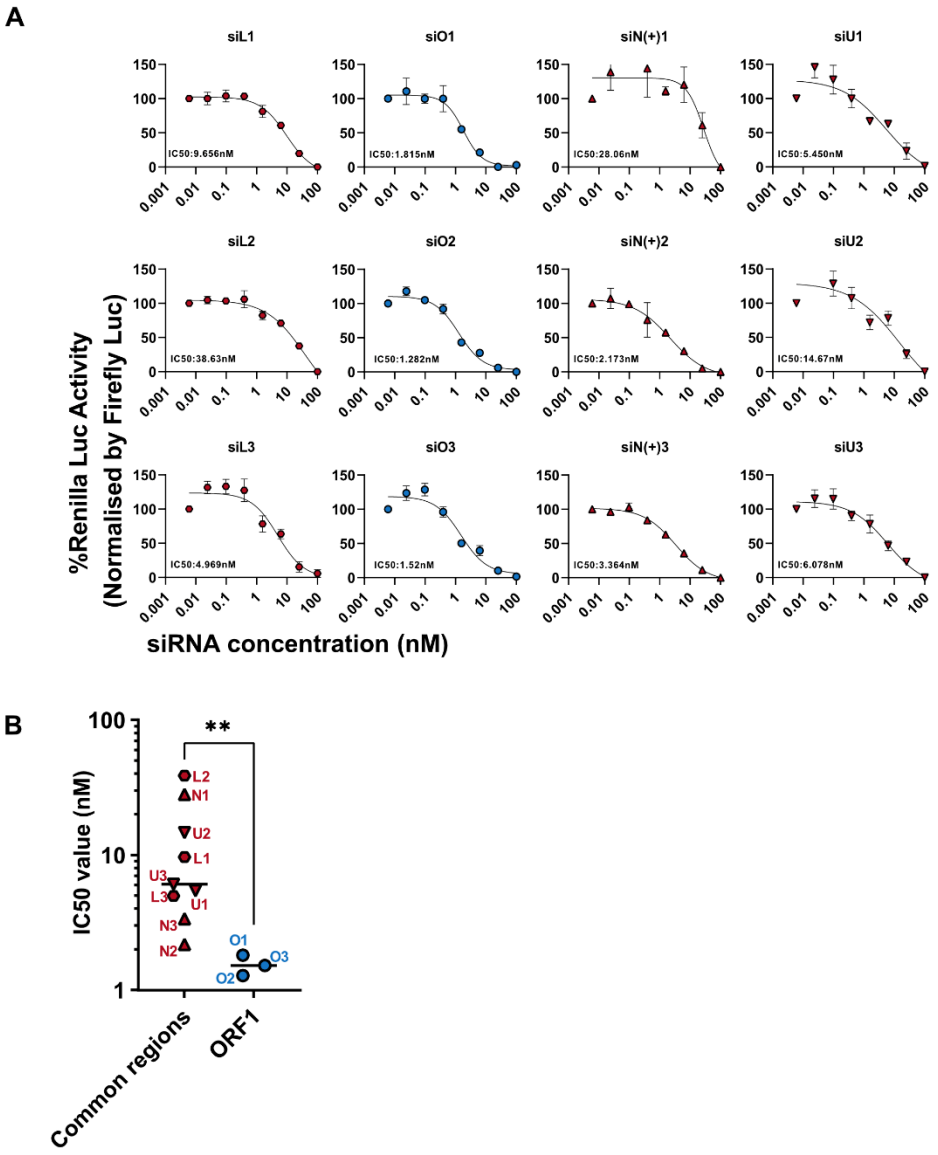

Figure 29: ORF1-specific siRNAs targeting only gRNA are more potent as compared to common region targeting siRNAs collectively in infection model [Adapted from: (Ambike et al., 2022)]. (A) Determination of mean inhibitory concentration (IC50) of siRNAs using rSARS-CoV-2-GFP infection model. Vero E6 were reverse-transfected with decreasing concentrations of siRNAs (100, 25, 6.25, 1.56, 0.39, 0.098, 0.024 and 0.006 nM) and were infected with rSARS-CoV-2-GFP (MOI 1.0) after 6h. The cells were monitored for viral spread for 24h in Incucyte© Live-Cell Imaging Analysis system. GFP+ cells were quantified using Incucyte S3 software. IC50 values were determined using non-linear regression in GraphPad 9.0. **(B)** Comparison of IC50 values between siRNAs targeting common regions of all viral transcripts (L, N and 3'UTR) and only genomic RNA (ORF1). (A) Arithmetic mean of triplicates with error bars indicating SEM or (B) median of arithmetic mean of triplicates for all groups is shown. Statistical significance was calculated using Mann-Whitney test in GraphPad 9.0. siL1-3 – Leader sequence specific siRNAs;

siO1-3 – ORF1 specific siRNAs, siN(+)1-3 – positive sense Nucleocapsid gene specific siRNA; siU1-6 3'UTR specific siRNAs; nM – nanomolar; ns – non-significant. **P< 0.01.

targeting only gRNA. In the initial approximation, the impact of viral replication on the siRNA activity was checked. A concentration of 50 nM employed in majority of the experiments proved repeatedly unsuccessful to pinpoint the varying efficacies of the siRNAs (data not shown). In brief, relatively low concentrations (1 nM) of siRNA targeting both gRNA and sgRNA (siN#2) or solely the gRNA (siORF1#2) were transfected individually in Vero E6 cells. The cells were then infected with increasing MOIs of rSARS-CoV-2-GFP (0.03, 0.3 and 3). The two siRNAs were chosen based on their comparable observed IC50 values. Interestingly, 24 hours post infection, both the siRNAs could achieve a similar level of inhibition of viral replication when the cells were infected with the lowest MOI of 0.03. However, with an increasing MOI, the sgRNA-RNA targeted siN#2 showed a significant loss of activity as compared to the gRNA-only targeting siORF1#2 (Figure 30 A). This served as an initial indication that the high-abundance of sgRNAs could render the siRNAs less effective by out-competition. Rationally, to substantiate these observations, it was further tested if an increased dosage could rectify this effect. Vero E6 cells were thus reverse-transfected with increasing dosage (0.1 nM, 1nM, 10 nM and 100 nM) of the same siRNAs and were infected with a relatively fair MOI (0.3) of rSARS-CoV-2-GFP. Interestingly, it was noted that the siORF1#2 was more efficacious than siN#2 only at the lower concentrations (0.1 and 1 nM). At the concentrations much higher than respective IC50s observed with rSARS-CoV-2GFP, both the siRNAs showed a similar antiviral activity (Figure 30 B). Thus, it was further confirmed that a competition with sgRNA could render the siRNAs that target the sgRNAs additionally less efficient and this effect could be compensated by an increased siRNA dosage.

To further corroborate the fact that viral replication influences the siRNA activity, a luciferase competition experiment was set up. 4 siRNAs targeting different regions of SARS-CoV-2 – siL#2, siORF1#2, siN#2 and siU#2 (chosen based on comparable IC50s) were co-transfected with respective luciferase reporters into HEK293T cells at a concentration of 10 nM. 6h after co-transfection, the cells were infected with *wildtype* SARS-CoV-2 and 24h post infection, the cells were lysed for dual luciferase assay (Figure 30 C, left). It must be understood that in such experimental setting, the mRNA transcribed from the luciferase reporter as well as SARS-CoV-2 RNA species generated during replication could constitute as target sites for all siRNAs. Therefore, a loss of

activity against the luciferase reporter could confirm the impact of competition by the target sites generated due to active viral replication.

Indeed, these results depicted that the ability to silence dual luciferase reporters of siRNAs targeting both genomic and sgRNAs was significantly impaired. On the other hand, the siRNAs targeting the gRNA exclusively, showed a similar level of silencing of luciferase reporters even in the presence of active viral replication (Figure 30 C, right). In conclusion, this data proved that the reduced efficiency of the siRNAs targeting sgRNAs additionally is a result of out-competition by highly abundant sgRNAs.

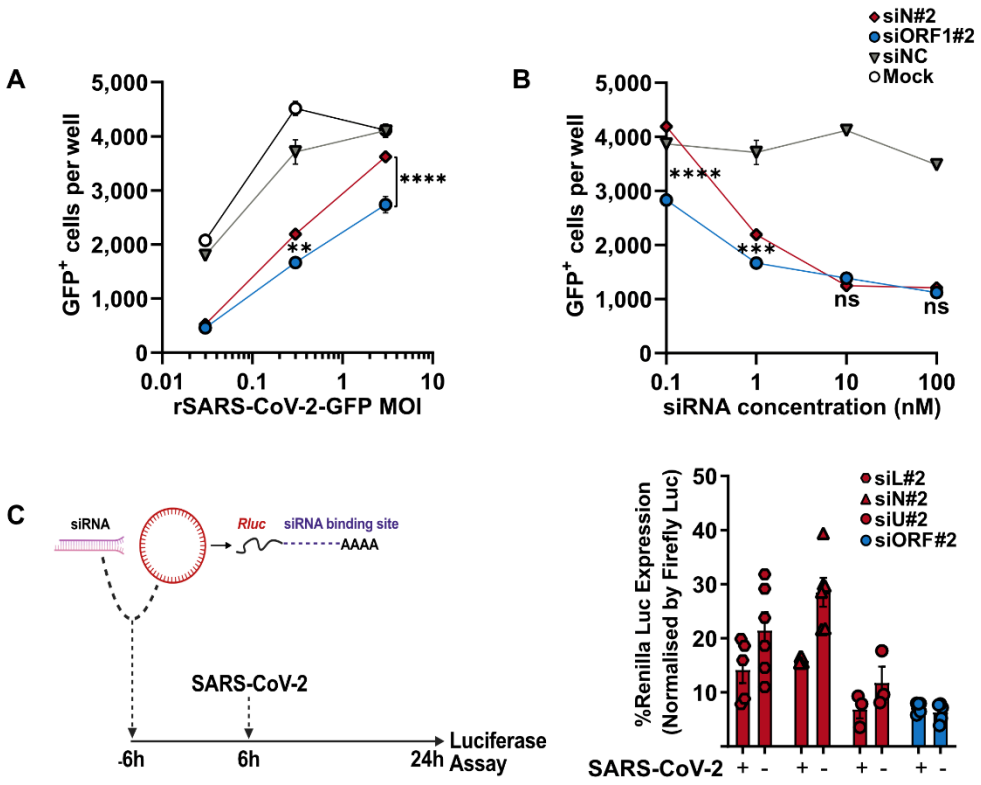

Figure 30: SARS-CoV-2 sgRNAs out-compete the siRNAs targeting sgRNAs additionally [Adapted from: (Ambike et al., 2022)]. (A, B) Vero E6 cells were reverse transfected with either (A) 1 nM or (B) varying dose of siRNAs targeting N or ORF1. 6 hours post transfections, the cells were infected with rSARS-CoV-2-GFP with either (A) varying MOIs or (B) MOI of 0.3. Number of GFP+ virus infected cells determined with Incucyte® Live-Cell Image Analysis after 24 hours of infection. **(A)** Comparison of activity of siRNAs targeting common regions or only gRNA at varying MOIs. **(B)** Comparison of activity at varying doses of siRNAs targeting common regions or only gRNA. siRNA targeting Firefly luciferase (siNC) served as negative control. **(C, left)** Experimental design for luciferase-competition experiment. HEK293T cells were co-transfected with individual siRNAs along with their luciferase reporters and were infected with *wildtype* SARS-CoV-2 (MOI 0.1) 6h post co-transfection. 24 hours after infection, the cells were lysed for dual luciferase assay.

(C, right) Dual-luciferase assay comparing siRNA activities from the competition experiment. Graphs indicate normalised Renilla luciferase activity corresponding to siRNA silencing activity. Cells co-transfected with negative control siRNA targeting GFP along with respective reporter vector served as negative control. Firefly luciferase activity was used for normalization and percent Renilla luciferase activity was calculated with respect to that of the negative control group. (A, B) Arithmetic means of triplicates or (C, right) individual values are indicated for each group. The error bars indicate SEM. Statistical significance was calculated using (A, B) two-way Anova and (C, right) unpaired t-test for independent samples. GFP – Green Fluorescent Protein; nM – nanomolar, MOI – multiplicity of infection; siL2 - L-specific siRNA #2, siO2 – ORF1-specific siRNA #2; siN2 – N-specific siRNA #2; siU2 – 3'UTR-specific siRNA #2; siNC – negative control siRNA, Mock – Mock transfected; h – hours, Rluc – Renilla luciferase. ns – non-significant; *P < 0.05; **P < 0.01; ***P < 0.001; ****P < 0.0001.

2.2.2.6 Physiologically more relevant *ex vivo* human lung model confirms the antiviral activity of ORF1-specific siRNAs

Final validation of the siRNA-therapy was achieved using a more sophisticated approach, where a highly relevant infection model of human precision cut lung slices (hPCLS) along with chemically modified siRNAs were employed. Initially, the siRNAs were subjected to chemical modifications and were tested for the retention of their silencing activities using the luciferase reporters in HEK293T cells. Interestingly, the results indicated a slight loss of activity for siORF1#1 and #2, whereas for #3, a slight gain in silencing activity was noted (Figure 31 A). Furthermore, with repeated dual-luciferase assays, the kinetics of siORF1#3 in either chemistry was compared for a stable knockdown. As expected, in line with the results reported in the section 2.1.2, the siRNA showed a stronger and prolonged knockdown upon chemical modifications (Figure 31 B).

Subsequently, the chemically modified siORF1#3 also showed improved control of viral spread than its chemically unmodified counterpart in Vero E6 cells (Figure 31 C). Finally, the ability of chemically modified siORF1#3 to suppress SARS-CoV-2 replication in hPCLS (kindly provided by Dr. Gerald Burgstaller, Comprehensive Pneumology Center, Helmholtz Munich) was tested. Since hPCLS are a complex ex vivo 3D tissue culture model of primary human lung cells, the siRNAs were delivered to the lung slices using Polyethyleneimine (PEI; kindly provided by Prof. Dr. Olivia Merkel, Department of Pharmacy, Ludwig Maximilian University of Munich), which has been previously proved suitable for an *in vivo* siRNA delivery (Mehta, Michler, & Merkel, 2021). A relatively higher dose (100 nM) of chemically modified siORF1#3 was transfected in the hPCLS, 6h

before infection with *wildtype* SARS-CoV-2 (MOI 1.0 assuming 300,000 cells per well) and the RT-qPCR to determine SARS-CoV-2 gRNA expression was performed 24h post infection. Indeed, in such a physiologically realistic model of human lung, ORF1-specific siRNA showed significant reduction of viral replication by more than 90 % (Figure 31 D). Overall, the results could shed a light upon the siRNA-accessible replication steps of SARS-CoV-2. It was evidently shown that the siRNAs, when transfected before infection, could target the incoming viral gRNA after cell entrance, stopping the replication before transcription and preventing virus-induced cell death. Surprisingly the low-abundant negative sense viral RNA transcripts were inaccessible for siRNAs. A single siRNA targeting common regions present in all viral RNA transcripts could simultaneously inhibit the genomic and sub-genomic viral RNAs. As the high abundant viral sgRNAs could not out-compete siRNAs targeting open reading frame 1 (ORF1), which is only in gRNA, therefore, ORF1-specific siRNAs suppressed viral replication the most. Lastly, the inhibition of viral replication in human lung slices with chemically modified siRNAs highlighted the potential of siRNA-based therapeutic strategy to combat COVID-19.

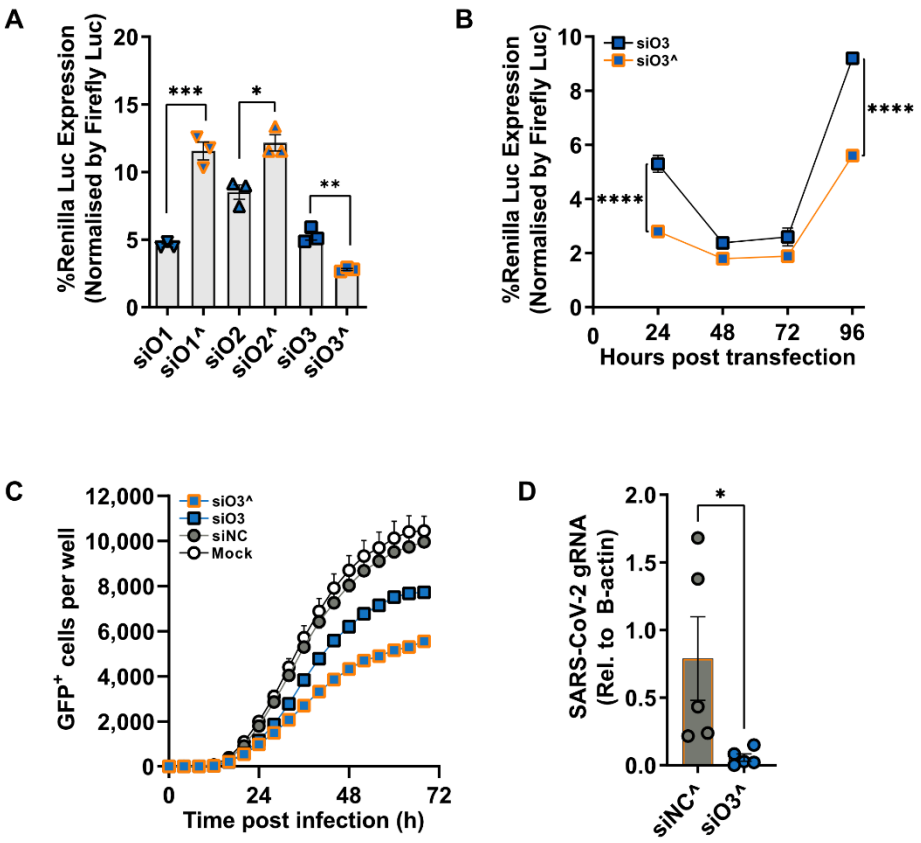

Figure 31: Chemically modified siRNAs show improved antiviral activity and are effective in ex vivo human lung model [Adapted from: (Ambike et al., 2022)]. (A, B) HEK293T cells were co-transfected with ORF1-specific siRNAs in either chemistry as well as the respective

luciferase reporters. Dual luciferase assay was performed either at (A) 24 hours post transfection or (B) at various time intervals. **(A)** Comparison of siRNA activity between chemically modified and unmodified ORF1-specific siRNAs. **(B)** Activity kinetics of siORF1#3 in either chemistry. Cells co-transfected with negative control siRNA targeting GFP along with respective reporter vector served as negative control. Firefly luciferase activity was used for normalization and percent Renilla luciferase activity was calculated with respect to that of the negative control group. **(C)** Real-time monitoring of viral spread upon siRNA treatment. Vero E6 cells were reverse transfected individually with siRNAs of either chemistry (50 nM) 6h before infection with rSARS-CoV-2-GFP (MOI 1.0). The GFP+ cells were visualized for 68h with images taken at the intervals of 4h, with Incucyte® Live-Cell Imaging Analysis system and GFP+ cells were quantified with Incucyte S3 software. **(D)** Suppression of SARS-CoV-2 gRNA by chemically modified siORF1#3 in human precision cut lung slices. Chemically modified siORF1#3 (100 nM) was transfected with PEI in hPCLS. 6h post transfection, the lung slices were infected with *wildtype* SARS-CoV-2 (MOI 1 considering 300,000 cells per well). RT-qPCR was performed 24h post infection to determine viral gRNA levels. siRNA targeting Firefly luciferase (siNC) and mock-transfected cells served as negative controls wherever indicated. (A, D) Individual values or (B, C) arithmetic mean of triplicates are shown for each group and error bars indicate SEM. Statistical significance was calculated with (A, D) unpaired t-tests for independent samples and (B, C) two-way Anova using GraphPad 9.0. Luc – Luciferase; siO1-3 – ORF1-specific siRNAs; siNC – negative control siRNA; Mock – Mock transfected; ^ - chemically modified siRNA; GFP –Green Fluorescent Protein; h-hours. *P < 0.05; **P < 0.01; ***P < 0.001; ****P < 0.0001.

3 Discussion

RNAi has been widely applied in developing antiviral therapeutic strategies. Novel therapeutic strategies against viruses causing chronic illness such as HBV as well as emerging viruses like SARS-CoV-2 are constantly under demand. This thesis is focused on utilizing RNAi-based suppression of immunomodulatory components in the liver, as a combinatorial immunotherapeutic strategy together with therapeutic vaccination to treat chronic hepatitis B. Additionally, the focus of this work was also extended towards identifying the most promising strategy to inhibit SARS-CoV-2 replication through RNAi.

3.1 Optimizing a combinatorial immunotherapy against chronic HBV infection constituting RNAi and therapeutic vaccination

3.1.1 Checkpoint inhibition to supplement immunotherapy in the immunosuppressive environment of the liver

In addition to a vital metabolic organ, the liver also function to filter our certain pathogens from the blood or food (Protzer et al., 2012). As a result of constant pathogenic exposure, the liver seemed to have developed a unique immune tolerant environment to avoid hypersensitivity (M. Zheng & Tian, 2019). Nevertheless, the liver is equipped with functional innate and adaptive immune responses with a potential to mount a robust response under certain conditions (Kubes & Jenne, 2018). However, a persistent infection of liver such as a chronic HBV infection could lead to a weakened adaptive immune response readily described as ‘exhaustion’, which is mainly associated with a poor or an absent $CD8^+$ T cell response (B. Ye et al., 2015). In an exhausted state, the antigen specific T cells exhibit a loss of cytokine production, and more importantly, an increased expression of inhibitory receptors such as PD-1 and TIM-3 (Jin et al., 2010; J. Ma et al., 2019). Therefore, several studies have underlined the enhancement of various therapeutic strategies by additional checkpoint inhibition in the context of HBV and other closely related pathogens (Bunse et al., 2022; J. Liu et al., 2014).

Additionally, regulatory T cells (T_{regs}) are known for their immune suppressive functions and have been reported in increased frequency in the liver as well as in the periphery during chronic HBV infection (Billerbeck, Bottler, & Thimme, 2007; Fu et al., 2006; Lapierre & Lamarre, 2015; D. Xu et al., 2006). A previous study at the institute has reported the involvement of T_{regs} in mitigating effector T cell response and prolonging the

viral clearance (Stross et al., 2012), suggesting, a systematic inhibition of T_{reg} induction could enhance the immune reactivation by therapeutic vaccine. One way to achieve this could be the local inhibition of TGF-ß1, which has been identified as one of the major regulators of the T_{regs} (Dardalhon et al., 2008; Wan & Flavell, 2007).
Administration of a therapeutic antibody for checkpoint inhibition in liver could have immune-related adverse effects (Y. Matsuda, Toda, Kato, Kuribayashi, & Kakimi, 2006; Nadeau, Fecher, Owens, & Razumilava, 2018; Poralla et al., 1987). Moreover, indiscriminative blocking of pleiotropic cytokine such as TGF-ß1 with antibodies can also lead to deleterious events (C. J. Martin et al., 2020; Shi et al., 2022), highlighting the need of a systematic and selective TGF-ß1 inhibition. One way to circumvent this is employing highly active siRNAs against ligands of the inhibitory receptors (PD-1, TIM-3) – PD-L1 and Gal-9 as well as against TGF-ß1 for an organ-specific or a cell-specific knockdown. In addition to these three factors, other factors such as IL-10 and Cytotoxic T-lymphocyte-associated protein 4 (CTLA4) have also been described as major contributors of immune suppression in the liver (Kalathil, Lugade, Miller, Iyer, & Thanavala, 2013; T. Y. Li, Yang, Zhou, & Tu, 2019; Saxena, Chawla, Verma, & Kaur, 2014), but were not the focus of this thesis.

3.1.2 *In vitro* screening and selection of candidate siRNAs

After two decades of the development process, five siRNA drugs are currently approved by the United States Food and Drug Administration (FDA) (Mullard, 2022; Padda, Mahtani, & Parmar, 2022). Given the recent advancements in the field, several siRNAs as well as anti-sense oligonucleotides (ASOs) as antivirals or immunotherapy, have been under clinical investigation (Proia et al., 2020; Qureshi, Tantray, Kirmani, & Ahangar, 2018; Yuen et al., 2020). Despite this, currently, two main challenges limit the application of siRNAs in clinical settings – a systematic delivery to a specific organ or a cell type and the off-target effects mediated by homologous gene sequences (Draz et al., 2014). Therefore, choosing the finest sequence with the *in vitro* screening of the siRNAs is an essential first step. To address these issues, while designing the siRNAs, the sequences were subjected to determination of potential off-targeting score or POTS score purely based on the bioinformatical predictions, in the very beginning (Boudreau et al., 2013). Here, a low POTS score was associated with lesser off-target activity of the siRNA sequences, predicted by homology comparison of the 7-mer seed sequence. As a result, a POTS score threshold of 50 was decided, and siRNAs with the lowest possible POTS score were chosen during the designing.

In vitro pre-screening of siRNAs could clearly suggest the candidate siRNAs for further development. In the beginning, similar levels of PD-L1 knockdown were observed with Lipofectamine 2000 and Lipofectamine RNAiMAX (see 2.1.1.1). However, as reported elsewhere (T. Wang, Larcher, Ma, & Veedu, 2018), RNAiMAX was chosen experiments for exhibiting lower cytotoxicity along with higher efficiency. Furthermore, the siRNAs could suppress the target mRNA efficiently 48h post transfection. However, the siRNA activity was demolished at 96h post transfection at mRNA levels (see 2.1.1.1). Such a drastic and rapid loss of siRNA activity suggested the intracellular degradation of the chemically unmodified siRNAs. This could be challenging to achieve a stable knockdown in clinical settings given the protein turnover and longer half-life of proteins such as PD-L1 (Hsu, Li, Lai, & Hung, 2018). Moreover, chemically unmodified siRNAs may induce type 1 Interferons (IFN) via pattern recognition receptors (Meng & Lu, 2017). This could result in a contrasting effect, as PD-L1 is an interferon-stimulated gene (ISG) (Garcia-Diaz et al., 2017). This could be the reason behind the observed upregulation of PD-L1 specifically upon siPD-L1#3 treatment (see 2.1.1.2). Such an effect highlights the potential drawbacks of employing RNAi against ISGs such as PD-L1. On the other hand, the basal expression of Gal-9 in RAW264.7 cells was found to be barely detectable and did not increase upon IFN treatment of cells (data not shown). Therefore, the conventional methods for siRNA screening for these two targets indeed proved unsuitable.

In comparison, the screening for siRNAs against TFG-ß1 was relatively uncomplicated. However, the bovine TGF-ß1 present in fetal bovine serum (FBS) supplemented for the cell growth and maintenance was cross-reactive upon HCL-based activation in the ELISA. This could lead to a loss of accuracy to determine the knockdown of secreted TGF-ß1 upon siRNA treatment. To circumvent these limitations of conventional screening methods, the dual-luciferase reporter system was chosen for the screening. This allowed a rapid, reliable, economical, and high throughput screening of the siRNAs in a single attempt, for all the genes of interest. Here, normalization with the *Fluc* proved advantageous for an accurate measurement of the siRNA knockdown. Since the complete target gene was cloned into the reporters, the potential effects of secondary RNA structures on the loss of siRNA activity were also accommodated in these readouts. Overall, the pre-screening of siRNAs is essential to point-out the potential candidates of interest from a relatively larger number of siRNAs.

3.1.3 Chemical modifications of the siRNAs

The obstacles associated with chemically unmodified siRNAs have been discussed earlier. A methodical, position-specific chemical modification of the siRNAs could bypass these challenges. The chemical modifications of the siRNAs have a broad application in drug discovery. Ideally, they must confer an enhanced stability, specificity, and potency to the siRNA (Selvam, Mutisya, Prakash, Ranganna, & Thilagavathi, 2017). Earlier extensive studies on position specific chemical modifications have reported that *2'-O* modifications in the ribose moiety of nucleotides were advantageous for RNAi (Kraynack & Baker, 2006; Selvam et al., 2017). The preferred chemical modifications typically include 2'-OMe, 2'-F and 2'-MOE modifications along with a phosphodiester linkage at the terminals of sense and anti-sense strands (Kenski et al., 2012; S. Y. Wu et al., 2014). In this thesis, the siRNAs were chemically modified based on a recently approved RNAi drug, Lumasiran, as it was a result of extensive clinical testing (CRASTO, 2020; Garrelfs et al., 2021) (see 2.1.2.1). The chemical modifications indeed conferred extracellular durability to the siRNAs. Furthermore, chemically modified siRNAs also allowed a prolonged knockdown of target gene (see 2.1.2.2), suggesting the intracellular stability of siRNA. This could be of benefit for *in vivo* or clinical applications of the siRNAs, where a prolonged, stable knockdown could prove essential over a stronger and shorter knockdown. Even though the chemical modifications are well-tolerated by the siRNAs, they may not always be favorable for the activity (J. Zheng et al., 2013). A similar effect was also observed with some of the siRNAs in this study. Particularly, siTGF-ß1#2 and 5 exhibited a significant loss of activity upon chemical modifications (see 2.1.2.2). Considering these facts, multiple siRNAs must be potentially tested as candidates, which however, could turn out less economical in the long run. Despite the discussed advantages of chemical modifications, it must be noted that due to the time constraints, an *in vivo* evaluation of any of the siRNAs could not be conducted. An extensive pre-clinical testing of the candidate siRNAs is therefore a must to corroborate the findings reported in this thesis.

3.1.4 Limitations of the *in vitro* based model systems

As mentioned previously, the success of an RNAi therapeutic intervention largely relies on precise delivery of the agent. Despite recent advancements and development of GalNac conjugated siRNAs, an extra-hepatocyte delivery of siRNAs remains as a major hurdle (Brown et al., 2022). Considering the focus of this thesis, identifying the cell type of interest or the virus permissive cell type in the organ is of high importance prior to

exploring a suitable delivery agent. This is especially relevant, due to the existence of tissue-specific immune cells (Weisberg, Ural, & Farber, 2021), where a non-systematic delivery to non-relevant immune cells could lead to induction of innate immune response. Following on these lines, HSCs were focused as the major producers of the TGF-ß1 in the liver based on previous studies (Tahashi et al., 2002). However, several other cells have also been proposed to be contributors of TGF-ß1 secretion in liver (Schon & Weiskirchen, 2014), which could argue against the flawed experimental design.

Due to unavailability of a mouse hepatic stellate cell-line, and failure of isolating primary murine hepatocytes, the initial experiments were performed with LX-2, a human hepatic stellate cell-line (L. Xu et al., 2005) (see 2.1.3.1). This could not allow the further testing of the siTGF-ß1#8 in co-culture settings. Moreover, during the co-culture experiments, the LX-2 could not tolerate the DMSO, which is essential for differentiation of HepG2-NTCP cells and HBV infection. Therefore, a considerable cytotoxicity was observed during the co-culture experiments. Looking at the unsuitability of the *in vitro* models, HSCs also exhibit a tendency to undergo self-activation when cultured for a longer duration (Mannaerts et al., 2020), which does not allow the assessment of upregulation of TGF-ß1 in co-culture setting for a longer period of time. Similarly, the pHSCs exhibited an identical tendency which was further circumvented to some extent with a serum-free culturing of the HSCs. However, this may not be ideal for a long-term maintenance of the cells and thus must be optimized further with serum-replacement alternatives. Given these limitations, an *in vivo* monitoring of activation of HSCs during chronic HBV infection through more sophisticated transcriptomic methods could shed a light on their role as the producers of TGF-ß1 in the liver.

3.1.5 Expression of HBV mosaic capsid particles from a single construct

The protein-prime phase of therapeutic vaccination comprising purified HBsAg and HBcAg is essential for priming the virus-specific adaptive immune response (Backes et al., 2016). For such purpose, each component of the vaccine must be thoroughly characterized and must meet the high standards of good manufacturing process (WHO, 2016). Considering the global distribution of major circulating HBV genotypes worldwide (Velkov et al., 2018), the novel mosaic capsid particles were designed to represent the complete T-cell epitope repertoire from all the major circulating HBV genotypes. Due to the high sequence homology in the core region (McNaughton, Revill, Littlejohn, Matthews, & Ansari, 2020), processed HBcAg of genotype C and D together can

contribute as T-cell epitopes for all the major genotypes. However, owing to the novelty of the mosaic capsid particles, preliminary, it was of great significance to confirm the occurrence of HBcAg from both genotypes from a single construct.

HBV capsids can self-assemble and thus, can be efficiently expressed in competent *E. coli* (Newman, Suk, Cajimat, Chua, & Shih, 2003). For the expression of the mosaic capsid particles, a pRSF construct (Novogene) was used harboring two individual promoters regulating individual HBV core genes of two genotypes. For a facile detection by the conventional analytical methods, genotype C HBcAg was C-terminally truncated (C_{Δ}) without compromising the ability to form functional capsids (Kang, Yu, & Jung, 2008). Upon initial assessment (see 2.1.4.1), both C_{Δ} and D HBcAg were successfully expressed from a single construct within 5 hours of induction. Initially the C_{Δ} HBcAg was expressed under AHT promoter, while D HBcAg was expressed under a T7 promoter. Such an arrangement could argue against achieve the equal levels of induction with two different chemical inducers – AHT and IPTG. Therefore, in the later parts, the AHT promoter was switched to a second T7 promoter to avoid the imbalance in expressing HBcAg due to variance in the promoter activities. However, it must be noted that, irrespective of the inducible promoters employed, a comparison between the expression ratios of HBcAg of either genotype within a preparation was not possible, primarily due to the protein aggregates. Furthermore, during the detection of HBcAg by western blotting, the AD09 antibody (Core facility, Helmholtz Munich) was observed to possess varying preferences to detect HBcAg of two genotypes in each experiment. Nevertheless, the results could qualitatively corroborate the occurrence of C_{Δ} and D HBcAg fairly.

3.1.6 Purification of the HBV mosaic capsid particles

Apart from vaccination or immunization studies, purified viral capsids or virus-like particles (VLPs) have a wide range of applications such as to study potential small molecule inhibitors as therapeutic agents, structural studies as well as in diagnostics (Le & Muller, 2021). To conduct any of such study, highly purified VLPs, free from any contaminants are a must. Considering the HBV capsids, primarily, sucrose-gradient ultracentrifugation or chromatography-based purification methods are being commonly used for purification (Z. Hu et al., 2020; Ng et al., 2018). Additionally, the expression and purification of single genotype HBV capsids composed of full length as well as C-terminally truncated HBcAg have been described (Newman et al., 2003). Despite the similar abundant reports on HBV capsids, the generation of mosaic capsid particles was

a first-of-its-kind study. Therefore, modifying the prior available methods, adequate purification protocols for sucrose-gradient and IEX-based purification of mosaic capsid particles were established in this thesis (see 2.1.4.2 and 2.1.4.3). The observations derived from the experiments also helped recognize the advantages and limitations of both the techniques. Firstly, both the purification methods could offer a suitable level of purification of mosaic capsid particles. Sucrose gradient-based purification was comparatively rapid with adequate resolving power whereas, the IEX-based purification offered a higher degree of purification with improved yield. Even though a significant loss of protein was observed during the consecutive runs of both methods, IEX-based purification was ascendable, yielding about 5-fold higher amount of purified capsids as compared to sucrose-gradient ultracentrifugation. Moreover, both methods required post-processing of the samples to remove excess sucrose or the elution buffer for a longer storage of the capsids. In essence, the SDS-PAGE analysis revealed that IEX-based purification proved superior with less detectable contaminants in the preparation. This could be justified by manual elution of the gradient in sucrose gradient-based purification as compared to more precise and automatic elution in the IEX. However, these observations clearly indicate the need of further optimizing purification methods for mosaic capsid particles.

3.1.7 Confirmation of occurrence of HBV mosaic capsid particles and the structural analysis

Given the novelty of the mosaic capsid particles, it was of high importance to confirm the formation of intact capsids composing HBcAg of both genotypes. A varied mobility of $C_{\Delta}D$ mosaic capsid particles in NAGE was the initial indication for the formation of HBV mosaic capsid particles (see 2.1.5.1). HBV capsids are able to encapsulate heterologous bacterial RNA (Porterfield et al., 2010). Normally, during the infection setting, the *wildtype* HBV capsids encapsulate about 3.5 kb of pre-genomic viral RNA. On the other hand, the truncated capsids were reported for their tendency to encapsulate a shorter, 2.2 kb of RNA species in addition (Le Pogam, Chua, Newman, & Shih, 2005). This could argue against the varied mobility of different HBV capsids however, a band representing $C_{\Delta}D$ appeared to have migrated between C_{Δ} and D capsids respectively. Till this point, a clear indication for the occurrence of $C_{\Delta}D$ mosaic capsid particles was still missing. To shed a light on this, a new construct coding for mosaic capsid particles, where D was replaced by a biotinylated D HBcAg using site-specific biotinylation. The site-specific biotinylation was achieved by *E. coli* biotin ligase (BirA) through linking free biotin to the lysine of 15

amino acid long AviTag peptide, added to the 5' terminal of the D HBcAg sequence. As a result of which, the mosaic capsid particles expressed by this construct harbored a biotinylated D and the C_{Δ} HBcAg ($C_{\Delta}D_{bt}$). Even the pull-down assay could confirm the co-presence of C_{Δ} HBcAg in D_{bt} containing pulled capsids, the experimental design could not completely disprove the occurrence of D-only HBV capsids. Interestingly, the western blot analysis performed from the final elutes of the pull-down assay showed rather higher amounts of C_{Δ} HBcAg in comparison to D_{bt} in pulled capsids (see 2.1.5.2), suggesting the lower-probability of the presence of D_{bt}-only capsids. Furthermore, a collaborative experiment for an in-depth analysis with NMR spectroscopy corroborated that the $C_{\Delta}D$ mosaic capsid particles are indeed expressed from a single construct and are composed of C_{Δ}- C_{Δ}, D-D homodimers as well as C_{Δ}-D chimeric heterodimers (data not shown).

3.2 Systematic Analysis of RNAi-accessible replication steps of Severe Acute Respiratory Syndrome Coronavirus 2 (SARS-CoV-2)

3.2.1 Designing of siRNAs against various regions of SARS-CoV-2

Application of siRNAs as a potential antiviral therapeutic strategy is not novel (Qureshi et al., 2018). Few recent reports provided a proof of concept that siRNAs could indeed target SARS-CoV-2 (Chang et al., 2022; Idris et al., 2021). However, none of these studies reported a detailed analysis of siRNA-accessible replication steps of an RNA virus, let alone SARS-CoV-2. Therefore, in this study, with a systematic analysis of intra-cellular replication steps of SARS-CoV-2, it was concluded that targeting of the incoming genome of SARS-CoV-2 could be the most efficient way of suppressing viral replication. Such in-detailed studies could prove key in devising novel antiviral strategies against emerging virus infections.

Four different regions of SARS-CoV-2 genome – L, ORF1, N and 3'UTR were chosen as the potential targets for the siRNA therapy. The ORF1 alone spans to over 2/3rd of the viral genome, whereas the rest of the ORFs take up the remaining 1/3rd of the genome (D. Kim et al., 2020). In contrast to ORF1, the N gene is about 1.5 kb long whereas the 3'UTR region and the 5' L sequence is about 330 bp and 60 bp long respectively. Since the siRNA-designing tools make use of the seed sequence provided manually, this could essentially raise a question whether the longer length of ORF1 region allowed selection of more efficient siRNAs to begin with. Therefore, the pre-screening of siRNAs was essential to answer these issues since the designing of the

siRNAs was purely based on predictive assessment. Apart from the results (see 2.2.2), the predictions for stability of secondary structures of the siRNAs corresponding to the activity of the siRNAs (Andrews, Roche, & Moss, 2018), showed no significant differences (data available in (Ambike et al., 2022)). This was enough evidence to deny the siRNA designing bias towards ORF1-specific siRNAs. Such confirmation is of significance especially when the findings of this project contradicted the previous report on the closely related SARS-CoV-1 to some extent. It was reported that the siRNA-based targeting of a common region, the Leader sequence, present in all RNA transcripts was proven superior to that of targeting the S ORF, which is present in relatively lesser number of RNA transcripts (T. Li et al., 2005). Nevertheless, screening of total 28 siRNAs against SARS-CoV-2 with at least 5 siRNAs designed against each region attributes as a major advantage of this study.

3.2.2 Preliminary screening of siRNAs of either sense

Assessment of antiviral activities of large number of siRNAs could be laborious and expensive, specifically with conventional methods such as qPCRs, plaque assays and in-cell ELISAs. Therefore, in such scenario, a pre-screening could prove rather utilitarian for a systematic assessment and narrowing down the number siRNAs with a rapid method. The benefits of the dual luciferase-based screening of the siRNAs have been discussed previously in this section. However, the results obtained during this project suggested that the siRNA activity observed with the luciferase reporters does not necessarily translate to the antiviral activity of the siRNA (further clarified in (Ambike et al., 2022)). Principally, the luciferase reporters do not produce high-abundant sub-genomic RNA transcripts containing binding sites, as observed in active SARS-CoV-2 replication. Therefore, only the siRNA activity due to the affinity towards the binding site, without undertaking the effects of viral replication and infection could be assessed with the luciferase reporters. In simpler words, such a screening method, although extensively utilized (Khaitov et al., 2021), are excellent preliminary indication, however, must not be the only deciding factor for screening especially antiviral RNAi agents.

Secondly, unlike the cellular genes such as TGF-ß1, the enormous size of the ORF1 impedes the construction of the luciferase vector harboring the complete gene. As a result, each siRNA required a respective luciferase reporter constructed, containing only a single binding site for a fair comparison of siRNA activities among different regions, except for the N(-) siRNAs. Considering these facts, more reliable yet rapid screening tools such as the SARS-CoV-2-GFP reporter virus (Thi Nhu Thao et al., 2020) could be

of high relevance in such studies. Due to the time constraints and the priority of this project however, the luciferase constructs were still mainly utilized for the preliminary screening (see 2.2.1).

Initially, it was not clear whether the N(-) specific siRNAs are active. It must be further noted that, both the strands of a siRNA possess silencing potentials. In such scenario, the luciferase reporters proved noteworthy to authenticate the sense-specific activities of N(+) and N(-) siRNAs (see 2.2.1.1). This confirmation was essential to attribute the observed antiviral effect to the antisense strand of N(-) specific siRNA, if observed. Surprisingly, the N(-) siRNAs did not show any effect on the replication of SARS-CoV-2, suggesting the inaccessibility of the negative-sense RNA intermediate for siRNA-based therapy. The probable reasons of the same are discussed later in this thesis.

3.2.3 Antiviral activity of the siRNAs

An important factor influencing the siRNA activity is the accessibility of the target RNA (Kretschmer-Kazemi Far & Sczakiel, 2003). In the cytoplasm of the host cell, the viral gRNA is immediately translated into two large polyproteins – ORF1a and ORF1ab, which later leads to formation of the double-membraned replication organelles (Conde, Allatif, Ohlmann, & de Breyne, 2022). Owing to this fact, it was hypothesized that ORF1 region of the gRNA could be immediately available for siRNA-based targeting and hence was chosen as the target to evaluate the potential of the siRNAs to target incoming viral genomes (see 2.2.2.1). Here, the SARS-CoV-2-GFP proved superlative for a rapid analysis in real-time. Since the siRNAs were not directed against the GFP transcript present in genomic and sgRNAs, a reduction of the GFP signal clearly indicated an effect of immediate suppression of incoming genomes on the viral spread. It must be noted that the main aim of these initial experiments was to only validate the capacity of the siRNAs to target the incoming genomes and hence, other siRNAs targeting different regions were not assessed in detailed at this step.

The paramount finding of this project was that the effectual targeting of SARS-CoV-2 gRNA could be key in controlling SARS-CoV-2 replication and spread. This must not be confused with ORF1 being the most promising target for siRNA-based therapy. It was rather later observed that ORF1-specific siRNAs were superior in suppressing SARS-CoV-2 gRNA more efficiently than other siRNAs in this study. The unlikeliness of a design-based bias causing such effect has been already discussed previously in this section. Interestingly, the ORF1-speicifc siRNAs exhibited better IC_{50} values only when tested in the infection setting and not with the luciferase reporters (see 2.2.1.3 and

2.2.2.5). Such observations undoubtedly confirmed that a virological factor was responsible for superior antiviral activities of the ORF1-specific siRNAs. However, it must be considered that another siRNA targeting any genomic region of SARS-CoV-2 could prove efficacious since activities of different siRNA sequences could differ strongly. Moreover, siRNAs against only four different genomic regions of SARS-CoV-2 were tested in this project. Therefore, it cannot be excluded that targeting another genomic region of SARS-CoV-2 could be superior in controlling SARS-CoV-2 replication than targeting the ORF1.

Coming back to the accessibility of viral RNA species, a possible reason for unavailability of negative-sense RNA species for siRNA-based therapy could be the double-membraned replication organelles. The negative-sense RNA intermediates could reside in the replication organelles and are not exported to the cytosol, as they do not code for viral proteins (Wolff et al., 2020). However, the absence of RISC complexes inside of the replication organelles limits the siRNA activity to the RNAs either exported from the organelle – the sgRNAs or that have not yet entered the organelles – the gRNA of incoming virus.

Out of the two siRNA-accessible target RNA species, it was quite evident that the sgRNAs are extremely abundant in comparison to the gRNA and the same has been reported earlier (D. Kim et al., 2020). Thus, it was hypothesized that a probable reason for the decreased activity of siRNAs additionally targeting sgRNAs could be that they were outnumbered by the sgRNAs. Subsequently, it was observed that a higher dose of the common region targeting siRNAs is necessary to control viral replication efficiently (see 2.2.2.5). However, an unreasonably high dose of siRNA could rather lead to a counter-effect inhibiting the RNAi effect (T. Ma, Pei, Li, & Zhu, 2019). Moreover, a higher dose of the siRNA could also cause induction of innate immune response and inflammation (Meng et al., 2013). Considering these observations, it is thus crucial to determine an ideal dose of the siRNA-carrier formulations.

3.2.4 Factors influencing clinical development of antiviral siRNA therapeutics

One of the highlights of this study was the use of a physiologically more relevant human lung explants – hPCLS. These explants contain all cell types including the immune cells present in the lung as well as the structural architecture of the human lung (G. Liu et al., 2019; Michalaki, Dean, & Johansson, 2022). In certain aspects, such a model system could be more relevant than the *in vivo* models for translational development of a

therapeutic strategy. A major disadvantage using hPCLS was the high autofluorescence exhibited in the GFP channel and thus, a real-time monitoring of effect on viral spread using SARS-CoV-2-GFP was not possible. Nevertheless, the two different cell culture infection models utilized in this study precisely covered some of the crucial factors varying conditions such as time points of siRNA treatment, siRNA dosage, viral inoculum, cell polarization in an organ, mucous production, and the induction of innate immune response. Another important factor negatively influencing siRNA activity is the resistance to different kinds of nucleases, found in serum or different cellular compartments. This issue was addressed by employing a clinically validated chemical modification pattern [60], where it was demonstrated that the most promising candidate siRNA (siO3) exhibited an improved and durable activity. Moreover, the chemically modified siRNA, when coupled with an improved delivery agent (PEI), showed significant reduction of SARS-CoV-2 gRNA in lung explants (see 2.2.2.6).

In addition to the factors mentioned earlier, other crucial factors such as delivery, stability, distribution, pharmacokinetics, and safety largely influence the clinical development of the RNAi agent (Ebenezer, Comoglio, Wong, & Tuszynski, 2023). These factors thus could be addressed well with *in vivo* studies. Therefore, lack of *in vivo* proof remains a major drawback of this study.

Efficient delivery of the siRNAs to relevant cell type still remains a major hurdle in the development of siRNA-based therapeutics (Sajid, Moazzam, Kato, Yeseom Cho, & Tiwari, 2020). An optimal career formulation and the precise route of delivery are the most important factors to be considered. Especially in the context of respiratory viruses such as SARS-CoV-2, an intranasal delivery of siRNAs is of special interest. Early efforts in this direction could yield promising results with Alnylam's siRNAs targeting RSV about a decade ago (DeVincenzo et al., 2010). Moreover, nasal drug delivery offers a rapid onset of drug administration and is non-invasive, maximizing patient comfort. It could also be beneficial to reduce first-pass metabolic effect seen with oral and intravenous medication, with a reduced risk of systemic adverse effects (Keller, Merkel, & Popp, 2022; Tai et al., 2022). Another major advantage for intranasal delivery of siRNAs could be the direct administration of a liquid formulation complexed with suitable lipid nanoparticles without nebulizing the formulation (Feldmann & Merkel, 2015; Lam, Liang, & Chan, 2012). This is particularly advantageous as the liposomal formulations are sensitive to stress endured during the nebulization (R. H. Muller, Radtke, & Wissing, 2002). On the alternative lines, pulmonary delivery of siRNAs in the form of dry powders has been also reported previously (Ito, Okuda, Takayama, & Okamoto, 2019; Okuda et al., 2013). The dry powder inhalers offer a superior shelf-life as well as confer enhanced

stability against chemical, physical and microbial factors (Zimmermann et al., 2022). An ideal delivery vehicle for pulmonary delivery must not only protect the payload from degradation but also should be non-cytotoxic and non-immunogenic. For such delivery approaches, numerous siRNA-nanoformulations are constantly in development based on variety of polymers, peptides, lipids, and inorganic materials (Merkel, Rubinstein, & Kissel, 2014). These approaches are of special relevance as the free nucleic acids may not efficiently diffuse through the mucous barrier in the airway for a successive uptake by the epithelium (Sanders, Rudolph, Braeckmans, De Smedt, & Demeester, 2009). Therefore, the delivery systems must be designed carefully to maximize the bioavailability and delivery to the infection cite of the organ while reducing the rapid clearance and degradation (Merkel & Kissel, 2012).

PEI has been previously reported for pulmonary delivery of siRNAs (Merkel et al., 2009) and was preferred for the delivery in the hPCLS (see 2.2.2.6), as RNAiMAX was unsuccessful (data not shown). Owing to its net positive surface charge, PEI could be easily complexed with the negatively charged nucleic acids for a systematic delivery. When coupled with the siRNAs, PEI ensured efficient siRNA encapsulation, protection of siRNA from RNases leading to a higher transfection efficiency as compared to naked siRNAs, even at lower N/P ratios (Merkel & Kissel, 2012).

3.2.5 Conclusions

Till today, chronic hepatitis B has no cure available. Current available treatment strategies can effectively reduce the viral replication to undetectable levels, but rarely achieve cure. Therefore, there is an urgent need of novel therapeutic strategies. Previously, therapeutic vaccination in combination with RNAi-based suppression of HBV antigens could regain the T-cell effector functions and achieve functional cure in the murine model (Michler et al., 2020). However, it was not clear whether a suppression of immunosuppressive genes of relevance in the liver could further enhance the efficacy of the therapeutic vaccine. To further improve upon the combinatorial strategies, primarily this thesis focused upon development of therapeutic siRNAs against immunosuppressive proteins of interest – PD-L1, LGALS-9 and TGFß-1.

Due to the time constraints, the focus of this project was later narrowed to a single target, TGFß-1. Nevertheless, about 90% of the siRNAs designed against all the three genes were functional. The dual luciferase-based reporter system proved greatly beneficial for a rapid screening of the siRNAs. Furthermore, the potency and stability of the candidate siRNAs was improved with incorporation of clinically validated chemical modifications.

Moreover, the potential of hepatic stellate cells as the major producers of TGFß-1 was assessed in *in vitro* and *ex vivo* testing systems.

In parallel, this project also focused on development of novel HBV mosaic capsid particles to further optimize the second component of the combinatorial approach. In this part, mosaic capsid particles composed of genotype C and D HBcAg were expressed and purified successfully. A single expression vector harboring the two genes was employed and the capsids were expressed in competent *E. coli*. This thesis reports the optimization of expression and purification methods to obtain highly pure mosaic capsid particles for the purpose of therapeutic vaccination. Furthermore, the structural assessment of the capsids revealed that mosaic capsid particles were composed of both homodimers as well as chimeric heterodimers. Moreover, further collaborative experiments proved that the mosaic capsid particles are antigenic, immunogenic, and stable at varying temperatures for long periods of time.

After the emergence of SARS-CoV-2, previously gained expertise in siRNA designing were further extended to devise a potential therapeutic strategy. In this part, about 40 siRNAs were designed against four genomic regions of SARS-CoV-2 – L, ORF1, N and 3'UTR. The chemically synthesized siRNAs, when transfected into the cells prior to infection, could successfully target the incoming viral genome, terminating the replication and preventing virus-induced cell death. Surprisingly, the negative sense RNA intermediates were inaccessible for siRNAs. All the candidate siRNAs against different regions showed similar levels of activity when tested against luciferase reporters. However, when tested in infection settings, the siRNAs targeting ORF1 showed superior targeting of gRNA as compared to other siRNAs, leading to a more efficient control of viral replication and spread. As suspected, the out-competition by highly abundant sgRNAs lead to a reduced siRNA activity of the common region targeting siRNAs. Lastly, the chemically modified ORF1-specific siRNAs were validated for their antiviral activity in human lung explants. Along these lines, it was concluded that an early therapy start or application of siRNAs in prophylactic setting could be of benefit to combat SARS-CoV-2.

This thesis evidently supports the development of siRNA-based therapeutic strategies to combat viral diseases. Further *in vivo* validation of these findings, however, is necessary to address important aspects such as delivery, distribution, and safety of the siRNAs.

4 Materials and Methods

4.1 Materials

4.1.1 Cell lines

Cell line	Details
AML-12	Mouse (CD1 strain) non-transformed hepatocyte cell line transgenic for human transforming growth factor alpha (J. C. Wu, Merlino, & Fausto, 1994)
HepG2-NTCP	HepG2 cells with a stable expressing of sodium taurocholate cotransporting polypeptide (Ko et al., 2018)
LX-2	Human hepatic stellate cell line immortalised with SV40 large T antigen (L. Xu et al., 2005)
RAW264.7	Mouse macrophage cell line established from a tumour in male mouse, induced with Abelson murine leukemia virus (Hartley et al., 2008)
Vero E6	African green monkey kidney epithelial cell line (Osada et al., 2014)

4.1.2 Competent *E. coli* derivatives

Product	Supplier
NEB10® beta	New England Biolabs
One Shot™ BL21(DE3)	Invitrogen
One Shot™ Stbl3™	Thermo Fisher Scientific
T7 Express competent *E. coli* (High Efficiency)	New England Biolabs

4.1.3 Cell culture media

Medium	Ingredients	Amount
Cell freezing medium	FCS DMSO	90 % 10 %

DMED full medium	DMEM FCS Pen/Strep (10,000 U/ml) L-Glutamine (200 mM) NEAA (100x) Sodium pyruvate (100 mM)	500 ml 50 ml 5.5 ml 5.5 ml 5.5 ml 5.5 ml
HepG2 differentiating medium	DMEM FCS Pen/Strep (10,000 U/ml) L-Glutamine (200 mM) NEAA (100x) Sodium pyruvate (100 mM) DMSO	500 ml 50 ml 5.5 ml 5.5 ml 5.5 ml 5.5 ml 10.5 ml
LB Medium	Tryptone Yeast extract NaCl (in 1 liter H2O)	10 g 5 g 10 g

1.1.4 Buffers

Buffer	Ingredient	Amount
10x SDS Running buffer	Tris Glycin 10 % SDS H2O	30.3 g 145 g 100 ml to 1000 ml
10x TBST (pH 7.4)	Tris NaCl H2O	12.1 g 40g to 500 ml
10x Transfer buffer	Tris Glycin H2O	30.3 g 144.1 g to 1000 ml
1x TAE buffer	50x TAE buffer H2O	20 ml 980 ml

1x TBST	10x TBS Tween20™ H2O	100 ml 1 ml to 1000 ml
50x TAE buffer	Tris 0.5M EDTA H2O	242 g 100 ml to 1000 ml
RIPA Cell lysis buffer (pH 7.4)	1M Tris/Cl NaCl Sodium Deoxycholate 0.5M EDTA SDS Sodium Fluoride H2O	50 ml 8.76 ml 5 g 2 ml 1 g 0.42 g to 1000 ml
SDS-Loading dye	1M Tris/Cl Glycerol SDS DTT Bromphenol Blue H2O	3.75 ml 6 ml 1.2 g 0.93 g 6 mg to 10 ml
Transfer buffer	10x Transfer buffer Methanol H2O	100 ml 200 ml to 1000ml
SDS-staining buffer	Coomassie R250 Methanol Acetic Acid Water	1 g 300 ml 50 ml to 1000 ml
Destaining buffer	Methanol Glacial Acetic acid Water	100 ml 100 ml to 1000 ml

4.1.4 Kits, assays, and enzymes

Product	**Supplier**
Amersham ECL Prime Western Blotting Detection Reagent	GE Healthcare
CellTiter-Blue® Cell Viability Assay	Promega

Dual-Luciferase Reporter Assay	Promega
Dynabeads™ M-280 Streptavidin	Invitrogen
Fix & Perm Cell Fixation & Permeabilization Kit	Thermo Fisher Scientific
FuGENE® HD Transfection Reagent	Promega
Gal-9 Mouse ELISA Kit	Cloud-Clone Corp
GeneJet Gel Extraction Kit	Thermo Fisher scientific
GeneJet Plasmid Miniprep Kit	Thermo Fisher scientific
High Pure PCR Cleanup Kit	Roche
HiScribe® T7 ARCA mRNA Kit	New England Biolabs
In-Fusion® HD Cloning Kit	Takara Bio Inc
Incucyte® Cytotox Red dye	Sartorius
LightCycler 480 SYBR green master mix	Roche
Lipofectamine™ 2000	Invitrogen
Lipofectamine™ MessengerMAX™	Invitrogen
Lipofectamine™ RNAiMAX	Invitrogen
NotI Fast Digest	Thermo Fisher Scientific
NucleoSpin RNA kit	Macherey-Nagel
Phusion Hot Start Flex 2x Master Mix	New England Biolabs
Plasmid Plus Midi Kit	Qiagen
siPORT™ NeoFX™ Transfection Agent	Invitrogen
SuperScript III First-Strand Synthesis SuperMix for qRT-PCR	Invitrogen
TA Cloning Kit	Invitrogen
TGF beta-1 Human/Mouse Uncoated ELISA Kit	Invitrogen
TRIzol™ Reagent	Invitrogen
XhoI Fast Digest	Thermo Fisher Scientific

4.1.5 Chemicals and Reagents

Product	**Supplier**
Agarose	PeqLab
Ammonium persulfate (APS)	Roth
Ampicillin	Roth

Antibiotics/Antimycotics, 100x	Thermo Fisher scientific
Bovine serum albumin (BSA)	Roth
Collagen R	Serva
Cytofix/Cytoperm	BD Biosciences
Dimethyl sulfoxide (DMSO)	Sigma-Aldrich
DMEM	Gibco
DMSO	Sigma-Aldrich
DNA ladder 1kb / 100bp	Eurogentec
Dulbecco's Modified Eagle's Medium	Gibco
EDTA	Roth
Ethanol	Roth
Ethidium bromide	Merck
FCS (heat-inactivated)	Gibco
IPTG	Roth
Isopropanol	Roth
LDS Sample Buffer, Non-Reducing (4X)	Thermo Fisher scientific
Methanol	Roth
Milk powder	Roth
NaCl	Roth
NaOH	Roth
Non-essential amino acids 100x	Gibco
OptiMEM	Gibco
Page Ruler Plus Prestained protein ladder	Thermo Fisher scientific
PBS	Gibco
PEG6000	Merck
Penicillin/streptomycin	Gibco
Pierce RIPA buffer	Thermo Fisher scientific
Polyacrylamide	Roth
Protease inhibitor (Complete)	Roth
RotiSafe	Roth
SDS	Roth
SmartLadder DNA (small fragment)	Eurogentec
Sodium citrate	Roth
Sodium pyruvate	Gibco
Sucrose	Roth

T5 exonuclease	New England Biolabs
TEMED	Roth
Tetracycline	Applichem
Tris base	Roth
Tris HCl	Roth
Trypan blue	Gibco
Trypsin	Gibco
Tryptone	Roth
Tween 20	Roth
Yeast extract	Roth

4.1.6 Laboratory equipment and consumables

Product	**Supplier**
Accu Jet® pro	Brand
Ambion™ mouse PD-L1 siRNA	Ambion
Amersham Hybond PVDF membrane	GE Healthcare
Amersham nylon membrane Hybond N+	GE Healthcare
Cell culture flasks and plates	TPP
Cell culture incubator HERAcell 150i	Thermo Fisher scientific
Centrifuge 5417C / 5417R	Eppendorf
Centrifuge Avanti J-26 XP	Beckman Coulter
Cryo vials	Greiner Bio One
Cytoflex S Flow Cytometer	Beckman Coulter
Digital lab scale balance analytical PC440	Mettler-Toledo
Dot blot device	GE Healthcare
ELISA 96well plates Nunc	Thermo Fisher scientific
ErgoOne® 8-channel Pipette (30-300 µl)	Starlab
Falcon tubes 15ml, 50ml	Greiner Bio One
FiveEasyPlusTM pH Meters	Mettler-Toledo
LSRFortessa™ Cell Analyzer	BD Biosciences
Fluorescence microscope DMi8	Leica
Freezing container	Thermo Fisher scientific
Fusion Fx7	Peqlab
Gel chambers (agarose gel electrophoresis)	Peqlab

Gel chambers (SDS-PAGE)	Bio-Rad
Heating block	Eppendorf
Hemocytometer	Brand
Hyperflask	Corning
Incucyte® Cytotox Red dye	Sartorius
Incucyte® Live-Cell imaging system	Sartorius
Light Cycler 480 II	Roche
Nanodrop Photometer	Implen
Pipette filter tips	Starlab
Pipette tips 2 - 50ml	Greiner Bio One
Pipettes	Eppendorf
PowerPac Basic	Bio-Rad
PowerPac HC	Bio-Rad
PVDF membrane	Bio-Rad
qPCR 96-well plates	4titude
Reaction tubes	Eppendorf
Reagent Reservoir (50 mL)	Corning
Shaker and incubator for bacteria	INFORS HT
Sterile filters 0.45µm	Merck
Sterile hood	Heraeus
Tecan plate reader Infinite F200	Tecan
Transwells 6 µm	Thermo Fisher Scientific
Ultracentrifuge Beckman SW40 rotor	Beckman Coulter
Western Blotting Chamber	Bio-Rad
Whatman filter paper	Bio-Rad

4.1.7 siRNAs

All siRNAs were purchased from Microsynth AG, Balgach, Switzerland.

Name	Sense strand (5'-3')	Anti-sense strand (5'-3')
siGal9#1	UUCCAUAUCAACCUUCGuUdTdT	AGCGAAGGUUGAUAUGGAACC
siGal9#2	GGCCAGAGCUUCUCGGUGUdTdT	ACACCGAGAAGCUCUGGCCUC
siGal9#3	CAAAUGGGCUUUACCCGUudTdT	GACGGGUAAAGCCCAUUUGGA

siGal9#4	GAAUGCUGUUGUCCGAAAudTdT	GUUUCGGACAACAGCAUUCUC
siGal9#5	CUCCAUACAUUAACCCGAUdTdT	AUCGGGUUAAUGUAUGGAGAC
siGal9#6	GUGAAUAUUACCACCGuuUdTdT	AGGCGGUGGUAAUAUUCACAC
siGal9#7	CAGUACCAACACCGCGUAudTdT	GUACGCGGUGUUGGUACUGCA
siGal9#8	GAGAAUGCUGUUGUCCGAAdTdT	UUCGGACAACAGCAUUCUCAU
siPDL1#1	CUGGCAUUUGCUGAACGCAdTdT	UGCGUUCAGCAAAUGCCAGUA
siPD-L1#10	GCUGGACCUGCUUGCGUUAdTdT	UAACGCAAGCAGGUCCAGCUC
siPD-L1#2	AGACGUAAGCAGUGUUGAAdTdT	UUCAACACUGCUUACGUCUCC
siPD-L1#3	GUGGAGAAAUGUGGCGUUGdTdT	uAACGCCACAUUUCUCCACAU
siPD-L1#4	GGAGAAAUGUGGCGUUGAAdTdT	UUCAACGCCACAUUUCUCCAC
siPD-L1#5	GCGGACUACAAGCGAAUuAdTdT	UGAUUCGCUUGUAGUCCGCAC
siPD-L1#6	GGUGCGGACUACAAGCGAAdTdT	UUCGCUUGUAGUCCGCACCAC
siPD-L1#7	GUGCGGACUACAAGCGAAUdTdT	AUUCGCUUGUAGUCCGCACCA
siPD-L1#8	GAGUAUGGCAGCAACGUuAdTdT	UGACGUUGCUGCCAUACUCCA
siPD-L1#9	GGUCAACGCCACAGCGAAUdTdT	AUUCGCUGUGGCGUUGACCCU
siTGF-ß1#1	GAACCAAGGAGACGGAAUAdTdT	UAUUCCGUCUCCUUGGUUCAG
siTGF-ß1#10	GUGGCUGUCUUUUGACGUudTdT	GACGUCAAAAGACAGCCACUC
siTGF-ß1#2	GGAAUACAGGGCUUUCGAUdTdT	AUCGAAAGCCCUGUAUUCCGU

siTGF-ß1#3	GAAUACAGGGCUUUCGAUUdTdT	AAUCGAAAGCCCUGUAUUCCG
siTGF-ß1#4	GCAACAAUUCCUGGCGUUAdTdT	UAACGCCAGGAAUUGUUGCUA
siTGF-ß1#5	GGAAGUGGAUCCACGAGuudTdT	GGCUCGUGGAUCCACUUCCAA
siTGF-ß1#6	AGGGCUACCAUGCCAAuUUdTdT	AAGUUGGCAUGGUAGCCCUUG
siTGF-ß1#7	GUCCAAACUAAGGCUCGuudTdT	GGCGAGCCUUAGUUUGGACAG
siTGF-ß1#8	CCAACAUGAUUGUGCGuUudTdT	GAGCGCACAAUCAUGUUGGAC
siTGF-ß1#9	GGCUGUCUUUUGACGUuAudTdT	GUGACGUCAAAAGACAGCCAC
siL#1	UCUGUUCUCUAAACGAAuUdTdT	AGUUCGUUUAGAGAACAGAUC
siL#2	CCAACCAACUUUCGAUuUudTdT	GAGAUCGAAAGUUGGUUGGUU
siL#3	AAACCAACCAACUUUCGAUdTdT	AUCGAAAGUUGGUUGGUUUGU
siL#4	ACCAACCAACUUUCGAUuUdTdT	AGAUCGAAAGUUGGUUGGUUU
siL#5	AACCAACCAACUUUCGAUudTdT	GAUCGAAAGUUGGUUGGUUUG
siN(-)#1	GGACGAUUGUUACGACGUUdTdT	AACGUCGUAACAAUCGUCCUA
siN(-)#10	CUAGUUCAGUAAAACGAUUdTdT	AGUCGUUUUACUGAACUAGAA
siN(-)#11	CUGAAGGGAUACCACGAUUdTdT	AAUCGUGGUAUCCCUUCAGGU
siN(-)#12	GUCUACUGGUUUAACCGAUdTdT	AUCGGUUAAACCAGUAGACCU
siN(-)#13	GUUUUCCGAAGAUGCGUUUdTdT	AGACGCAUCUUCGGAAAACCG
siN(-)#2	GCCUGGGGUUUUAGUCGUUdTdT	AGCGACUAAAACCCCAGGCAA
siN(-)#3	CCCUUGAAGAGGACGAUUUdTdT	AGAUCGUCCUCUUCAAGGGGA
siN(-)#4	CGUGGGCGUUAGGACGAUUdTdT	AAUCGUCCUAACGCCCACGGU
siN(-)#5	GAUUGUUUCUGCCGUAGUAdTdT	UACUACGGCAGAAACAAUCGU

siN(-)#6	GGGUGGUUGUCUCGGAUUUdTdT	AAAUCCGAGACAACCACCCUU
siN(-)#7	GUUCCUUGUUGUAACGGUUdTdT	AACCGUUACAACAAGGAACUC
siN(-)#8	GAGAGUGAGUUGUACCGUUdTdT	AACGGUACAACUCACUCUCGC
siN(-)#9	GACGAUUGUUACGACGUUAdTdT	UAACGUCGUAACAAUCGUCCU
siN(+)#1	GAAUAAGCAUAUUGACGuAdTdT	UGCGUCAAUAUGCUUAUUCAG
siN(+)#10	GACGAUUGUUACGACGUUAdTdT	UAACGUCGUAACAAUCGUCCU
siN(+)#11	CUAGUUCAGUAAAACGAuUdTdT	AGUCGUUUUACUGAACUAGAA
siN(+)#2	CAAAUUGGCUACUACCGAAdTdT	UUCGGUAGUAGCCAAUUUGGU
siN(+)#3	CGCUUCAGCGUUCUUCGGAAUdTdT	AUUCCGAAGAACGCUGAAGCG
siN(+)#4	GGACGAUUGUUACGACGUUdTdT	AACGUCGUAACAAUCGUCCUA
siN(+)#5	CCCUUGAAGAGGACGAUuUdTdT	AGAUCGUCCUCUUCAAGGGGA
siN(+)#6	CGUGGGCGUUAGGACGAUUdTdT	AAUCGUCCUAACGCCCACGGU
siN(+)#7	GAUUGUUUCUGCCGUAGUAdTdT	UACUACGGCAGAAACAAUCGU
siN(+)#8	GGGUGGUUGUCUCGGAUUUdTdT	AAAUCCGAGACAACCACCCUU
siN(+)#9	GUUCCUUGUUGUAACGGUUdTdT	AACCGUUACAACAAGGAACUC
siORF1#1	CCAAAUGUGCCUUUCAACUdTdT	AGUUGAAAGGCACAUUUGGUU
siORF1#2	GUUACAUGCACCAUAUGGAdTdT	UCCAUAUGGUGCAUGUAACAA
siORF1#3	GGUACUUGGUAGUUUAGCUdTdT	AGCUAAACUACCAAGUACCAU
siORF1#4	CAUAGACGGUGCUUUACUUdTdT	AAGUAAAGCACCGUCUAUGCA
siORF1#5	GCUAACACCUGUACUGAAAdTdT	UUUCAGUACAGGUGUUAGCUA

siORF1#6	GGACAUUGCUGCUAAUACUdTdT	AGUAUUAGCAGCAAUGUCCAC
siU#1	CUUUAAUCAGUGUGUAACAdTdT	UGUUACACACUGAUUAAAGAU
siU#2	CCUAAUGUGUAAAAUUAAUdTdT	AUUAAUUUUACACAUUAGGGC
siU#3	CAUGUGAUUUUAAUAGCUUdTdT	AAGCUAUUAAAAUCACAUGGG
siU#4	CCCUAAUGUGUAAAAUUAAdTdT	UUAAUUUUACACAUUAGGGCU
siU#5	CUAAUGUGUAAAAUUAAUUdTdT	AAUUAAUUUUACACAUUAGGG
siU#6	GUGUAAAAUUAAUUUUAGUdTdT	ACUAAAAUUAAUUUUACACAU
siGFP	GCAGCACGACUUCUUCAAGdTdT	CUUGAAGAAGUCGUGCUGCdTdT
siLuc	CGUACGCGGAAUACUUCGAdTdT	UCGAAGUAUUCCGCGUACGdTdT

4.1.8 Primers and Oligonucleotides

Primers were purchased from Microsynth AG, Balgach, Switzerland.

Name	**Sequence**
18S cDNA 1	CCTTCCGCAGGTTCACCTAC
18S cDNA 2	CCTCCAATGGATCCTCGT
18S cDNA 3	TAATCATGGCCTCAGTTCCG
18S_Fw	AAACGGCTACCACATCCA
18S_Re	CCTCCAATGGATCCTCGT
CDC_N1_Fw	GACCCCAAAATCAGCGAAAT
CDC_N1_Re	TCTGGTTACTGCCAGTTGAATCTG
Gal-9_Fw	CTGGAATCCCTCCTGTGGTGTA
Gal-9_Re	CCTCGTAGCATCTGGCAAGACA
Gal-9_recom_Fw	AATTCTAGGCGATCGCATGGCTCTCTTCAGTGCCCAG
Gal-9_recom_Re	TAAACGAATTCCCGGGCTATGTCTGCACGTGGGTCAG
L1_target site	TCGAGTCTGTTCTCTAAACGAACTGC
L2_target site	TCGAGCCAACCAACTTTCGATCTCGC
L3_target site	TCGAGAAACCAACCAACTTTCGATGC
L4_target site	TCGAGACCAACCAACTTTCGATCTGC
L5_target site	TCGAGAACCAACCAACTTTCGATCGC
N(-) gene forward	TCGAGTACAGACTATTGCCTGGGGTTTTAGTCGCT TTGCGTGGGGCGTAATGCAAACCACCTGGGAGTC TAAGTTGACCGTCATTGGTCTTGCCTCTTGCGTCA

	CCCCGCGCTAGTTTTGTTGCAGCCGGGGTTCCAA ATGGGTTATTATGACGCAGAACCAAGTGGCGAGA GTGAGTTGTACCGTTCCTTCTGGAATTTAAGGGAG CTCCTGTTCCGCAAGGTTAATTGTGGTTATCGTCA GGTCTACTGGTTTAACCGATGATGGCTTCTCGATG GTCTGCTTAAGCACCACCACTGCCCTTTTACTTTC TAGAGTCAGGTTCTACCATAAAGATGATGGATCCT TGACCCGGTCTTCGACCTGAAGGGATACCACGAT TGTTTCTGCCGTAGTATACCCAACGTTGACTCCCT CGGAACTTATGTGGTTTTCTAGTGTAACCGTGGGC GTTAGGACGATTGTTACGACGTTAGCACGATGTTG AAGGAGTTCCTTGTTGTAACGGTTTTCCGAAGATG CGTCTTCCCTCGTCTCCGCCGTCAGTTCGGAGAA GAGCAAGGAGTAGTGCATCAGCGTTGTCAAGTTC TTTAAGTTGAGGTCCGTCGTCATCCCCTTGAAGAG GACGATCTTACCGACCGTTACCGCCACTACGACG AGAACGAAACGACGACGAACTGTCTGAGTTGGTC GAACTCTCGTTTTACAGACCATTTCCGGTTGTTGT TGTTCCGGTTTGACAGTGATTCTTTAGACGACGAC TCCGAAGATTCTTCGGAGCCGTTTTTGCATGACGG TGATTTCGTATGTTACATTGTGTTCGAAAGCCGTC TGCACCAGGTCTTGTTTGGGTTCCTTTAAAACCCC TGGTCCTTGATTAGTCTGTTCCTTGACTAATGTTTG TAACCGGCGTTTAACGTGTTAAACGGGGGAGGCG ATCGCGCAAGAAGCCTTACAGCGCGTAACCGTAC CTTCAGTGTGGAAGCCCTTGCACCAACTGGATGT GTCCCCGGTAGTTTAACCTACTGTTTCTAGGTTTA AAGTTTCTAGTTCAGTAAAACGACTTATTCGTATAA CTGCGTATGTTTTGTAAGGGTGGTTGTCTCGGATT TTTCCTGTTTTTCTTCTTCCGACTACTTTGAGTTCG GAATGGCGTCTCTGTCTTCTTTGTCGTTTGACACT GAGAAGAAGGACGACGGCTAAACCTACTAAAGAG GTTTGTTAACGTTGTTAGGTACTCGTCACGACTGA GTTGAGTCCGGGC
N(-) gene reverse	GCCCGGACTCAACTCAGTCGTGACGAGTACCTAACA ACGTTAACAAACCTCTTTAGTAGGTTTAGCCGTCGT

	CCTTCTTCTCAGTGTCAAACGACAAAGAAGACAGAG ACGCCATTCCGAACTCAAAGTAGTCGGAAGAAGAAA AACAGGAAAAATCCGAGACAACCACCCTTACAAAAC ATACGCAGTTATACGAATAAGTCGTTTTACTGAACTA GAAACTTTAAACCTAGAAACAGTAGGTTAAACTACC GGGGACACATCCAGTTGGTGCAAGGGCTTCCACAC TGAAGGTACGGTTACGCGCTGTAAGGCTTCTTGCGC GATCGCCTCCCCCGTTTAACACGTTAAACGCCGGTT ACAAACATTAGTCAAGGAACAGACTAATCAAGGACC AGGGGTTTTAAAGGAACCCAAACAAGACCTGGTGCA GACGGCTTTCGAACACAATGTAACATACGAAATCAC CGTCATGCAAAAACGGCTCCGAAGAATCTTCGGAGT CGTCGTCTAAAGAATCACTGTCAAACCGGAACAACA ACAACCGGAAATGGTCTGTAAAACGAGAGTTCGACC AACTCAGACAGTTCGTCGTCGTTTCGTTCTCGTCGT AGTGGCGGTAACGGTCGGTAAGATCGTCCTCTTCAA GGGGATGACGACGGACCTCAACTTAAAGAACTTGAC AACGCTGATGCACTACTCCTTGCTCTTCTCCGAACT GACGGCGGAGACGAGGGAAGACGCATCTTCGGAAA ACCGTTACAACAAGGAACTCCTTCAACATCGTGCTA ACGTCGTAACAATCGTCCTAACGCCCACGGTTACAC TAGAAAACCACATAAGTTCCGAGGGAGTCAACGTTG GGTATACTACGGCAGAAACAATCGTGGTATCCCTTC AGGTCGAAGACCGGGTCAAGGATCCATCATCTTTAT GGTAGAACCTGACTCTAGAAAGTAAAAGGGCAGTG GTGGTGCTTAAGCAGACCATCGAGAAGCCATCATCG GTTAAACCAGTAGACCTGACGATAACCACAATTAAC CTTGCGGAACAGGAGCTCCCTTAAATTCCAGAAGGA ACGGTACAACTCACTCTCGCCACTTGGTTCTGCGTC ATAATAACCCATTTGGAACCCCGGCTGCAACAAAAC TAGCGCGGGGTGACGCAAGAGGCAAGACCAATGAC GGTCAACTTAGACTCCCAGGTGGTTTGCATTACGCC CCACGCAAAGCGACTAAAACCCCAGGCAATAGTCTG TACTCGA
N(+)1_target site	TCGAGGAATAAGCATATTGACGCAGC
N(+)10_target site	TCGAGGACGATTGTTACGACGTTAGC

N(+)11_target site	TCGAGCTAGTTCAGTAAAACGACTGC
N(+)2_target site	TCGAGCAAATTGGCTACTACCGAAGC
N(+)3_target site	TCGAGCGCTTCAGCGTTCTTCGGAATGC
N(+)4_target site	TCGAGGGACGATTGTTACGACGTTGC
N(+)5_target site	TCGAGCCCTTGAAGAGGACGATCTGC
N(+)6_target site	TCGAGCGTGGGCGTTAGGACGATTGC
N(+)7_target site	TCGAGGATTGTTTCTGCCGTAGTAGC
N(+)8_target site	TCGAGGGGTGGTTGTCTCGGATTTGC
N(+)9_target site	TCGAGGTTCCTTGTTGTAACGGTTGC
O1_target site	TCGAGAACCAAATGTGCCTTTCAACTGC
O2_target site	TCGAGTGCATAGACGGTGCTTTACTTGC
O3_target site	TCGAGTTGTTACATGCACCATATGGAGC
O4_target site	TCGAGATGGTACTTGGTAGTTTAGCTGC
O5_target site	TCGAGTAGCTAACACCTGTACTGAAAGC
O6_target site	TCGAGGTGGACATTGCTGCTAATACTGC
O7_target site	TCGAGGTGTAAAGATGGCCATGTAGAGC
Oligo$(dA)_{20}$	AAAAAAAAAAAAAAAAAAAA
Oligo$(dT)_{20}$	TTTTTTTTTTTTTTTTTTTT
PD-L1_Fw	TGCGGACTACAAGCGAATCACG
PD-L1_Re	CTCAGCTTCTGGATAACCCTCG
PD-L1_recom_Fw	AATTCTAGGCGATCGCATGAGGATATTTGCTGGCATTA
PD-L1_recom_Re	TAAACGAATTCCCGGGTTACGTCTCCTCGAATTGTGTA
Psicheck2_seq_Fw	ACGCTCCAGATGAAATGGGTA
Psicheck2_seq_Re	AGACTCATTTAGATCCTCACAC
RDRP_Fw	CGTCTGCGGTATGTGGAAAG
RDRP_Re	TAAGACGGGCTGCACTTACA
TGF-ß1_Fw	TGATACGCCTGAGTGGCTGTCT
TGF-ß1_Re	CACAAGAGCAGTGAGCGCTGAA
TGF-ß1_recom_Fw	AATTCTAGGCGATCGCATGCCGCCCTCGGGGCTG
TGF-ß1_recom_Re	TAAACGAATTCCCGGGTCAGCTGCACTTGCAGGAGC
U1_target site	TCGAGATCTTTAATCAGTGTGTAACAGC
U2_target site	TCGAGAGCCCTAATGTGTAAAATTAAGC
U3_target site	TCGAGGCCCTAATGTGTAAAATTAATGC
U4_target site	TCGAGCCCTAATGTGTAAAATTAATTGC
U5_target site	TCGAGATGTGTAAAATTAATTTTAGTGC

U6_target site	TCGAGCCCATGTGATTTTAATAGCTTGC

4.1.9 Antibodies

Antibody/Dye	Supplier
aSMA – eF660	Invitrogen
CD271 – eF488	Miltenyi Biotec
LAP (TGF-ß1) – PE	Biolegend
LAP (TGF-ß1) – PE/Cy7	Biolegend
Fixable Viability Dye – eF789	Thermo Fisher Scientific
Goat anti-mouse IgG	Thermo Fisher Scientific
Goat anti-Rabbit IgG	Thermo Fisher Scientific

4.1.10 Proteins and Viruses

Product	Supplier/source
Recombinant human TGF-ß1 protein	R&D Systems
Recombinant HBcAg	Dr. Andris Dišlers
HBV	AG Protzer
SARS-CoV-2	AG Protzer
rSARS-CoV-2-GFP	AG Pichlmair

4.1.11 Softwares and tools

Program	Supplier/source	Application
FlowJo, Version 10.4	BD Biosciences	Flow Cytometry analysis
Incucyte® S3 software	Sartorius	Live-cell imaging analysis
LightCycler 480 SW 1.5.1	Roche	qPCR analysis
Prism 9.0	GraphPad Software inc.	Graph design, statistics
Serial Cloner	SerialBasics	DNA analysis
siSPOTR	University of Iowa	siRNA designing
siDirect 2.0	University of Tokyo	siRNA designing

4.2 Methods

4.2.1 siRNA designing, chemical modifications and curating

4.2.1.1 siRNA designing against PD-L1, LGALS-9 and TGFß-1

Coding sequences (CDS) of all the genes of interest were obtained from NCBI RefSeq database. The siRNA sequences were generated using an online available tool siSPOTR (https://sispotr.icts.uiowa.edu/sispotr/index.html) (Boudreau et al., 2013). siSPOTR generates potential siRNA sequences based on the POTS score as described before. The top siRNA hits obtained based on a POTS score less than 50 were further subjected to manual curation in two rounds. Primarily, siRNA sequences following either one of the designing rules based on previous reports (Reynolds et al., 2004; Ui-Tei, Naito, & Saigo, 2006) and mentioned below were selected. In the second round, the siRNA sequences exhibiting the lowest POTS score previously were finalized. At least 8 siRNAs per target gene were purchased as chemically unmodified, desalted siRNAs from Micosynth AG. siRNAs were resuspended in sterile, RNAse-free water at the stock concentration of 40uM and stored at -20^{0}C until further use.

Number	Rules for designing siRNAs (based on 5'-3' of sense strand)
1	G/C at position 1, A/U at position 19 and >3 A/Us between positions 13-19
2	G/C at position 1, 11 and 19 and >6 A/Us between positions 5-19
3	A/U at position 1 and 19 and >3 A/Us between positions 13-19

4.2.1.2 siRNA designing against various genomic regions of SARS-CoV-2

A full-length mRNA sequence of SARS-CoV-2 (Wuhan strain) genomic RNA was obtained from NCBI RefSeq. The siRNAs were designed against four different regions of SARS-CoV-2 – 5'UTR Leader sequence (L), ORF1ab, Nucleocapsid gene (N) and the 3'UTR region. The sequences were directly subjected to two siRNA designing tools, siSPOTR and siDirect 2.0, available online (http://sidirect2.rnai.jp/). Potential siRNA sequences were then manually curated as described before. Additionally, siRNAs against negative sense N gene, targeting all the negative sense replication intermediates of SARS-CoV-2 were designed in identical way. In the end, at least 5 siRNAs targeting each intended region of SARS-CoV-2 were purchased as chemically modified, desalted siRNAs from Micosynth AG. siRNAs were resuspended in sterile, RNAse-free water at the stock concentration of 40μM and stored at -20^{0}C until further use.

4.2.1.3 Chemically modified siRNAs

Well performing, chemically unmodified siRNAs upon testing, were subjected to chemical modification following the design of a recently approved siRNA based therapeutic, Lumasiran (Shah & Pyle, 2021). All the nucleotides of sense and anti-sense strand of the siRNAs were modified with 2' O-Methyl modification except positions 7, 9, 10 and 11 from 5' end sense strand and positions 2, 6, 8, 9, 14, 16 from 5' end of antisense strand, which were modified with 2'-Fluoro modifications. In addition to that, first two phosphate linkages at 5' end of sense strand and of both the ends of antisense strand were modified to phosphorothioate linkages. Chemically modified siRNAs were purchased from Eurogentec, Germany and were resuspended in sterile, RNAse-free water at the stock concentration of 20μM and stored at -20^{0}C until further use.

4.2.2 Mammalian cell culture and *in vitro* assays

4.2.2.1 Maintenance of mammalian cell lines

All adherent cell lines of human, monkey and murine origins were cultured under sterile conditions in full DMEM and incubated at 37^{0}C, 95 % humidity and 5 % CO2. Cells were passaged when they reached about 90 % confluency. Cells were treated with 0.05 % Trypsinfor 3-5 minutes at 37^{0}C to obtain a single cell suspension. Cell lines of hepatic origin were seeded and cultured on pre-collagenated flasks and plates.

4.2.2.2 Cell counting

A trypsinised single suspension of cells was diluted 1:2 or 1:5 with trypan blue and number of cells per ml was determined using a Neubauer chamber.

4.2.2.3 siRNA transfection

Chemically synthesized siRNAs were transfected in cell lines in majority of experiments using Lipofectamine™ RNAiMAX irrespective of cell-type. Other transfection agents such as siPORT™ *NeoFX™* Transfection Agent and Lipofectamine™ 2000 were also used where indicated. Briefly, siRNA-polymer complexes were diluted to desired concentrations in Opti-MEM, mixed and incubated for 20 minutes at room temperature. For reverse transfections, the trypsinized cells were added on top of siRNA-polymer

complexes. For forward transfections, siRNA-polymer complexes were added on top of 65-80 % confluent cells plated a day before.

4.2.2.4 siRNA-plasmid co-transfection

200,000 HEK293T cells in 500 µl complete media were seeded on Poly-L-Lysin coated 24-well plates to achieve 65-80 % confluency the next day. Lipofectamine™ 2000 was then used for co-transfection of siRNAs and reporter plasmid the following day. Briefly, in 100 µl Opti-MEM, 0.6 µl of 10 µM siRNA together with 200 ng of luciferase reporter plasmid and 1 µl Lipofectamine™ 2000 were diluted. The polymer-nucleic acid mixture was incubated for 20 minutes at room temperature and added on top of the plated cells. The medium was replaced 24 hours after co-transfection.

4.2.2.5 RNA extraction

RNA was extracted using the Nucleo Spin RNA kit from mammalian cell lines according to the manufacturer's instruction. For RNA extraction from the tissues, the samples were first disrupted using a Tissue lyser LT according to manufacturer's instruction followed by the RNA extraction as per manufacturer's instructions.

4.2.2.6 Preparation of cDNA

First strand cDNA was synthesized from 4 µl extracted RNA using SuperScript™ III One-Step RT-PCR system with *Taq* DNA polymerase as per the manufacturer's instruction. Synthesized cDNA was diluted as required in sterile molecular biology grade water prior to further use.

4.2.2.7 Quantitative PCR

Quantitative PCR from cDNA was performed in LightCycler 480 system with the SYBR™ Green PCR Master Mix according to manufacturer's instruction. Briefly, 4 µl of synthesized cDNA was supplemented with 0.5 µl of forward and reverse primers in 5 µl master mix containing SYBR green. Conditions used for qPCR throughout this thesis are given below.

	T [°C]	t [sec]	Ramp [°C/sec]	Acquisition mode	Cycles
Denaturation	95	300	4.4		1
Amplification	95	15	4.4		40
	60	10	2.2		
	72	25	4.4	single	
Melting	95	10	4.4		1
	65	60	2.2		
	95		0.11	Continuous: 5/°C	
Cooling	40	1	2.2		1

4.2.2.8 Dual Luciferase assay

siRNAs were co-transfected with respective psiCHECK™-2 constructs harbouring either the siRNA binding sites or the whole target gene in HEK293T cells seeded a day before, using Lipofectamine™ 2000. 48 hours post co-transfection, the cells were lysed with the passive lysis buffer. 5 µl of cell lysate was thereafter used for the dual luciferase assay in the Infinite® 2000 PRO plate reader. Both Renilla and and Firefly luminescence was measured for 10 seconds from each lysate. Relative Renilla luciferase luminescence was then calculated by normalizing with Firefly luciferase activity.

4.2.2.9 Differentiation of hepatoma cell lines and HBV infection

HepG2 and AML12 derived cell lines were differentiated using differentiating media containing 2.5 % DMSO for 72 hours. The HBV stocks were kindly provided by Lea Hansen-Palmus and Dr. Jochen Wettengel (Institute of Virology, TU Munich). Differentiated hepatoma cells were then infected with HBV, with a desired MOI in presence of 5 % PEI in differentiating medium. The infection was allowed for 24 hours and later the infected cells were supplemented with fresh differentiating media.

4.2.2.10 Co-culture assays

HepG2-NTCP and HSC co-cultures were performed using Nunc™ Polycarbonate tissue culture inserts allowing cell contact. HBV infected HepG2-NTCP cells were maintained for 4 days before start of co-culture. HSCs (LX-2 or primary HSCs) were then plated at HepG2: HSCs ratio of 4:1 on the tissue culture inserts. The inserts containing the stellate

cells were then transferred carefully on top of HepG2-NTCP cells in 6-well plate containing differentiation media with 1 % DMSO.

4.2.2.11 SARS-CoV-2 and rSARS-CoV-2-GFP infection

VeroE6 and HEK293T cells were plated at approximately 80 % confluency in the desired well plate format. SARS-CoV-2 and rSARS-CoV-2-GFP infections were kindly performed by Cho-Chin Cheng and Dr. Chunkyu Ko (Institute of Virology, TU Munich) in the BSL3 facility at the Institute of Virology, TU Munich. SARS-CoV-2 and rSARS-CoV-2-GFP with specific MOIs in full growth medium was incubated for one hour with the host cells. Cells were then washed and supplemented with full growth media.

4.2.2.12 IncuCyte® Live-Cell analysis

VeroE6 cells infected with rSARS-CoV-2-GFP were subjected to live-cell imaging in real-time using Incucyte® Live-Cell Analysis device. GFP^+ cells depicted the number of infected cells, thereby, the real-time viral spread. Infected cells were quantified using GFP channel. Quantification of dead cells was performed using IncuCyte® Cytotox Red dye to monitor the loss of cell membrane integrity. Fluorescence signal (631nm) from dead cells was measured by red channel. The real-time monitoring was done by acquisition of phase contrast and fluorescent pictures every 4 hours, for three days. The analysis was performed in Incucyte® S3 software.

4.2.2.13 Half Maximal Inhibitory concentration (IC_{50}) of siRNAs

For IC_{50} analysis based on dual luciferase assay, candidate siRNAs in varying concentrations were co-transfected with respective psiCHECK™-2 constructs in HEKC293T cells. Dual luciferase assay was performed 48h post transfection and relative Renilla luciferase luminescence, to that of the negative control siRNA was used as an indication of siRNA activity. To determine antiviral IC_{50} values of siRNAs against SARS-CoV-2, VeroE6 cells were reverse transfected with siRNAs 16h before infection in varying concentrations. Transfected host cells were then infected with rSARS-CoV-2-GFP with an MOI of 1. Difference in GFP+ cells relative to negative control siRNA were used as indication of siRNA activity. The respective IC_{50} values were calculated by fitting a nonlinear curve with variable slope using the nonlinear regression model in Prism 9.0.

4.2.2.14 siRNA stability assay

To assess the stability of chemically modified siRNAs in mouse serum, equal concentrations of chemically modified and unmodified siRNA were incubated in 10 % mouse serum for varying amounts of time. Upon incubation, the samples were subjected to reducing RNA-PAGE. Presence of uncut RNA strands were observed upon staining by Roti®Gel-Stain.

4.2.3 Molecular cloning methods

4.2.3.1 Inducible constructs for expression of HBC mosaic capsid particles

All the expression constructs harbouring various forms of HBcAg were kindly provided by Prof. Dr. Michael Nassal (University clinic, University of Freiburg). Different constructs used for expression of varying types of HBV capsids are denoted in the table below.

Constructs	**Genes and Promoters**	**Resulting HBV capsids**
pRSF1b_TetC_{Δ}_T7D	Tet-C_{Δ} T7-D	$C_{\Delta}D$
pRSF1b_ T7C_{Δ}_T7D	T7-C_{Δ} T7-D	$C_{\Delta}D$
pRSF1b_ T7C_{Δ}_T7NBioD	T7-C_{Δ} T7-NBioD	$C_{\Delta}D_{bt}$

All the expression constructs were provided in pRSF1b backbone with codon optimisation. A single construct harbouring C-terminally truncated HBV genotype C or C_{Δ} HBcAg under either Tetracycline (Tet) or T7 inducible promoter together with full-length genotype D or D HBcAg under T7 promoter yielded the mosaic capsid particles. Single genotype capsid particles were used synthesized using the former mosaic capsid construct inducing either Tet promoter or T7 promoter for C_{Δ} and D capsids respectively. pRSF1b_ T7C_{Δ}_T7NBioD additionally harboured D core gene with an upstream AviTag™ sequence. This construct was utilised to generate mosaic capsid particles containing a biotinylated D HBcAg together with C_{Δ}.

4.2.3.2 Polymerase Chain Reaction (PCR)

Cloning PCR was performed using the Phusion Hot Start Flex 2 Master Mix with 1 µl template cDNA and 20 pmol forward and reverse primers, containing 15 nucleotides identical to the nucleotides present upstream and downstream of the cloning site for recombination cloning. Optimal primer annealing temperature was determined using TM-calculator software available online (https://tmcalculator.neb.com/#!/main). Conditions and duration for cycles were determined based on in-house protocols. PCR was performed in a T professional Trio Thermocycler and further analysed by agarose gel-electrophoresis (1 % Agarose) with Fusion Fx7 gel documentation device. Upon successful amplification, the PCR products were either purified directly using High Pure PCR Cleanup Kit or extracted from agarose gels using GeneJet Gel extraction kit. Purified DNA was either immediately subjected to digestion or stored at -20^{0}C till further use. Primers used for cloning are listed in 4.1.8.

4.2.3.3 Restriction digestion, ligation, and transformation.

For conventional cloning methods, FastDigest XhoI and NotI enzymes were used. Digestions of amplified fragments was performed according to the manufacturer's instructions. Upon digestion of inserts and digestion/linearization of plasmids, respective fragments were extracted from agarose gels using GeneJet Gel extraction kit. Alternatively, various siRNA binding sites were purchased as chemically synthesized ssDNA fragments mimicking XhoI-NotI digested products. The siRNA binding sites were *in vitro* annealed at 95 °C for 5 minutes and gradual cooling to form dsDNA insert fragments. Ligation reactions were performed with T4 DNA Ligase according to manufacturer's instructions. All ligation reactions were performed at 1:5 vactor-to-insert ratio. For 50 ng psiCHECK^{TM}-2 vector, 250 ng of insert was used in presence of 1 µl of 10x Ligase buffer and 1 µl of T4 DNA Ligase Enzyme. The reaction was adjusted to a total of 10 µl with nuclease-free water and was incubated overnight at 16 °C in thermocycler. The ligation products or capsid constructs were transformed into chemically competent *E. coli* using a heat-shock method. Transformed bacteria were allowed to grow overnight under antibiotic selection.

4.2.3.4 Isolation of Plasmid DNA and sequencing

5 ml of bacterial culture grown overnight was subjected to plasmid isolation using GeneJet Plasmid Miniprep kit. To obtain higher amounts of plasmid DNA, midi-preps were performed using Plasmid Plus Midi Kit with 200 ml bacterial culture grown overnight. All procedures were performed as per the manufacturer's instructions. Concentration of obtained DNA was assessed using Nano Drop One. To confirm the presence of desired constructs, all obtained plasmids were sequenced through Eurofins Genomics SupremeRun Tube sequencing using 10 pmol primers. The primers used for sequencing various psiCHECK^{TM}-2 and HBV capsid constructs are enlisted in 4.1.8. All sequence-confirmed DNA samples were stored at -20^{0}C.

4.2.4 Immunological techniques

4.2.4.1 Flow Cytometric Analysis of Hepatic stellate cells

Primary HSCs or LX-2 cells were analyzed for intracellular activation markers and TGFß-1 expression by flow cytometry. In brief, the cells were harvested by trypsinisation and washed with FACS buffer (PBS with 0.5 % FCS) twice, followed by surface staining with 50 µl mix containing 1:100 diluted anti-CD271 AF488 as well as FVD Live-dead stain for 30 minutes at 4^{0}C in dark. Thereafter washing the cells twice with 200 µl FACS buffer, the cells were then fixed with 70 µl Fix & Perm Cell Fixation & Cell Permeabilization kit for 30 minutes. Upon washing once with 200 µl FACS buffer, the cells were intracellularly stained with a master mix containing 1:50 diluted anti-TGFß-1 PE or PE/Cy-7, and anti-αSMA APC. The cells were incubated for 1 hour at 4^{0}C in dark. Following the intracellular staining, the cells were washed twice with 200 µl FACS buffer and analyzed by either CytoFLEX S Flow Cytometer or LSR-Fortessa^{TM} flow cytometer.

4.2.5 Protein production, purification, and analytical Methods

4.2.5.1 Bacterial pre-cultures and expression cultures for HBV capsids

To prepare bacterial pre-cultures, single *E. coli* colonies harbouring HBV capsid constructs were picked up and grown overnight at 37 °C in 6 or 200 ml Lysogeny broth containing Kanamycin (LB_{kan}) with constant shaking. The optical density at 600 nm (OD600) of the pre-cultures were determined using spectrophotometer. The expression cultures for inducible expression of HBV capsids were initiated with an OD600 of 0.1 per

ml, using the pre-cultures as inoculum. The expression cultures of 200 ml – 1 litre were carried out in antibiotic free LB medium. Upon reaching the desired OD600 of 1.0 per ml, the expression cultures were induced with 1 mM IPTG for T7 promoter; and/or with 250 ng/ml AHT. After induction, the cultures were grown for 16 hours at 25 °C with a constant mixing at 140-160 rpm. Following to that, the bacteria were harvested by centrifugation at 4000 x *g* for 15 minutes at 4 °C and the pallets were either stored at -80 °C or processed for further extraction of intact HBV capsids.

4.2.5.2 Sonication of bacterial pallets

Harvested bacterial pallets were weighed and resuspended in 10 ml extraction buffer (50 mM NaH_2PO_4, 100mM NaCl, 10 % Triton-X, in 200 ml water supplemented with 2 mM $MgCl_2$ and DNase) by heavy vortexing. Sonication was performed on suspended bacteria with Brandelin Sonicator, with 2 cycles of 2 minutes each at 85-87 % intensity. Bacterial pallets and suspension were always maintained on ice during the whole process. After sonication, the residual debris was collected by centrifuging times at 3200 x *g* for 15 minutes at 4 °C. After two rounds of centrifugation, the supernatant was carefully transferred to new clean falcon tubes and either used for sucrose gradient-based purification or stored at -80 °C till further use.

4.2.5.3 Bradford assay for protein estimation

Protein estimation was performed using Bradford Assay. Briefly, in a 96-well plate, to the 10 µl of sample to be measured, 200 µl of Bradford reagent was added. The samples were incubated at 37 °C for 30 minutes. After incubation, the assay was measured at 595 nM using Infinte® 200 Pro plate reader. Protein concentration per ml was extrapolated from the standard curve generated from in-run BSA standards.

4.2.5.4 Sucrose gradient ultracentrifugation

Supernatants harvested from sonicated bacteria were subjected to purification by two successive rounds of sucrose gradient ultracentrifugation. Briefly, 15 mg total soluble protein was resuspended in 15 ml of 1x PBS supplemented with cOmplete™ protease inhibitor and loaded carefully on top of the first sucrose gradient. The samples were centrifuged at 32,000 RPM in Beckman L90 Optima centrifuge with SW 32 Ti Swinging-Bucket rotor at 8 °C for 3.5 hours. Post ultracentrifugation, the fractions were harvested

manually. Presence of HBV core protein in different fractions was verified with SDS-PAGE followed by Coomassie Brilliant Blue CCB R250 staining. Elutes showing distinct presence of HBV core protein were pulled together and concentrated and washed with 1x PBS supplemented with protease inhibitor, using Vivaspin® 100,000 MWCO PES columns. Immediately after that, the samples were subjected to second round of sucrose gradient ultracentrifugation. Post recovery of fractions, analysis by SDS-PAGE and concentration of proteins were carried out as mentioned before. Estimation of concentration of purified capsids was done using Bradford assay. Purified capsids were stored at -20 °C till further use.

4.2.5.5 SDS-PAGE and Western blot

SDS-PAGE and WB analysis were performed to assess the purity and presence of HBV core protein and capsids as well as to confirm the silencing efficacy of siRNAs. The samples were prepared by heating at 95 °C for 10 minutes, suspended in SDS-PAGE loading buffer supplemented with ß-Mercaptoethanol. Either equal volumes of protein solutions or equal amounts of total protein were separated on a 15 % SDS-PAGE under reducing conditions and stained for 2 hours with Coomassie Brilliant Blue R-250. Stained gels were destained overnight in approximately 100 ml of destaining buffer. The bands of protein of interest were visualized in ECL ChemoCam Imager. For WB analysis, the proteins separated by SDS-PAGE and transferred to a polyvinylidene fluoride membrane at 300 mA for 1 hour 45 minutes. After blocking the membrane with 5 % skimmed milk prepared in PBST for 1 hour at room temperature, the membranes were incubated on a rocker with sufficient concentrations of primary antibody overnight at 4 °C. The membranes were then washed 3x with approximately 50 ml PBST and incubated with appropriate HRP-labelled secondary antibody diluted 1:10000 in PBST for 2 hours at room temperature. The staining was again followed by 3x washing with PBST. Thereafter, the blots were developed using Amersham™ ECL Prime Western Blotting Detection Reagent and the bands were visualized in ECL ChemoCam Imager.

4.2.5.6 Native Agarose Gel Electrophoresis

NAGE was performed to assess the integrity of various HBV capsids. Equal amounts of total protein were mixed with 6x DNA gel loading dye and separated on 50 ml 1 % Agarose gel containing 10 µl Roti® Gel stain in native conditions at 100 Volts for one hour. Bands representing HBV capsids carrying bacterial nucleic acids were visualized

in Fusion Fx7 gel documentation system. The gels were then subjected to protein staining with SDS-staining buffer for 2 hours. Stained gels were then destained overnight with the destaining solution as described previously. The bands representing intact HBV capsids were visualized under Fusion Fx7 gel documentation system.

5 List of Figures

6 References

Adami, R. C., Seth, S., Harvie, P., Johns, R., Fam, R., Fosnaugh, K., . . . Houston, M. E., Jr. (2011). An amino acid-based amphoteric liposomal delivery system for systemic administration of siRNA. *Mol Ther, 19*(6), 1141-1151. Retrieved from https://www.ncbi.nlm.nih.gov/pubmed/21505423. doi:10.1038/mt.2011.56

Adams, D., Gonzalez-Duarte, A., O'Riordan, W. D., Yang, C. C., Ueda, M., Kristen, A. V., . . . Suhr, O. B. (2018). Patisiran, an RNAi Therapeutic, for Hereditary Transthyretin Amyloidosis. *N Engl J Med, 379*(1), 11-21. Retrieved from https://www.ncbi.nlm.nih.gov/pubmed/29972753. doi:10.1056/NEJMoa1716153

Adrian, M., Zeman, J., Erdley, C., Lisa, L., & Sim, L. (2011). Emotional dysregulation and interpersonal difficulties as risk factors for nonsuicidal self-injury in adolescent girls. *J Abnorm Child Psychol, 39*(3), 389-400. Retrieved from https://www.ncbi.nlm.nih.gov/pubmed/20953828. doi:10.1007/s10802-010-9465-3

Aguilar, J. C., Aguiar, J. A., & Akbar, S. M. F. (2022). Action Mechanisms and Scientific Rationale of Using Nasal Vaccine (HeberNasvac) for the Treatment of Chronic Hepatitis B. *Vaccines (Basel), 10*(12). Retrieved from https://www.ncbi.nlm.nih.gov/pubmed/36560498. doi:10.3390/vaccines10122087

Akinc, A., Zumbuehl, A., Goldberg, M., Leshchiner, E. S., Busini, V., Hossain, N., . . . Anderson, D. G. (2008). A combinatorial library of lipid-like materials for delivery of RNAi therapeutics. *Nat Biotechnol, 26*(5), 561-569. Retrieved from https://www.ncbi.nlm.nih.gov/pubmed/18438401. doi:10.1038/nbt1402

Al Mahtab, M., Akbar, S. M. F., Aguilar, J. C., Guillen, G., Penton, E., Tuero, A., . . . Onji, M. (2018). Treatment of chronic hepatitis B naive patients with a therapeutic vaccine containing HBs and HBc antigens (a randomized, open and treatment controlled phase III clinical trial). *PLoS One, 13*(8), e0201236. Retrieved from https://www.ncbi.nlm.nih.gov/pubmed/30133478. doi:10.1371/journal.pone.0201236

Alberti, A., Clumeck, N., Collins, S., Gerlich, W., Lundgren, J., Palu, G., . . . Jury, E. C. C. (2005). Short statement of the first European Consensus Conference on the treatment of chronic hepatitis B and C in HIV co-infected patients. *J Hepatol, 42*(5), 615-624. Retrieved from https://www.ncbi.nlm.nih.gov/pubmed/15916745. doi:10.1016/j.jhep.2005.03.003

Alexandersen, S., Chamings, A., & Bhatta, T. R. (2020). SARS-CoV-2 genomic and subgenomic RNAs in diagnostic samples are not an indicator of active replication. *Nat Commun, 11*(1), 6059. Retrieved from https://www.ncbi.nlm.nih.gov/pubmed/33247099. doi:10.1038/s41467-020-19883-7

Alimohamadi, Y., Sepandi, M., Taghdir, M., & Hosamirudsari, H. (2020). Determine the most common clinical symptoms in COVID-19 patients: a systematic review and meta-analysis. *J Prev Med Hyg, 61*(3), E304-E312. Retrieved from https://www.ncbi.nlm.nih.gov/pubmed/33150219. doi:10.15167/2421-4248/jpmh2020.61.3.1530

Allerson, C. R., Sioufi, N., Jarres, R., Prakash, T. P., Naik, N., Berdeja, A., . . . Bhat, B. (2005). Fully 2'-modified oligonucleotide duplexes with improved in vitro potency and stability compared to unmodified small interfering RNA. *J Med Chem, 48*(4), 901-904. Retrieved from https://www.ncbi.nlm.nih.gov/pubmed/15715458. doi:10.1021/jm049167j

Alshaer, W., Zureigat, H., Al Karaki, A., Al-Kadash, A., Gharaibeh, L., Hatmal, M. M., . . . Awidi, A. (2021). siRNA: Mechanism of action, challenges, and therapeutic approaches. *Eur J Pharmacol, 905*, 174178. Retrieved from https://www.ncbi.nlm.nih.gov/pubmed/34044011. doi:10.1016/j.ejphar.2021.174178

Amarzguioui, M., Holen, T., Babaie, E., & Prydz, H. (2003). Tolerance for mutations and chemical modifications in a siRNA. *Nucleic Acids Res, 31*(2), 589-595. Retrieved from https://www.ncbi.nlm.nih.gov/pubmed/12527766. doi:10.1093/nar/gkg147

Ambike, S., Cheng, C. C., Feuerherd, M., Velkov, S., Baldassi, D., Afridi, S. Q., . . . Michler, T. (2022). Targeting genomic SARS-CoV-2 RNA with siRNAs allows efficient inhibition of viral replication and spread. *Nucleic Acids Res, 50*(1), 333-349. Retrieved from https://www.ncbi.nlm.nih.gov/pubmed/34928377. doi:10.1093/nar/gkab1248

Andrews, R. J., Roche, J., & Moss, W. N. (2018). ScanFold: an approach for genome-wide discovery of local RNA structural elements-applications to Zika virus and HIV. *PeerJ, 6*,

e6136. Retrieved from https://www.ncbi.nlm.nih.gov/pubmed/30627482. doi:10.7717/peerj.6136

Asabe, S., Wieland, S. F., Chattopadhyay, P. K., Roederer, M., Engle, R. E., Purcell, R. H., & Chisari, F. V. (2009). The size of the viral inoculum contributes to the outcome of hepatitis B virus infection. *J Virol, 83*(19), 9652-9662. Retrieved from https://www.ncbi.nlm.nih.gov/pubmed/19625407. doi:10.1128/JVI.00867-09

Ayensu, W. K., & Tchounwou, P. B. (2006). Microarray analysis of mercury-induced changes in gene expression in human liver carcinoma (HepG2) cells: importance in immune responses. *Int J Environ Res Public Health, 3*(2), 141-173. Retrieved from https://www.ncbi.nlm.nih.gov/pubmed/16823088. doi:10.3390/ijerph2006030018

Baatartsogt, N., Kashiwakura, Y., Hiramoto, T., Hayakawa, M., Kamoshita, N., & Ohmori, T. (2023). Successful liver transduction by re-administration of different adeno-associated virus vector serotypes in mice. *J Gene Med*, e3505. Retrieved from https://www.ncbi.nlm.nih.gov/pubmed/36972408. doi:10.1002/jgm.3505

Backes, S., Jager, C., Dembek, C. J., Kosinska, A. D., Bauer, T., Stephan, A. S., . . . Protzer, U. (2016). Protein-prime/modified vaccinia virus Ankara vector-boost vaccination overcomes tolerance in high-antigenemic HBV-transgenic mice. *Vaccine, 34*(7), 923-932. Retrieved from https://www.ncbi.nlm.nih.gov/pubmed/26776470. doi:10.1016/j.vaccine.2015.12.060

Balkhair, A., Al-Zakwani, I., Al Busaidi, M., Al-Khirbash, A., Al Mubaihsi, S., BaTaher, H., . . . Balkhair, O. (2020). Anakinra in hospitalized patients with severe COVID-19 pneumonia requiring oxygen therapy: results of a prospective, open-label, interventional study. *Int J Infect Dis*. Retrieved from https://www.ncbi.nlm.nih.gov/pubmed/33217576. doi:10.1016/j.ijid.2020.11.149

Barbier, A. J., Jiang, A. Y., Zhang, P., Wooster, R., & Anderson, D. G. (2022). The clinical progress of mRNA vaccines and immunotherapies. *Nat Biotechnol, 40*(6), 840-854. Retrieved from https://www.ncbi.nlm.nih.gov/pubmed/35534554. doi:10.1038/s41587-022-01294-2

Bartas, M., Volna, A., Beaudoin, C. A., Poulsen, E. T., Cerven, J., Brazda, V., . . . Pecinka, P. (2022). Unheeded SARS-CoV-2 proteins? A deep look into negative-sense RNA. *Brief Bioinform, 23*(3). Retrieved from https://www.ncbi.nlm.nih.gov/pubmed/35229157. doi:10.1093/bib/bbac045

Baselga, M., Guemes, A., Alba, J. J., & Schuhmacher, A. J. (2022). SARS-CoV-2 Droplet and Airborne Transmission Heterogeneity. *J Clin Med, 11*(9). Retrieved from https://www.ncbi.nlm.nih.gov/pubmed/35566733. doi:10.3390/jcm11092607

Beigel, J. H., Tomashek, K. M., Dodd, L. E., Mehta, A. K., Zingman, B. S., Kalil, A. C., . . . Members, A.-S. G. (2020). Remdesivir for the Treatment of Covid-19 - Final Report. *N Engl J Med, 383*(19), 1813-1826. Retrieved from https://www.ncbi.nlm.nih.gov/pubmed/32445440. doi:10.1056/NEJMoa2007764

Bengsch, B., Martin, B., & Thimme, R. (2014). Restoration of HBV-specific CD8+ T cell function by PD-1 blockade in inactive carrier patients is linked to T cell differentiation. *J Hepatol, 61*(6), 1212-1219. Retrieved from https://www.ncbi.nlm.nih.gov/pubmed/25016223. doi:10.1016/j.jhep.2014.07.005

Benseler, V., Warren, A., Vo, M., Holz, L. E., Tay, S. S., Le Couteur, D. G., . . . Bertolino, P. (2011). Hepatocyte entry leads to degradation of autoreactive CD8 T cells. *Proc Natl Acad Sci U S A, 108*(40), 16735-16740. Retrieved from https://www.ncbi.nlm.nih.gov/pubmed/21933957. doi:10.1073/pnas.1112251108

Bernstein, E., Caudy, A. A., Hammond, S. M., & Hannon, G. J. (2001). Role for a bidentate ribonuclease in the initiation step of RNA interference. *Nature, 409*(6818), 363-366. Retrieved from https://www.ncbi.nlm.nih.gov/pubmed/11201747. doi:10.1038/35053110

Bertoletti, A., & Ferrari, C. (2016). Adaptive immunity in HBV infection. *J Hepatol, 64*(1 Suppl), S71-S83. Retrieved from https://www.ncbi.nlm.nih.gov/pubmed/27084039. doi:10.1016/j.jhep.2016.01.026

Bettini, E., & Locci, M. (2021). SARS-CoV-2 mRNA Vaccines: Immunological Mechanism and Beyond. *Vaccines (Basel), 9*(2). Retrieved from https://www.ncbi.nlm.nih.gov/pubmed/33673048. doi:10.3390/vaccines9020147

Billerbeck, E., Bottler, T., & Thimme, R. (2007). Regulatory T cells in viral hepatitis. *World J Gastroenterol, 13*(36), 4858-4864. Retrieved from https://www.ncbi.nlm.nih.gov/pubmed/17828817. doi:10.3748/wjg.v13.i36.4858

Bitko, V., Musiyenko, A., Shulyayeva, O., & Barik, S. (2005). Inhibition of respiratory viruses by nasally administered siRNA. *Nat Med, 11*(1), 50-55. Retrieved from https://www.ncbi.nlm.nih.gov/pubmed/15619632. doi:10.1038/nm1164

Boni, C., Fisicaro, P., Valdatta, C., Amadei, B., Di Vincenzo, P., Giuberti, T., . . . Ferrari, C. (2007). Characterization of hepatitis B virus (HBV)-specific T-cell dysfunction in chronic HBV infection. *J Virol, 81*(8), 4215-4225. Retrieved from https://www.ncbi.nlm.nih.gov/pubmed/17287266. doi:10.1128/JVI.02844-06

Boudreau, R. L., Spengler, R. M., Hylock, R. H., Kusenda, B. J., Davis, H. A., Eichmann, D. A., & Davidson, B. L. (2013). siSPOTR: a tool for designing highly specific and potent siRNAs for human and mouse. *Nucleic Acids Res, 41*(1), e9. Retrieved from https://www.ncbi.nlm.nih.gov/pubmed/22941647. doi:10.1093/nar/gks797

Braasch, D. A., Jensen, S., Liu, Y., Kaur, K., Arar, K., White, M. A., & Corey, D. R. (2003). RNA interference in mammalian cells by chemically-modified RNA. *Biochemistry, 42*(26), 7967-7975. Retrieved from https://www.ncbi.nlm.nih.gov/pubmed/12834349. doi:10.1021/bi0343774

Brown, K. M., Nair, J. K., Janas, M. M., Anglero-Rodriguez, Y. I., Dang, L. T. H., Peng, H., . . . Jadhav, V. (2022). Expanding RNAi therapeutics to extrahepatic tissues with lipophilic conjugates. *Nat Biotechnol, 40*(10), 1500-1508. Retrieved from https://www.ncbi.nlm.nih.gov/pubmed/35654979. doi:10.1038/s41587-022-01334-x

Bruss, V., & Ganem, D. (1991). The role of envelope proteins in hepatitis B virus assembly. *Proc Natl Acad Sci U S A, 88*(3), 1059-1063. Retrieved from https://www.ncbi.nlm.nih.gov/pubmed/1992457. doi:10.1073/pnas.88.3.1059

Buchmann, P., Dembek, C., Kuklick, L., Jager, C., Tedjokusumo, R., von Freyend, M. J., . . . Protzer, U. (2013). A novel therapeutic hepatitis B vaccine induces cellular and humoral immune responses and breaks tolerance in hepatitis B virus (HBV) transgenic mice. *Vaccine, 31*(8), 1197-1203. Retrieved from https://www.ncbi.nlm.nih.gov/pubmed/23306359. doi:10.1016/j.vaccine.2012.12.074

Bunse, T., Kosinska, A. D., Michler, T., & Protzer, U. (2022). PD-L1 Silencing in Liver Using siRNAs Enhances Efficacy of Therapeutic Vaccination for Chronic Hepatitis B. *Biomolecules, 12*(3). Retrieved from https://www.ncbi.nlm.nih.gov/pubmed/35327662. doi:10.3390/biom12030470

Burnett, J. C., Rossi, J. J., & Tiemann, K. (2011). Current progress of siRNA/shRNA therapeutics in clinical trials. *Biotechnol J, 6*(9), 1130-1146. Retrieved from https://www.ncbi.nlm.nih.gov/pubmed/21744502. doi:10.1002/biot.201100054

Cai, Q., Yang, M., Liu, D., Chen, J., Shu, D., Xia, J., . . . Liu, L. (2020). Experimental Treatment with Favipiravir for COVID-19: An Open-Label Control Study. *Engineering (Beijing), 6*(10), 1192-1198. Retrieved from https://www.ncbi.nlm.nih.gov/pubmed/32346491. doi:10.1016/j.eng.2020.03.007

Carpino, G., Morini, S., Ginanni Corradini, S., Franchitto, A., Merli, M., Siciliano, M., . . . Gaudio, E. (2005). Alpha-SMA expression in hepatic stellate cells and quantitative analysis of hepatic fibrosis in cirrhosis and in recurrent chronic hepatitis after liver transplantation. *Dig Liver Dis, 37*(5), 349-356. Retrieved from https://www.ncbi.nlm.nih.gov/pubmed/15843085. doi:10.1016/j.dld.2004.11.009

Carthew, R. W., & Sontheimer, E. J. (2009). Origins and Mechanisms of miRNAs and siRNAs. *Cell, 136*(4), 642-655. Retrieved from https://www.ncbi.nlm.nih.gov/pubmed/19239886. doi:10.1016/j.cell.2009.01.035

Cassidy, A., Mossman, S., Olivieri, A., De Ridder, M., & Leroux-Roels, G. (2011). Hepatitis B vaccine effectiveness in the face of global HBV genotype diversity. *Expert Rev Vaccines, 10*(12), 1709-1715. Retrieved from https://www.ncbi.nlm.nih.gov/pubmed/22085174. doi:10.1586/erv.11.151

CDC, C. f. D. C. a. P. (2021). Scientific Brief: SARS-CoV-2 Transmission. Retrieved from https://www.cdc.gov/coronavirus/2019-ncov/science/science-briefs/sars-cov-2-transmission.html#:~:text=Inhalation%20of%20air%20carrying%20very,droplets%20and%20particles%20is%20greatest.

CDC, C. f. D. C. a. P. (2023a). COVID-19 Treatments and Medications. Retrieved from https://www.cdc.gov/coronavirus/2019-ncov/your-health/treatments-for-severe-illness.html

CDC, C. f. D. C. a. P. (2023b). How Vaccines are Developed and Approved for Use. Retrieved from https://www.cdc.gov/vaccines/basics/test-approve.html

Cha, J. H., Chan, L. C., Li, C. W., Hsu, J. L., & Hung, M. C. (2019). Mechanisms Controlling PD-L1 Expression in Cancer. *Mol Cell, 76*(3), 359-370. Retrieved from https://www.ncbi.nlm.nih.gov/pubmed/31668929. doi:10.1016/j.molcel.2019.09.030

Chang, Y. C., Yang, C. F., Chen, Y. F., Yang, C. C., Chou, Y. L., Chou, H. W., . . . Yang, P. C. (2022). A siRNA targets and inhibits a broad range of SARS-CoV-2 infections including Delta variant. *EMBO Mol Med, 14*(4), e15298. Retrieved from https://www.ncbi.nlm.nih.gov/pubmed/35138028. doi:10.15252/emmm.202115298

Chen, C., Wang, J. C., & Zlotnick, A. (2011). A kinase chaperones hepatitis B virus capsid assembly and captures capsid dynamics in vitro. *PLoS Pathog, 7*(11), e1002388. Retrieved from https://www.ncbi.nlm.nih.gov/pubmed/22114561. doi:10.1371/journal.ppat.1002388

Chernikov, I. V., Vlassov, V. V., & Chernolovskaya, E. L. (2019). Current Development of siRNA Bioconjugates: From Research to the Clinic. *Front Pharmacol, 10*, 444. Retrieved from https://www.ncbi.nlm.nih.gov/pubmed/31105570. doi:10.3389/fphar.2019.00444

Chin, A. W. H., & Poon, L. L. M. (2020). Stability of SARS-CoV-2 in different environmental conditions - Authors' reply. *Lancet Microbe, 1*(4), e146. Retrieved from https://www.ncbi.nlm.nih.gov/pubmed/33521712. doi:10.1016/S2666-5247(20)30095-1

Chisari, F. V., Isogawa, M., & Wieland, S. F. (2010). Pathogenesis of hepatitis B virus infection. *Pathol Biol (Paris), 58*(4), 258-266. Retrieved from https://www.ncbi.nlm.nih.gov/pubmed/20116937. doi:10.1016/j.patbio.2009.11.001

Chiu, Y. L., & Rana, T. M. (2003). siRNA function in RNAi: a chemical modification analysis. *RNA, 9*(9), 1034-1048. Retrieved from https://www.ncbi.nlm.nih.gov/pubmed/12923253. doi:10.1261/rna.5103703

Choung, S., Kim, Y. J., Kim, S., Park, H. O., & Choi, Y. C. (2006). Chemical modification of siRNAs to improve serum stability without loss of efficacy. *Biochem Biophys Res Commun, 342*(3), 919-927. Retrieved from https://www.ncbi.nlm.nih.gov/pubmed/16598842. doi:10.1016/j.bbrc.2006.02.049

Chu, D. K., Akl, E. A., Duda, S., Solo, K., Yaacoub, S., Schunemann, H. J., & authors, C.-S. U. R. G. E. s. (2020). Physical distancing, face masks, and eye protection to prevent person-to-person transmission of SARS-CoV-2 and COVID-19: a systematic review and meta-analysis. *Lancet, 395*(10242), 1973-1987. Retrieved from https://www.ncbi.nlm.nih.gov/pubmed/32497510. doi:10.1016/S0140-6736(20)31142-9

Coelho, T., Adams, D., Silva, A., Lozeron, P., Hawkins, P. N., Mant, T., . . . Suhr, O. B. (2013). Safety and efficacy of RNAi therapy for transthyretin amyloidosis. *N Engl J Med, 369*(9), 819-829. Retrieved from https://www.ncbi.nlm.nih.gov/pubmed/23984729. doi:10.1056/NEJMoa1208760

Colantuoni, A., Martini, R., Caprari, P., Ballestri, M., Capecchi, P. L., Gnasso, A., . . . Caimi, G. (2020). COVID-19 Sepsis and Microcirculation Dysfunction. *Front Physiol, 11*, 747. Retrieved from https://www.ncbi.nlm.nih.gov/pubmed/32676039. doi:10.3389/fphys.2020.00747

Conde, L., Allatif, O., Ohlmann, T., & de Breyne, S. (2022). Translation of SARS-CoV-2 gRNA Is Extremely Efficient and Competitive despite a High Degree of Secondary Structures and the Presence of an uORF. *Viruses, 14*(7). Retrieved from https://www.ncbi.nlm.nih.gov/pubmed/35891485. doi:10.3390/v14071505

Copin, R., Baum, A., Wloga, E., Pascal, K. E., Giordano, S., Fulton, B. O., . . . Kyratsous, C. A. (2021). The monoclonal antibody combination REGEN-COV protects against SARS-CoV-2 mutational escape in preclinical and human studies. *Cell, 184*(15), 3949-3961 e3911. Retrieved from https://www.ncbi.nlm.nih.gov/pubmed/34161776. doi:10.1016/j.cell.2021.06.002

Coronaviridae Study Group of the International Committee on Taxonomy of, V. (2020). The species Severe acute respiratory syndrome-related coronavirus: classifying 2019-nCoV and naming it SARS-CoV-2. *Nat Microbiol, 5*(4), 536-544. Retrieved from https://www.ncbi.nlm.nih.gov/pubmed/32123347. doi:10.1038/s41564-020-0695-z

CRASTO, D. A. M. (2020). Lumasiran. Retrieved from https://newdrugapprovals.org/2020/12/15/lumasiran/

Crehuet Gramatyka, D., Domenech Tarrega, A., Driller, C., Mangas Alvarez, L., Maupoey Ibanez, J., Dieguez Hernandez-Baquero, I., . . . Vila Carbo, J. J. (2022). Pediatric living donor liver transplantation: results of laparoscopic vs. open graft removal. *Cir Pediatr, 35*(2), 63-69.

Retrieved from https://www.ncbi.nlm.nih.gov/pubmed/35485753. doi:10.54847/cp.2022.02.13

Cubuk, J., Alston, J. J., Incicco, J. J., Singh, S., Stuchell-Brereton, M. D., Ward, M. D., . . . Holehouse, A. S. (2021). The SARS-CoV-2 nucleocapsid protein is dynamic, disordered, and phase separates with RNA. *Nat Commun, 12*(1), 1936. Retrieved from https://www.ncbi.nlm.nih.gov/pubmed/33782395. doi:10.1038/s41467-021-21953-3

Cucinotta, D., & Vanelli, M. (2020). WHO Declares COVID-19 a Pandemic. *Acta Biomed, 91*(1), 157-160. Retrieved from https://www.ncbi.nlm.nih.gov/pubmed/32191675. doi:10.23750/abm.v91i1.9397

D'Souza, A. A., & Devarajan, P. V. (2015). Asialoglycoprotein receptor mediated hepatocyte targeting - strategies and applications. *J Control Release, 203*, 126-139. Retrieved from https://www.ncbi.nlm.nih.gov/pubmed/25701309. doi:10.1016/j.jconrel.2015.02.022

Dai, F., Yusuf, F., Farjah, G. H., & Brand-Saberi, B. (2005). RNAi-induced targeted silencing of developmental control genes during chicken embryogenesis. *Dev Biol, 285*(1), 80-90. Retrieved from https://www.ncbi.nlm.nih.gov/pubmed/16055113. doi:10.1016/j.ydbio.2005.06.005

Dande, P., Prakash, T. P., Sioufi, N., Gaus, H., Jarres, R., Berdeja, A., . . . Bhat, B. (2006). Improving RNA interference in mammalian cells by 4'-thio-modified small interfering RNA (siRNA): effect on siRNA activity and nuclease stability when used in combination with 2'-O-alkyl modifications. *J Med Chem, 49*(5), 1624-1634. Retrieved from https://www.ncbi.nlm.nih.gov/pubmed/16509579. doi:10.1021/jm050822c

Dane, D. S., Cameron, C. H., & Briggs, M. (1970). Virus-like particles in serum of patients with Australia-antigen-associated hepatitis. *Lancet, 1*(7649), 695-698. Retrieved from https://www.ncbi.nlm.nih.gov/pubmed/4190997. doi:10.1016/s0140-6736(70)90926-8

Dardalhon, V., Awasthi, A., Kwon, H., Galileos, G., Gao, W., Sobel, R. A., . . . Kuchroo, V. K. (2008). IL-4 inhibits TGF-beta-induced Foxp3+ T cells and, together with TGF-beta, generates IL-9+ IL-10+ Foxp3(-) effector T cells. *Nat Immunol, 9*(12), 1347-1355. Retrieved from https://www.ncbi.nlm.nih.gov/pubmed/18997793. doi:10.1038/ni.1677

Das, P. R., & Sherif, S. M. (2020). Application of Exogenous dsRNAs-induced RNAi in Agriculture: Challenges and Triumphs. *Front Plant Sci, 11*, 946. Retrieved from https://www.ncbi.nlm.nih.gov/pubmed/32670336. doi:10.3389/fpls.2020.00946

Datta, S., Chatterjee, S., Veer, V., & Chakravarty, R. (2012). Molecular biology of the hepatitis B virus for clinicians. *J Clin Exp Hepatol, 2*(4), 353-365. Retrieved from https://www.ncbi.nlm.nih.gov/pubmed/25755457. doi:10.1016/j.jceh.2012.10.003

Deeks, E. D. (2021). Casirivimab/Imdevimab: First Approval. *Drugs, 81*(17), 2047-2055. Retrieved from https://www.ncbi.nlm.nih.gov/pubmed/34716907. doi:10.1007/s40265-021-01620-z

Deleavey, G. F., Watts, J. K., & Damha, M. J. (2009). Chemical modification of siRNA. *Curr Protoc Nucleic Acid Chem, Chapter 16*, Unit 16 13. Retrieved from https://www.ncbi.nlm.nih.gov/pubmed/20013783. doi:10.1002/0471142700.nc1603s39

Dembek, C., Protzer, U., & Roggendorf, M. (2018). Overcoming immune tolerance in chronic hepatitis B by therapeutic vaccination. *Curr Opin Virol, 30*, 58-67. Retrieved from https://www.ncbi.nlm.nih.gov/pubmed/29751272. doi:10.1016/j.coviro.2018.04.003

DeVincenzo, J., Lambkin-Williams, R., Wilkinson, T., Cehelsky, J., Nochur, S., Walsh, E., . . . Vaishnaw, A. (2010). A randomized, double-blind, placebo-controlled study of an RNAi-based therapy directed against respiratory syncytial virus. *Proc Natl Acad Sci U S A, 107*(19), 8800-8805. Retrieved from https://www.ncbi.nlm.nih.gov/pubmed/20421463. doi:10.1073/pnas.0912186107

Donnelly, J. J., Wahren, B., & Liu, M. A. (2005). DNA vaccines: progress and challenges. *J Immunol, 175*(2), 633-639. Retrieved from https://www.ncbi.nlm.nih.gov/pubmed/16002657. doi:10.4049/jimmunol.175.2.633

Dorsett, Y., & Tuschl, T. (2004). siRNAs: applications in functional genomics and potential as therapeutics. *Nat Rev Drug Discov, 3*(4), 318-329. Retrieved from https://www.ncbi.nlm.nih.gov/pubmed/15060527. doi:10.1038/nrd1345

Draz, M. S., Fang, B. A., Zhang, P., Hu, Z., Gu, S., Weng, K. C., . . . Chen, F. F. (2014). Nanoparticle-mediated systemic delivery of siRNA for treatment of cancers and viral infections. *Theranostics, 4*(9), 872-892. Retrieved from https://www.ncbi.nlm.nih.gov/pubmed/25057313. doi:10.7150/thno.9404

Du, X., Liu, Y., Ma, L., Lu, J., Jin, Y., Ren, S., . . . Chen, X. (2017). Virological and serological features of acute hepatitis B in adults. *Medicine (Baltimore), 96*(7), e6088. Retrieved from https://www.ncbi.nlm.nih.gov/pubmed/28207518. doi:10.1097/MD.0000000000006088

Dynavax. (2011). Dynavax Reports Additional Positive Phase 1B Immunogenicity Data for Hepatitis B Therapy Candidate [Press release]. Retrieved from https://investors.dynavax.com/news-releases/news-release-details/dynavax-reports-additional-positive-phase-1b-immunogenicity-data

EASL. (2017). EASL 2017 Clinical Practice Guidelines on the management of hepatitis B virus infection. *J Hepatol, 67*(2), 370-398. Retrieved from https://www.ncbi.nlm.nih.gov/pubmed/28427875. doi:10.1016/j.jhep.2017.03.021

Ebenezer, O., Comoglio, P., Wong, G. K., & Tuszynski, J. A. (2023). Development of Novel siRNA Therapeutics: A Review with a Focus on Inclisiran for the Treatment of Hypercholesterolemia. *Int J Mol Sci, 24*(4). Retrieved from https://www.ncbi.nlm.nih.gov/pubmed/36835426. doi:10.3390/ijms24044019

Elbashir, S. M., Harborth, J., Lendeckel, W., Yalcin, A., Weber, K., & Tuschl, T. (2001). Duplexes of 21-nucleotide RNAs mediate RNA interference in cultured mammalian cells. *Nature, 411*(6836), 494-498. Retrieved from https://www.ncbi.nlm.nih.gov/pubmed/11373684. doi:10.1038/35078107

Elmen, J., Thonberg, H., Ljungberg, K., Frieden, M., Westergaard, M., Xu, Y., . . . Wahlestedt, C. (2005). Locked nucleic acid (LNA) mediated improvements in siRNA stability and functionality. *Nucleic Acids Res, 33*(1), 439-447. Retrieved from https://www.ncbi.nlm.nih.gov/pubmed/15653644. doi:10.1093/nar/gki193

Essalmani, R., Jain, J., Susan-Resiga, D., Andreo, U., Evagelidis, A., Derbali, R. M., . . . Seidah, N. G. (2022). Distinctive Roles of Furin and TMPRSS2 in SARS-CoV-2 Infectivity. *J Virol, 96*(8), e0012822. Retrieved from https://www.ncbi.nlm.nih.gov/pubmed/35343766. doi:10.1128/jvi.00128-22

Fairhead, M., & Howarth, M. (2015). Site-specific biotinylation of purified proteins using BirA. *Methods Mol Biol, 1266*, 171-184. Retrieved from https://www.ncbi.nlm.nih.gov/pubmed/25560075. doi:10.1007/978-1-4939-2272-7_12

Fedorov, Y., Anderson, E. M., Birmingham, A., Reynolds, A., Karpilow, J., Robinson, K., . . . Khvorova, A. (2006). Off-target effects by siRNA can induce toxic phenotype. *RNA, 12*(7), 1188-1196. Retrieved from https://www.ncbi.nlm.nih.gov/pubmed/16682561. doi:10.1261/rna.28106

Feldmann, D. P., & Merkel, O. M. (2015). The advantages of pulmonary delivery of therapeutic siRNA. *Ther Deliv, 6*(4), 407-409. Retrieved from https://www.ncbi.nlm.nih.gov/pubmed/25996039. doi:10.4155/tde.15.8

Ferrari, C., Bertoletti, A., Penna, A., Cavalli, A., Valli, A., Missale, G., . . . et al. (1991). Identification of immunodominant T cell epitopes of the hepatitis B virus nucleocapsid antigen. *J Clin Invest, 88*(1), 214-222. Retrieved from https://www.ncbi.nlm.nih.gov/pubmed/1711541. doi:10.1172/JCI115280

Fire, A., Albertson, D., Harrison, S. W., & Moerman, D. G. (1991). Production of antisense RNA leads to effective and specific inhibition of gene expression in C. elegans muscle. *Development, 113*(2), 503-514. Retrieved from https://www.ncbi.nlm.nih.gov/pubmed/1782862. doi:10.1242/dev.113.2.503

Fire, A., Xu, S., Montgomery, M. K., Kostas, S. A., Driver, S. E., & Mello, C. C. (1998). Potent and specific genetic interference by double-stranded RNA in Caenorhabditis elegans. *Nature, 391*(6669), 806-811. Retrieved from https://www.ncbi.nlm.nih.gov/pubmed/9486653. doi:10.1038/35888

Fontaine, H., Kahi, S., Chazallon, C., Bourgine, M., Varaut, A., Buffet, C., . . . group, A. H. s. (2015). Anti-HBV DNA vaccination does not prevent relapse after discontinuation of analogues in the treatment of chronic hepatitis B: a randomised trial--ANRS HB02 VAC-ADN. *Gut, 64*(1), 139-147. Retrieved from https://www.ncbi.nlm.nih.gov/pubmed/24555998. doi:10.1136/gutjnl-2013-305707

Fopase, R., Panda, C., Rajendran, A. P., Uludag, H., & Pandey, L. M. (2023). Potential of siRNA in COVID-19 therapy: Emphasis on in silico design and nanoparticles based delivery. *Front Bioeng Biotechnol, 11*, 1112755. Retrieved from https://www.ncbi.nlm.nih.gov/pubmed/36814718. doi:10.3389/fbioe.2023.1112755

Foster, D. J., Brown, C. R., Shaikh, S., Trapp, C., Schlegel, M. K., Qian, K., . . . Milstein, S. (2018). Advanced siRNA Designs Further Improve In Vivo Performance of GalNAc-siRNA

Conjugates. *Mol Ther, 26*(3), 708-717. Retrieved from https://www.ncbi.nlm.nih.gov/pubmed/29456020. doi:10.1016/j.ymthe.2017.12.021

Friedrich, M., & Aigner, A. (2022). Therapeutic siRNA: State-of-the-Art and Future Perspectives. *BioDrugs, 36*(5), 549-571. Retrieved from https://www.ncbi.nlm.nih.gov/pubmed/35997897. doi:10.1007/s40259-022-00549-3

Fu, J. L., Xu, D. P., Zhao, P., Chen, L. M., Zhang, H., Zhou, C. B., . . . Wang, F. S. (2006). [The characterization of regulatory T cells in peripheral blood of HBV-infected patients]. *Zhonghua Yi Xue Za Zhi, 86*(22), 1522-1525. Retrieved from https://www.ncbi.nlm.nih.gov/pubmed/16854276.

Fung, S. Y., Yuen, K. S., Ye, Z. W., Chan, C. P., & Jin, D. Y. (2020). A tug-of-war between severe acute respiratory syndrome coronavirus 2 and host antiviral defence: lessons from other pathogenic viruses. *Emerg Microbes Infect, 9*(1), 558-570. Retrieved from https://www.ncbi.nlm.nih.gov/pubmed/32172672. doi:10.1080/22221751.2020.1736644

Gan, W., Gao, N., Gu, L., Mo, Z., Pang, X., Lei, Z., & Gao, Z. (2023). Reduction in Intrahepatic cccDNA and Integration of HBV in Chronic Hepatitis B Patients with a Functional Cure. *J Clin Transl Hepatol, 11*(2), 314-322. Retrieved from https://www.ncbi.nlm.nih.gov/pubmed/36643049. doi:10.14218/JCTH.2022.00177

Ganem, D., & Prince, A. M. (2004). Hepatitis B virus infection--natural history and clinical consequences. *N Engl J Med, 350*(11), 1118-1129. Retrieved from https://www.ncbi.nlm.nih.gov/pubmed/15014185. doi:10.1056/NEJMra031087

Gao, Y. D., Ding, M., Dong, X., Zhang, J. J., Kursat Azkur, A., Azkur, D., . . . Akdis, C. A. (2021). Risk factors for severe and critically ill COVID-19 patients: A review. *Allergy, 76*(2), 428-455. Retrieved from https://www.ncbi.nlm.nih.gov/pubmed/33185910. doi:10.1111/all.14657

Garcia-Diaz, A., Shin, D. S., Moreno, B. H., Saco, J., Escuin-Ordinas, H., Rodriguez, G. A., . . . Ribas, A. (2017). Interferon Receptor Signaling Pathways Regulating PD-L1 and PD-L2 Expression. *Cell Rep, 19*(6), 1189-1201. Retrieved from https://www.ncbi.nlm.nih.gov/pubmed/28494868. doi:10.1016/j.celrep.2017.04.031

Garrelfs, S. F., Frishberg, Y., Hulton, S. A., Koren, M. J., O'Riordan, W. D., Cochat, P., . . . Collaborators, I.-A. (2021). Lumasiran, an RNAi Therapeutic for Primary Hyperoxaluria Type 1. *N Engl J Med, 384*(13), 1216-1226. Retrieved from https://www.ncbi.nlm.nih.gov/pubmed/33789010. doi:10.1056/NEJMoa2021712

Gaziova, Z., Baumann, V., Winkler, A. M., & Winkler, J. (2014). Chemically defined polyethylene glycol siRNA conjugates with enhanced gene silencing effect. *Bioorg Med Chem, 22*(7), 2320-2326. Retrieved from https://www.ncbi.nlm.nih.gov/pubmed/24613624. doi:10.1016/j.bmc.2014.02.004

Gehring, A. J., & Protzer, U. (2019). Targeting Innate and Adaptive Immune Responses to Cure Chronic HBV Infection. *Gastroenterology, 156*(2), 325-337. Retrieved from https://www.ncbi.nlm.nih.gov/pubmed/30367834. doi:10.1053/j.gastro.2018.10.032

Gerlich, W. H. (2015). Prophylactic vaccination against hepatitis B: achievements, challenges and perspectives. *Med Microbiol Immunol, 204*(1), 39-55. Retrieved from https://www.ncbi.nlm.nih.gov/pubmed/25523195. doi:10.1007/s00430-014-0373-y

Gong, W., Ren, Y., Zhou, H., Wang, Y., Kang, S., & Li, T. (2008). siDRM: an effective and generally applicable online siRNA design tool. *Bioinformatics, 24*(20), 2405-2406. Retrieved from https://www.ncbi.nlm.nih.gov/pubmed/18718944. doi:10.1093/bioinformatics/btn442

Gottlieb, J., Zamora, M. R., Hodges, T., Musk, A. W., Sommerwerk, U., Dilling, D., . . . Glanville, A. R. (2016). ALN-RSV01 for prevention of bronchiolitis obliterans syndrome after respiratory syncytial virus infection in lung transplant recipients. *J Heart Lung Transplant, 35*(2), 213-221. Retrieved from https://www.ncbi.nlm.nih.gov/pubmed/26452996. doi:10.1016/j.healun.2015.08.012

Grimm, D., Pandey, K., Nakai, H., Storm, T. A., & Kay, M. A. (2006). Liver transduction with recombinant adeno-associated virus is primarily restricted by capsid serotype not vector genotype. *J Virol, 80*(1), 426-439. Retrieved from https://www.ncbi.nlm.nih.gov/pubmed/16352567. doi:10.1128/JVI.80.1.426-439.2006

Hadziyannis, S. J., Vassilopoulos, D., & Hadziyannis, E. (2013). The natural course of chronic hepatitis B virus infection and its management. *Adv Pharmacol, 67*, 247-291. Retrieved from https://www.ncbi.nlm.nih.gov/pubmed/23886003. doi:10.1016/B978-0-12-405880-4.00007-X

Hamilton, B., Dong, Y., Shindo, M., Liu, W., Odell, I., Ruvkun, G., & Lee, S. S. (2005). A systematic RNAi screen for longevity genes in C. elegans. *Genes Dev, 19*(13), 1544-1555. Retrieved from https://www.ncbi.nlm.nih.gov/pubmed/15998808. doi:10.1101/gad.1308205

Hang, J., Sun, Z., & Li, L. (2020). [Prevention and control of SARS-CoV-2 infection in clinical laboratories: implementation of contingency plan and postpandemic response strategies]. *Nan Fang Yi Ke Da Xue Xue Bao, 40*(4), 606-608. Retrieved from https://www.ncbi.nlm.nih.gov/pubmed/32895124. doi:10.12122/j.issn.1673-4254.2020.04.25

Haraszti, R. A., Miller, R., Didiot, M. C., Biscans, A., Alterman, J. F., Hassler, M. R., . . . Khvorova, A. (2018). Optimized Cholesterol-siRNA Chemistry Improves Productive Loading onto Extracellular Vesicles. *Mol Ther, 26*(8), 1973-1982. Retrieved from https://www.ncbi.nlm.nih.gov/pubmed/29937418. doi:10.1016/j.ymthe.2018.05.024

Hardenbrook, N. J., & Zhang, P. (2022). A structural view of the SARS-CoV-2 virus and its assembly. *Curr Opin Virol, 52*, 123-134. Retrieved from https://www.ncbi.nlm.nih.gov/pubmed/34915287. doi:10.1016/j.coviro.2021.11.011

Hartley, J. W., Evans, L. H., Green, K. Y., Naghashfar, Z., Macias, A. R., Zerfas, P. M., & Ward, J. M. (2008). Expression of infectious murine leukemia viruses by RAW264.7 cells, a potential complication for studies with a widely used mouse macrophage cell line. *Retrovirology, 5*, 1. Retrieved from https://www.ncbi.nlm.nih.gov/pubmed/18177500. doi:10.1186/1742-4690-5-1

He, L., & Hannon, G. J. (2004). MicroRNAs: small RNAs with a big role in gene regulation. *Nat Rev Genet, 5*(7), 522-531. Retrieved from https://www.ncbi.nlm.nih.gov/pubmed/15211354. doi:10.1038/nrg1379

Henderson, N. C., Mackinnon, A. C., Farnworth, S. L., Poirier, F., Russo, F. P., Iredale, J. P., . . . Sethi, T. (2006). Galectin-3 regulates myofibroblast activation and hepatic fibrosis. *Proc Natl Acad Sci U S A, 103*(13), 5060-5065. Retrieved from https://www.ncbi.nlm.nih.gov/pubmed/16549783. doi:10.1073/pnas.0511167103

Heo, Y. A. (2022). Sotrovimab: First Approval. *Drugs, 82*(4), 477-484. Retrieved from https://www.ncbi.nlm.nih.gov/pubmed/35286623. doi:10.1007/s40265-022-01690-7

Herrscher, C., Roingeard, P., & Blanchard, E. (2020). Hepatitis B Virus Entry into Cells. *Cells, 9*(6). Retrieved from https://www.ncbi.nlm.nih.gov/pubmed/32570893. doi:10.3390/cells9061486

Ho, K. J., Bass, C. E., Kroemer, A. H., Ma, C., Terwilliger, E., & Karp, S. J. (2008). Optimized adeno-associated virus 8 produces hepatocyte-specific Cre-mediated recombination without toxicity or affecting liver regeneration. *Am J Physiol Gastrointest Liver Physiol, 295*(2), G412-419. Retrieved from https://www.ncbi.nlm.nih.gov/pubmed/18535290. doi:10.1152/ajpgi.00590.2007

Holz, L. E., Benseler, V., Bowen, D. G., Bouillet, P., Strasser, A., O'Reilly, L., . . . Bertolino, P. (2008). Intrahepatic murine CD8 T-cell activation associates with a distinct phenotype leading to Bim-dependent death. *Gastroenterology, 135*(3), 989-997. Retrieved from https://www.ncbi.nlm.nih.gov/pubmed/18619445. doi:10.1053/j.gastro.2008.05.078

Honer Zu Siederdissen, C., & Cornberg, M. (2016). Management of HBV and HBV/HDV-Associated Liver Cirrhosis. *Visc Med, 32*(2), 86-94. Retrieved from https://www.ncbi.nlm.nih.gov/pubmed/27413725. doi:10.1159/000445518

Hou, X., Zaks, T., Langer, R., & Dong, Y. (2021). Lipid nanoparticles for mRNA delivery. *Nat Rev Mater, 6*(12), 1078-1094. Retrieved from https://www.ncbi.nlm.nih.gov/pubmed/34394960. doi:10.1038/s41578-021-00358-0

Hsu, J. M., Li, C. W., Lai, Y. J., & Hung, M. C. (2018). Posttranslational Modifications of PD-L1 and Their Applications in Cancer Therapy. *Cancer Res, 78*(22), 6349-6353. Retrieved from https://www.ncbi.nlm.nih.gov/pubmed/30442814. doi:10.1158/0008-5472.CAN-18-1892

Hu, B., Zhong, L., Weng, Y., Peng, L., Huang, Y., Zhao, Y., & Liang, X. J. (2020). Therapeutic siRNA: state of the art. *Signal Transduct Target Ther, 5*(1), 101. Retrieved from https://www.ncbi.nlm.nih.gov/pubmed/32561705. doi:10.1038/s41392-020-0207-x

Hu, J., & Liu, K. (2017). Complete and Incomplete Hepatitis B Virus Particles: Formation, Function, and Application. *Viruses, 9*(3). Retrieved from https://www.ncbi.nlm.nih.gov/pubmed/28335554. doi:10.3390/v9030056

Hu, J. F., Zhang, W., Zuo, W., Tan, H. Q., & Bai, W. (2020). Inhibition of the PD-1/PD-L1 signaling pathway enhances innate immune response of alveolar macrophages to mycobacterium

tuberculosis in mice. *Pulm Pharmacol Ther, 60*, 101842. Retrieved from https://www.ncbi.nlm.nih.gov/pubmed/31541762. doi:10.1016/j.pupt.2019.101842

Hu, Z., Ban, H., Zheng, H., Liu, M., Chang, J., & Guo, J. T. (2020). Protein phosphatase 1 catalyzes HBV core protein dephosphorylation and is co-packaged with viral pregenomic RNA into nucleocapsids. *PLoS Pathog, 16*(7), e1008669. Retrieved from https://www.ncbi.nlm.nih.gov/pubmed/32702076. doi:10.1371/journal.ppat.1008669

Huang, Y., Yang, C., Xu, X. F., Xu, W., & Liu, S. W. (2020). Structural and functional properties of SARS-CoV-2 spike protein: potential antivirus drug development for COVID-19. *Acta Pharmacol Sin, 41*(9), 1141-1149. Retrieved from https://www.ncbi.nlm.nih.gov/pubmed/32747721. doi:10.1038/s41401-020-0485-4

Huovila, A. P., Eder, A. M., & Fuller, S. D. (1992). Hepatitis B surface antigen assembles in a post-ER, pre-Golgi compartment. *J Cell Biol, 118*(6), 1305-1320. Retrieved from https://www.ncbi.nlm.nih.gov/pubmed/1522109. doi:10.1083/jcb.118.6.1305

Hwang, Y. C., Lu, R. M., Su, S. C., Chiang, P. Y., Ko, S. H., Ke, F. Y., . . . Wu, H. C. (2022). Monoclonal antibodies for COVID-19 therapy and SARS-CoV-2 detection. *J Biomed Sci, 29*(1), 1. Retrieved from https://www.ncbi.nlm.nih.gov/pubmed/34983527. doi:10.1186/s12929-021-00784-w

Idris, A., Davis, A., Supramaniam, A., Acharya, D., Kelly, G., Tayyar, Y., . . . Morris, K. V. (2021). A SARS-CoV-2 targeted siRNA-nanoparticle therapy for COVID-19. *Mol Ther, 29*(7), 2219-2226. Retrieved from https://www.ncbi.nlm.nih.gov/pubmed/33992805. doi:10.1016/j.ymthe.2021.05.004

Imaeda, A., Tomoike, F., Hayakawa, M., Nakamoto, K., Kimura, Y., Abe, N., & Abe, H. (2019). N(6)-methyl adenosine in siRNA evades immune response without reducing RNAi activity. *Nucleosides Nucleotides Nucleic Acids, 38*(12), 972-979. Retrieved from https://www.ncbi.nlm.nih.gov/pubmed/31298608. doi:10.1080/15257770.2019.1641205

Ito, T., Okuda, T., Takayama, R., & Okamoto, H. (2019). Establishment of an Evaluation Method for Gene Silencing by Serial Pulmonary Administration of siRNA and pDNA Powders: Naked siRNA Inhalation Powder Suppresses Luciferase Gene Expression in the Lung. *J Pharm Sci, 108*(8), 2661-2667. Retrieved from https://www.ncbi.nlm.nih.gov/pubmed/30954524. doi:10.1016/j.xphs.2019.03.029

Ivashchenko, A. A., Dmitriev, K. A., Vostokova, N. V., Azarova, V. N., Blinow, A. A., Egorova, A. N., . . . Ivachtchenko, A. V. (2021). AVIFAVIR for Treatment of Patients With Moderate Coronavirus Disease 2019 (COVID-19): Interim Results of a Phase II/III Multicenter Randomized Clinical Trial. *Clin Infect Dis, 73*(3), 531-534. Retrieved from https://www.ncbi.nlm.nih.gov/pubmed/32770240. doi:10.1093/cid/ciaa1176

Iwakawa, H. O., & Tomari, Y. (2022). Life of RISC: Formation, action, and degradation of RNA-induced silencing complex. *Mol Cell, 82*(1), 30-43. Retrieved from https://www.ncbi.nlm.nih.gov/pubmed/34942118. doi:10.1016/j.molcel.2021.11.026

Jack, A. D., Hall, A. J., Maine, N., Mendy, M., & Whittle, H. C. (1999). What level of hepatitis B antibody is protective? *J Infect Dis, 179*(2), 489-492. Retrieved from https://www.ncbi.nlm.nih.gov/pubmed/9878036. doi:10.1086/314578

Jackson, A. L., Bartz, S. R., Schelter, J., Kobayashi, S. V., Burchard, J., Mao, M., . . . Linsley, P. S. (2003). Expression profiling reveals off-target gene regulation by RNAi. *Nat Biotechnol, 21*(6), 635-637. Retrieved from https://www.ncbi.nlm.nih.gov/pubmed/12754523. doi:10.1038/nbt831

Jackson, A. L., Burchard, J., Schelter, J., Chau, B. N., Cleary, M., Lim, L., & Linsley, P. S. (2006). Widespread siRNA "off-target" transcript silencing mediated by seed region sequence complementarity. *RNA, 12*(7), 1179-1187. Retrieved from https://www.ncbi.nlm.nih.gov/pubmed/16682560. doi:10.1261/rna.25706

Jahns, H., Roos, M., Imig, J., Baumann, F., Wang, Y., Gilmour, R., & Hall, J. (2015). Stereochemical bias introduced during RNA synthesis modulates the activity of phosphorothioate siRNAs. *Nat Commun, 6*, 6317. Retrieved from https://www.ncbi.nlm.nih.gov/pubmed/25744034. doi:10.1038/ncomms7317

Janas, M. M., Harbison, C. E., Perry, V. K., Carito, B., Sutherland, J. E., Vaishnaw, A. K., . . . Warner, G. (2018). The Nonclinical Safety Profile of GalNAc-conjugated RNAi Therapeutics in Subacute Studies. *Toxicol Pathol, 46*(7), 735-745. Retrieved from https://www.ncbi.nlm.nih.gov/pubmed/30139307. doi:10.1177/0192623318792537

Jayk Bernal, A., Gomes da Silva, M. M., Musungaie, D. B., Kovalchuk, E., Gonzalez, A., Delos Reyes, V., . . . Group, M. O.-O. S. (2022). Molnupiravir for Oral Treatment of Covid-19 in

Nonhospitalized Patients. *N Engl J Med, 386*(6), 509-520. Retrieved from https://www.ncbi.nlm.nih.gov/pubmed/34914868. doi:10.1056/NEJMoa2116044

Ji, M., & Hu, K. (2017). Recent advances in the study of hepatitis B virus covalently closed circular DNA. *Virol Sin, 32*(6), 454-464. Retrieved from https://www.ncbi.nlm.nih.gov/pubmed/29280054. doi:10.1007/s12250-017-4009-4

Jin, H. T., Anderson, A. C., Tan, W. G., West, E. E., Ha, S. J., Araki, K., . . . Ahmed, R. (2010). Cooperation of Tim-3 and PD-1 in CD8 T-cell exhaustion during chronic viral infection. *Proc Natl Acad Sci U S A, 107*(33), 14733-14738. Retrieved from https://www.ncbi.nlm.nih.gov/pubmed/20679213. doi:10.1073/pnas.1009731107

Joe, C. C. D., Jiang, J., Linke, T., Li, Y., Fedosyuk, S., Gupta, G., . . . Douglas, A. D. (2022). Manufacturing a chimpanzee adenovirus-vectored SARS-CoV-2 vaccine to meet global needs. *Biotechnol Bioeng, 119*(1), 48-58. Retrieved from https://www.ncbi.nlm.nih.gov/pubmed/34585736. doi:10.1002/bit.27945

Kabinger, F., Stiller, C., Schmitzova, J., Dienemann, C., Kokic, G., Hillen, H. S., . . . Cramer, P. (2021). Mechanism of molnupiravir-induced SARS-CoV-2 mutagenesis. *Nat Struct Mol Biol, 28*(9), 740-746. Retrieved from https://www.ncbi.nlm.nih.gov/pubmed/34381216. doi:10.1038/s41594-021-00651-0

Kalathil, S., Lugade, A. A., Miller, A., Iyer, R., & Thanavala, Y. (2013). Higher frequencies of GARP(+)CTLA-4(+)Foxp3(+) T regulatory cells and myeloid-derived suppressor cells in hepatocellular carcinoma patients are associated with impaired T-cell functionality. *Cancer Res, 73*(8), 2435-2444. Retrieved from https://www.ncbi.nlm.nih.gov/pubmed/23423978. doi:10.1158/0008-5472.CAN-12-3381

Kang, H., Yu, J., & Jung, G. (2008). Phosphorylation of hepatitis B virus core C-terminally truncated protein (Cp149) by PKC increases capsid assembly and stability. *Biochem J, 416*(1), 47-54. Retrieved from https://www.ncbi.nlm.nih.gov/pubmed/18605987. doi:10.1042/BJ20080724

Kaptein, S. J. F., Jacobs, S., Langendries, L., Seldeslachts, L., Ter Horst, S., Liesenborghs, L., . . . Delang, L. (2020). Favipiravir at high doses has potent antiviral activity in SARS-CoV-2-infected hamsters, whereas hydroxychloroquine lacks activity. *Proc Natl Acad Sci U S A, 117*(43), 26955-26965. Retrieved from https://www.ncbi.nlm.nih.gov/pubmed/33037151. doi:10.1073/pnas.2014441117

Kara, G., Calin, G. A., & Ozpolat, B. (2022). RNAi-based therapeutics and tumor targeted delivery in cancer. *Adv Drug Deliv Rev, 182*, 114113. Retrieved from https://www.ncbi.nlm.nih.gov/pubmed/35063535. doi:10.1016/j.addr.2022.114113

Keller, L. A., Merkel, O., & Popp, A. (2022). Intranasal drug delivery: opportunities and toxicologic challenges during drug development. *Drug Deliv Transl Res, 12*(4), 735-757. Retrieved from https://www.ncbi.nlm.nih.gov/pubmed/33491126. doi:10.1007/s13346-020-00891-5

Kenski, D. M., Butora, G., Willingham, A. T., Cooper, A. J., Fu, W., Qi, N., . . . Flanagan, W. M. (2012). siRNA-optimized Modifications for Enhanced In Vivo Activity. *Mol Ther Nucleic Acids, 1*(1), e5. Retrieved from https://www.ncbi.nlm.nih.gov/pubmed/23344622. doi:10.1038/mtna.2011.4

Khailany, R. A., Safdar, M., & Ozaslan, M. (2020). Genomic characterization of a novel SARS-CoV-2. *Gene Rep, 19*, 100682. Retrieved from https://www.ncbi.nlm.nih.gov/pubmed/32300673. doi:10.1016/j.genrep.2020.100682

Khaitov, M., Nikonova, A., Shilovskiy, I., Kozhikhova, K., Kofiadi, I., Vishnyakova, L., . . . Skvortsova, V. (2021). Silencing of SARS-CoV-2 with modified siRNA-peptide dendrimer formulation. *Allergy, 76*(9), 2840-2854. Retrieved from https://www.ncbi.nlm.nih.gov/pubmed/33837568. doi:10.1111/all.14850

Khan, A. A., Alanazi, A. M., Jabeen, M., Chauhan, A., & Ansari, M. A. (2019). Therapeutic potential of functionalized siRNA nanoparticles on regression of liver cancer in experimental mice. *Sci Rep, 9*(1), 15825. Retrieved from https://www.ncbi.nlm.nih.gov/pubmed/31676815. doi:10.1038/s41598-019-52142-4

Khanna, R. C., Cicinelli, M. V., Gilbert, S. S., Honavar, S. G., & Murthy, G. S. V. (2020). COVID-19 pandemic: Lessons learned and future directions. *Indian J Ophthalmol, 68*(5), 703-710. Retrieved from https://www.ncbi.nlm.nih.gov/pubmed/32317432. doi:10.4103/ijo.IJO_843_20

Kim, D., Lee, J. Y., Yang, J. S., Kim, J. W., Kim, V. N., & Chang, H. (2020). The Architecture of SARS-CoV-2 Transcriptome. *Cell, 181*(4), 914-921 e910. Retrieved from https://www.ncbi.nlm.nih.gov/pubmed/32330414. doi:10.1016/j.cell.2020.04.011

Kim, H., Ko, C., Lee, J. Y., & Kim, M. (2021). Current Progress in the Development of Hepatitis B Virus Capsid Assembly Modulators: Chemical Structure, Mode-of-Action and Efficacy. *Molecules, 26*(24). Retrieved from https://www.ncbi.nlm.nih.gov/pubmed/34946502. doi:10.3390/molecules26247420

Kim, J., Eygeris, Y., Gupta, M., & Sahay, G. (2021). Self-assembled mRNA vaccines. *Adv Drug Deliv Rev, 170*, 83-112. Retrieved from https://www.ncbi.nlm.nih.gov/pubmed/33400957. doi:10.1016/j.addr.2020.12.014

Kim, M. S., Seong, D., Li, H., Chung, S. K., Park, Y., Lee, M., . . . Smith, L. (2022). Comparative effectiveness of N95, surgical or medical, and non-medical facemasks in protection against respiratory virus infection: A systematic review and network meta-analysis. *Rev Med Virol, 32*(5), e2336. Retrieved from https://www.ncbi.nlm.nih.gov/pubmed/35218279. doi:10.1002/rmv.2336

Klein, C., Bock, C. T., Wedemeyer, H., Wustefeld, T., Locarnini, S., Dienes, H. P., . . . Trautwein, C. (2003). Inhibition of hepatitis B virus replication in vivo by nucleoside analogues and siRNA. *Gastroenterology, 125*(1), 9-18. Retrieved from https://www.ncbi.nlm.nih.gov/pubmed/12851866. doi:10.1016/s0016-5085(03)00720-0

Ko, C., Chakraborty, A., Chou, W. M., Hasreiter, J., Wettengel, J. M., Stadler, D., . . . Protzer, U. (2018). Hepatitis B virus genome recycling and de novo secondary infection events maintain stable cccDNA levels. *J Hepatol, 69*(6), 1231-1241. Retrieved from https://www.ncbi.nlm.nih.gov/pubmed/30142426. doi:10.1016/j.jhep.2018.08.012

Ko, C., Michler, T., & Protzer, U. (2017). Novel viral and host targets to cure hepatitis B. *Curr Opin Virol, 24*, 38-45. Retrieved from https://www.ncbi.nlm.nih.gov/pubmed/28433762. doi:10.1016/j.coviro.2017.03.019

Koda, H., Okuno, M., Imai, S., Moriwaki, H., Muto, Y., Kawada, N., & Kojima, S. (1996). Retinoic acid-stimulated liver stellate cells suppress the production of albumin from parenchymal cells via TGF-beta. *Biochem Biophys Res Commun, 221*(3), 565-569. Retrieved from https://www.ncbi.nlm.nih.gov/pubmed/8630001. doi:10.1006/bbrc.1996.0636

Kokic, G., Hillen, H. S., Tegunov, D., Dienemann, C., Seitz, F., Schmitzova, J., . . . Cramer, P. (2021). Mechanism of SARS-CoV-2 polymerase stalling by remdesivir. *Nat Commun, 12*(1), 279. Retrieved from https://www.ncbi.nlm.nih.gov/pubmed/33436624. doi:10.1038/s41467-020-20542-0

Koornneef, A., Maczuga, P., van Logtenstein, R., Borel, F., Blits, B., Ritsema, T., . . . Konstantinova, P. (2011). Apolipoprotein B knockdown by AAV-delivered shRNA lowers plasma cholesterol in mice. *Mol Ther, 19*(4), 731-740. Retrieved from https://www.ncbi.nlm.nih.gov/pubmed/21304496. doi:10.1038/mt.2011.6

Kosinska, A. D., Moeed, A., Kallin, N., Festag, J., Su, J., Steiger, K., . . . Knolle, P. A. (2019). Synergy of therapeutic heterologous prime-boost hepatitis B vaccination with CpG-application to improve immune control of persistent HBV infection. *Sci Rep, 9*(1), 10808. Retrieved from https://www.ncbi.nlm.nih.gov/pubmed/31346211. doi:10.1038/s41598-019-47149-w

Kosinska, A. D., Zhang, E., Lu, M., & Roggendorf, M. (2010). Therapeutic vaccination in chronic hepatitis B: preclinical studies in the woodchuck. *Hepat Res Treat, 2010*, 817580. Retrieved from https://www.ncbi.nlm.nih.gov/pubmed/21188201. doi:10.1155/2010/817580

Kraft, C. S., Hewlett, A. L., Koepsell, S., Winkler, A. M., Kratochvil, C. J., Larson, L., . . . the Emory Serious Communicable Diseases, U. (2015). The Use of TKM-100802 and Convalescent Plasma in 2 Patients With Ebola Virus Disease in the United States. *Clin Infect Dis, 61*(4), 496-502. Retrieved from https://www.ncbi.nlm.nih.gov/pubmed/25904375. doi:10.1093/cid/civ334

Kraynack, B. A., & Baker, B. F. (2006). Small interfering RNAs containing full 2'-O-methylribonucleotide-modified sense strands display Argonaute2/eIF2C2-dependent activity. *RNA, 12*(1), 163-176. Retrieved from https://www.ncbi.nlm.nih.gov/pubmed/16301602. doi:10.1261/rna.2150806

Kretschmer-Kazemi Far, R., & Sczakiel, G. (2003). The activity of siRNA in mammalian cells is related to structural target accessibility: a comparison with antisense oligonucleotides. *Nucleic Acids Res, 31*(15), 4417-4424. Retrieved from https://www.ncbi.nlm.nih.gov/pubmed/12888501. doi:10.1093/nar/gkg649

Kristen, A. V., Ajroud-Driss, S., Conceicao, I., Gorevic, P., Kyriakides, T., & Obici, L. (2019). Patisiran, an RNAi therapeutic for the treatment of hereditary transthyretin-mediated

amyloidosis. *Neurodegener Dis Manag, 9*(1), 5-23. Retrieved from https://www.ncbi.nlm.nih.gov/pubmed/30480471

https://www.futuremedicine.com/doi/pdf/10.2217/nmt-2018-0033?download=true. doi:10.2217/nmt-2018-0033

Kronbichler, A., Anders, H. J., Fernandez-Juarez, G. M., Floege, J., Goumenos, D., Segelmark, M., . . . Immunonephrology Working Group of the, E.-E. (2021). Recommendations for the use of COVID-19 vaccines in patients with immune-mediated kidney diseases. *Nephrol Dial Transplant*. Retrieved from https://www.ncbi.nlm.nih.gov/pubmed/33693778. doi:10.1093/ndt/gfab064

Kronbichler, A., Kresse, D., Yoon, S., Lee, K. H., Effenberger, M., & Shin, J. I. (2020). Asymptomatic patients as a source of COVID-19 infections: A systematic review and meta-analysis. *Int J Infect Dis, 98*, 180-186. Retrieved from https://www.ncbi.nlm.nih.gov/pubmed/32562846. doi:10.1016/j.ijid.2020.06.052

Kubes, P., & Jenne, C. (2018). Immune Responses in the Liver. *Annu Rev Immunol, 36*, 247-277. Retrieved from https://www.ncbi.nlm.nih.gov/pubmed/29328785. doi:10.1146/annurev-immunol-051116-052415

Kulkarni, J. A., Darjuan, M. M., Mercer, J. E., Chen, S., van der Meel, R., Thewalt, J. L., . . . Cullis, P. R. (2018). On the Formation and Morphology of Lipid Nanoparticles Containing Ionizable Cationic Lipids and siRNA. *ACS Nano, 12*(5), 4787-4795. Retrieved from https://www.ncbi.nlm.nih.gov/pubmed/29614232. doi:10.1021/acsnano.8b01516

Kulkarni, J. A., Witzigmann, D., Chen, S., Cullis, P. R., & van der Meel, R. (2019). Lipid Nanoparticle Technology for Clinical Translation of siRNA Therapeutics. *Acc Chem Res, 52*(9), 2435-2444. Retrieved from https://www.ncbi.nlm.nih.gov/pubmed/31397996. doi:10.1021/acs.accounts.9b00368

Kurreck, J. (2009). RNA interference: from basic research to therapeutic applications. *Angew Chem Int Ed Engl, 48*(8), 1378-1398. Retrieved from https://www.ncbi.nlm.nih.gov/pubmed/19153977. doi:10.1002/anie.200802092

Lai, S., Ruktanonchai, N. W., Zhou, L., Prosper, O., Luo, W., Floyd, J. R., . . . Tatem, A. J. (2020). Effect of non-pharmaceutical interventions to contain COVID-19 in China. *Nature, 585*(7825), 410-413. Retrieved from https://www.ncbi.nlm.nih.gov/pubmed/32365354. doi:10.1038/s41586-020-2293-x

Lam, J. K., Liang, W., & Chan, H. K. (2012). Pulmonary delivery of therapeutic siRNA. *Adv Drug Deliv Rev, 64*(1), 1-15. Retrieved from https://www.ncbi.nlm.nih.gov/pubmed/21356260. doi:10.1016/j.addr.2011.02.006

Lancet, E. T. (2023). The COVID-19 pandemic in 2023: far from over. *Lancet, 401*(10371), 79. Retrieved from https://www.ncbi.nlm.nih.gov/pubmed/36641201. doi:10.1016/S0140-6736(23)00050-8

Lapierre, P., & Lamarre, A. (2015). Regulatory T Cells in Autoimmune and Viral Chronic Hepatitis. *J Immunol Res, 2015*, 479703. Retrieved from https://www.ncbi.nlm.nih.gov/pubmed/26106627. doi:10.1155/2015/479703

Laursen, M. B., Pakula, M. M., Gao, S., Fluiter, K., Mook, O. R., Baas, F., . . . Bramsen, J. B. (2010). Utilization of unlocked nucleic acid (UNA) to enhance siRNA performance in vitro and in vivo. *Mol Biosyst, 6*(5), 862-870. Retrieved from https://www.ncbi.nlm.nih.gov/pubmed/20567772. doi:10.1039/b918869j

Le Bouvier, G. L., McCollum, R. W., Hierholzer, W. J., Jr., Irwin, G. R., Krugman, S., & Giles, J. P. (1972). Subtypes of Australia antigen and hepatitis-B virus. *JAMA, 222*(8), 928-930. Retrieved from https://www.ncbi.nlm.nih.gov/pubmed/4120331. doi:10.1001/jama.222.8.928

Le, D. T., & Muller, K. M. (2021). In Vitro Assembly of Virus-Like Particles and Their Applications. *Life (Basel), 11*(4). Retrieved from https://www.ncbi.nlm.nih.gov/pubmed/33920215. doi:10.3390/life11040334

Le Page, M. (2022). Could vaccines end the pandemic? *New Sci, 255*(3398), 16-17. Retrieved from https://www.ncbi.nlm.nih.gov/pubmed/35958698. doi:10.1016/S0262-4079(22)01381-1

Le Pogam, S., Chua, P. K., Newman, M., & Shih, C. (2005). Exposure of RNA templates and encapsidation of spliced viral RNA are influenced by the arginine-rich domain of human hepatitis B virus core antigen (HBcAg 165-173). *J Virol, 79*(3), 1871-1887. Retrieved from https://www.ncbi.nlm.nih.gov/pubmed/15650211. doi:10.1128/JVI.79.3.1871-1887.2005

Levanova, A., & Poranen, M. M. (2018). RNA Interference as a Prospective Tool for the Control of Human Viral Infections. *Front Microbiol, 9*, 2151. Retrieved from https://www.ncbi.nlm.nih.gov/pubmed/30254624. doi:10.3389/fmicb.2018.02151

Levanova, A. A., Kalke, K. M., Lund, L. M., Sipari, N., Sadeghi, M., Nyman, M. C., . . . Poranen, M. M. (2020). Enzymatically synthesized 2'-fluoro-modified Dicer-substrate siRNA swarms against herpes simplex virus demonstrate enhanced antiviral efficacy and low cytotoxicity. *Antiviral Res, 182*, 104916. Retrieved from https://www.ncbi.nlm.nih.gov/pubmed/32798603. doi:10.1016/j.antiviral.2020.104916

Levrero, M., & Zucman-Rossi, J. (2016). Mechanisms of HBV-induced hepatocellular carcinoma. *J Hepatol, 64*(1 Suppl), S84-S101. Retrieved from https://www.ncbi.nlm.nih.gov/pubmed/27084040. doi:10.1016/j.jhep.2016.02.021

Li, B. J., Tang, Q., Cheng, D., Qin, C., Xie, F. Y., Wei, Q., . . . Lu, P. Y. (2005). Using siRNA in prophylactic and therapeutic regimens against SARS coronavirus in Rhesus macaque. *Nat Med, 11*(9), 944-951. Retrieved from https://www.ncbi.nlm.nih.gov/pubmed/16116432. doi:10.1038/nm1280

Li, H. Y., McSharry, M., Bullock, B., Nguyen, T. T., Kwak, J., Poczobutt, J. M., . . . Nemenoff, R. A. (2017). The Tumor Microenvironment Regulates Sensitivity of Murine Lung Tumors to PD-1/PD-L1 Antibody Blockade. *Cancer Immunol Res, 5*(9), 767-777. Retrieved from https://www.ncbi.nlm.nih.gov/pubmed/28819064. doi:10.1158/2326-6066.CIR-16-0365

Li, M. Y., Li, L., Zhang, Y., & Wang, X. S. (2020). Expression of the SARS-CoV-2 cell receptor gene ACE2 in a wide variety of human tissues. *Infect Dis Poverty, 9*(1), 45. Retrieved from https://www.ncbi.nlm.nih.gov/pubmed/32345362. doi:10.1186/s40249-020-00662-x

Li, S., Zhang, Y., Guan, Z., Li, H., Ye, M., Chen, X., . . . Peng, K. (2020). SARS-CoV-2 triggers inflammatory responses and cell death through caspase-8 activation. *Signal Transduct Target Ther, 5*(1), 235. Retrieved from https://www.ncbi.nlm.nih.gov/pubmed/33037188. doi:10.1038/s41392-020-00334-0

Li, T., Zhang, Y., Fu, L., Yu, C., Li, X., Li, Y., . . . Chang, Z. (2005). siRNA targeting the leader sequence of SARS-CoV inhibits virus replication. *Gene Ther, 12*(9), 751-761. Retrieved from https://www.ncbi.nlm.nih.gov/pubmed/15772689. doi:10.1038/sj.gt.3302479

Li, T. Y., Yang, Y., Zhou, G., & Tu, Z. K. (2019). Immune suppression in chronic hepatitis B infection associated liver disease: A review. *World J Gastroenterol, 25*(27), 3527-3537. Retrieved from https://www.ncbi.nlm.nih.gov/pubmed/31367154. doi:10.3748/wjg.v25.i27.3527

Li, X., Zhang, Z., Wang, Z., Gutierrez-Castrellon, P., & Shi, H. (2022). Cell deaths: Involvement in the pathogenesis and intervention therapy of COVID-19. *Signal Transduct Target Ther, 7*(1), 186. Retrieved from https://www.ncbi.nlm.nih.gov/pubmed/35697684. doi:10.1038/s41392-022-01043-6

Li, Y., Fu, Y., Hu, X., Sun, L., Tang, D., Li, N., . . . Fan, X. G. (2019). The HBx-CTTN interaction promotes cell proliferation and migration of hepatocellular carcinoma via CREB1. *Cell Death Dis, 10*(6), 405. Retrieved from https://www.ncbi.nlm.nih.gov/pubmed/31138777. doi:10.1038/s41419-019-1650-x

Liang, T. J., Block, T. M., McMahon, B. J., Ghany, M. G., Urban, S., Guo, J. T., . . . Lok, A. S. (2015). Present and future therapies of hepatitis B: From discovery to cure. *Hepatology, 62*(6), 1893-1908. Retrieved from https://www.ncbi.nlm.nih.gov/pubmed/26239691. doi:10.1002/hep.28025

Lin, C. L., & Kao, J. H. (2011). The clinical implications of hepatitis B virus genotype: Recent advances. *J Gastroenterol Hepatol, 26 Suppl 1*, 123-130. Retrieved from https://www.ncbi.nlm.nih.gov/pubmed/21199523. doi:10.1111/j.1440-1746.2010.06541.x

Linton, N. M., Kobayashi, T., Yang, Y., Hayashi, K., Akhmetzhanov, A. R., Jung, S. M., . . . Nishiura, H. (2020). Incubation Period and Other Epidemiological Characteristics of 2019 Novel Coronavirus Infections with Right Truncation: A Statistical Analysis of Publicly Available Case Data. *J Clin Med, 9*(2). Retrieved from https://www.ncbi.nlm.nih.gov/pubmed/32079150. doi:10.3390/jcm9020538

Liu, G., Betts, C., Cunoosamy, D. M., Aberg, P. M., Hornberg, J. J., Sivars, K. B., & Cohen, T. S. (2019). Use of precision cut lung slices as a translational model for the study of lung biology. *Respir Res, 20*(1), 162. Retrieved from https://www.ncbi.nlm.nih.gov/pubmed/31324219. doi:10.1186/s12931-019-1131-x

Liu, J., Carmell, M. A., Rivas, F. V., Marsden, C. G., Thomson, J. M., Song, J. J., . . . Hannon, G. J. (2004). Argonaute2 is the catalytic engine of mammalian RNAi. *Science, 305*(5689),

1437-1441. Retrieved from https://www.ncbi.nlm.nih.gov/pubmed/15284456. doi:10.1126/science.1102513

Liu, J., Zhang, E., Ma, Z., Wu, W., Kosinska, A., Zhang, X., . . . Roggendorf, M. (2014). Enhancing virus-specific immunity in vivo by combining therapeutic vaccination and PD-L1 blockade in chronic hepadnaviral infection. *PLoS Pathog, 10*(1), e1003856. Retrieved from https://www.ncbi.nlm.nih.gov/pubmed/24391505. doi:10.1371/journal.ppat.1003856

Lobaina, Y., & Michel, M. L. (2017). Chronic hepatitis B: Immunological profile and current therapeutic vaccines in clinical trials. *Vaccine, 35*(18), 2308-2314. Retrieved from https://www.ncbi.nlm.nih.gov/pubmed/28351734. doi:10.1016/j.vaccine.2017.03.049

Love, K. T., Mahon, K. P., Levins, C. G., Whitehead, K. A., Querbes, W., Dorkin, J. R., . . . Anderson, D. G. (2010). Lipid-like materials for low-dose, in vivo gene silencing. *Proc Natl Acad Sci U S A, 107*(5), 1864-1869. Retrieved from https://www.ncbi.nlm.nih.gov/pubmed/20080679. doi:10.1073/pnas.0910603106

Lucifora, J., Arzberger, S., Durantel, D., Belloni, L., Strubin, M., Levrero, M., . . . Protzer, U. (2011). Hepatitis B virus X protein is essential to initiate and maintain virus replication after infection. *J Hepatol, 55*(5), 996-1003. Retrieved from https://www.ncbi.nlm.nih.gov/pubmed/21376091. doi:10.1016/j.jhep.2011.02.015

Lumley, S. F., McNaughton, A. L., Klenerman, P., Lythgoe, K. A., & Matthews, P. C. (2018). Hepatitis B Virus Adaptation to the CD8+ T Cell Response: Consequences for Host and Pathogen. *Front Immunol, 9*, 1561. Retrieved from https://www.ncbi.nlm.nih.gov/pubmed/30061882. doi:10.3389/fimmu.2018.01561

Luo, W. C., & Lu, X. (2023). Solid Lipid Nanoparticles for Drug Delivery. *Methods Mol Biol, 2622*, 139-146. Retrieved from https://www.ncbi.nlm.nih.gov/pubmed/36781757. doi:10.1007/978-1-0716-2954-3_12

Ma, J., Zheng, B., Goswami, S., Meng, L., Zhang, D., Cao, C., . . . Zhang, X. (2019). PD1(Hi) CD8(+) T cells correlate with exhausted signature and poor clinical outcome in hepatocellular carcinoma. *J Immunother Cancer, 7*(1), 331. Retrieved from https://www.ncbi.nlm.nih.gov/pubmed/31783783. doi:10.1186/s40425-019-0814-7

Ma, L., Yang, X., Wei, R., Ye, T., Zhou, J. K., Wen, M., . . . Peng, Y. (2018). MicroRNA-214 promotes hepatic stellate cell activation and liver fibrosis by suppressing Sufu expression. *Cell Death Dis, 9*(7), 718. Retrieved from https://www.ncbi.nlm.nih.gov/pubmed/29915227. doi:10.1038/s41419-018-0752-1

Ma, T., Pei, Y., Li, C., & Zhu, M. (2019). Periodicity and dosage optimization of an RNAi model in eukaryotes cells. *BMC Bioinformatics, 20*(1), 340. Retrieved from https://www.ncbi.nlm.nih.gov/pubmed/31208316. doi:10.1186/s12859-019-2925-z

Maini, M. K., Boni, C., Ogg, G. S., King, A. S., Reignat, S., Lee, C. K., . . . Bertoletti, A. (1999). Direct ex vivo analysis of hepatitis B virus-specific CD8(+) T cells associated with the control of infection. *Gastroenterology, 117*(6), 1386-1396. Retrieved from https://www.ncbi.nlm.nih.gov/pubmed/10579980. doi:10.1016/s0016-5085(99)70289-1

Maini, M. K., & Pallett, L. J. (2018). Defective T-cell immunity in hepatitis B virus infection: why therapeutic vaccination needs a helping hand. *Lancet Gastroenterol Hepatol, 3*(3), 192-202. Retrieved from https://www.ncbi.nlm.nih.gov/pubmed/29870733. doi:10.1016/S2468-1253(18)30007-4

Mancini-Bourgine, M., Fontaine, H., Scott-Algara, D., Pol, S., Brechot, C., & Michel, M. L. (2004). Induction or expansion of T-cell responses by a hepatitis B DNA vaccine administered to chronic HBV carriers. *Hepatology, 40*(4), 874-882. Retrieved from https://www.ncbi.nlm.nih.gov/pubmed/15382173. doi:10.1002/hep.20408

Manjunath, N., Wu, H., Subramanya, S., & Shankar, P. (2009). Lentiviral delivery of short hairpin RNAs. *Adv Drug Deliv Rev, 61*(9), 732-745. Retrieved from https://www.ncbi.nlm.nih.gov/pubmed/19341774. doi:10.1016/j.addr.2009.03.004

Mannaerts, I., Eysackers, N., Anne van Os, E., Verhulst, S., Roosens, T., Smout, A., . . . van Grunsven, L. A. (2020). The fibrotic response of primary liver spheroids recapitulates in vivo hepatic stellate cell activation. *Biomaterials, 261*, 120335. Retrieved from https://www.ncbi.nlm.nih.gov/pubmed/32891040. doi:10.1016/j.biomaterials.2020.120335

Martin, B., Sainlos, M., Aissaoui, A., Oudrhiri, N., Hauchecorne, M., Vigneron, J. P., . . . Lehn, P. (2005). The design of cationic lipids for gene delivery. *Curr Pharm Des, 11*(3), 375-394. Retrieved from https://www.ncbi.nlm.nih.gov/pubmed/15723632. doi:10.2174/1381612053382133

Martin, C. J., Datta, A., Littlefield, C., Kalra, A., Chapron, C., Wawersik, S., . . . Schurpf, T. (2020). Selective inhibition of TGFbeta1 activation overcomes primary resistance to checkpoint blockade therapy by altering tumor immune landscape. *Sci Transl Med, 12*(536). Retrieved from https://www.ncbi.nlm.nih.gov/pubmed/32213632. doi:10.1126/scitranslmed.aay8456

Martin, P., Dubois, C., Jacquier, E., Dion, S., Mancini-Bourgine, M., Godon, O., . . . Inchauspe, G. (2015). TG1050, an immunotherapeutic to treat chronic hepatitis B, induces robust T cells and exerts an antiviral effect in HBV-persistent mice. *Gut, 64*(12), 1961-1971. Retrieved from https://www.ncbi.nlm.nih.gov/pubmed/25429051. doi:10.1136/gutjnl-2014-308041

Mashima, R., & Takada, S. (2022). Lipid Nanoparticles: A Novel Gene Delivery Technique for Clinical Application. *Curr Issues Mol Biol, 44*(10), 5013-5027. Retrieved from https://www.ncbi.nlm.nih.gov/pubmed/36286056. doi:10.3390/cimb44100341

Matsuda, S., Keiser, K., Nair, J. K., Charisse, K., Manoharan, R. M., Kretschmer, P., . . . Manoharan, M. (2015). siRNA conjugates carrying sequentially assembled trivalent N-acetylgalactosamine linked through nucleosides elicit robust gene silencing in vivo in hepatocytes. *ACS Chem Biol, 10*(5), 1181-1187. Retrieved from https://www.ncbi.nlm.nih.gov/pubmed/25730476. doi:10.1021/cb501028c

Matsuda, Y., Toda, M., Kato, T., Kuribayashi, K., & Kakimi, K. (2006). Fulminant liver failure triggered by therapeutic antibody treatment in a mouse model. *Int J Oncol, 29*(5), 1119-1125. Retrieved from https://www.ncbi.nlm.nih.gov/pubmed/17016642.

McNaughton, A. L., Revill, P. A., Littlejohn, M., Matthews, P. C., & Ansari, M. A. (2020). Analysis of genomic-length HBV sequences to determine genotype and subgenotype reference sequences. *J Gen Virol, 101*(3), 271-283. Retrieved from https://www.ncbi.nlm.nih.gov/pubmed/32134374. doi:10.1099/jgv.0.001387

Medeiros, I. G., Khayat, A. S., Stransky, B., Santos, S., Assumpcao, P., & de Souza, J. E. S. (2021). A small interfering RNA (siRNA) database for SARS-CoV-2. *Sci Rep, 11*(1), 8849. Retrieved from https://www.ncbi.nlm.nih.gov/pubmed/33893357. doi:10.1038/s41598-021-88310-8

Mehta, A., Michler, T., & Merkel, O. M. (2021). siRNA Therapeutics against Respiratory Viral Infections-What Have We Learned for Potential COVID-19 Therapies? *Adv Healthc Mater*, e2001650. Retrieved from https://www.ncbi.nlm.nih.gov/pubmed/33506607. doi:10.1002/adhm.202001650

Melo, A., de Macedo, L. S., Invencao, M., de Moura, I. A., da Gama, M., de Melo, C. M. L., . . . Freitas, A. C. (2022). Third-Generation Vaccines: Features of Nucleic Acid Vaccines and Strategies to Improve Their Efficiency. *Genes (Basel), 13*(12). Retrieved from https://www.ncbi.nlm.nih.gov/pubmed/36553554. doi:10.3390/genes13122287

Meng, Z., & Lu, M. (2017). RNA Interference-Induced Innate Immunity, Off-Target Effect, or Immune Adjuvant? *Front Immunol, 8*, 331. Retrieved from https://www.ncbi.nlm.nih.gov/pubmed/28386261. doi:10.3389/fimmu.2017.00331

Meng, Z., Zhang, X., Wu, J., Pei, R., Xu, Y., Yang, D., . . . Lu, M. (2013). RNAi induces innate immunity through multiple cellular signaling pathways. *PLoS One, 8*(5), e64708. Retrieved from https://www.ncbi.nlm.nih.gov/pubmed/23700487. doi:10.1371/journal.pone.0064708

Merkel, O. M., Beyerle, A., Librizzi, D., Pfestroff, A., Behr, T. M., Sproat, B., . . . Kissel, T. (2009). Nonviral siRNA delivery to the lung: investigation of PEG-PEI polyplexes and their in vivo performance. *Mol Pharm, 6*(4), 1246-1260. Retrieved from https://www.ncbi.nlm.nih.gov/pubmed/19606864. doi:10.1021/mp900107v

Merkel, O. M., & Kissel, T. (2012). Nonviral pulmonary delivery of siRNA. *Acc Chem Res, 45*(7), 961-970. Retrieved from https://www.ncbi.nlm.nih.gov/pubmed/21905687. doi:10.1021/ar200110p

Merkel, O. M., Rubinstein, I., & Kissel, T. (2014). siRNA delivery to the lung: what's new? *Adv Drug Deliv Rev, 75*, 112-128. Retrieved from https://www.ncbi.nlm.nih.gov/pubmed/24907426. doi:10.1016/j.addr.2014.05.018

Michalaki, C., Dean, C., & Johansson, C. (2022). The Use of Precision-Cut Lung Slices for Studying Innate Immunity to Viral Infections. *Curr Protoc, 2*(8), e505. Retrieved from https://www.ncbi.nlm.nih.gov/pubmed/35938685. doi:10.1002/cpz1.505

Michler, T., Kosinska, A. D., Festag, J., Bunse, T., Su, J., Ringelhan, M., . . . Protzer, U. (2020). Knockdown of Virus Antigen Expression Increases Therapeutic Vaccine Efficacy in High-

Titer Hepatitis B Virus Carrier Mice. *Gastroenterology, 158*(6), 1762-1775 e1769. Retrieved from https://www.ncbi.nlm.nih.gov/pubmed/32001321. doi:10.1053/j.gastro.2020.01.032

Miguez-Rey, E., Choi, D., Kim, S., Yoon, S., & Sandulescu, O. (2022). Monoclonal antibody therapies in the management of SARS-CoV-2 infection. *Expert Opin Investig Drugs, 31*(1), 41-58. Retrieved from https://www.ncbi.nlm.nih.gov/pubmed/35164631. doi:10.1080/13543784.2022.2030310

Milich, D., & Liang, T. J. (2003). Exploring the biological basis of hepatitis B e antigen in hepatitis B virus infection. *Hepatology, 38*(5), 1075-1086. Retrieved from https://www.ncbi.nlm.nih.gov/pubmed/14578844. doi:10.1053/jhep.2003.50453

Morais da Silva, M., Lira de Lucena, A. S., Paiva Junior, S. S. L., Florencio De Carvalho, V. M., Santana de Oliveira, P. S., da Rosa, M. M., . . . Pereira, M. C. (2022). Cell death mechanisms involved in cell injury caused by SARS-CoV-2. *Rev Med Virol, 32*(3), e2292. Retrieved from https://www.ncbi.nlm.nih.gov/pubmed/34590761. doi:10.1002/rmv.2292

Morrissey, D. V., Lockridge, J. A., Shaw, L., Blanchard, K., Jensen, K., Breen, W., . . . Polisky, B. (2005). Potent and persistent in vivo anti-HBV activity of chemically modified siRNAs. *Nat Biotechnol, 23*(8), 1002-1007. Retrieved from https://www.ncbi.nlm.nih.gov/pubmed/16041363. doi:10.1038/nbt1122

Mullard, A. (2022). FDA approves fifth RNAi drug - Alnylam's next-gen hATTR treatment. *Nat Rev Drug Discov, 21*(8), 548-549. Retrieved from https://www.ncbi.nlm.nih.gov/pubmed/35794463. doi:10.1038/d41573-022-00118-x

Muller, M., Fazi, F., & Ciaudo, C. (2019). Argonaute Proteins: From Structure to Function in Development and Pathological Cell Fate Determination. *Front Cell Dev Biol, 7*, 360. Retrieved from https://www.ncbi.nlm.nih.gov/pubmed/32039195. doi:10.3389/fcell.2019.00360

Muller, R. H., Radtke, M., & Wissing, S. A. (2002). Solid lipid nanoparticles (SLN) and nanostructured lipid carriers (NLC) in cosmetic and dermatological preparations. *Adv Drug Deliv Rev, 54 Suppl 1*, S131-155. Retrieved from https://www.ncbi.nlm.nih.gov/pubmed/12460720. doi:10.1016/s0169-409x(02)00118-7

Mullol, J., Alobid, I., Marino-Sanchez, F., Izquierdo-Dominguez, A., Marin, C., Klimek, L., . . . Liu, Z. (2020). The Loss of Smell and Taste in the COVID-19 Outbreak: a Tale of Many Countries. *Curr Allergy Asthma Rep, 20*(10), 61. Retrieved from https://www.ncbi.nlm.nih.gov/pubmed/32748211. doi:10.1007/s11882-020-00961-1

Muthusamy, V., Bosenberg, M., & Wajapeyee, N. (2010). Redefining regulation of DNA methylation by RNA interference. *Genomics, 96*(4), 191-198. Retrieved from https://www.ncbi.nlm.nih.gov/pubmed/20620207. doi:10.1016/j.ygeno.2010.07.001

Nadeau, B. A., Fecher, L. A., Owens, S. R., & Razumilava, N. (2018). Liver Toxicity with Cancer Checkpoint Inhibitor Therapy. *Semin Liver Dis, 38*(4), 366-378. Retrieved from https://www.ncbi.nlm.nih.gov/pubmed/30357774. doi:10.1055/s-0038-1667358

Naito, Y., Yamada, T., Ui-Tei, K., Morishita, S., & Saigo, K. (2004). siDirect: highly effective, target-specific siRNA design software for mammalian RNA interference. *Nucleic Acids Res, 32*(Web Server issue), W124-129. Retrieved from https://www.ncbi.nlm.nih.gov/pubmed/15215364. doi:10.1093/nar/gkh442

Nassal, M. (2015). HBV cccDNA: viral persistence reservoir and key obstacle for a cure of chronic hepatitis B. *Gut, 64*(12), 1972-1984. Retrieved from https://www.ncbi.nlm.nih.gov/pubmed/26048673. doi:10.1136/gutjnl-2015-309809

Newman, M., Suk, F. M., Cajimat, M., Chua, P. K., & Shih, C. (2003). Stability and morphology comparisons of self-assembled virus-like particles from wild-type and mutant human hepatitis B virus capsid proteins. *J Virol, 77*(24), 12950-12960. Retrieved from https://www.ncbi.nlm.nih.gov/pubmed/14645551. doi:10.1128/jvi.77.24.12950-12960.2003

Ng, H. W., Lee, M. F. X., Chua, G. K., Gan, B. K., Tan, W. S., Ooi, C. W., . . . Tey, B. T. (2018). Size-selective purification of hepatitis B virus-like particle in flow-through chromatography: Types of ion exchange adsorbent and grafted polymer architecture. *J Sep Sci, 41*(10), 2119-2129. Retrieved from https://www.ncbi.nlm.nih.gov/pubmed/29427396. doi:10.1002/jssc.201700823

NIH, N. I. o. H. (2023). *COVID-19 Treatment Guidelines Panel. Coronavirus Disease 2019 (COVID-19) Treatment Guidelines. National Institutes of*

Health. Available at https://www.covid19treatmentguidelines.nih.gov/. Accessed [25.05.2023]. Retrieved from https://files.covid19treatmentguidelines.nih.gov/guidelines/covid19treatmentguidelines.pdf

Niklasch, M., Zimmermann, P., & Nassal, M. (2021). The Hepatitis B Virus Nucleocapsid-Dynamic Compartment for Infectious Virus Production and New Antiviral Target. *Biomedicines, 9*(11). Retrieved from https://www.ncbi.nlm.nih.gov/pubmed/34829806. doi:10.3390/biomedicines9111577

Ning, X., Luckenbaugh, L., Liu, K., Bruss, V., Sureau, C., & Hu, J. (2018). Common and Distinct Capsid and Surface Protein Requirements for Secretion of Complete and Genome-Free Hepatitis B Virions. *J Virol, 92*(14). Retrieved from https://www.ncbi.nlm.nih.gov/pubmed/29743374. doi:10.1128/JVI.00272-18

The Nobel Prize in Physiology or Medicine 2006. (2006). [Press release]. Retrieved from https://www.nobelprize.org/prizes/medicine/2006/prize-announcement/

Noordeen, F. (2015). Hepatitis B virus infection: An insight into infection outcomes and recent treatment options. *Virusdisease, 26*(1-2), 1-8. Retrieved from https://www.ncbi.nlm.nih.gov/pubmed/26436115. doi:10.1007/s13337-015-0247-y

Novina, C. D., Murray, M. F., Dykxhoorn, D. M., Beresford, P. J., Riess, J., Lee, S. K., . . . Sharp, P. A. (2002). siRNA-directed inhibition of HIV-1 infection. *Nat Med, 8*(7), 681-686. Retrieved from https://www.ncbi.nlm.nih.gov/pubmed/12042777. doi:10.1038/nm725

Novina, C. D., & Sharp, P. A. (2004). The RNAi revolution. *Nature, 430*(6996), 161-164. Retrieved from https://www.ncbi.nlm.nih.gov/pubmed/15241403. doi:10.1038/430161a

Obeng-Adjei, N., Choo, D. K., Saini, J., Yan, J., Pankhong, P., Parikh, A., . . . Weiner, D. B. (2012). Synthetic DNA immunogen encoding hepatitis B core antigen drives immune response in liver. *Cancer Gene Ther, 19*(11), 779-787. Retrieved from https://www.ncbi.nlm.nih.gov/pubmed/23037809. doi:10.1038/cgt.2012.61

Okuda, T., Kito, D., Oiwa, A., Fukushima, M., Hira, D., & Okamoto, H. (2013). Gene silencing in a mouse lung metastasis model by an inhalable dry small interfering RNA powder prepared using the supercritical carbon dioxide technique. *Biol Pharm Bull, 36*(7), 1183-1191. Retrieved from https://www.ncbi.nlm.nih.gov/pubmed/23811567. doi:10.1248/bpb.b13-00167

Orban, T. I., & Izaurralde, E. (2005). Decay of mRNAs targeted by RISC requires XRN1, the Ski complex, and the exosome. *RNA, 11*(4), 459-469. Retrieved from https://www.ncbi.nlm.nih.gov/pubmed/15703439. doi:10.1261/rna.7231505

Osada, N., Kohara, A., Yamaji, T., Hirayama, N., Kasai, F., Sekizuka, T., . . . Hanada, K. (2014). The genome landscape of the african green monkey kidney-derived vero cell line. *DNA Res, 21*(6), 673-683. Retrieved from https://www.ncbi.nlm.nih.gov/pubmed/25267831. doi:10.1093/dnares/dsu029

Osiowy, C. (2018). From infancy and beyond... ensuring a lifetime of hepatitis B virus (HBV) vaccine-induced immunity. *Hum Vaccin Immunother, 14*(8), 2093-2097. Retrieved from https://www.ncbi.nlm.nih.gov/pubmed/29641290. doi:10.1080/21645515.2018.1462428

Padda, I. S., Mahtani, A. U., & Parmar, M. (2022). Small Interfering RNA (siRNA) Based Therapy. In *StatPearls*. Treasure Island (FL).

Padda, I. S., Mahtani, A. U., & Parmar, M. (2023). Small Interfering RNA (siRNA) Based Therapy. In *StatPearls*. Treasure Island (FL).

Paroo, Z., Liu, Q., & Wang, X. (2007). Biochemical mechanisms of the RNA-induced silencing complex. *Cell Res, 17*(3), 187-194. Retrieved from https://www.ncbi.nlm.nih.gov/pubmed/17310219. doi:10.1038/sj.cr.7310148

Pascarella, G., Strumia, A., Piliego, C., Bruno, F., Del Buono, R., Costa, F., . . . Agro, F. E. (2020). COVID-19 diagnosis and management: a comprehensive review. *J Intern Med, 288*(2), 192-206. Retrieved from https://www.ncbi.nlm.nih.gov/pubmed/32348588. doi:10.1111/joim.13091

Peacock, T. P., Goldhill, D. H., Zhou, J., Baillon, L., Frise, R., Swann, O. C., . . . Barclay, W. S. (2021). The furin cleavage site in the SARS-CoV-2 spike protein is required for transmission in ferrets. *Nat Microbiol, 6*(7), 899-909. Retrieved from https://www.ncbi.nlm.nih.gov/pubmed/33907312. doi:10.1038/s41564-021-00908-w

Peeridogaheh, H., Meshkat, Z., Habibzadeh, S., Arzanlou, M., Shahi, J. M., Rostami, S., . . . Teimourpour, R. (2018). Current concepts on immunopathogenesis of hepatitis B virus

infection. *Virus Res, 245*, 29-43. Retrieved from https://www.ncbi.nlm.nih.gov/pubmed/29273341. doi:10.1016/j.virusres.2017.12.007

Pereira, T. C., & Lopes-Cendes, I. (2013). Medical applications of RNA interference (RNAi). *BMC Proc, 7 Suppl 2*(Suppl 2), K21. Retrieved from https://www.ncbi.nlm.nih.gov/pubmed/24764479. doi:10.1186/1753-6561-7-S2-K21

Pharmaceuticals, A. (2016). Arrowhead Pharmaceuticals Focuses Resources on Subcutaneous and Extra-Hepatic RNAi Therapeutics [Press release]. Retrieved from https://ir.arrowheadpharma.com/news-releases/news-release-details/arrowhead-pharmaceuticals-focuses-resources-subcutaneous-and

Polack, F. P., Thomas, S. J., Kitchin, N., Absalon, J., Gurtman, A., Lockhart, S., . . . Group, C. C. T. (2020). Safety and Efficacy of the BNT162b2 mRNA Covid-19 Vaccine. *N Engl J Med, 383*(27), 2603-2615. Retrieved from https://www.ncbi.nlm.nih.gov/pubmed/33301246. doi:10.1056/NEJMoa2034577

Poralla, T., Ramadori, G., Dienes, H. P., Manns, M., Gerken, G., Dippold, W., . . . Meyer zum Buschenfelde, K. H. (1987). Liver cell damage caused by monoclonal antibody against an organ-specific membrane antigen in vivo and in vitro. *J Hepatol, 4*(3), 373-380. Retrieved from https://www.ncbi.nlm.nih.gov/pubmed/3598165. doi:10.1016/s0168-8278(87)80548-2

Porterfield, J. Z., Dhason, M. S., Loeb, D. D., Nassal, M., Stray, S. J., & Zlotnick, A. (2010). Full-length hepatitis B virus core protein packages viral and heterologous RNA with similarly high levels of cooperativity. *J Virol, 84*(14), 7174-7184. Retrieved from https://www.ncbi.nlm.nih.gov/pubmed/20427522. doi:10.1128/JVI.00586-10

Prakash, T. P., Naik, N., Sioufi, N., Bhat, B., & Swayze, E. E. (2009). Activity of siRNAs with 2-thio-2'-O-methyluridine modification in mammalian cells. *Nucleosides Nucleotides Nucleic Acids, 28*(10), 902-910. Retrieved from https://www.ncbi.nlm.nih.gov/pubmed/20183560. doi:10.1080/15257770903316145

Proal, A. D., & VanElzakker, M. B. (2021). Long COVID or Post-acute Sequelae of COVID-19 (PASC): An Overview of Biological Factors That May Contribute to Persistent Symptoms. *Front Microbiol, 12*, 698169. Retrieved from https://www.ncbi.nlm.nih.gov/pubmed/34248921. doi:10.3389/fmicb.2021.698169

Proia, T. A., Singh, M., Woessner, R., Carnevalli, L., Bommakanti, G., Magiera, L., . . . McCoon, P. (2020). STAT3 Antisense Oligonucleotide Remodels the Suppressive Tumor Microenvironment to Enhance Immune Activation in Combination with Anti-PD-L1. *Clin Cancer Res, 26*(23), 6335-6349. Retrieved from https://www.ncbi.nlm.nih.gov/pubmed/32943458. doi:10.1158/1078-0432.CCR-20-1066

Protzer, U., Maini, M. K., & Knolle, P. A. (2012). Living in the liver: hepatic infections. *Nat Rev Immunol, 12*(3), 201-213. Retrieved from https://www.ncbi.nlm.nih.gov/pubmed/22362353. doi:10.1038/nri3169

Qureshi, A., Tantray, V. G., Kirmani, A. R., & Ahangar, A. G. (2018). A review on current status of antiviral siRNA. *Rev Med Virol, 28*(4), e1976. Retrieved from https://www.ncbi.nlm.nih.gov/pubmed/29656441. doi:10.1002/rmv.1976

Ragab, D., Salah Eldin, H., Taeimah, M., Khattab, R., & Salem, R. (2020). The COVID-19 Cytokine Storm; What We Know So Far. *Front Immunol, 11*, 1446. Retrieved from https://www.ncbi.nlm.nih.gov/pubmed/32612617. doi:10.3389/fimmu.2020.01446

Raghav, S., Ghosh, A., Turuk, J., Kumar, S., Jha, A., Madhulika, S., . . . Parida, A. (2020). Analysis of Indian SARS-CoV-2 Genomes Reveals Prevalence of D614G Mutation in Spike Protein Predicting an Increase in Interaction With TMPRSS2 and Virus Infectivity. *Front Microbiol, 11*, 594928. Retrieved from https://www.ncbi.nlm.nih.gov/pubmed/33329480. doi:10.3389/fmicb.2020.594928

Rahmani, K., Shavaleh, R., Forouhi, M., Disfani, H. F., Kamandi, M., Oskooi, R. K., . . . Dianatinasab, M. (2022). The effectiveness of COVID-19 vaccines in reducing the incidence, hospitalization, and mortality from COVID-19: A systematic review and meta-analysis. *Front Public Health, 10*, 873596. Retrieved from https://www.ncbi.nlm.nih.gov/pubmed/36091533. doi:10.3389/fpubh.2022.873596

Raveendran, A. V., Jayadevan, R., & Sashidharan, S. (2021). Long COVID: An overview. *Diabetes Metab Syndr, 15*(3), 869-875. Retrieved from https://www.ncbi.nlm.nih.gov/pubmed/33892403. doi:10.1016/j.dsx.2021.04.007

Redondo, N., Zaldivar-Lopez, S., Garrido, J. J., & Montoya, M. (2021). SARS-CoV-2 Accessory Proteins in Viral Pathogenesis: Knowns and Unknowns. *Front Immunol, 12*, 708264.

Retrieved from https://www.ncbi.nlm.nih.gov/pubmed/34305949. doi:10.3389/fimmu.2021.708264

Rehermann, B., Ferrari, C., Pasquinelli, C., & Chisari, F. V. (1996). The hepatitis B virus persists for decades after patients' recovery from acute viral hepatitis despite active maintenance of a cytotoxic T-lymphocyte response. *Nat Med, 2*(10), 1104-1108. Retrieved from https://www.ncbi.nlm.nih.gov/pubmed/8837608. doi:10.1038/nm1096-1104

Reynolds, A., Leake, D., Boese, Q., Scaringe, S., Marshall, W. S., & Khvorova, A. (2004). Rational siRNA design for RNA interference. *Nat Biotechnol, 22*(3), 326-330. Retrieved from https://www.ncbi.nlm.nih.gov/pubmed/14758366. doi:10.1038/nbt936

Rezaei, M., & Nazari, M. (2022). New Generation Vaccines for COVID-19 Based on Peptide, Viral Vector, Artificial Antigen Presenting Cell, DNA or mRNA. *Avicenna J Med Biotechnol, 14*(1), 30-36. Retrieved from https://www.ncbi.nlm.nih.gov/pubmed/35509358. doi:10.18502/ajmb.v14i1.8167

Rezvani, M., Espanol-Suner, R., Malato, Y., Dumont, L., Grimm, A. A., Kienle, E., . . . Willenbring, H. (2016). In Vivo Hepatic Reprogramming of Myofibroblasts with AAV Vectors as a Therapeutic Strategy for Liver Fibrosis. *Cell Stem Cell, 18*(6), 809-816. Retrieved from https://www.ncbi.nlm.nih.gov/pubmed/27257763. doi:10.1016/j.stem.2016.05.005

Richards, F., Kodjamanova, P., Chen, X., Li, N., Atanasov, P., Bennetts, L., . . . El Khoury, A. C. (2022). Economic Burden of COVID-19: A Systematic Review. *Clinicoecon Outcomes Res, 14*, 293-307. Retrieved from https://www.ncbi.nlm.nih.gov/pubmed/35509962. doi:10.2147/CEOR.S338225

Roingeard, P., Eymieux, S., Burlaud-Gaillard, J., Hourioux, C., Patient, R., & Blanchard, E. (2022). The double-membrane vesicle (DMV): a virus-induced organelle dedicated to the replication of SARS-CoV-2 and other positive-sense single-stranded RNA viruses. *Cell Mol Life Sci, 79*(8), 425. Retrieved from https://www.ncbi.nlm.nih.gov/pubmed/35841484. doi:10.1007/s00018-022-04469-x

Rolland, D., Gauthier, M., Dugua, J. M., Fournier, C., Delpech, L., Watelet, B., . . . Jolivet, M. (2001). Purification of recombinant HBc antigen expressed in Escherichia coli and Pichia pastoris: comparison of size-exclusion chromatography and ultracentrifugation. *J Chromatogr B Biomed Sci Appl, 753*(1), 51-65. Retrieved from https://www.ncbi.nlm.nih.gov/pubmed/11302448. doi:10.1016/s0378-4347(00)00538-7

Safari, F., Rahmani Barouji, S., & Tamaddon, A. M. (2017). Strategies for Improving siRNA-Induced Gene Silencing Efficiency. *Adv Pharm Bull, 7*(4), 603-609. Retrieved from https://www.ncbi.nlm.nih.gov/pubmed/29399550. doi:10.15171/apb.2017.072

Sajid, M. I., Mandal, D., El-Sayed, N. S., Lohan, S., Moreno, J., & Tiwari, R. K. (2022). Oleyl Conjugated Histidine-Arginine Cell-Penetrating Peptides as Promising Agents for siRNA Delivery. *Pharmaceutics, 14*(4). Retrieved from https://www.ncbi.nlm.nih.gov/pubmed/35456715. doi:10.3390/pharmaceutics14040881

Sajid, M. I., Moazzam, M., Kato, S., Yeseom Cho, K., & Tiwari, R. K. (2020). Overcoming Barriers for siRNA Therapeutics: From Bench to Bedside. *Pharmaceuticals (Basel), 13*(10). Retrieved from https://www.ncbi.nlm.nih.gov/pubmed/33036435. doi:10.3390/ph13100294

Salomon, W. E., Jolly, S. M., Moore, M. J., Zamore, P. D., & Serebrov, V. (2015). Single-Molecule Imaging Reveals that Argonaute Reshapes the Binding Properties of Its Nucleic Acid Guides. *Cell, 162*(1), 84-95. Retrieved from https://www.ncbi.nlm.nih.gov/pubmed/26140592. doi:10.1016/j.cell.2015.06.029

Samaranayake, L. P., Fakhruddin, K. S., & Panduwawala, C. (2020). Sudden onset, acute loss of taste and smell in coronavirus disease 2019 (COVID-19): a systematic review. *Acta Odontol Scand, 78*(6), 467-473. Retrieved from https://www.ncbi.nlm.nih.gov/pubmed/32762282. doi:10.1080/00016357.2020.1787505

Sanders, N., Rudolph, C., Braeckmans, K., De Smedt, S. C., & Demeester, J. (2009). Extracellular barriers in respiratory gene therapy. *Adv Drug Deliv Rev, 61*(2), 115-127. Retrieved from https://www.ncbi.nlm.nih.gov/pubmed/19146894. doi:10.1016/j.addr.2008.09.011

Sawicki, S. G., & Sawicki, D. L. (1995). Coronaviruses use discontinuous extension for synthesis of subgenome-length negative strands. *Adv Exp Med Biol, 380*, 499-506. Retrieved from https://www.ncbi.nlm.nih.gov/pubmed/8830530. doi:10.1007/978-1-4615-1899-0_79

Saxena, R., Chawla, Y. K., Verma, I., & Kaur, J. (2014). Association of interleukin-10 with hepatitis B virus (HBV) mediated disease progression in Indian population. *Indian J Med Res, 139*(5), 737-745. Retrieved from https://www.ncbi.nlm.nih.gov/pubmed/25027084.

Schinagl, M., Tomin, T., Gindlhuber, J., Honeder, S., Pfleger, R., Schittmayer, M., . . . Birner-Gruenberger, R. (2021). Proteomic Changes of Activated Hepatic Stellate Cells. *Int J Mol Sci, 22*(23). Retrieved from https://www.ncbi.nlm.nih.gov/pubmed/34884585. doi:10.3390/ijms222312782

Schlegel, M. K., Janas, M. M., Jiang, Y., Barry, J. D., Davis, W., Agarwal, S., . . . Maier, M. A. (2022). From bench to bedside: Improving the clinical safety of GalNAc-siRNA conjugates using seed-pairing destabilization. *Nucleic Acids Res, 50*(12), 6656-6670. Retrieved from https://www.ncbi.nlm.nih.gov/pubmed/35736224. doi:10.1093/nar/gkac539

Schluep, T., Lickliter, J., Hamilton, J., Lewis, D. L., Lai, C. L., Lau, J. Y., . . . Given, B. D. (2017). Safety, Tolerability, and Pharmacokinetics of ARC-520 Injection, an RNA Interference-Based Therapeutic for the Treatment of Chronic Hepatitis B Virus Infection, in Healthy Volunteers. *Clin Pharmacol Drug Dev, 6*(4), 350-362. Retrieved from https://www.ncbi.nlm.nih.gov/pubmed/27739230. doi:10.1002/cpdd.318

Schnichels, S., Simmang, D., Loscher, M., Herrmann, A., de Vries, J. W., Spitzer, M. S., & Hurst, J. (2023). Lipid-DNA Nanoparticles as Drug-Delivery Vehicles for the Treatment of Retinal Diseases. *Pharmaceutics, 15*(2). Retrieved from https://www.ncbi.nlm.nih.gov/pubmed/36839853. doi:10.3390/pharmaceutics15020532

Schon, H. T., & Weiskirchen, R. (2014). Immunomodulatory effects of transforming growth factor-beta in the liver. *Hepatobiliary Surg Nutr, 3*(6), 386-406. Retrieved from https://www.ncbi.nlm.nih.gov/pubmed/25568862. doi:10.3978/j.issn.2304-3881.2014.11.06

Scott, J. T., Sharma, R., Meredith, L. W., Dunning, J., Moore, C. E., Sahr, F., . . . team, R.-T. t. (2020). Pharmacokinetics of TKM-130803 in Sierra Leonean patients with Ebola virus disease: plasma concentrations exceed target levels, with drug accumulation in the most severe patients. *EBioMedicine, 52*, 102601. Retrieved from https://www.ncbi.nlm.nih.gov/pubmed/31953031. doi:10.1016/j.ebiom.2019.102601

Seeger, C., & Mason, W. S. (2015). Molecular biology of hepatitis B virus infection. *Virology, 479-480*, 672-686. Retrieved from https://www.ncbi.nlm.nih.gov/pubmed/25759099. doi:10.1016/j.virol.2015.02.031

Selvam, C., Mutisya, D., Prakash, S., Ranganna, K., & Thilagavathi, R. (2017). Therapeutic potential of chemically modified siRNA: Recent trends. *Chem Biol Drug Des, 90*(5), 665-678. Retrieved from https://www.ncbi.nlm.nih.gov/pubmed/28378934. doi:10.1111/cbdd.12993

Senefeld, J. W., Franchini, M., Mengoli, C., Cruciani, M., Zani, M., Gorman, E. K., . . . Joyner, M. J. (2023). COVID-19 Convalescent Plasma for the Treatment of Immunocompromised Patients: A Systematic Review and Meta-analysis. *JAMA Netw Open, 6*(1), e2250647. Retrieved from https://www.ncbi.nlm.nih.gov/pubmed/36633846. doi:10.1001/jamanetworkopen.2022.50647

Sepp-Lorenzino, L. (2016). *ALN-HBV*. Alnylam. Retrieved from https://www.liver-institute.org/HBV_MeetingSlides_PDFs/08_161111_LIFER_Alnylam.pdf

Shah, V. N., & Pyle, L. (2021). Lumasiran, an RNAi Therapeutic for Primary Hyperoxaluria Type 1. *N Engl J Med, 385*(20), e69. Retrieved from https://www.ncbi.nlm.nih.gov/pubmed/34758264. doi:10.1056/NEJMc2107661

Shawan, M., Sharma, A. R., Bhattacharya, M., Mallik, B., Akhter, F., Shakil, M. S., . . . Chakraborty, C. (2021). Designing an effective therapeutic siRNA to silence RdRp gene of SARS-CoV-2. *Infect Genet Evol, 93*, 104951. Retrieved from https://www.ncbi.nlm.nih.gov/pubmed/34089909. doi:10.1016/j.meegid.2021.104951

Shi, N., Wang, Z., Zhu, H., Liu, W., Zhao, M., Jiang, X., . . . Luo, L. (2022). Research progress on drugs targeting the TGF-beta signaling pathway in fibrotic diseases. *Immunol Res, 70*(3), 276-288. Retrieved from https://www.ncbi.nlm.nih.gov/pubmed/35147920. doi:10.1007/s12026-022-09267-y

Siolas, D., Lerner, C., Burchard, J., Ge, W., Linsley, P. S., Paddison, P. J., . . . Cleary, M. A. (2005). Synthetic shRNAs as potent RNAi triggers. *Nat Biotechnol, 23*(2), 227-231. Retrieved from https://www.ncbi.nlm.nih.gov/pubmed/15619616. doi:10.1038/nbt1052

Song, X., Wang, X., Ma, Y., Liang, Z., Yang, Z., & Cao, H. (2017). Site-Specific Modification Using the 2'-Methoxyethyl Group Improves the Specificity and Activity of siRNAs. *Mol Ther Nucleic Acids, 9*, 242-250. Retrieved from https://www.ncbi.nlm.nih.gov/pubmed/29246303. doi:10.1016/j.omtn.2017.10.003

Spellman M, M. J. T. (2011). *TREATMENT OF CHRONIC HEPATITIS B INFECTION WITH DV-601,*

A THERAPEUTIC VACCINE. Poster. Dynavax Technologies. J Hepatol. Retrieved from https://www.journal-of-hepatology.eu/article/S0168-8278(11)60753-8/pdf

Springer, A. D., & Dowdy, S. F. (2018). GalNAc-siRNA Conjugates: Leading the Way for Delivery of RNAi Therapeutics. *Nucleic Acid Ther, 28*(3), 109-118. Retrieved from https://www.ncbi.nlm.nih.gov/pubmed/29792572. doi:10.1089/nat.2018.0736

Stadnytskyi, V., Bax, C. E., Bax, A., & Anfinrud, P. (2020). The airborne lifetime of small speech droplets and their potential importance in SARS-CoV-2 transmission. *Proc Natl Acad Sci U S A, 117*(22), 11875-11877. Retrieved from https://www.ncbi.nlm.nih.gov/pubmed/32404416. doi:10.1073/pnas.2006874117

Stramer, S. L., Wend, U., Candotti, D., Foster, G. A., Hollinger, F. B., Dodd, R. Y., . . . Gerlich, W. (2011). Nucleic acid testing to detect HBV infection in blood donors. *N Engl J Med, 364*(3), 236-247. Retrieved from https://www.ncbi.nlm.nih.gov/pubmed/21247314. doi:10.1056/NEJMoa1007644

Stross, L., Gunther, J., Gasteiger, G., Asen, T., Graf, S., Aichler, M., . . . Protzer, U. (2012). Foxp3+ regulatory T cells protect the liver from immune damage and compromise virus control during acute experimental hepatitis B virus infection in mice. *Hepatology, 56*(3), 873-883. Retrieved from https://www.ncbi.nlm.nih.gov/pubmed/22487943. doi:10.1002/hep.25765

Stuart Milstein, T. N., Adam Castoreno, Abigail Liebow, Vasant Jadhav, Martin Maier, Laura Sepp-Lorenzino. (2017). *Preclinical Development of an RNAi*

Therapeutic Drug Candidate Targeting

Hepatitis B Virus. Poster. Alnylam. Retrieved from https://www.alnylam.de/wp-content/uploads/2017/09/OTS-2017_Poster-4_Milstein-et-al..pdf

Su, J., Brunner, L., Ates Oz, E., Sacherl, J., Frank, G., Kerth, H. A., . . . Protzer, U. (2023). Activation of CD4 T cells during prime immunization determines the success of a therapeutic hepatitis B vaccine in HBV-carrier mouse models. *J Hepatol, 78*(4), 717-730. Retrieved from https://www.ncbi.nlm.nih.gov/pubmed/36634821. doi:10.1016/j.jhep.2022.12.013

Sun, D., & Lu, Z. R. (2023). Structure and Function of Cationic and Ionizable Lipids for Nucleic Acid Delivery. *Pharm Res, 40*(1), 27-46. Retrieved from https://www.ncbi.nlm.nih.gov/pubmed/36600047. doi:10.1007/s11095-022-03460-2

Swadling, L., Pallett, L. J., Diniz, M. O., Baker, J. M., Amin, O. E., Stegmann, K. A., . . . Maini, M. K. (2020). Human Liver Memory CD8(+) T Cells Use Autophagy for Tissue Residence. *Cell Rep, 30*(3), 687-698 e686. Retrieved from https://www.ncbi.nlm.nih.gov/pubmed/31968246. doi:10.1016/j.celrep.2019.12.050

Tahashi, Y., Matsuzaki, K., Date, M., Yoshida, K., Furukawa, F., Sugano, Y., . . . Inoue, K. (2002). Differential regulation of TGF-beta signal in hepatic stellate cells between acute and chronic rat liver injury. *Hepatology, 35*(1), 49-61. Retrieved from https://www.ncbi.nlm.nih.gov/pubmed/11786959. doi:10.1053/jhep.2002.30083

Tai, J., Han, M., Lee, D., Park, I. H., Lee, S. H., & Kim, T. H. (2022). Different Methods and Formulations of Drugs and Vaccines for Nasal Administration. *Pharmaceutics, 14*(5). Retrieved from https://www.ncbi.nlm.nih.gov/pubmed/35631663. doi:10.3390/pharmaceutics14051073

Takahashi, K., Machida, A., Funatsu, G., Nomura, M., Usuda, S., Aoyagi, S., . . . Mayumi, M. (1983). Immunochemical structure of hepatitis B e antigen in the serum. *J Immunol, 130*(6), 2903-2907. Retrieved from https://www.ncbi.nlm.nih.gov/pubmed/6189903.

Tan, L. Y., Komarasamy, T. V., & Rmt Balasubramaniam, V. (2021). Hyperinflammatory Immune Response and COVID-19: A Double Edged Sword. *Front Immunol, 12*, 742941. Retrieved from https://www.ncbi.nlm.nih.gov/pubmed/34659238. doi:10.3389/fimmu.2021.742941

Tan, Z., Pionek, K., Unchwaniwala, N., Maguire, M. L., Loeb, D. D., & Zlotnick, A. (2015). The interface between hepatitis B virus capsid proteins affects self-assembly, pregenomic RNA packaging, and reverse transcription. *J Virol, 89*(6), 3275-3284. Retrieved from https://www.ncbi.nlm.nih.gov/pubmed/25568211. doi:10.1128/JVI.03545-14

Taniuchi, K., Yawata, T., Tsuboi, M., Ueba, T., & Saibara, T. (2019). Efficient delivery of small interfering RNAs targeting particular mRNAs into pancreatic cancer cells inhibits

invasiveness and metastasis of pancreatic tumors. *Oncotarget, 10*(30), 2869-2886. Retrieved from https://www.ncbi.nlm.nih.gov/pubmed/31080558. doi:10.18632/oncotarget.26880

Taverniti, V., Ligat, G., Debing, Y., Kum, D. B., Baumert, T. F., & Verrier, E. R. (2022). Capsid Assembly Modulators as Antiviral Agents against HBV: Molecular Mechanisms and Clinical Perspectives. *J Clin Med, 11*(5). Retrieved from https://www.ncbi.nlm.nih.gov/pubmed/35268440. doi:10.3390/jcm11051349

Terrault, N. A., Bzowej, N. H., Chang, K. M., Hwang, J. P., Jonas, M. M., Murad, M. H., & American Association for the Study of Liver, D. (2016). AASLD guidelines for treatment of chronic hepatitis B. *Hepatology, 63*(1), 261-283. Retrieved from https://www.ncbi.nlm.nih.gov/pubmed/26566064. doi:10.1002/hep.28156

Terrazas, M., & Kool, E. T. (2009). RNA major groove modifications improve siRNA stability and biological activity. *Nucleic Acids Res, 37*(2), 346-353. Retrieved from https://www.ncbi.nlm.nih.gov/pubmed/19042976. doi:10.1093/nar/gkn958

Thi Nhu Thao, T., Labroussaa, F., Ebert, N., V'Kovski, P., Stalder, H., Portmann, J., . . . Thiel, V. (2020). Rapid reconstruction of SARS-CoV-2 using a synthetic genomics platform. *Nature, 582*(7813), 561-565. Retrieved from https://www.ncbi.nlm.nih.gov/pubmed/32365353. doi:10.1038/s41586-020-2294-9

Thimme, R., Wieland, S., Steiger, C., Ghrayeb, J., Reimann, K. A., Purcell, R. H., & Chisari, F. V. (2003). CD8(+) T cells mediate viral clearance and disease pathogenesis during acute hepatitis B virus infection. *J Virol, 77*(1), 68-76. Retrieved from https://www.ncbi.nlm.nih.gov/pubmed/12477811. doi:10.1128/jvi.77.1.68-76.2003

Thomson, A. W., & Knolle, P. A. (2010). Antigen-presenting cell function in the tolerogenic liver environment. *Nat Rev Immunol, 10*(11), 753-766. Retrieved from https://www.ncbi.nlm.nih.gov/pubmed/20972472. doi:10.1038/nri2858

Tinoco, R., Alcalde, V., Yang, Y., Sauer, K., & Zuniga, E. I. (2009). Cell-intrinsic transforming growth factor-beta signaling mediates virus-specific CD8+ T cell deletion and viral persistence in vivo. *Immunity, 31*(1), 145-157. Retrieved from https://www.ncbi.nlm.nih.gov/pubmed/19604493. doi:10.1016/j.immuni.2009.06.015

Tokatlian, T., & Segura, T. (2010). siRNA applications in nanomedicine. *Wiley Interdiscip Rev Nanomed Nanobiotechnol, 2*(3), 305-315. Retrieved from https://www.ncbi.nlm.nih.gov/pubmed/20135697. doi:10.1002/wnan.81

Tomczyk, M., Kraszewska, I., Maka, R., Waligorska, A., Dulak, J., & Jazwa-Kusior, A. (2020). Characterization of hepatic macrophages and evaluation of inflammatory response in heme oxygenase-1 deficient mice exposed to scAAV9 vectors. *PLoS One, 15*(10), e0240691. Retrieved from https://www.ncbi.nlm.nih.gov/pubmed/33057437. doi:10.1371/journal.pone.0240691

Tripathi, N., & Mousa, O. Y. (2023). Hepatitis B. In *StatPearls*. Treasure Island (FL) ineligible companies. Disclosure: Omar Mousa declares no relevant financial relationships with ineligible companies.

Truong, L. B., Medina-Cruz, D., & Mostafavi, E. (2023). Current state of RNA delivery using lipid nanoparticles to extrahepatic tissues: A review towards clinical translation. *Int J Biol Macromol, 242*(Pt 4), 125185. Retrieved from https://www.ncbi.nlm.nih.gov/pubmed/37276899. doi:10.1016/j.ijbiomac.2023.125185

Tsukuda, S., & Watashi, K. (2020). Hepatitis B virus biology and life cycle. *Antiviral Res, 182*, 104925. Retrieved from https://www.ncbi.nlm.nih.gov/pubmed/32866519. doi:10.1016/j.antiviral.2020.104925

Ui-Tei, K., Naito, Y., & Saigo, K. (2006). Essential notes regarding the design of functional siRNAs for efficient mammalian RNAi. *J Biomed Biotechnol, 2006*(4), 65052. Retrieved from https://www.ncbi.nlm.nih.gov/pubmed/17057367. doi:10.1155/JBB/2006/65052

Ui-Tei, K., Naito, Y., Takahashi, F., Haraguchi, T., Ohki-Hamazaki, H., Juni, A., . . . Saigo, K. (2004). Guidelines for the selection of highly effective siRNA sequences for mammalian and chick RNA interference. *Nucleic Acids Res, 32*(3), 936-948. Retrieved from https://www.ncbi.nlm.nih.gov/pubmed/14769950. doi:10.1093/nar/gkh247

Umar, M., Hamama Tul, B., Umar, S., & Khan, H. A. (2013). HBV perinatal transmission. *Int J Hepatol, 2013*, 875791. Retrieved from https://www.ncbi.nlm.nih.gov/pubmed/23738081. doi:10.1155/2013/875791

V'Kovski, P., Kratzel, A., Steiner, S., Stalder, H., & Thiel, V. (2021). Coronavirus biology and replication: implications for SARS-CoV-2. *Nat Rev Microbiol, 19*(3), 155-170. Retrieved from https://www.ncbi.nlm.nih.gov/pubmed/33116300. doi:10.1038/s41579-020-00468-6

van de Veerdonk, F. L., Giamarellos-Bourboulis, E., Pickkers, P., Derde, L., Leavis, H., van Crevel, R., . . . Netea, M. G. (2022). A guide to immunotherapy for COVID-19. *Nat Med, 28*(1), 39-50. Retrieved from https://www.ncbi.nlm.nih.gov/pubmed/35064248. doi:10.1038/s41591-021-01643-9

van den Berg, F., Limani, S. W., Mnyandu, N., Maepa, M. B., Ely, A., & Arbuthnot, P. (2020). Advances with RNAi-Based Therapy for Hepatitis B Virus Infection. *Viruses, 12*(8). Retrieved from https://www.ncbi.nlm.nih.gov/pubmed/32759756. doi:10.3390/v12080851

Velkov, S., Ott, J. J., Protzer, U., & Michler, T. (2018). The Global Hepatitis B Virus Genotype Distribution Approximated from Available Genotyping Data. *Genes (Basel), 9*(10). Retrieved from https://www.ncbi.nlm.nih.gov/pubmed/30326600. doi:10.3390/genes9100495

Voysey, M., Clemens, S. A. C., Madhi, S. A., Weckx, L. Y., Folegatti, P. M., Aley, P. K., . . . Oxford, C. V. T. G. (2021). Safety and efficacy of the ChAdOx1 nCoV-19 vaccine (AZD1222) against SARS-CoV-2: an interim analysis of four randomised controlled trials in Brazil, South Africa, and the UK. *Lancet, 397*(10269), 99-111. Retrieved from https://www.ncbi.nlm.nih.gov/pubmed/33306989. doi:10.1016/S0140-6736(20)32661-1

Wan, Y. Y., & Flavell, R. A. (2007). 'Yin-Yang' functions of transforming growth factor-beta and T regulatory cells in immune regulation. *Immunol Rev, 220*, 199-213. Retrieved from https://www.ncbi.nlm.nih.gov/pubmed/17979848. doi:10.1111/j.1600-065X.2007.00565.x

Wang, C., Han, B., Zhou, R., & Zhuang, X. (2016). Real-Time Imaging of Translation on Single mRNA Transcripts in Live Cells. *Cell, 165*(4), 990-1001. Retrieved from https://www.ncbi.nlm.nih.gov/pubmed/27153499. doi:10.1016/j.cell.2016.04.040

Wang, T., Larcher, L. M., Ma, L., & Veedu, R. N. (2018). Systematic Screening of Commonly Used Commercial Transfection Reagents towards Efficient Transfection of Single-Stranded Oligonucleotides. *Molecules, 23*(10). Retrieved from https://www.ncbi.nlm.nih.gov/pubmed/30297632. doi:10.3390/molecules23102564

Watanabe, T., Sorensen, E. M., Naito, A., Schott, M., Kim, S., & Ahlquist, P. (2007). Involvement of host cellular multivesicular body functions in hepatitis B virus budding. *Proc Natl Acad Sci U S A, 104*(24), 10205-10210. Retrieved from https://www.ncbi.nlm.nih.gov/pubmed/17551004. doi:10.1073/pnas.0704000104

Watts, J. K., Choubdar, N., Sadalapure, K., Robert, F., Wahba, A. S., Pelletier, J., . . . Damha, M. J. (2007). 2'-fluoro-4'-thioarabino-modified oligonucleotides: conformational switches linked to siRNA activity. *Nucleic Acids Res, 35*(5), 1441-1451. Retrieved from https://www.ncbi.nlm.nih.gov/pubmed/17284457. doi:10.1093/nar/gkl1153

Watts, J. K., Deleavey, G. F., & Damha, M. J. (2008). Chemically modified siRNA: tools and applications. *Drug Discov Today, 13*(19-20), 842-855. Retrieved from https://www.ncbi.nlm.nih.gov/pubmed/18614389. doi:10.1016/j.drudis.2008.05.007

Watts, N. R., Conway, J. F., Cheng, N., Stahl, S. J., Belnap, D. M., Steven, A. C., & Wingfield, P. T. (2002). The morphogenic linker peptide of HBV capsid protein forms a mobile array on the interior surface. *EMBO J, 21*(5), 876-884. Retrieved from https://www.ncbi.nlm.nih.gov/pubmed/11867516. doi:10.1093/emboj/21.5.876

Webster, G. J., Reignat, S., Brown, D., Ogg, G. S., Jones, L., Seneviratne, S. L., . . . Bertoletti, A. (2004). Longitudinal analysis of CD8+ T cells specific for structural and nonstructural hepatitis B virus proteins in patients with chronic hepatitis B: implications for immunotherapy. *J Virol, 78*(11), 5707-5719. Retrieved from https://www.ncbi.nlm.nih.gov/pubmed/15140968. doi:10.1128/JVI.78.11.5707-5719.2004

Wei, J. X., Yang, J., Sun, J. F., Jia, L. T., Zhang, Y., Zhang, H. Z., . . . Yang, A. G. (2009). Both strands of siRNA have potential to guide posttranscriptional gene silencing in mammalian cells. *PLoS One, 4*(4), e5382. Retrieved from https://www.ncbi.nlm.nih.gov/pubmed/19401777. doi:10.1371/journal.pone.0005382

Weisberg, S. P., Ural, B. B., & Farber, D. L. (2021). Tissue-specific immunity for a changing world. *Cell, 184*(6), 1517-1529. Retrieved from https://www.ncbi.nlm.nih.gov/pubmed/33740452. doi:10.1016/j.cell.2021.01.042

Weldemhret, L. (2021). Epidemiology and Challenges of HBV/HIV Co-Infection Amongst HIV-Infected Patients in Endemic Areas: Review. *HIV AIDS (Auckl), 13*, 485-490. Retrieved from https://www.ncbi.nlm.nih.gov/pubmed/33981165. doi:10.2147/HIV.S273649

Wen, W. H., Chen, H. L., Ni, Y. H., Hsu, H. Y., Kao, J. H., Hu, F. C., & Chang, M. H. (2011). Secular trend of the viral genotype distribution in children with chronic hepatitis B virus infection after universal infant immunization. *Hepatology, 53*(2), 429-436. Retrieved from https://www.ncbi.nlm.nih.gov/pubmed/21274864. doi:10.1002/hep.24061

WHO. (2015). Guidelines for the prevention, care and treatment of persons with chronic hepatitis B infection. Retrieved from https://www.who.int/publications/i/item/9789241549059.

WHO. (2016). *Annex 2 WHO good manufacturing practices for biological products*. Retrieved from https://cdn.who.int/media/docs/default-source/biologicals/gmp/annex-2-who-good-manufacturing-practices-for-biological-products.pdf?sfvrsn=995d5518_2&download=true

WHO. (2022). Hepatitis B. Retrieved from https://www.who.int/news-room/fact-sheets/detail/hepatitis-b

Wieland, S., Thimme, R., Purcell, R. H., & Chisari, F. V. (2004). Genomic analysis of the host response to hepatitis B virus infection. *Proc Natl Acad Sci U S A, 101*(17), 6669-6674. Retrieved from https://www.ncbi.nlm.nih.gov/pubmed/15100412. doi:10.1073/pnas.0401771101

Wieland, S. F., Spangenberg, H. C., Thimme, R., Purcell, R. H., & Chisari, F. V. (2004). Expansion and contraction of the hepatitis B virus transcriptional template in infected chimpanzees. *Proc Natl Acad Sci U S A, 101*(7), 2129-2134. Retrieved from https://www.ncbi.nlm.nih.gov/pubmed/14764900. doi:10.1073/pnas.0308478100

Wolff, G., Limpens, R., Zevenhoven-Dobbe, J. C., Laugks, U., Zheng, S., de Jong, A. W. M., . . . Barcena, M. (2020). A molecular pore spans the double membrane of the coronavirus replication organelle. *Science, 369*(6509), 1395-1398. Retrieved from https://www.ncbi.nlm.nih.gov/pubmed/32763915. doi:10.1126/science.abd3629

Won, J. E., Byeon, Y., Wi, T. I., Lee, C. M., Lee, J. H., Kang, T. H., . . . Han, H. D. (2022). Immune checkpoint silencing using RNAi-incorporated nanoparticles enhances antitumor immunity and therapeutic efficacy compared with antibody-based approaches. *J Immunother Cancer, 10*(2). Retrieved from https://www.ncbi.nlm.nih.gov/pubmed/35228265. doi:10.1136/jitc-2021-003928

Wooddell, C. I., Rozema, D. B., Hossbach, M., John, M., Hamilton, H. L., Chu, Q., . . . Lewis, D. L. (2013). Hepatocyte-targeted RNAi therapeutics for the treatment of chronic hepatitis B virus infection. *Mol Ther, 21*(5), 973-985. Retrieved from https://www.ncbi.nlm.nih.gov/pubmed/23439496. doi:10.1038/mt.2013.31

Wooddell, C. I., Yuen, M. F., Chan, H. L., Gish, R. G., Locarnini, S. A., Chavez, D., . . . Lewis, D. L. (2017). RNAi-based treatment of chronically infected patients and chimpanzees reveals that integrated hepatitis B virus DNA is a source of HBsAg. *Sci Transl Med, 9*(409). Retrieved from https://www.ncbi.nlm.nih.gov/pubmed/28954926. doi:10.1126/scitranslmed.aan0241

Wu, J. C., Merlino, G., & Fausto, N. (1994). Establishment and characterization of differentiated, nontransformed hepatocyte cell lines derived from mice transgenic for transforming growth factor alpha. *Proc Natl Acad Sci U S A, 91*(2), 674-678. Retrieved from https://www.ncbi.nlm.nih.gov/pubmed/7904757. doi:10.1073/pnas.91.2.674

Wu, Q., Wang, K., Wang, X., Liang, G., & Li, J. (2020). Delivering siRNA to control osteogenic differentiation and real-time detection of cell differentiation in human mesenchymal stem cells using multifunctional gold nanoparticles. *J Mater Chem B, 8*(15), 3016-3027. Retrieved from https://www.ncbi.nlm.nih.gov/pubmed/32207489. doi:10.1039/c9tb02899d

Wu, S. Y., Yang, X., Gharpure, K. M., Hatakeyama, H., Egli, M., McGuire, M. H., . . . Sood, A. K. (2014). 2'-OMe-phosphorodithioate-modified siRNAs show increased loading into the RISC complex and enhanced anti-tumour activity. *Nat Commun, 5*, 3459. Retrieved from https://www.ncbi.nlm.nih.gov/pubmed/24619206. doi:10.1038/ncomms4459

Wu, W., Cheng, Y., Zhou, H., Sun, C., & Zhang, S. (2023). The SARS-CoV-2 nucleocapsid protein: its role in the viral life cycle, structure and functions, and use as a potential target in the development of vaccines and diagnostics. *Virol J, 20*(1), 6. Retrieved from https://www.ncbi.nlm.nih.gov/pubmed/36627683. doi:10.1186/s12985-023-01968-6

Wu, W., Shi, Y., Li, S., Zhang, Y., Liu, Y., Wu, Y., & Chen, Z. (2012). Blockade of Tim-3 signaling restores the virus-specific CD8(+) T-cell response in patients with chronic hepatitis B. *Eur J Immunol, 42*(5), 1180-1191. Retrieved from https://www.ncbi.nlm.nih.gov/pubmed/22539292. doi:10.1002/eji.201141852

Xu, D., Fu, J., Jin, L., Zhang, H., Zhou, C., Zou, Z., . . . Wang, F. S. (2006). Circulating and liver resident CD4+CD25+ regulatory T cells actively influence the antiviral immune response and disease progression in patients with hepatitis B. *J Immunol, 177*(1), 739-747. Retrieved from https://www.ncbi.nlm.nih.gov/pubmed/16785573. doi:10.4049/jimmunol.177.1.739

Xu, J., Gu, M., Hooi, L., Toh, T. B., Thng, D. K. H., Lim, J. J., & Chow, E. K. (2021). Enhanced penetrative siRNA delivery by a nanodiamond drug delivery platform against hepatocellular carcinoma 3D models. *Nanoscale, 13*(38), 16131-16145. Retrieved from https://www.ncbi.nlm.nih.gov/pubmed/34542130. doi:10.1039/d1nr03502a

Xu, L., Hui, A. Y., Albanis, E., Arthur, M. J., O'Byrne, S. M., Blaner, W. S., . . . Eng, F. J. (2005). Human hepatic stellate cell lines, LX-1 and LX-2: new tools for analysis of hepatic fibrosis. *Gut, 54*(1), 142-151. Retrieved from https://www.ncbi.nlm.nih.gov/pubmed/15591520. doi:10.1136/gut.2004.042127

Yan, W., Zheng, Y., Zeng, X., He, B., & Cheng, W. (2022). Structural biology of SARS-CoV-2: open the door for novel therapies. *Signal Transduct Target Ther, 7*(1), 26. Retrieved from https://www.ncbi.nlm.nih.gov/pubmed/35087058. doi:10.1038/s41392-022-00884-5

Yang, Y., Wu, Y., Meng, X., Wang, Z., Younis, M., Liu, Y., . . . Huang, X. (2022). SARS-CoV-2 membrane protein causes the mitochondrial apoptosis and pulmonary edema via targeting BOK. *Cell Death Differ, 29*(7), 1395-1408. Retrieved from https://www.ncbi.nlm.nih.gov/pubmed/35022571. doi:10.1038/s41418-022-00928-x

Yata, Y., Gotwals, P., Koteliansky, V., & Rockey, D. C. (2002). Dose-dependent inhibition of hepatic fibrosis in mice by a TGF-beta soluble receptor: implications for antifibrotic therapy. *Hepatology, 35*(5), 1022-1030. Retrieved from https://www.ncbi.nlm.nih.gov/pubmed/11981752. doi:10.1053/jhep.2002.32673

Ye, B., Liu, X., Li, X., Kong, H., Tian, L., & Chen, Y. (2015). T-cell exhaustion in chronic hepatitis B infection: current knowledge and clinical significance. *Cell Death Dis, 6*(3), e1694. Retrieved from https://www.ncbi.nlm.nih.gov/pubmed/25789969. doi:10.1038/cddis.2015.42

Ye, H., Teng, J., Lin, Z., Wang, Y., & Fu, X. (2020). Analysis of HBsAg mutations in the 25 years after the implementation of the hepatitis B vaccination plan in China. *Virus Genes, 56*(5), 546-556. Retrieved from https://www.ncbi.nlm.nih.gov/pubmed/32542478. doi:10.1007/s11262-020-01773-1

Yonezawa, S., Koide, H., & Asai, T. (2020). Recent advances in siRNA delivery mediated by lipid-based nanoparticles. *Adv Drug Deliv Rev, 154-155*, 64-78. Retrieved from https://www.ncbi.nlm.nih.gov/pubmed/32768564. doi:10.1016/j.addr.2020.07.022

Yoshimoto, F. K. (2020). The Proteins of Severe Acute Respiratory Syndrome Coronavirus-2 (SARS CoV-2 or n-COV19), the Cause of COVID-19. *Protein J, 39*(3), 198-216. Retrieved from https://www.ncbi.nlm.nih.gov/pubmed/32447571. doi:10.1007/s10930-020-09901-4

Yuen, M. F., Sablon, E., Wong, D. K., Yuan, H. J., Wong, B. C., Chan, A. O., & Lai, C. L. (2003). Role of hepatitis B virus genotypes in chronic hepatitis B exacerbation. *Clin Infect Dis, 37*(4), 593-597. Retrieved from https://www.ncbi.nlm.nih.gov/pubmed/12905145. doi:10.1086/376988

Yuen, M. F., Schiefke, I., Yoon, J. H., Ahn, S. H., Heo, J., Kim, J. H., . . . Gish, R. G. (2020). RNA Interference Therapy With ARC-520 Results in Prolonged Hepatitis B Surface Antigen Response in Patients With Chronic Hepatitis B Infection. *Hepatology, 72*(1), 19-31. Retrieved from https://www.ncbi.nlm.nih.gov/pubmed/31654573. doi:10.1002/hep.31008

Zhang, Z., Nomura, N., Muramoto, Y., Ekimoto, T., Uemura, T., Liu, K., . . . Shimizu, T. (2022). Structure of SARS-CoV-2 membrane protein essential for virus assembly. *Nat Commun, 13*(1), 4399. Retrieved from https://www.ncbi.nlm.nih.gov/pubmed/35931673. doi:10.1038/s41467-022-32019-3

Zhao, X., Shi, X., Lv, M., Yuan, B., & Wu, J. (2021). Prevalence and factors associated with hepatitis B virus infection among household members: a cross-sectional study in Beijing. *Hum Vaccin Immunother, 17*(6), 1818-1824. Retrieved from https://www.ncbi.nlm.nih.gov/pubmed/33606606. doi:10.1080/21645515.2020.1847951

Zhao, Y., Sun, J., Li, Y., Li, Z., Xie, Y., Feng, R., . . . Hu, Y. (2021). The strand-biased transcription of SARS-CoV-2 and unbalanced inhibition by remdesivir. *iScience, 24*(8), 102857. Retrieved from https://www.ncbi.nlm.nih.gov/pubmed/34278249. doi:10.1016/j.isci.2021.102857

Zheng, J., Zhang, L., Zhang, J., Wang, X., Ye, K., Xi, Z., . . . Liang, Z. (2013). Single modification at position 14 of siRNA strand abolishes its gene-silencing activity by decreasing both RISC loading and target degradation. *FASEB J, 27*(10), 4017-4026. Retrieved from https://www.ncbi.nlm.nih.gov/pubmed/23771927. doi:10.1096/fj.13-228668

Zheng, M., & Tian, Z. (2019). Liver-Mediated Adaptive Immune Tolerance. *Front Immunol, 10*, 2525. Retrieved from https://www.ncbi.nlm.nih.gov/pubmed/31787967. doi:10.3389/fimmu.2019.02525

Zhu, N., Zhang, D., Wang, W., Li, X., Yang, B., Song, J., . . . Research, T. (2020). A Novel Coronavirus from Patients with Pneumonia in China, 2019. *N Engl J Med, 382*(8), 727-733. Retrieved from https://www.ncbi.nlm.nih.gov/pubmed/31978945. doi:10.1056/NEJMoa2001017

Zimmermann, C. M., Baldassi, D., Chan, K., Adams, N. B. P., Neumann, A., Porras-Gonzalez, D. L., . . . Merkel, O. M. (2022). Spray drying siRNA-lipid nanoparticles for dry powder pulmonary delivery. *J Control Release, 351*, 137-150. Retrieved from https://www.ncbi.nlm.nih.gov/pubmed/36126785. doi:10.1016/j.jconrel.2022.09.021

Zoulim, F., Fournier, C., Habersetzer, F., Sprinzl, M., Pol, S., Coffin, C. S., . . . Inchauspe, G. (2020). Safety and immunogenicity of the therapeutic vaccine TG1050 in chronic hepatitis B patients: a phase 1b placebo-controlled trial. *Hum Vaccin Immunother, 16*(2), 388-399. Retrieved from https://www.ncbi.nlm.nih.gov/pubmed/31373537. doi:10.1080/21645515.2019.1651141

Acknowledgements

I begin with thanking my supervisor Prof. Dr. Ulrike Protzer for allowing me to pursue my doctorate under her eminent supervision and for her guidance throughout my studies. She constantly provided valuable input for my projects, nurturing my ideas and helped me become a better researcher.

Next, I thank my second supervisor Prof. Dr. Matthias Feige for his time and guidance on my projects especially during the thesis committee meetings.

Special thanks to my mentor and friend, Dr. med. Thomas Michler, who took me under his wings as a new doctoral student. I thank him for teaching me all the laboratory work, his constant support, scientific input and most importantly, providing funds for my projects. I will always cherish the experiments we did together and our conversations at professional as well as private level.

I thank all our collaborators, especially Mr. Cho-Chin Cheng, Mr. Philipp Hagen, Prof. Dr. Olivia Merkel and Ms. Domizia Baldassi for their immense support during the SARS-CoV-2 project. Special thanks to Mr. Florian Wilsch for kick-starting the mosaic capsid particles project with me and to Dr. Arie Geerlof for his patience and constant help in purifying capsid particles for more than 4 years. I also thank Dr. Laura Pallet and Prof. Dr. Mala Maini for hosting me as a visiting researcher at the UCL and Ms. Stephanie Kucykowicz for helping me to conduct experiments.

I also thank my students - Ms. Krupa Krishna, Mr. Alexander Seidler and Mr. Pratik Mallick, who worked or are working under my supervision in our lab. While supervising these motivated students, I also learned a great deal about being a better team player and managing various scientific projects efficiently.

I thank all my colleagues at the Institute of Virology, not just for their scientific contributions but also for making me feel welcomed at every stage of my studies. Special thanks to Theresa, Romina, Fenna, Bo-Hung, Merve, Omid, Kathi, Sophia, Laura, Luis, Ecem, Helen and Alex for making this journey full of fun! I feel very lucky and honored to have worked alongside with such amazing people.

I also thank all my friends in India and in Europe. You all have contributed in some way in my development as a researcher. I am very grateful to have you all in my life. Special mention to my friends – Suliman, Abdul, Sainitin and Aman for supporting me during my first few months in Germany.

I thank the Deutscher Akademischer Austauschdienst (DAAD) for funding my doctorate. I also thank Gilead Sciences for our research funding. Also, thanks to European Molecular Biology Organization (EMBO) for funding my research visit at the UCL.

For all my achievements, I owe the most to my family. Very special thanks to my loving wife Khushboo, my parents – Mrs. Megha Ambike and Mr. Sunil Ambike, my sister, and my brother-in-law – Mrs. Gandhali Ambike-Kulkarni and Mr. Avadhoot Kulkarni. Thank you for believing in me, always being there for me and supporting me unconditionally. I would not be here without you.

Publications and Conferences

1. Conferences

- **Controlled Released Society (CRS) Local Chapters – 2021**

  Systematic analysis identifies factors that enable efficient inhibition of SARS-CoV-2 replication with siRNAs – Shubhankar Ambike, Cho-Chin Cheng, Martin Feuerherd, Domizia Baldassi, Suliman Quadir Afridi, Vincent Grass, Andreas Pichlmair, Olivia Merkel and Thomas Michler.

- **Controlled Released Society (CRS) Annual International Meeting – 2021**

  Systematic analysis of RNAi-accessible replication steps of SARS-CoV-2 identifies ORF1 as promising target - Shubhankar Ambike, Cho-Chin Cheng, Domizia Baldassi, Martin Feuerherd, Gerald Burgstaller, Chunkyu Ko, Olivia Merkel and Thomas Michler.

- **Annual Meeting for the Society of Virology - 2021**

  Systematic analysis identifies RNAi-accessible SARS-CoV-2 replication steps - Shubhankar Ambike, Cho-Chin Cheng, Martin Feuerherd, Domizia Baldassi, , Olivia Merkel Andreas Pichlmair, Chunkyu Ko and Thomas Michler.

- **Conference on Retroviruses and Opportunistic Infections (CROI) – 2022**

  Systematic analysis reveals ORF1 region of SARS-CoV-2 genomic RNA as a promising target for siRNA-based therapy - Shubhankar Ambike, Domizia Baldassi, Cho-Chin Cheng, Martin Feuerherd, Gerald Burgstaller, Chunkyu Ko, Olivia Merkel and Thomas Michler.

- **International HBV Meeting – 2022**

  Recombinant mosaic HBV capsids allow activating immunity against the most prevalent HBV genotypes by therapeutic vaccination - Shubhankar Ambike, Julia Sacherl, Arie Geerlof, Anna Kosinska, Sophia Schreiber, Frank Thiele, Tanja Bauer, Michael Nassal, Anne Schütz and Ulrike Protzer.

2. Publications

- **Targeting genomic SARS-CoV-2 RNA with siRNAs allows efficient inhibition of viral replication and spread, Nucleic Acids Research. Volume 50, Issue 1, 11 January 2022, Pages 333-349, https://doi.org/10.1093/nar/gkab1248 - Shubhankar Ambike*,** Cho-Chin Cheng*, Martin Feuerherd, Stoyan Velkov, Domizia Baldassi, Suliman Afridi, Diana Porras-Gonzalez, Xin Wei, Philipp Hagen, Nikolaus Kneidiger, Mircea Gabriel Stoleriu, Vincent Grass, Gerald Burgstaller, Andreas Pichlmair, Olivia Merkel, Chunkyu Ko and Thomas Michler.

- **Inhibition of SARS-CoV-2 replication in the lung with siRNA/VIPER polyplexes. J Control Release. 2022 May; 345:661-674, 10.1016/j.jconrel.2022.03.051** – Domizia Baldassi, **Shubhankar Ambike**, Martin Feuerherd, Cho-Chin Cheng, David Peeler, Daniel Feldmann, Diana Porras-Gonzalez, Xin Wei, Lea Keller, Nikolaus Kneidiger, Mircea Gabriel Stoleriu, Andreas Popp, Gerald Burgstaller, Suzie Pun, Thomas Michler and Olivia Merkel.